

# Verisk Typhoon Model for Southeast Asia

Publication Date: May 2023

## Revision History

Date	Description
1 July 2016	Original document release.
21 July 2016	<p>Facts at a Glance: Stochastic Catalog</p> <ul style="list-style-type: none"> <li>The stochastic catalog statistics included in this section were updated to ensure the number of landfalling events, bypassing events, and total events affecting each modeled country and the Southeast Asia domain were included.</li> <li>For each country, the reported maximum number of landfalling events in a simulated year was corrected.</li> </ul> <p>Facts at a Glance: Modeled Industry Losses</p> <ul style="list-style-type: none"> <li>Additional text was added to the description of the “typhoon risk (loss costs) in Southeast Asia” map.</li> </ul> <p>Event Generation: Stochastic Catalog Summary Statistics</p> <ul style="list-style-type: none"> <li>The reported maximum number of landfalling events in a simulated year was corrected.</li> </ul> <p>M64 Southeast Asia Typhoon Supplement</p> <ul style="list-style-type: none"> <li>The Excel Supplement available on the Verisk <a href="#">Client Portal</a> was updated.</li> </ul>
26 April 2017	<p>Event Generation: Storm Surge Model Domain</p> <ul style="list-style-type: none"> <li>Changed the resolution within the Philippines from 250-meter grid spacing to 500-meter grid spacing.</li> </ul>
12 May 2023	Updated <a href="#">Figure 112</a> Precipitation was extracted for a given day for a given station if it was within 3.5 degrees of the typhoon track, rather than the previous 6 degrees of the typhoon track.
12 May 2023	Added Accounting for Climate Change chapter

# Table of Contents

REVISION HISTORY.....	ii
1 FACTS AT A GLANCE.....	1
1.1 Model abstract.....	1
1.2 Model facts.....	1
1.3 Country facts—Southeast Asia.....	2
1.4 Data sources.....	3
1.5 Historical catalog.....	3
1.6 Stochastic catalog.....	3
1.7 Model resolution and physical properties.....	14
1.8 Modeled lines of business.....	15
1.9 Construction and occupancy classes.....	15
1.10 Modeled industry losses.....	15
1.11 Navigating the document.....	32
2 TYPHOONS IN SOUTHEAST ASIA.....	33
2.1 Typhoons: An overview.....	33
2.2 Southeast Asia typhoon risk.....	35
2.3 Significant historical Southeast Asia typhoons.....	46
3 EVENT GENERATION.....	63
3.1 Annual frequency and location.....	64
3.2 Storm tracks.....	68
3.3 Forward speed, central pressure, and radius of maximum winds.....	69
3.4 Storm filling.....	72
3.5 Peak rainfall intensity and rainfall radius.....	72
3.6 Extratropical transition.....	74
3.7 Stochastic catalog statistics.....	75
3.8 World Scenarios event set.....	76
3.9 Validating stochastic event generation.....	77
3.10 Generating simulated storm surge events.....	83
4 LOCAL INTENSITY CALCULATION.....	85
4.1 Local wind intensity.....	85
4.2 Typhoon-induced precipitation and inland flood intensity.....	95

4.3 Storm surge intensity.....	100
4.4 Validating local intensity.....	106
5 DAMAGE ESTIMATION.....	115
5.1 Building classifications.....	115
5.2 Wind damage functions for residential, commercial, and small industrial buildings.....	124
5.3 Flood damage functions for residential, commercial, and small industrial buildings.....	133
5.4 Storm surge damage functions for residential, commercial, and small industrial buildings.....	142
5.5 Combined damage from multiple sub-perils.....	144
5.6 Time element (business interruption) damage functions for commercial and small industrial buildings.....	145
5.7 Distribution of damage: Uncertainty in damage estimation.....	147
5.8 CRESTA-level damage functions for unknown construction, occupancy, or height classes.....	148
5.9 Estimating damage to large-scale industrial facilities.....	150
5.10 Damage functions for additional lines of business.....	163
5.11 Validating the model's damage functions.....	169
6 INSURED LOSS CALCULATION.....	170
6.1 Aggregating losses probabilistically.....	170
6.2 Demand surge.....	171
6.3 Validating modeled losses.....	172
7 ACCOUNTING FOR CLIMATE CHANGE.....	183
7.1 Historical trends.....	185
7.2 Model and catalog development.....	200
7.3 Model validation.....	201
7.4 Conclusion.....	206
8 VERISK TYPHOON MODEL FOR SOUTHEAST ASIA IN CATRADER.....	207
8.1 Available catalogs.....	207
8.2 Resolution of analysis results.....	207
8.3 Verisk Industry Exposure Database.....	208
8.4 Supported lines of business for reporting model losses.....	208
8.5 Policy conditions.....	209
9 VERISK TYPHOON MODEL FOR SOUTHEAST ASIA IN TOUCHSTONE.....	216
9.1 Available catalogs.....	216
9.2 Supported geographic resolutions.....	216
9.3 Modeling aggregate data.....	218

9.4 Modeled coverages.....	218
9.5 Construction and occupancy classes, year built and height bands, and relative vulnerabilities.....	218
9.6 Supported secondary risk characteristics.....	219
9.7 Supported policy terms.....	220
A CRESTA ZONES.....	221
A.1 Guam.....	221
A.2 Hong Kong.....	221
A.3 Macau.....	222
A.4 Philippines.....	223
A.5 Saipan.....	227
A.6 Taiwan.....	227
A.7 Vietnam.....	229
SELECTED REFERENCES.....	232
SELECTED REFERENCES FOR ACCOUNTING FOR CLIMATE CHANGE.....	245

# List of Figures

- Figure 1. Model domain for the Verisk Typhoon Model for Southeast Asia..... 2
- Figure 2. Historical vs. simulated annual landfall frequency by intensity category – Guam..... 4
- Figure 3. Historical vs. simulated annual landfall frequency by intensity category – Hong Kong.....4
- Figure 4. Historical vs. simulated annual landfall frequency by intensity category – The Philippines..... 5
- Figure 5. Historical vs. simulated annual landfall frequency by intensity category – Taiwan..... 5
- Figure 6. Historical vs. simulated annual landfall frequency by intensity category – Macau.....6
- Figure 7. Historical vs. simulated annual landfall frequency by intensity category – Saipan.....6
- Figure 8. Historical vs. simulated annual landfall frequency by intensity category – Vietnam..... 7
- Figure 9. Historical vs. simulated annual landfall distribution – Guam.....8
- Figure 10. Historical vs. simulated distribution of landfalling events by month – Guam..... 8
- Figure 11. Historical vs. simulated annual landfall distribution – Hong Kong..... 9
- Figure 12. Historical vs. simulated distribution of landfalling events by month – Hong Kong.....9
- Figure 13. Historical vs. simulated annual landfall distribution – Macau..... 10
- Figure 14. Historical vs. simulated distribution of landfalling events by month – Macau.....10
- Figure 15. Historical vs. simulated annual landfall distribution – The Philippines..... 11
- Figure 16. Historical vs. simulated distribution of landfalling events by month – The Philippines.....11
- Figure 17. Historical vs. simulated annual landfall distribution – Saipan..... 12
- Figure 18. Historical vs. simulated distribution of landfalling events by month – Saipan.....12
- Figure 19. Historical vs. simulated annual landfall distribution – Taiwan.....13
- Figure 20. Historical vs. simulated distribution of landfalling events by month – Taiwan..... 13
- Figure 21. Historical vs. simulated annual landfall distribution – Vietnam.....14
- Figure 22. Historical vs. simulated distribution of landfalling events by month – Vietnam..... 14
- Figure 23. Insurable/insured average annual aggregate losses – Guam..... 17
- Figure 24. Insurable average annual aggregate losses – Hong Kong..... 18
- Figure 25. Insured average annual aggregate losses – Hong Kong..... 18
- Figure 26. Insurable average annual aggregate losses – Macau..... 19
- Figure 27. Insured average annual aggregate losses – Macau..... 19



Figure 28. Insurable average annual aggregate losses – The Philippines.....	20
Figure 29. Insured average annual aggregate losses – The Philippines.....	20
Figure 30. Insurable/insured average annual aggregate losses – Saipan.....	21
Figure 31. Insurable average annual aggregate losses – Taiwan.....	21
Figure 32. Insured average annual aggregate losses – Taiwan.....	22
Figure 33. Insurable average annual aggregate losses – Vietnam.....	22
Figure 34. Insured average annual aggregate losses – Vietnam.....	23
Figure 35. Insurable average annual aggregate losses – all modeled countries/territories and top loss zones.....	23
Figure 36. Insured average annual aggregate losses – all modeled countries/territories and top loss zones.....	24
Figure 37. Typhoon risk (loss costs) in Southeast Asia.....	25
Figure 38. Components of the Verisk model.....	32
Figure 39. Average number of typhoon formations per year by ocean basin.....	35
Figure 40. Typhoon landfall counts in Southeast Asia by intensity.....	36
Figure 41. Population density in the modeled countries of Southeast Asia.....	39
Figure 42. Population density in Guam and Saipan.....	40
Figure 43. Population density in Hong Kong and Macau.....	41
Figure 44. Population density in Hong Kong and Macau.....	42
Figure 45. Population density in the Philippines.....	43
Figure 46. Population density in Guam and Saipan.....	44
Figure 47. Population density in Taiwan.....	45
Figure 48. Population density in Vietnam.....	46
Figure 49. Track of Typhoon Joan (1970).....	48
Figure 50. Track of Typhoon Ellen (1983).....	49
Figure 51. Track of Typhoon Angela (1995).....	50
Figure 52. Track of Typhoon Paka (1997).....	51
Figure 53. Track of Typhoon Sam (1999).....	52
Figure 54. Track of Typhoon Nari (2001).....	53
Figure 55. Track of Typhoon Haitang (2005).....	54

Figure 56. Track of Typhoon Durian (2006).....	55
Figure 57. Track of Typhoon Fengshen (2008).....	56
Figure 58. Track of Typhoon Nuri (2008).....	57
Figure 59. Track of Typhoon Morakot (2009).....	58
Figure 60. Track of Typhoon Nesat (2011).....	60
Figure 61. Track of Typhoon Vicente (2012).....	62
Figure 62. Domain of the Verisk Typhoon Model for the Northwest Pacific Basin, highlighting the countries modeled in the Verisk Typhoon Model for Southeast Asia.....	65
Figure 63. Annual frequency (Poisson) distribution of simulated typhoons in the Verisk Typhoon Model for the Northwest Pacific Basin domain.....	66
Figure 64. Annual frequency distribution of simulated typhoon landfalls in the Verisk Typhoon Model for Southeast Asia domain.....	66
Figure 65. Distribution by month of simulated events in the model domain from the 10,000 year catalog.....	67
Figure 66. Historical storm genesis locations and smoothed historical genesis locations.....	68
Figure 67. Storm track generation in the Verisk Typhoon Model for the Northwest Pacific Basin.....	69
Figure 68. Storm parameters vary along the storm track.....	70
Figure 69. Simulated storm counts by intensity category at landfall.....	71
Figure 70. Peak rainfall intensity distribution.....	73
Figure 71. Rainfall radius distribution.....	73
Figure 72. Extratropical transitioning by month and latitude, historical.....	75
Figure 73. Extratropical transitioning by month and latitude, simulated.....	75
Figure 74. Historical vs. simulated annual frequency of typhoons in the model domain.....	77
Figure 75. Comparison of historical and simulated annual frequency at genesis for typhoons in the model domain.....	78
Figure 76. Historical vs. simulated annual frequency of landfalling typhoons in Southeast Asia.....	78
Figure 77. Historical vs. simulated number of landfalls per event in Southeast Asia.....	79
Figure 78. Historical and Verisk-simulated typhoon tracks for a 25-year period.....	80
Figure 79. Historical and Verisk-modeled typhoon intensity category at landfall.....	81
Figure 80. Comparison between historical and simulated annual storm track density.....	82
Figure 81. Simulated multi-country loss-causing events for Southeast Asia.....	83

Figure 82. Specific location (500-m resolution) grids, nested within region grids (2,250-m resolution), nested within country grids (6,750-m resolution), nested within the model domain.....	84
Figure 83. Relationship between central pressure and wind speed.....	87
Figure 84. Effects of topography on wind.....	88
Figure 85. Terrain effects on wind velocity profiles.....	89
Figure 86. Verisk friction factors used in the Verisk Typhoon Model for the Northwest Pacific Basin – the Philippines, Taiwan, and Vietnam.....	90
Figure 87. Verisk friction factors used in the Verisk Typhoon Model for the Northwest Pacific Basin – Guam and Saipan.....	91
Figure 88. Verisk friction factors used in the Verisk Typhoon Model for the Northwest Pacific Basin – Macau and Hong Kong.....	91
Figure 89. Verisk gust factors used in the Verisk Typhoon Model for the Northwest Pacific Basin – the Philippines, Taiwan, and Vietnam.....	92
Figure 90. Verisk gust factors used in the Verisk Typhoon Model for the Northwest Pacific Basin – Guam and Saipan.....	93
Figure 91. Verisk gust factors used in the Verisk Typhoon Model for the Northwest Pacific Basin – Macau and Hong Kong.....	93
Figure 92. Storm track and modeled wind field of Typhoon Haiyan (2013).....	94
Figure 93. TRMM average pre-extratropical transition (left panel) and post extratropical transition (right panel) precipitation 24 hours before JMA extratropical transition hour, for 2000 to 2008.....	96
Figure 94. Storm track and modeled accumulated precipitation levels for Typhoon Nari (2001).....	97
Figure 95. Storm track and modeled accumulated precipitation levels for Typhoon Ketsana (2009).....	97
Figure 96. Schematic of CASC2D showing how a fraction of rainfall at each grid cell is absorbed and the rest runs off to the next cell.....	99
Figure 97. Storm track and modeled accumulated runoff for Typhoon Nari (2001).....	99
Figure 98. Storm track and modeled accumulated runoff for Typhoon Ketsana (2009).....	100
Figure 99. Water depth and land elevation for the model domain, produced using 30 arc second GEBCO data for bathymetry and a combination of SRTM90 and InterMap Data products for terrain height.....	101
Figure 100. Location of levees in Hong Kong.....	102
Figure 101. Location of levees in Taipei and Keelung, Taiwan.....	102
Figure 102. Location of levees in Kaohsiung, Taiwan.....	103
Figure 103. Location of levees in Tacloban, Philippines.....	103
Figure 104. Location of levees in Manila, Philippines.....	104

Figure 105. Location of levees in Cebu, Philippines.....	104
Figure 106. Modeled astronomical tidal range for each 250-m computational domain.....	106
Figure 107. Verisk-modeled and JMA-estimated maximum wind speeds at landfall for historical events.....	107
Figure 108. Maximum modeled and observed wind speeds for historical typhoons affecting Hong Kong.....	108
Figure 109. Verisk-modeled 100-year return period wind speeds for the Philippines (left) and a similar analysis as determined by PAGASA (right).....	109
Figure 110. Verisk-modeled 100-year return period wind speeds for Taiwan and similar analysis from a wind engineering study.....	110
Figure 111. Maximum modeled and observed wind speeds for historical typhoons affecting Guam.....	110
Figure 112. Verisk-modeled and observed 5-year (occurrence) return period typhoon related precipitation amounts. Observed values are computed from the National Climatic Data Center's Global Summary of the Day data.....	111
Figure 113. Verisk-modeled 100-year return period flood footprint (right) and flood footprint from PAGASA (left) (Ketsana was considered to be a 100 year event for the Manila region; dashed rectangle on PAGASA analysis shows only the flood in the Manila region, which is also identified in the modeled result).....	112
Figure 114. Verisk-modeled 200-year return period flood footprint (left) and Taiwan Government Agency 250-year flood footprint (right) for Taipei Region (Taiwan).....	113
Figure 115. Verisk-modeled maximum and observed storm surge heights for selected historical events for Hong Kong.....	114
Figure 116. Verisk-modeled maximum storm surge heights (m) for Typhoon Haiyan (2013) and selected observations (color-filled circles).....	114
Figure 117. Construction type distribution for residential buildings in Hong Kong, the Philippines, Taiwan, Vietnam, Macau, Guam, and Saipan.....	118
Figure 118. Construction type distribution for commercial and industrial buildings in Guam, Hong Kong, Macau, the Philippines, Saipan, Taiwan, and Vietnam.....	119
Figure 119. Construction type distribution for agricultural buildings in the Philippines, Taiwan, and Vietnam.....	120
Figure 120. Examples of large industrial facilities.....	121
Figure 121. Examples of large industrial facility components.....	122
Figure 122. Examples of typical types of infrastructures.....	123
Figure 123. Wind building damage functions for selected construction types, including unknown, for a single-family home in Southeast Asia.....	125

Figure 124. Wind building damage functions for selected construction types, including unknown construction, for unknown-height apartment in Southeast Asia.....	125
Figure 125. Wind speed profile and corresponding damage ratios.....	126
Figure 126. Measuring the cumulative effects of winds.....	127
Figure 127. Relationship between wind mean building damage and wind mean contents damage for different lines of business, including unknown.....	128
Figure 128. Regional vulnerability for engineered and non-engineered buildings in the Philippines.....	130
Figure 129. Regional vulnerability for engineered and non-engineered buildings in Taiwan.....	130
Figure 130. Regional vulnerability for engineered and non-engineered buildings in Vietnam.....	131
Figure 131. Temporal modifier for engineered building in the model (x-axis represents the year built, y-axis represents the temporal vulnerability).....	133
Figure 132. Flood building damage functions for reinforced-concrete, low-rise buildings for single-family, condominium, commercial, and industrial in Southeast Asia.....	134
Figure 133. Flood building damage functions for selected construction types, including unknown, for low-rise single-family buildings in Southeast Asia.....	135
Figure 134. Flood building damage functions for selected construction types, including unknown, for 3-story condominium in Southeast Asia.....	136
Figure 135. Flood building damage functions for selected construction types, including unknown, for 3-story commercial in Southeast Asia.....	137
Figure 136. Relative vulnerability of contents for residential buildings.....	138
Figure 137. Flood content damage functions with reinforced concrete, mid rise building for general occupancy types in Southeast Asia.....	138
Figure 138. Relative flood vulnerability of building and content for general occupancies with reinforced concrete in Southeast Asia.....	139
Figure 139. Flood damage functions for supported height categories for concrete apartment building in Southeast Asia.....	141
Figure 140. Storm surge vulnerability for supported height categories for a concrete commercial building in Southeast Asia.....	144
Figure 141. Hypothetical event tree of BI estimation for an office and a hotel.....	146
Figure 142. Time element (BI) damage functions for different buildings of varying occupancy classes.....	147
Figure 143. Representative damage function.....	148
Figure 144. Comparison of building inventory with CRESTA areas by occupancy and height class in Taiwan.....	150
Figure 145. Distribution of wind pressure around a tank wall.....	154

Figure 146. Deflection of tank wall due to elastic buckling.....	154
Figure 147. West Ford Flat power plant geothermal cooling tower.....	155
Figure 148. Example of a process tower.....	156
Figure 149. Examples of flare tower types: freestanding (left), guyed flare (middle), and derrick-supported (right).....	157
Figure 150. Buckling of a derrick-supported flare tower.....	157
Figure 151. Wind damage to selected industrial facilities.....	158
Figure 152. Flood damage to selected industrial facilities.....	159
Figure 153. Storm surge damage to selected industrial facilities.....	159
Figure 154. Wind damage to selected industrial facility components.....	160
Figure 155. Flood damage to selected industrial facility components.....	161
Figure 156. Time element ratios for wind damage to selected large-scale industrial facilities.....	162
Figure 157. Time element ratios for flood and storm surge damage to selected large-scale industrial facilities.....	162
Figure 158. Examples of automobile damage due to water inundation.....	164
Figure 159. Damage to railway tracks and bridges.....	168
Figure 160. Observed and Verisk-modeled gross losses – Guam.....	174
Figure 161. Observed and Verisk-modeled gross losses – Hong Kong.....	175
Figure 162. Observed and Verisk-modeled gross losses – the Philippines.....	175
Figure 163. Observed and Verisk-modeled gross losses – Taiwan.....	176
Figure 164. Observed and Verisk-modeled gross losses – Vietnam.....	176
Figure 165. Benchmarking historical losses on Verisk's insurable occurrence exceedance probability curve – Guam.....	177
Figure 166. Benchmarking historical losses on Verisk's insurable occurrence exceedance probability curve – Hong Kong (all sub-perils).....	178
Figure 167. Benchmarking historical losses on Verisk's insurable occurrence exceedance probability curve – the Philippines (all sub-perils).....	178
Figure 168. Benchmarking historical losses on Verisk's insurable occurrence exceedance probability curve – the Philippines (surge only).....	179
Figure 169. Benchmarking historical losses on Verisk's insurable occurrence exceedance probability curve – Taiwan (all sub-perils).....	179

Figure 170. Benchmarking historical losses on Verisk's insurable occurrence exceedance probability curve – Taiwan (precipitation-induced flood only).....	180
Figure 171. Benchmarking historical losses on Verisk's insurable occurrence exceedance probability curve – Vietnam (all sub-perils).....	180
Figure 172. Observed and Verisk-modeled gross losses by company with different events (linear scale) – the Philippines.....	181
Figure 173. Observed and Verisk-modeled gross losses by company with different events (logarithmic scale) – the Philippines.....	182
Figure 174. Relative degree of confidence that climate change is impacting various weather phenomena.....	183
Figure 175. Recent increases in tropical cyclone frequency by Saffir-Simpson Hurricane Wind Scale....	184
Figure 176. Summary of tropical cyclone projections for a 2°C global anthropogenic warming.....	185
Figure 177. Observed trends in tropical cyclone frequency (number per year) over the period 1980 to 2018.....	187
Figure 178. Annual typhoon numbers over basin the from 1884 to 2018, for Philippines, Hong Kong, Shanghai, Japan and IBTrACS data.....	188
Figure 179. Annual average minimum central pressure of storms that make landfall in Hong Kong.....	189
Figure 180. Annual frequency of landfalling typhoons in Hong Kong.....	190
Figure 181. Annual average minimum central pressure of storms that make landfall in Philippines.....	190
Figure 182. Annual frequency of landfalling typhoons in Philippines.....	190
Figure 183. Annual average minimum central pressure of storms that make landfall in Taiwan.....	191
Figure 184. Annual frequency of landfalling typhoons in Taiwan.....	191
Figure 185. Annual average minimum central pressure of storms that make landfall in Vietnam.....	191
Figure 186. Annual frequency of landfalling typhoons in Vietnam.....	192
Figure 187. Mean latitude of lifetime maximum intensity (LMI).....	193
Figure 188. Time series of annual-mean tropical-cyclone forward speed (labeled "translation speed") and their linear trends in different regions.....	195
Figure 189. Forward speed of typhoons at landfall – Hong Kong.....	196
Figure 190. Forward speed of typhoons at landfall – Philippines.....	196
Figure 191. Forward speed of typhoons at landfall –Taiwan forward.....	197
Figure 192. Forward speed of typhoons at landfall –Vietnam.....	197
Figure 193. Hong Kong typhoon-day precipitation.....	198

Figure 194. Philippines typhoon-day precipitation.....	199
Figure 195. Taiwan typhoon-day precipitation.....	199
Figure 196. Vietnam typhoon-day precipitation.....	200
Figure 197. Comparison of modeled and historic frequencies of typhoons making landfall across domain.....	202
Figure 198. Comparison of modeled and historic frequencies of typhoons making landfall– Hong Kong.....	202
Figure 199. Comparison of modeled and historic frequencies of typhoons making landfall– Taiwan.....	202
Figure 200. Comparison of modeled and historic frequencies of typhoons making landfall– Philippines.....	203
Figure 201. Comparison of modeled and historic frequencies of typhoons making landfall– Vietnam.....	203
Figure 202. Comparison of modeled and historic forward speed – model domain.....	203
Figure 203. Comparison of modeled and historic forward speed – Hong Kong.....	204
Figure 204. Comparison of modeled and historic forward speed – Philippines.....	204
Figure 205. Comparison of modeled and historic forward speed – Taiwan.....	204
Figure 206. Comparison of modeled and historic forward speed – Vietnam.....	205
Figure 207. Verisk modeled and observed 5-year (occurrence) return period typhoon related precipitation amounts.....	206
Figure 208. CRESTA zone in Guam.....	221
Figure 209. CRESTA zones in Hong Kong.....	222
Figure 210. CRESTA zone in Macau.....	223
Figure 211. CRESTA zones in the Philippines.....	224
Figure 212. CRESTA zone in Saipan.....	227
Figure 213. CRESTA zones in Taiwan.....	228
Figure 214. CRESTA zones in Vietnam.....	229

# List of Tables

- Table 1. Modeled insurable occurrence loss estimates..... 16
- Table 2. Modeled insured occurrence loss estimates..... 17
- Table 3. Modeled insurable/insured losses for historical typhoons – Guam (USD millions)..... 25
- Table 4. Modeled insurable losses for historical typhoons – Hong Kong (HKD millions)..... 26
- Table 5. Modeled insured losses for historical typhoons – Hong Kong (HKD millions)..... 26
- Table 6. Modeled insurable losses for historical typhoons – Macau (MOP millions)..... 26
- Table 7. Modeled insured losses for historical typhoons – Macau (MOP millions)..... 27
- Table 8. Modeled insurable losses for historical typhoons – The Philippines (PHP millions)..... 27
- Table 9. Modeled insured losses for historical typhoons – The Philippines (PHP millions)..... 28
- Table 10. Modeled insurable/insured losses for historical typhoons – Saipan (USD millions)..... 29
- Table 11. Modeled insurable losses for historical typhoons – Taiwan (NTD millions)..... 29
- Table 12. Modeled insured losses for historical typhoons – Taiwan (NTD millions)..... 30
- Table 13. Modeled insurable losses for historical typhoons – Vietnam (VND millions)..... 30
- Table 14. Modeled insured losses for historical typhoons – Vietnam (VND millions)..... 30
- Table 15. Modeled insurable losses for Extreme Disaster Scenarios available in Touchstone and CATRADER..... 31
- Table 16. Modeled insured losses for Extreme Disaster Scenarios available in Touchstone and CATRADER..... 31
- Table 17. The Saffir-Simpson hurricane wind scale..... 34
- Table 18. Historical event set for the Verisk Typhoon Model for Southeast Asia..... 46
- Table 19. Extreme Disaster Scenarios in the World Scenarios event set for the Verisk Typhoon Model for Southeast Asia available in CATRADER 18.0 and Touchstone 4.0..... 76
- Table 20. Historical vs. simulated typhoon variable values at landfall..... 81
- Table 21. Manning coefficients assigned by Verisk to LULC categories in Southeast Asia..... 98
- Table 22. Definition of engineered and non-engineered buildings..... 116
- Table 23. Supported height bands for construction and occupancy classes for wind..... 128
- Table 24. Relative wind risk and vulnerability across regions..... 131
- Table 25. Supported height bands for construction and occupancy classes for flood..... 139



Table 26. Relative flood risk and vulnerability for Southeast Asia modeled countries/territories.....	142
Table 27. Example of combined MDR calculation using sub-peril MDRs.....	145
Table 28. Industrial facility components used in the Verisk Typhoon Model for Southeast Asia.....	152
Table 29. The historical event set available in CATRADER for the Verisk Typhoon Model for Southeast Asia.....	207
Table 30. Deductibles by line of business by country/territory.....	209
Table 31. Limits by line of business by country/territory.....	210
Table 32. Assumed typhoon take-up rates by country/territory.....	210
Table 33. Assumed typhoon take-up rates by CRESTA zone – the Philippines.....	210
Table 34. Assumed typhoon take-up rates by CRESTA zone – Taiwan.....	213
Table 35. Assumed typhoon take-up rates by CRESTA zone – Vietnam.....	214
Table 36. The historical event set available in Touchstone for the Verisk Typhoon Model for Southeast Asia.....	216
Table 37. Supported geographic resolutions in Touchstone.....	217
Table 38. CRESTA zone name in Guam.....	221
Table 39. CRESTA zone names in Hong Kong.....	222
Table 40. CRESTA zone name in Macau.....	223
Table 41. CRESTA zone names in the Philippines.....	224
Table 42. CRESTA zone name in Saipan.....	227
Table 43. CRESTA zone names in Taiwan.....	228
Table 44. CRESTA zone names in Vietnam.....	230

# 1 Facts at a Glance

## 1.1 Model abstract

The Verisk Typhoon Model for Southeast Asia is part of the Verisk Typhoon Model for the Northwest Pacific Basin. The Verisk Typhoon Model for Southeast Asia is a stochastic, event based model that shares a catalog with other Verisk-modeled countries in the region, including mainland China, Japan, and South Korea. The Verisk Typhoon Model for Southeast Asia captures the effects of tropical storm and typhoon winds, precipitation-induced flooding, and storm surge induced flooding on insured properties in Southeast Asia. Wind intensity computations are based on a storm's intensity, size, location, forward speed, and direction, as well as the underlying terrain and land use in the region. The effect of extratropical transitioning is also included to accurately assess the full impact on properties due to precipitation from a typhoon. Moreover, the model captures wind duration to accurately estimate the damage at a location.

For the local intensity component of the model, the effects of surface friction, filling, and gustiness on wind intensity are all considered in order to properly calculate the damage of onshore properties. Flood intensity computations are based on total accumulated precipitation, soil type, land use/land cover data, and topography.

The model includes separate damage functions for wind, precipitation-induced flood, and storm surge sub-perils. These functions vary by building characteristics, such as occupancy class, construction type, and building height. Additionally, the model explicitly accounts for the regional variability in wind vulnerability due to differences in regional construction practices. The model also considers the effects of existing flood mitigation measures. Several new lines of business are also introduced in the model, including, marine cargo and hull, large industrial facilities, and infrastructure.

All model components and model losses are validated with the latest available data and science. The model is built to meet the wide spectrum of typhoon risk management needs of all stakeholders, including the insurance and reinsurance industry, and accounts for insurance policy conditions specific to each country/territory.

## 1.2 Model facts

<b>Model Name</b>	Verisk Typhoon Model for Southeast Asia
<b>Release Date</b>	June 15, 2016
<b>Software Systems</b>	<ul style="list-style-type: none"><li>• Touchstone 4.0</li><li>• CATRADER 18.0</li></ul>
<b>Model Domain</b>	4.57 to 26.62 latitude, 102.00 to 146.15 longitude

<b>Modeled Countries</b>	Wind, precipitation, and precipitation-induced flooding are modeled in Guam, Hong Kong, Macau, the Philippines, Saipan, Taiwan, and Vietnam. Storm surge is modeled in Hong Kong, the Philippines, and Taiwan.
<b>Modeled Perils</b>	The modeled sub-perils include typhoon 1-minute sustained winds (from tropical storm strength—with wind speeds of at least 63 km/h—to Category 5 strength—with wind speeds of at least 252 km/h), precipitation-induced flooding, and storm surge. Flood defenses, such as those constructed by the Drainage Services Department of the Government of the Hong Kong Special Administrative Region, are included so that precipitation-induced flooding does not occur until the capacities of such defenses are exceeded. Catastrophic failures of the defenses are not considered.

### 1.3 Country facts—Southeast Asia

Outlined in red in [Figure 1](#) is the domain (4.57 to 26.62 latitude, 102.00 to 146.15 longitude) for the Verisk Typhoon Model for Southeast Asia, which includes Guam, Hong Kong, Macau, the Philippines, Saipan, Taiwan, and Vietnam. Country/territory specific CRESTA zones and zone names are presented in Appendix A.

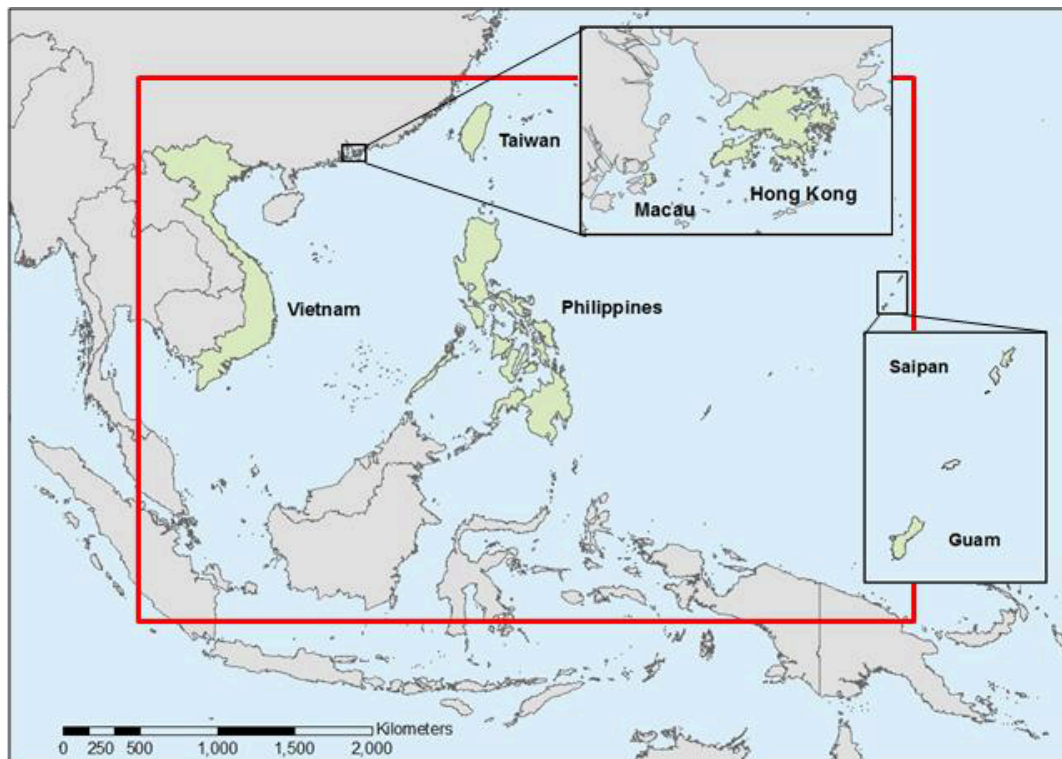


**Figure 1. Model domain for the Verisk Typhoon Model for Southeast Asia**

**See Also**  
[CRESTA Zones](#)

## 1.4 Data sources

Key data sources used in the development of the stochastic catalog of the Verisk Typhoon Model for the Northwest Pacific Basin include typhoon track information from the Japan Meteorological Agency (JMA) and the Shanghai Typhoon Institute (STI). Precipitation data came from the Tropical Rainfall Measurement Mission (TRMM), NOAA's Global Summary of the Day (GSOD), the Hong Kong Observatory (HKO), the Philippine Atmospheric Geophysical and Astronomical Services Administration (PAGASA), and Taiwan's Central Weather Bureau (CWB). Satellite imagery came from Digital Typhoon and Soil data for the flood sub-peril came from the Harmonized World Soil Database (HWSD).

Land use land cover (LULC) data was collected from the Moderate Resolution Imaging Spectroradiometer (MODIS) retrieved courtesy of the NASA EOSDIS Land Processes Distributed Active Archive Center (LP DAAC) and USGS/Earth Resources Observation and Science (EROS) Center, Sioux Falls, South Dakota, at a 1-km resolution. For coastal regions, Verisk used 1 arc-minute global relief data from the General Bathymetric Chart of the Oceans (GEBCO).

### See Also

[Verisk Industry Exposure Database](#)

## 1.5 Historical catalog

The stochastic catalog for the Verisk Typhoon Model for the Northwest Pacific Basin was constructed by blending meteorological and track information from the Japan Meteorological Agency (JMA) and the Shanghai Typhoon Institute (STI) for more than 1,800 storms that occurred in the Northwest Pacific Basin between 1951 and 2008. Precipitation data from the Tropical Rainfall Measurement Mission (TRMM) as well as satellite imagery from Digital Typhoon were primarily used to specify the precipitation characteristics of the catalog.

The catalog for the Verisk Typhoon Model for the Northwest Pacific Basin includes events that occurred in or near China, Guam, Hong Kong, Japan, Macau, the Philippines, Saipan, South Korea, Taiwan, and Vietnam.

## 1.6 Stochastic catalog

The Verisk Typhoon Model for the Northwest Pacific Basin has a 10,000-year catalog containing 293,235 simulated events in the basinwide domain. The catalog includes events with intensities that range from tropical storm (1-minute sustained wind speeds of 63 km/h) to Category 5 (1-minute sustained wind speeds of at least 252 km/h). Note that wind intensity is modeled according to the Saffir-Simpson hurricane wind scale (SSHWS). After the model's industry loss filter is applied, the number of loss-causing simulated typhoons in the

catalog that make landfall in Southeast Asia is 92,006 with the number of bypassing events being 29,576, totaling 121,581 events. [Figure 2](#) through [Figure 8](#) show the landfall counts by Saffir-Simpson intensity category for Guam, Hong Kong, Macau, the Philippines, Saipan, Taiwan, and Vietnam, respectively. The figures show weak typhoons dominate the intensity distributions for these regions, but much stronger storms are also common, particularly in the Philippines and Taiwan.

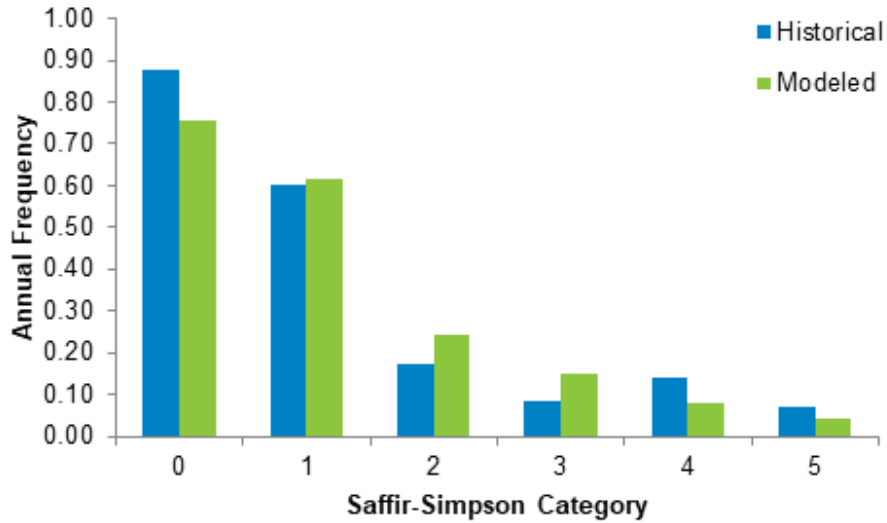


**Figure 2. Historical vs. simulated annual landfall frequency by intensity category – Guam**

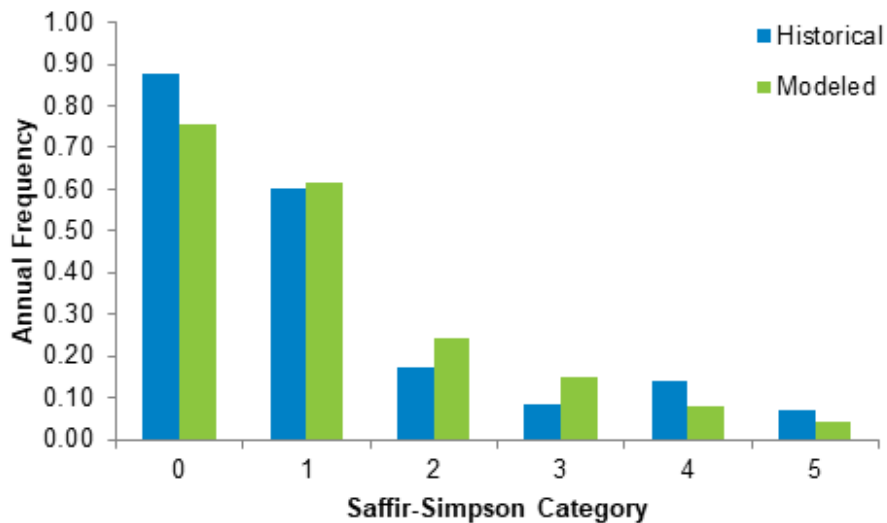


**Figure 3. Historical vs. simulated annual landfall frequency by intensity category – Hong Kong**

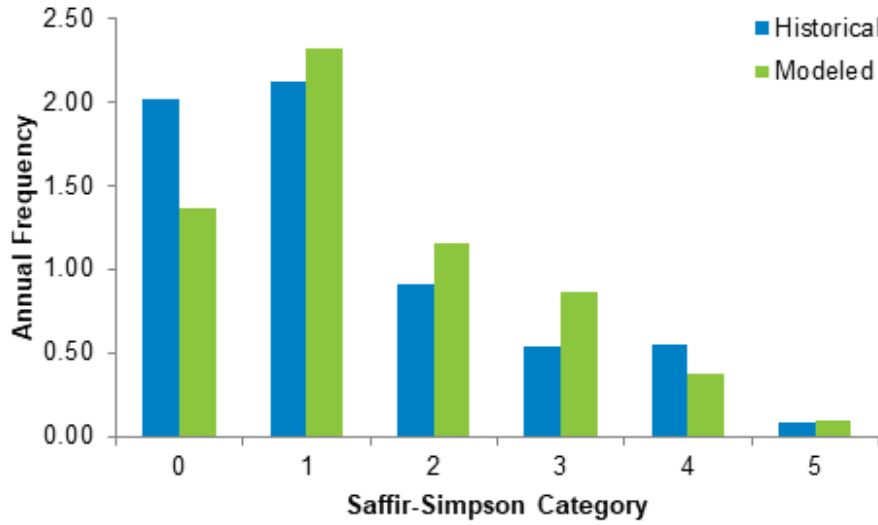


Figure 4. Historical vs. simulated annual landfall frequency by intensity category – The Philippines

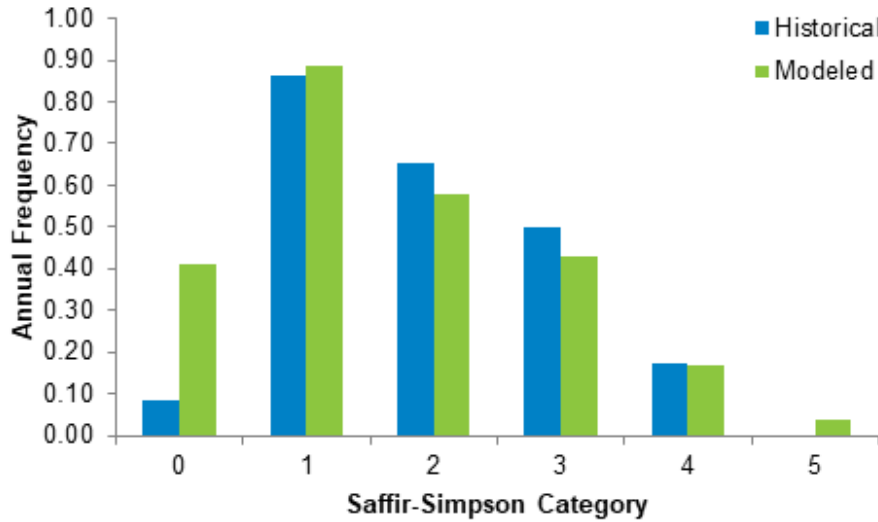


Figure 5. Historical vs. simulated annual landfall frequency by intensity category – Taiwan

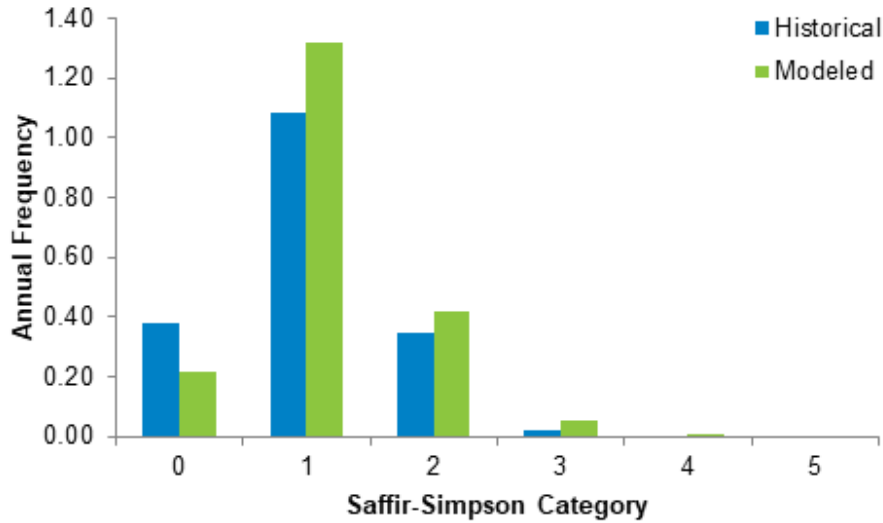


Figure 6. Historical vs. simulated annual landfall frequency by intensity category – Macau

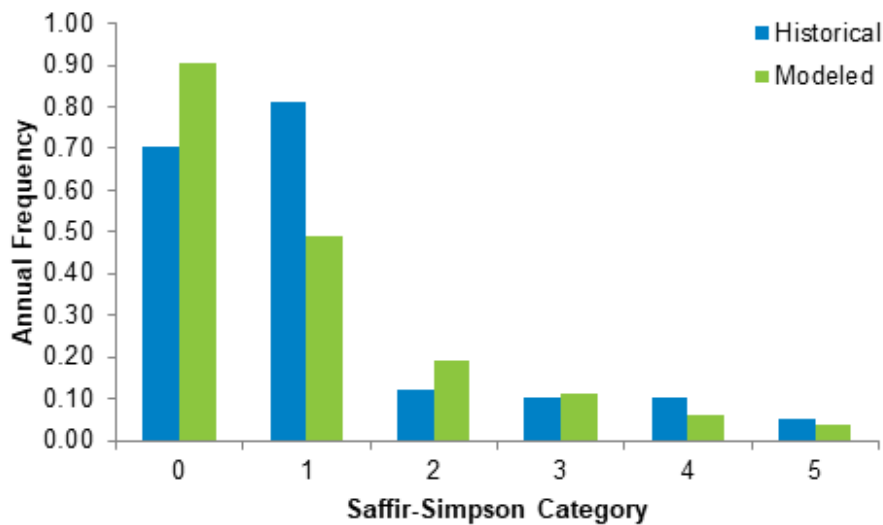
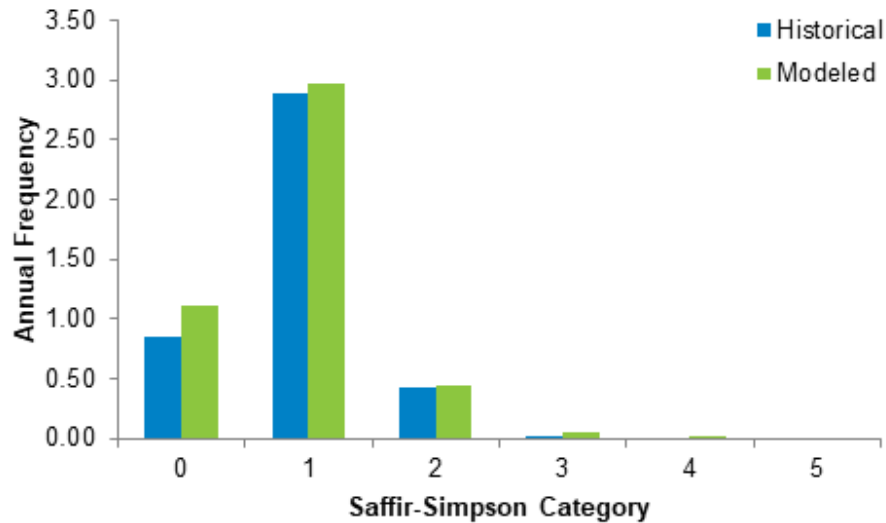


Figure 7. Historical vs. simulated annual landfall frequency by intensity category – Saipan



**Figure 8. Historical vs. simulated annual landfall frequency by intensity category – Vietnam**

Accounting for a third of the global typhoon activity, the Northwest Pacific Basin is the world's most active basin. Though typhoons can occur in the Northwest Pacific Basin at any time of the year, the months of February and March are comparatively calmer. The distribution of simulated multiple landfalling events and the distribution of simulated landfalling events by month are illustrated below for each modeled country/territory (Guam, Hong Kong, Macau, the Philippines, Saipan, Taiwan, and Vietnam).

## Guam

The total number of simulated events that cause loss in Guam is 12,673 – 3,134 of which are landfalling events while 9,539 are bypassing events. The maximum number of landfalling events in a single simulated year is eight, though the probability of such an occurrence is low; note that a single storm can make multiple landfalls. Like actual typhoons in the Northwest Pacific Basin, simulated events can occur in any month of the year. [Figure 9](#) and [Figure 10](#) show the comparison between historical and simulated annual landfall distributions and the distribution of landfall events by month for Guam, respectively.

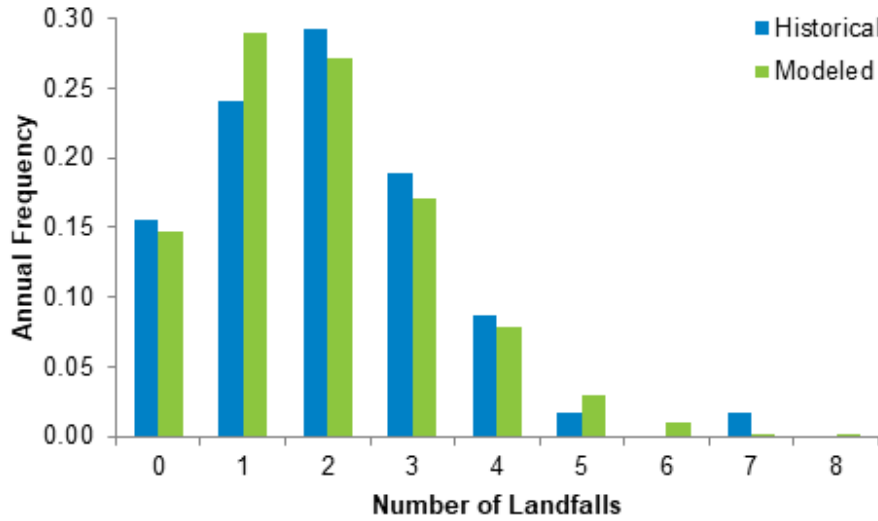


Figure 9. Historical vs. simulated annual landfall distribution – Guam

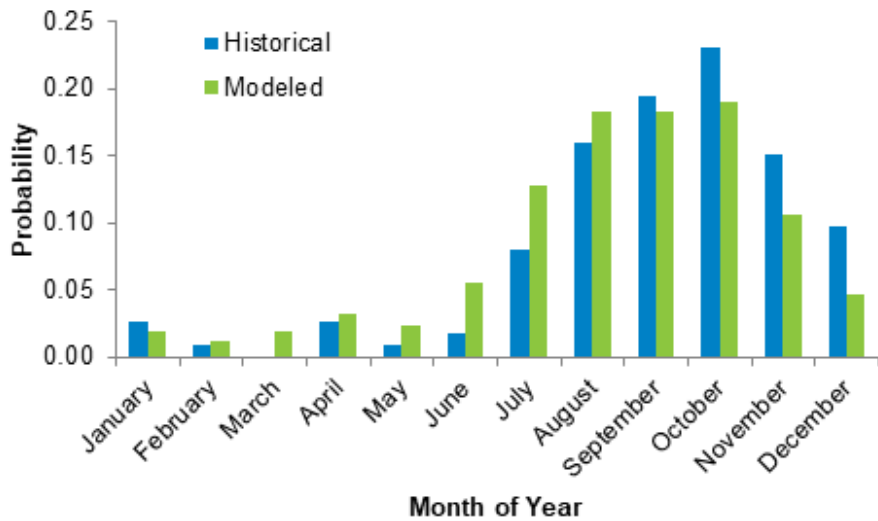


Figure 10. Historical vs. simulated distribution of landfalling events by month – Guam

## Hong Kong

The total number of simulated events that cause loss in Hong Kong is 14,058 – 4,191 of which are landfalling events while 9,867 are bypassing events. The maximum number of landfalling events in a single simulated year is 10, though the probability of this is very small. Like actual typhoons in the Northwest Pacific Basin, simulated events can occur in any month of the year. [Figure 11](#) and [Figure 12](#) show the comparison between historical and simulated annual landfall distributions and the distribution of landfall events by month for Hong Kong, respectively.

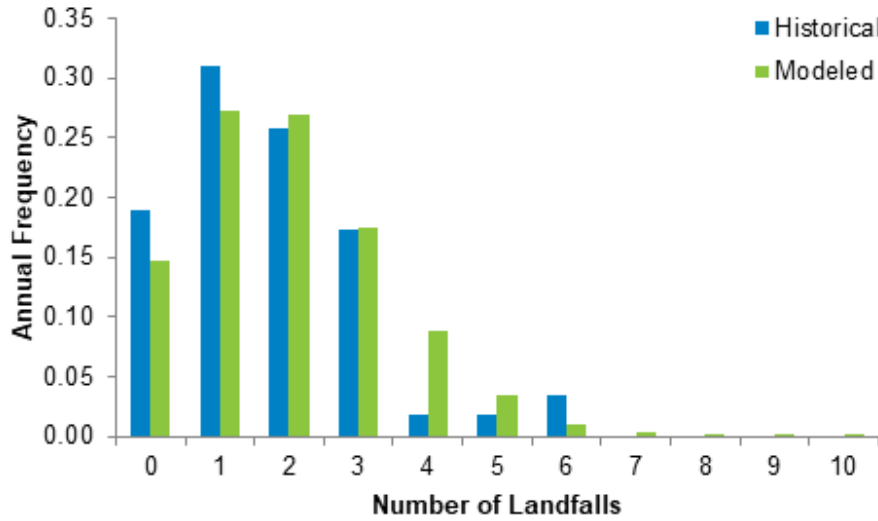


Figure 11. Historical vs. simulated annual landfall distribution – Hong Kong

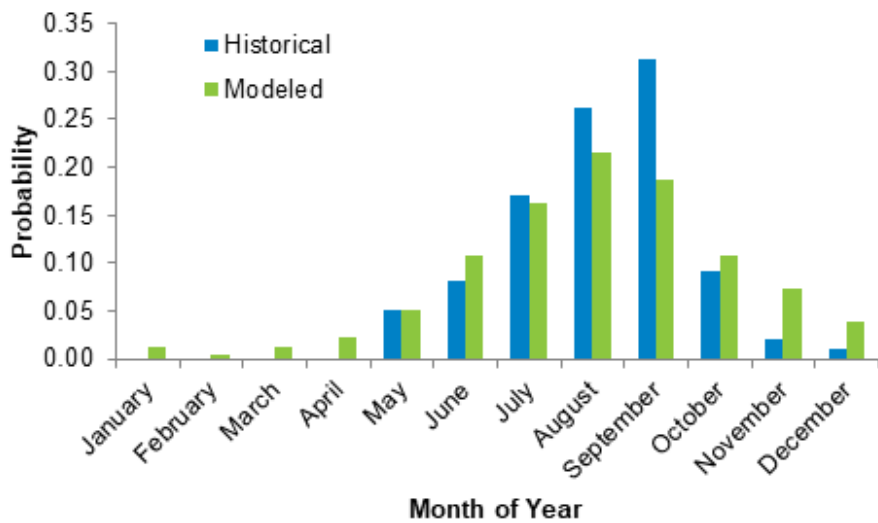


Figure 12. Historical vs. simulated distribution of landfalling events by month – Hong Kong

## Macau

The total number of simulated events that cause loss in Macau is 16,225 - 10,244 of which are landfalling events while 5,981 are bypassing events. The maximum number of landfalling events in a single simulated year is nine, though the probability of such an occurrence is low; note that a single storm can make multiple landfalls. Like actual typhoons in the Northwest Pacific Basin, simulated events can occur in any month of the year. [Figure 13](#) and [Figure 14](#) show the comparison between historical and simulated annual landfall distributions and the distribution of landfall events by month for Macau, respectively.

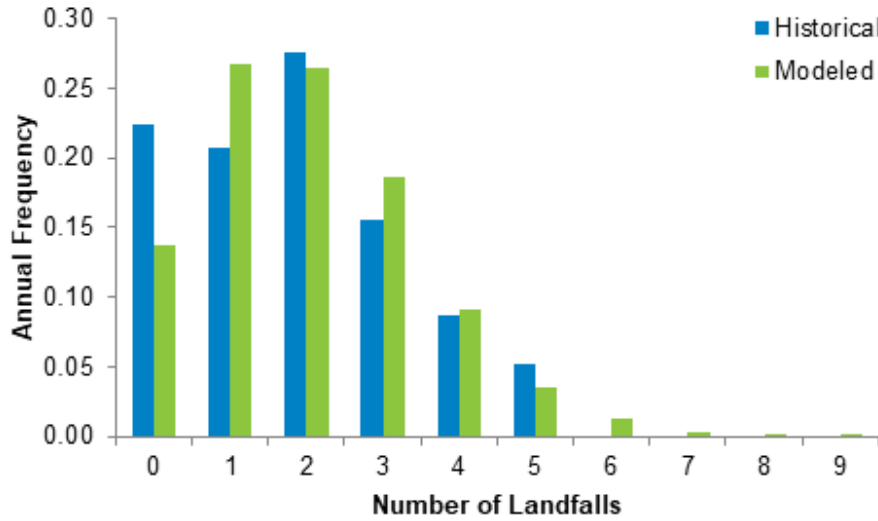


Figure 13. Historical vs. simulated annual landfall distribution – Macau

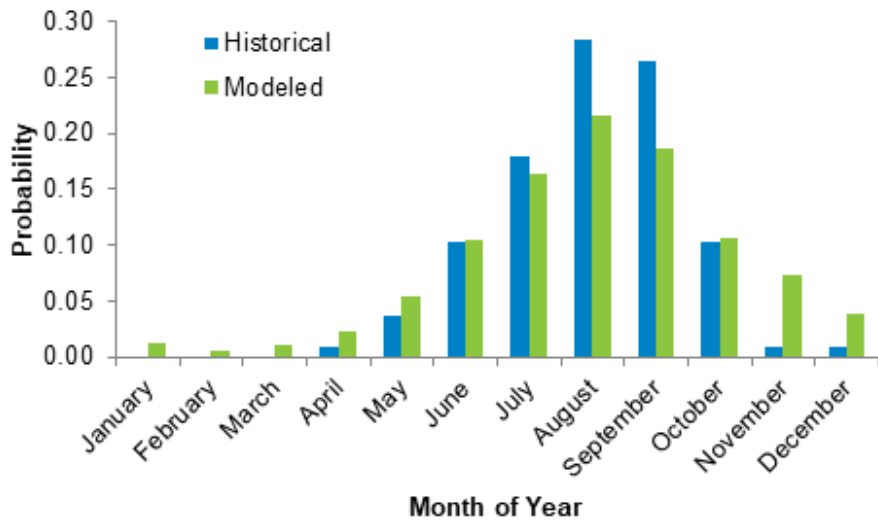


Figure 14. Historical vs. simulated distribution of landfalling events by month – Macau

## The Philippines

The total number of simulated events that cause loss in the Philippines is 66,549 – 51,228 of which are landfalling events while 15,321 are bypassing events. The maximum number of landfalling events in a single simulated year is 18, though the probability of such an occurrence is low; note that a single storm can make multiple landfalls. Like actual typhoons in the Northwest Pacific Basin, simulated events can occur in any month of the year. [Figure 15](#) and [Figure 16](#) show the comparison between historical and simulated annual landfall distributions and the distribution of landfall events by month for The Philippines, respectively.

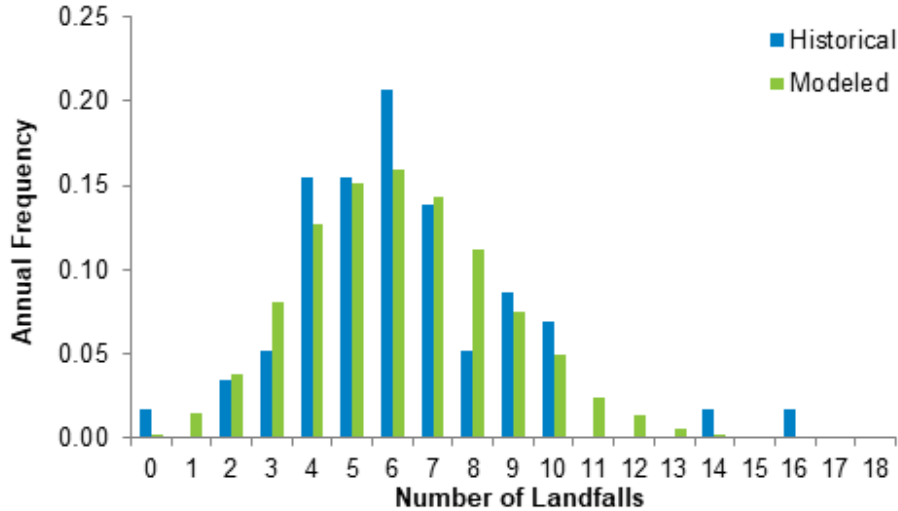


Figure 15. Historical vs. simulated annual landfall distribution – The Philippines

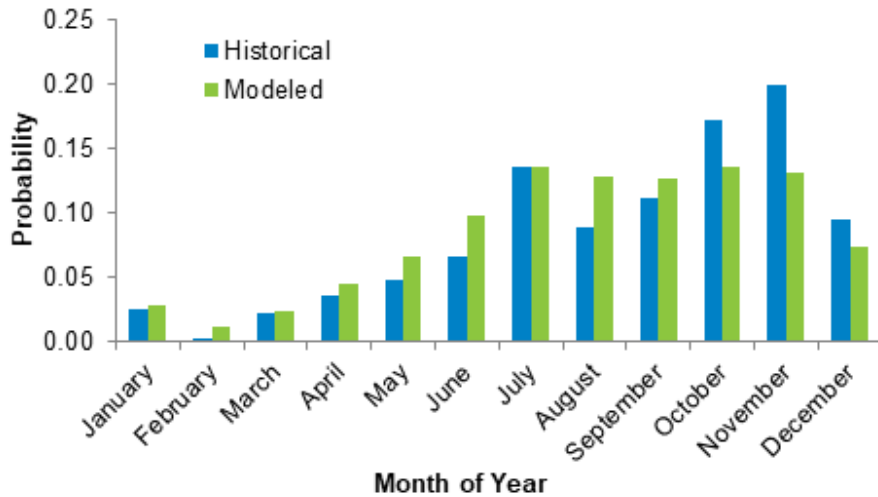


Figure 16. Historical vs. simulated distribution of landfalling events by month – The Philippines

## Saipan

The total number of simulated events that cause loss in Saipan is 6,865 – 1,381 of which are landfalling events while 5,484 are bypassing events. The maximum number of landfalling events in a single simulated year is 10, though the probability of such an occurrence is low; note that a single storm can make multiple landfalls. Like actual typhoons in the Northwest Pacific Basin, simulated events can occur in any month of the year. [Figure 17](#) and [Figure 18](#) show the comparison between historical and simulated annual landfall distributions and the distribution of landfall events by month for Saipan, respectively.

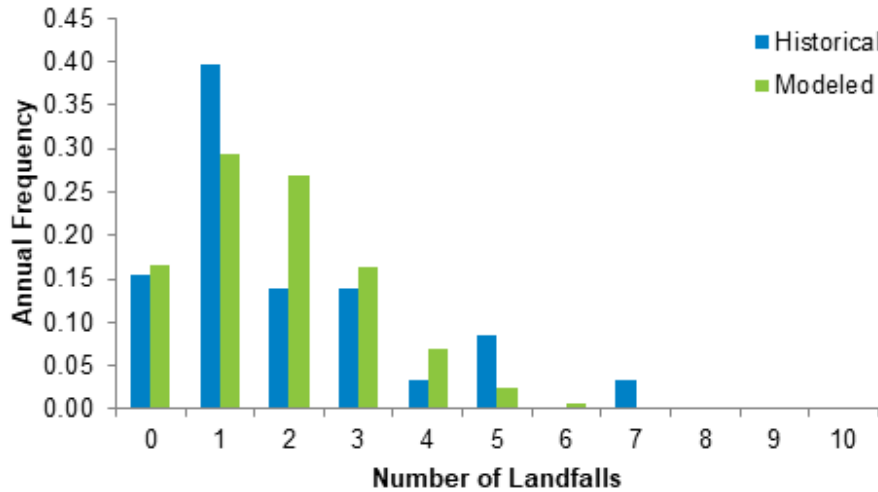


Figure 17. Historical vs. simulated annual landfall distribution – Saipan

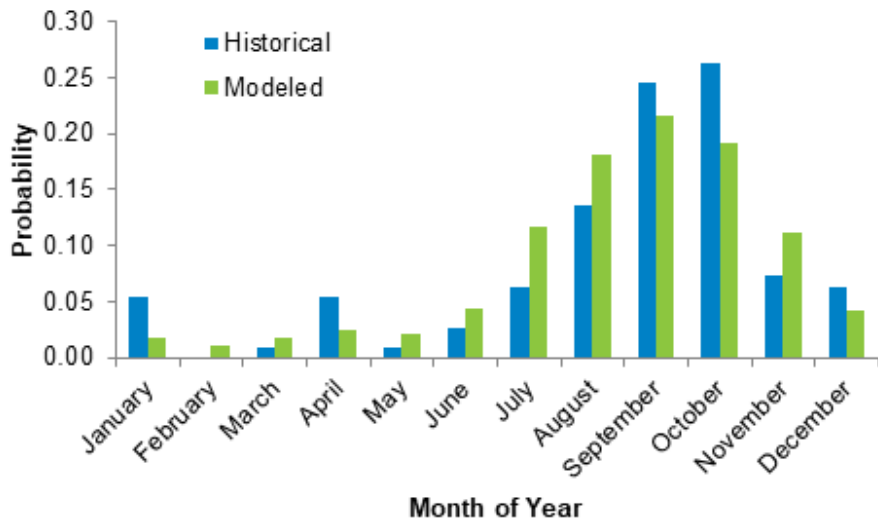


Figure 18. Historical vs. simulated distribution of landfalling events by month – Saipan

## Taiwan

The total number of simulated events that cause loss in Taiwan is 36,613 – 28,502 of which are landfalling events while 8,111 are bypassing events. The maximum number of landfalling events in a single simulated year is 12, though the probability of such an occurrence is low; note that a single storm can make multiple landfalls. Like actual typhoons in the Northwest Pacific Basin, simulated events can occur in any month of the year. [Figure 19](#) and [Figure 20](#) show the comparison between historical and simulated annual landfall distributions and the distribution of landfall events by month for Taiwan, respectively.

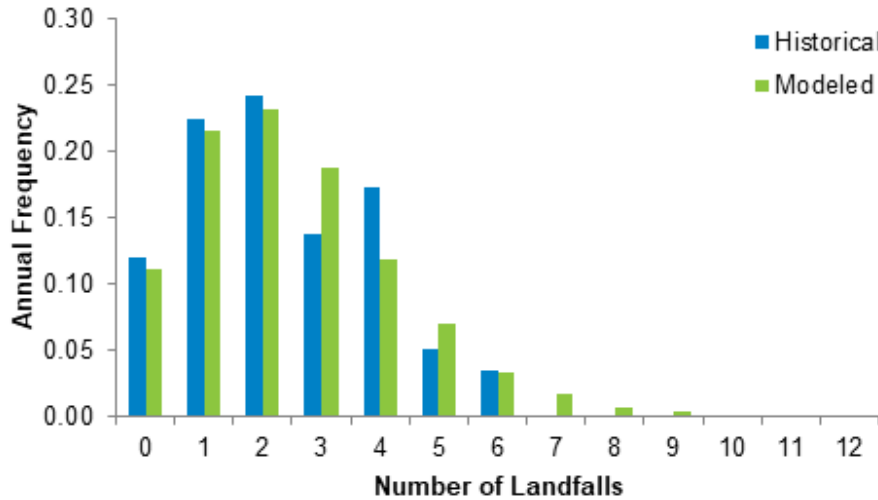


Figure 19. Historical vs. simulated annual landfall distribution – Taiwan

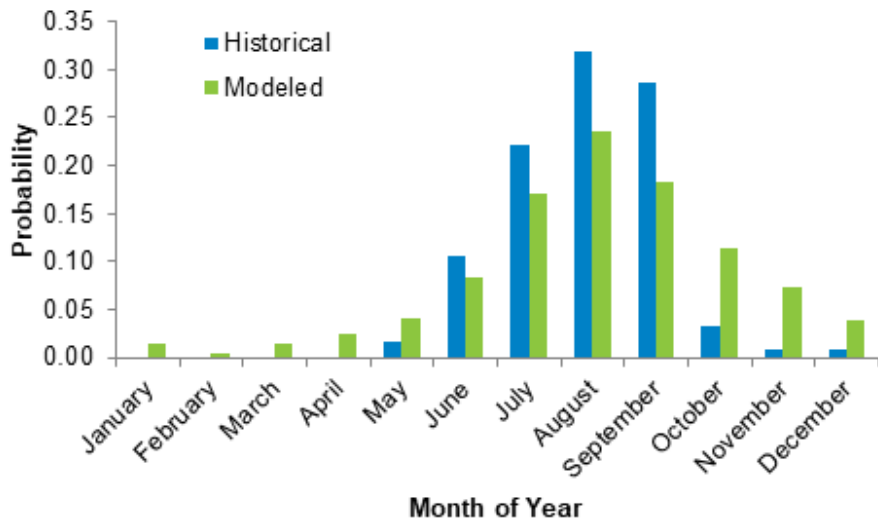


Figure 20. Historical vs. simulated distribution of landfalling events by month – Taiwan

## Vietnam

The total number of simulated events that cause loss in Vietnam is 24,873 – 12,829 of which are landfalling events while 12,044 are bypassing events. The maximum number of landfalling events in a single simulated year is 16, though the probability of such an occurrence is low; note that a single storm can make multiple landfalls. Like actual typhoons in the Northwest Pacific Basin, simulated events can occur in any month of the year. [Figure 21](#) and [Figure 22](#) show the comparison between historical and simulated annual landfall distributions and the distribution of landfall events by month for Vietnam, respectively.

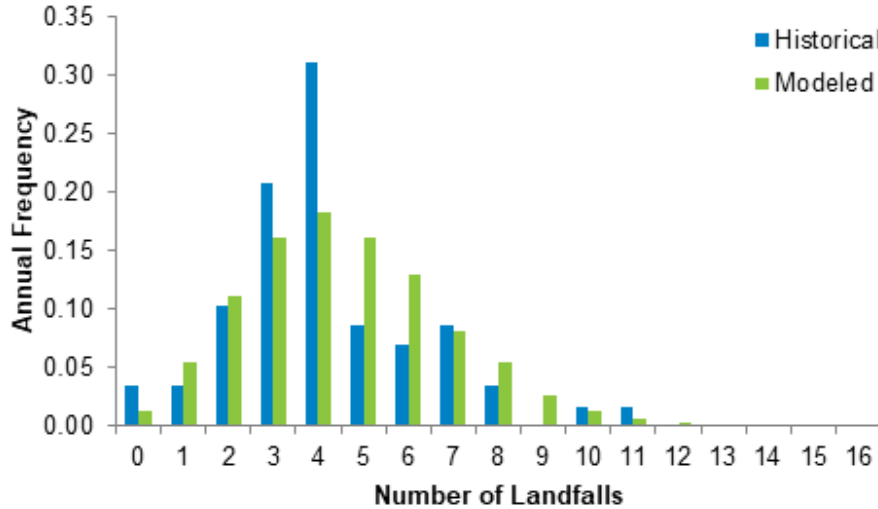


Figure 21. Historical vs. simulated annual landfall distribution – Vietnam

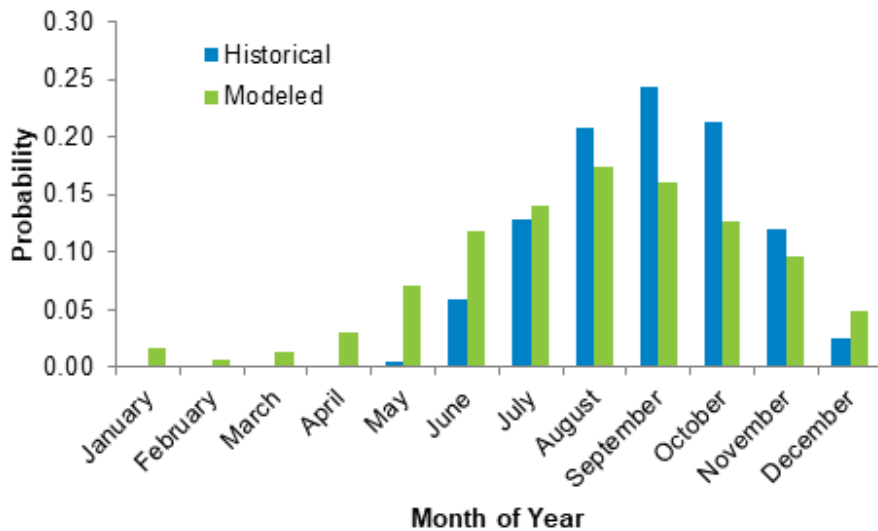


Figure 22. Historical vs. simulated distribution of landfalling events by month – Vietnam

## 1.7 Model resolution and physical properties

The resolution of the model is 1 km. Central pressure is estimated on a 2.5° x 2.5° grid, and storm track is modeled on a 1.25° x 1.25° grid. The model’s flood module relies on elevation data from NASA’S Shuttle Radar Topography Mission (SRTM) made available by the U.S. Geological Survey’s EROS Data Center at a 90-m resolution and soil data from the Harmonized World Soil Database (HWSD) made available by the Food and Agriculture Organization of the United Nations (FAO) the International Institute for Applied Systems Analysis (IIASA), International Soil Reference and Information Centre (ISRIC), Institute of Soil

Science – Chinese Academy of Sciences (ISSCAS) or Joint Research Centre of the European Commission (JRC) at a 925-m resolution.

Model physical properties were developed using the SRTM elevation data and MODIS/LULC data, which were both previously mentioned.

## 1.8 Modeled lines of business

The lines of business (LOBs) included in the Verisk Typhoon Model for Southeast Asia in CATRADER are residential, commercial/industrial, marine, and automobile. Touchstone also supports industrial facilities.

**See Also**

[Supported lines of business for reporting model losses](#)

## 1.9 Construction and occupancy classes

The model supports numerous construction and occupancy classes, as listed below.

<b>Construction Classes</b>	116
<b>Occupancy Classes</b>	116 (of which 62 classes are large industrial facilities)

For a complete list of construction classes, occupancy classes, and supported combinations, see the *Verisk Typhoon Model for Southeast Asia Supplement* available with login on the [Client Portal](#).

**See Also**

[Construction and occupancy classes, year built and height bands, and relative vulnerabilities](#)

## 1.10 Modeled industry losses

It is important to distinguish between insurable and insured losses when modeling the industry exposure.

<b>Insurable exposure</b>	Total replacement value and number of properties (risk counts) that are eligible for insurance.
---------------------------	---

<b>Insured exposure</b>	Although eligible for insurance, “take-up” or purchase of insurance coverage for eligible properties varies by peril and region. For example, coverage for some natural perils may be mandatory in a region, and consequently the insurance take-up rate would be 100%. For other natural perils, insurance may be voluntary, and take-up may be as low as single-digit percentage values. Based on available information, Verisk provides estimates of take-up rates for each modeled region and simulated peril. Insured exposure is calculated by multiplying the take-up rate by the insurable risk count and replacement values.
<b>Insurable losses</b>	Estimated losses to insurable exposures.
<b>Insured losses</b>	Estimated losses to insured exposures.

Modeled insurable occurrence loss estimates for selected exceedance probabilities are provided below. The losses do not incorporate demand surge. Note that the current default Verisk demand surge function was developed using economic principles and validated based on U.S. loss levels and component cost analyses. Development of country/region demand surge functions is currently underway at Verisk. In the meantime, for countries other than the U.S., clients may choose to apply the U.S. demand surge function or a user-defined demand surge function, at their discretion.

Note that modeled losses for the Verisk Typhoon Model for Southeast Asia include losses from wind, precipitation-induced flood, and storm surge.

**See Also**

[Policy conditions](#)

## Insurable occurrence losses

**Table 1. Modeled insurable occurrence loss estimates**

Insurable Occurrence Losses			
Country/Territory	Local Currency (Billions)		Currency
	1% Exceedance Probability (100-yr)	0.4% Exceedance Probability (250-yr)	
Guam <sup>1</sup>	1.705	3.826	USD
Hong Kong	10.089	13.599	HKD
Macau	1.925	2.975	MOP
The Philippines	835.183	1,473.557	PHP
Saipan <sup>1</sup>	0.667	1.497	USD
Taiwan	361.264	518.170	NTD
Vietnam	40,250.791	67,887.163	VND

<sup>1</sup> Insurable and insured occurrence losses are the same for this territory.

## Insured occurrence loss estimates

**Table 2. Modeled insured occurrence loss estimates**

Insured Occurrence Losses			
Country/Territory	Local Currency (Billions)		
	1% Exceedance Probability (100-yr)	0.4% Exceedance Probability (250-yr)	Currency
Guam <sup>2</sup>	1.705	3.826	USD
Hong Kong	7.801	10.751	HKD
Macau	1.572	2.429	MOP
The Philippines	93.037	170.553	PHP
Saipan <sup>2</sup>	0.667	1.497	USD
Taiwan	33.615	47.334	NTD
Vietnam	6,922.882	11,545.852	VND

## Insurable and insured average annual aggregate loss estimates for selected regions

Average annual insurable and insured aggregate losses for each country or territory and selected at-risk zones are shown below. Note that insurable and insured average annual aggregate losses are the same for Guam and for Saipan.

### Guam

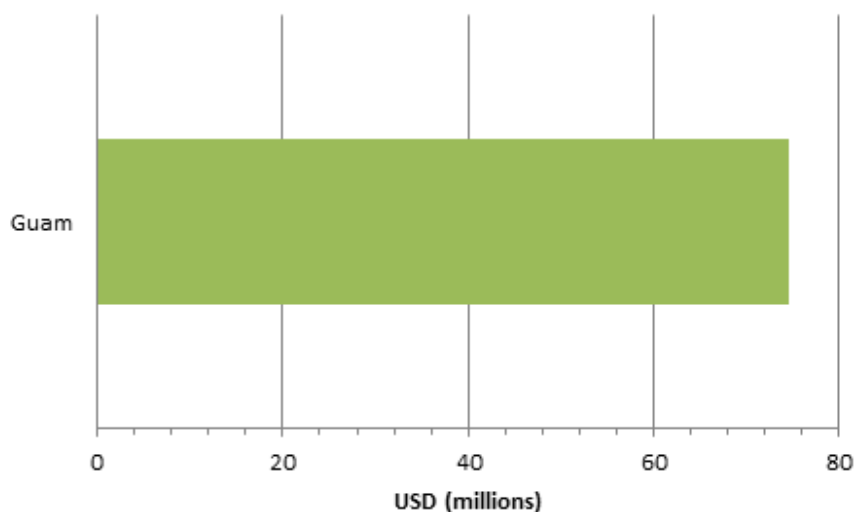


**Figure 23. Insurable/insured average annual aggregate losses – Guam**

<sup>2</sup> Insurable and insured occurrence losses are the same for this territory.

Hong Kong

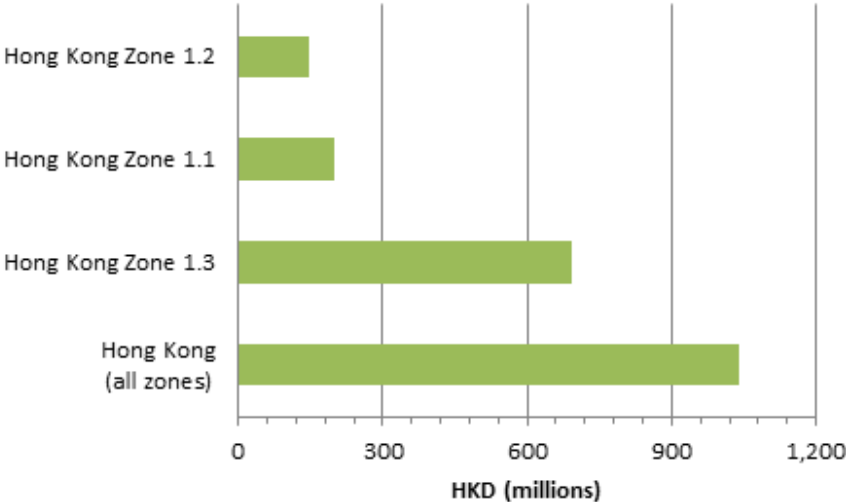


Figure 24. Insurable average annual aggregate losses – Hong Kong

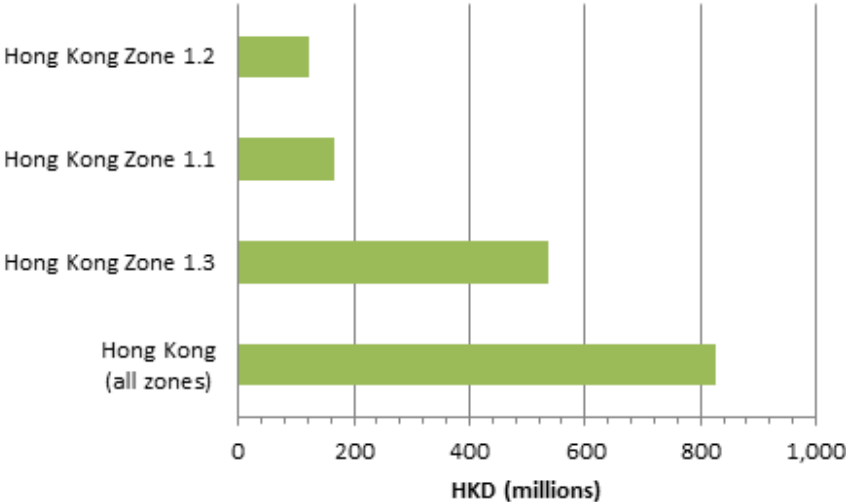


Figure 25. Insured average annual aggregate losses – Hong Kong

Macau

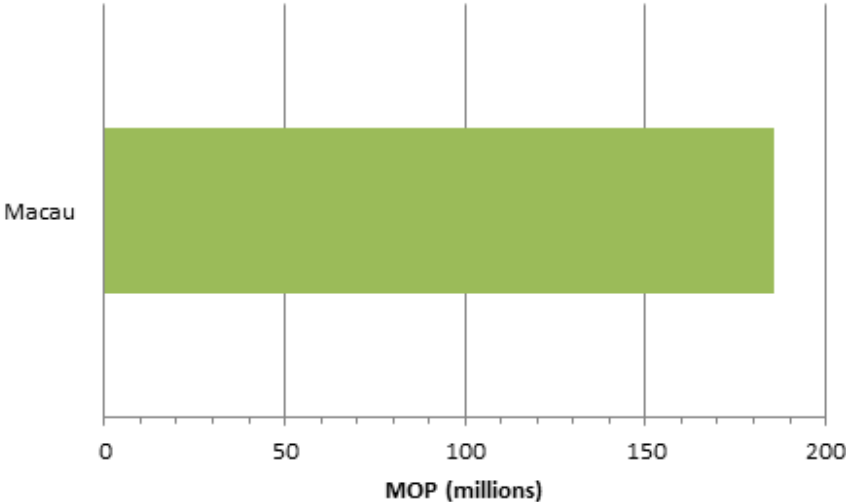


Figure 26. Insurable average annual aggregate losses – Macau

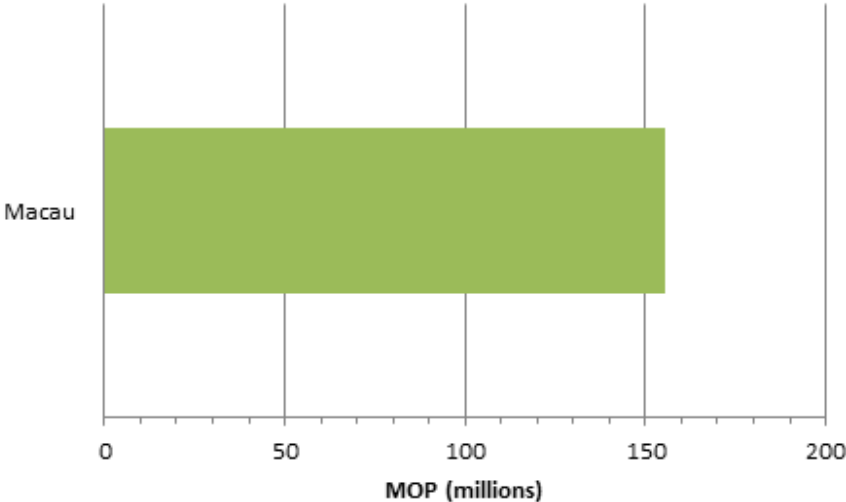


Figure 27. Insured average annual aggregate losses – Macau

The Philippines

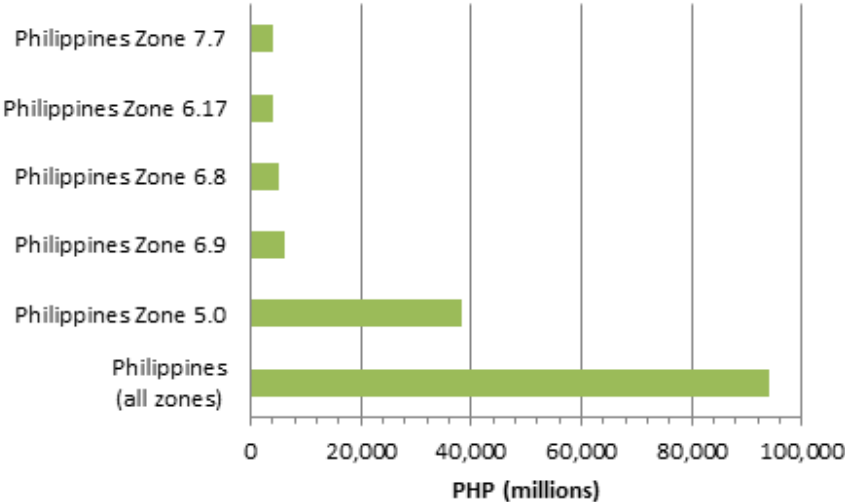


Figure 28. Insurable average annual aggregate losses – The Philippines

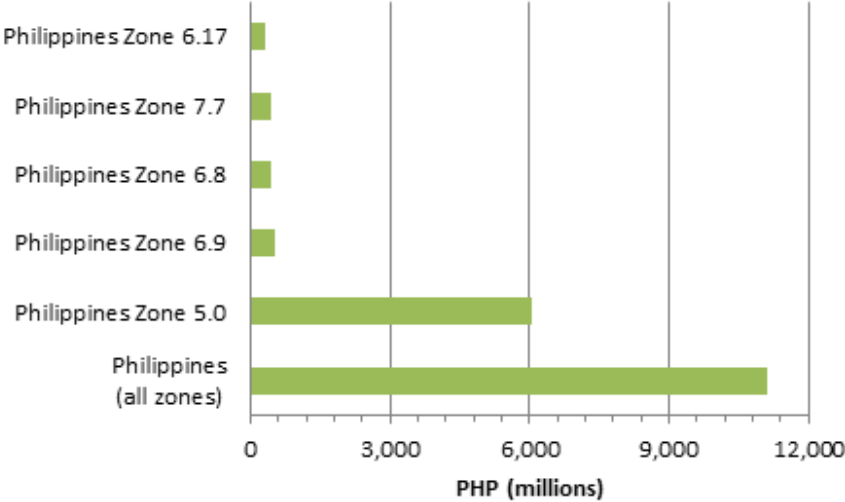


Figure 29. Insured average annual aggregate losses – The Philippines

Saipan

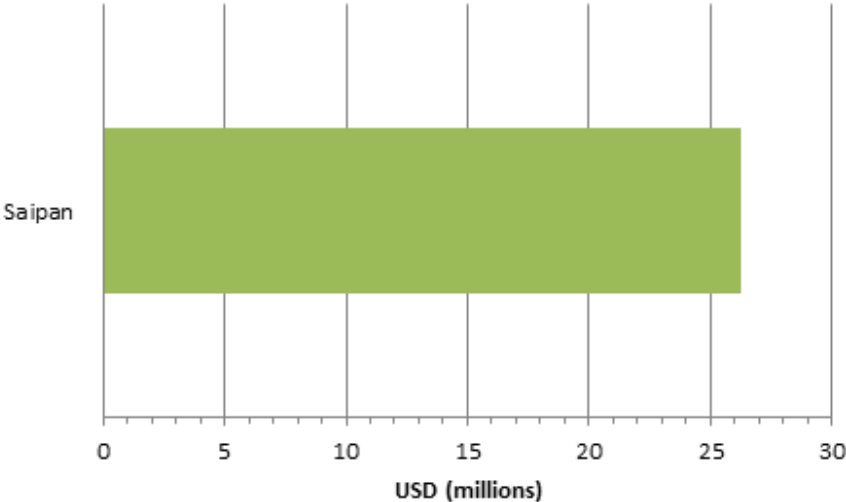


Figure 30. Insurable/insured average annual aggregate losses – Saipan

Taiwan

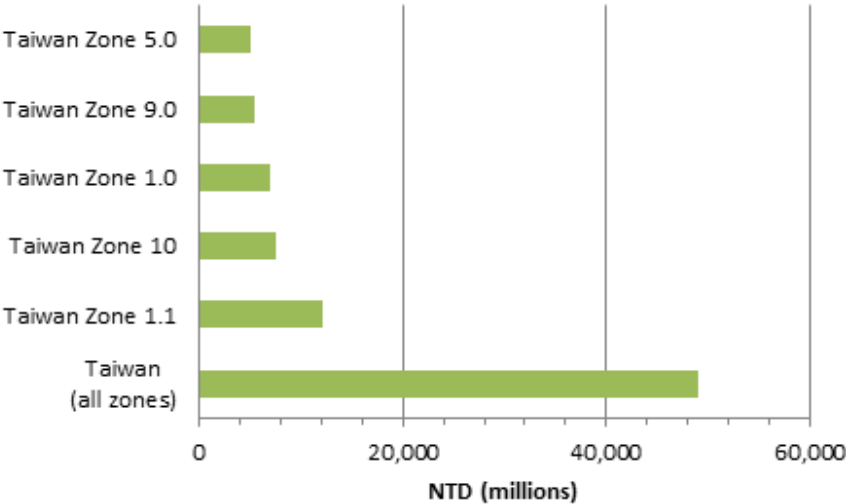


Figure 31. Insurable average annual aggregate losses – Taiwan

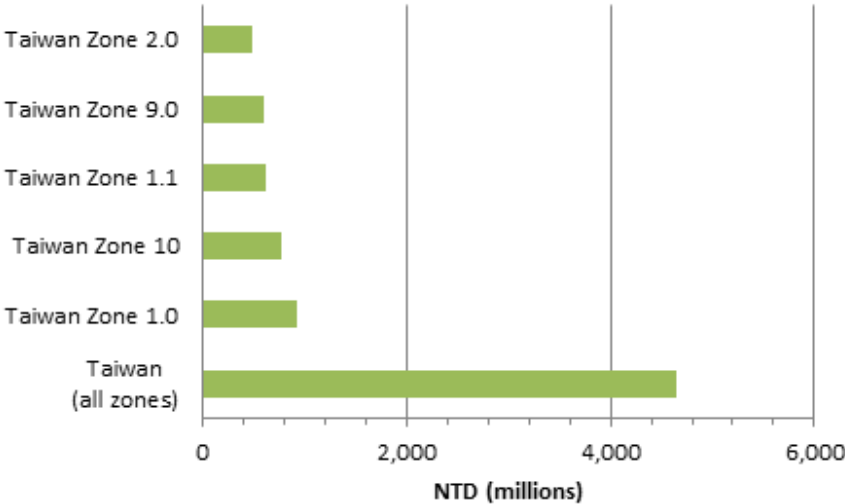


Figure 32. Insured average annual aggregate losses – Taiwan

Vietnam

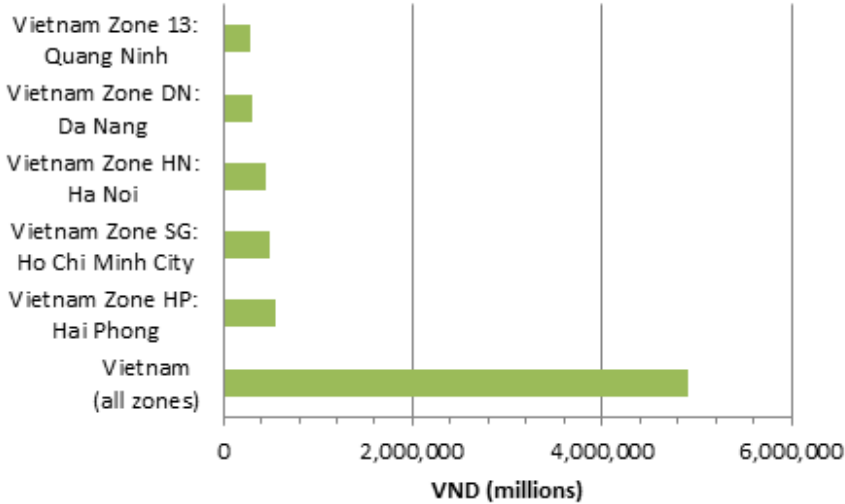


Figure 33. Insurable average annual aggregate losses – Vietnam

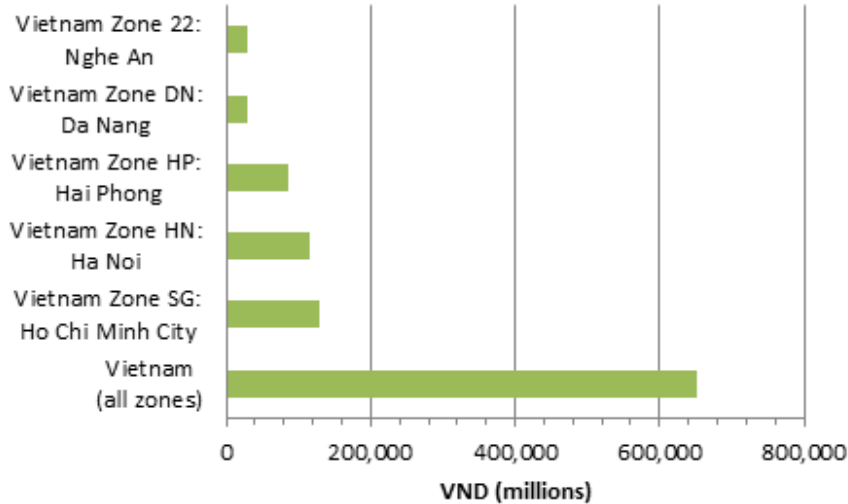


Figure 34. Insured average annual aggregate losses – Vietnam

Southeast Asia Region

Figure 35 and Figure 36 compare the insurable and insured average annual aggregate losses, respectively, for all modeled countries and top loss zones using USD as the common currency.

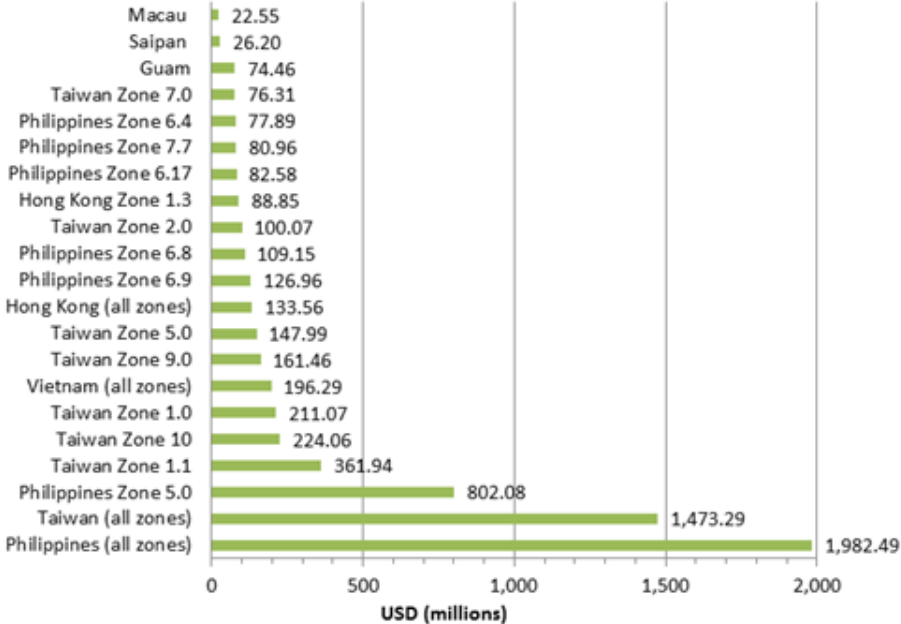
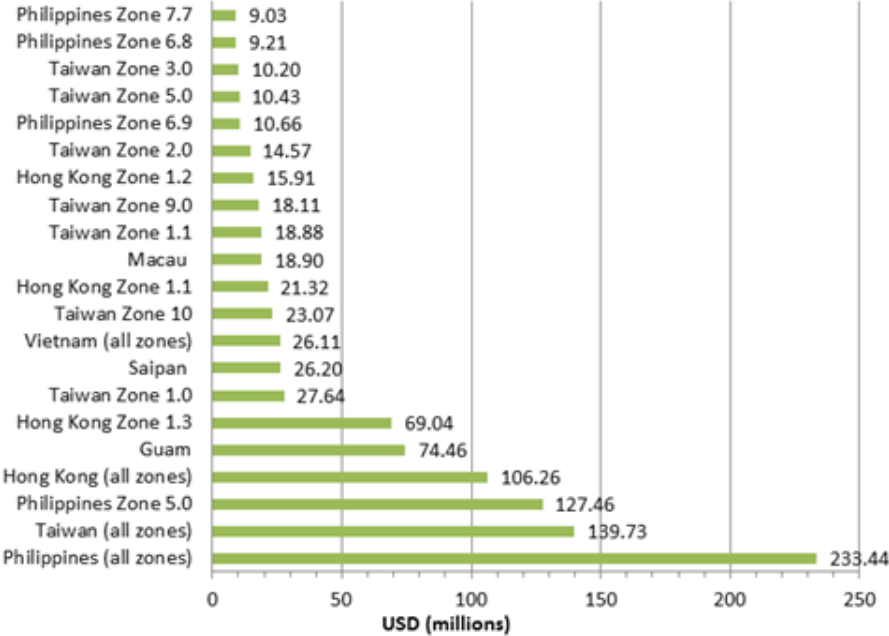


Figure 35. Insurable average annual aggregate losses – all modeled countries/territories and top loss zones



**Figure 36. Insured average annual aggregate losses – all modeled countries/territories and top loss zones**

### Loss cost

Combined loss costs for all sub-perils (wind, precipitation-induced flood, and storm surge or wind and precipitation-induced flood, depending on country/territory) are shown in [Figure 37](#). The map depicts the average annual loss to Coverage A (buildings) of a uniform exposure type (construction class 100, occupancy class 301, unknown building height, and unknown age) with a uniform exposure value, calculated at a 1-km grid resolution. Note that Average Properties was turned on, and demand surge was not included in the calculation.

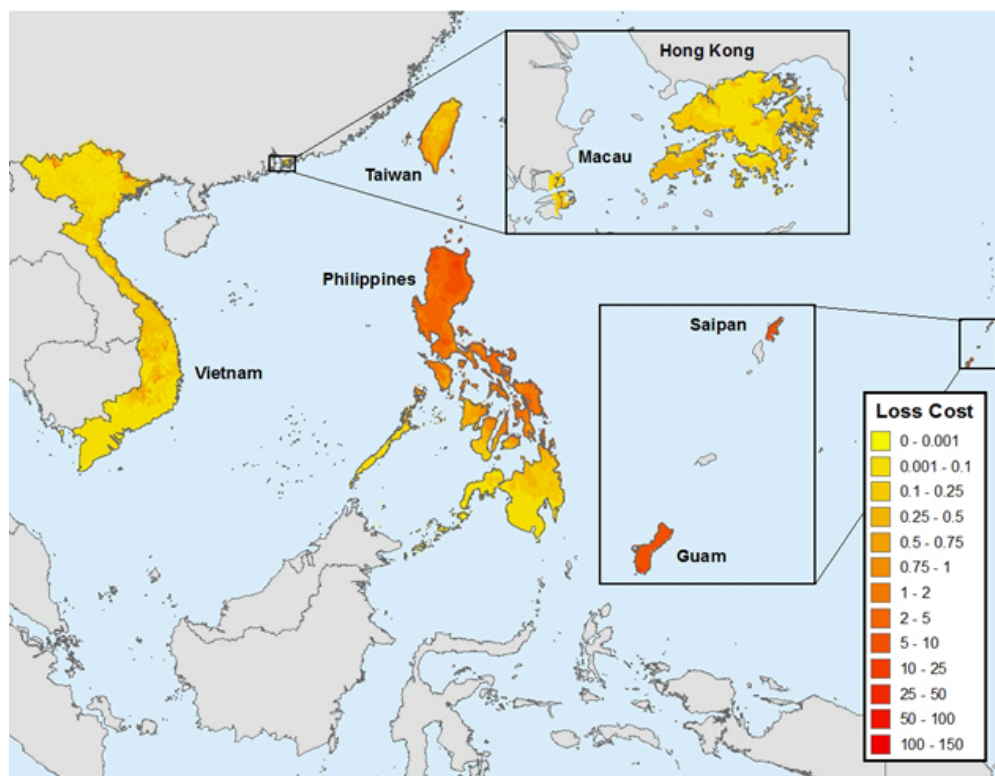


**Figure 37. Typhoon risk (loss costs) in Southeast Asia**

## Modeled losses for historical typhoons

Modeled insurable and insured loss estimates for significant historical typhoons affecting the modeled countries/territories of the Verisk Typhoon Model for Southeast Asia, based on Verisk industry exposures (2015), are provided in [Table 3](#) through [Table 14](#). See Section 7 for Verisk take-up rate assumptions. For further details about these historical typhoons, refer to Section 2.

**Table 3. Modeled insurable/insured losses for historical typhoons – Guam (USD millions)**

Modeled Insured Losses (USD Millions)				
Event Name	Residential	Commercial	Auto	Total
Ida 1958	2.3	0.60	0.074	2.9
Sarah 1959	0.027	0.048	0.0034	0.078
Karen 1962	741	403	44	1,187
Pamela 1976	352	158	12	522
Thelma 1987	0.14	0.13	0.015	0.29
Paka 1997	143	45	2.8	191
Pongsona 2002	318	93	8.8	420
Chaba 2004	0.46	0.088	0.012	0.56

Modeled Insured Losses (USD Millions)				
Event Name	Residential	Commercial	Auto	Total
Saomai 2006	0.33	0.29	0.035	0.65

**Table 4. Modeled insurable losses for historical typhoons – Hong Kong (HKD millions)**

Modeled Insured Losses (HKD Millions)				
Event Name	Residential	Commercial	Auto	Total
Rose 1971	1,765	1,295	11	3,072
Hope 1979	1,184	953	6.3	2,143
Ellen 1983	1,403	977	8.8	2,389
Sam 1999	147	106	0.94	253
Billis 2006	-	17	-	17
Fengshen 2008	0.022	18	0.00	18
Nuri 2008	160	87	0.57	247
Hagupit 2008	262	153	1.6	417
Nesat 2011	-	19	-	19
Vicente 2012	246	143	1.4	390

**Table 5. Modeled insured losses for historical typhoons – Hong Kong (HKD millions)**

Modeled Insured Losses (HKD Millions)				
Event Name	Residential	Commercial	Auto	Total
Rose 1971	1,465	1,149	4.5	2,618
Hope 1979	989	852	2.5	1,844
Ellen 1983	1,131	849	3.5	1,984
Sam 1999	112	90	0.37	202
Billis 2006	-	17	-	17
Fengshen 2008	0.022	18	0.000024	18
Nuri 2008	115	75	0.23	190
Hagupit 2008	236	137	0.66	373
Nesat 2011	-	19	-	19
Vicente 2012	220	128	0.58	348

**Table 6. Modeled insurable losses for historical typhoons – Macau (MOP millions)**

Modeled Insured Losses (MOP Millions)				
Event Name	Residential	Commercial	Auto	Total
Rose 1971	17	18	0.12	34
Hope 1979	10	7.9	0.031	18

Modeled Insured Losses (MOP Millions)				
Event Name	Residential	Commercial	Auto	Total
Ellen 1983	408	470	3.1	882
Sam 1999	-	1.4	-	1.4
Bilis 2006	-	0.97	-	0.97
Fengshen 2008	-	1.0	-	1.0
Nuri 2008	1.6	3.5	0.0024	5.1
Hagupit 2008	169	166	1.0	336
Nesat 2011	-	1.4	-	1.4
Vicente 2012	253	272	1.6	527

**Table 7. Modeled insured losses for historical typhoons – Macau (MOP millions)**

Modeled Insured Losses (MOP Millions)				
Event Name	Residential	Commercial	Auto	Total
Rose 1971	14	16	0.047	30
Hope 1979	8.7	7.2	0.013	16
Ellen 1983	321	419	1.2	741
Sam 1999	-	1.4	-	1.39
Bilis 2006	-	0.97	-	0.97
Fengshen 2008	-	1.0	-	1.0
Nuri 2008	1.4	3.3	0.00097	4.7
Hagupit 2008	139	149	0.42	289
Nesat 2011	-	1.4	-	1.4
Vicente 2012	205	243	0.62	449

**Table 8. Modeled insurable losses for historical typhoons – The Philippines (PHP millions)**

Modeled Insured Losses (PHP Millions)					
Event Name	Residential	Commercial	Agricultural	Auto	Total
Joan 1970	138,235	227,974	3,857	12,258	382,324
Rose 1971	20	3.4	2.3	2.5	29
Hope 1979	127	101	36	40	304
Ellen 1983	1,188	381	193	111	1,873
Mike 1990	19,955	40,701	1,159	1,669	63,484
Angela 1995	26,833	54,507	343	2,282	83,965
Vicki 1998	4,616	3,442	320	461	8,839
Sam 1999	7.9	0.92	0.75	1.2	11
Toraji 2001	4.0	2.3	0.43	0.90	7.6

Modeled Insured Losses (PHP Millions)					
Event Name	Residential	Commercial	Agricultural	Auto	Total
Xangsane 2006	35,092	79,003	697	3,809	118,601
Durian 2006	11,513	13,442	663	886	26,504
Sepat 2007	3.0	1.7	0.42	0.70	5.9
Fengshen 2008	7,122	14,112	260	787	22,280
Nuri 2008	122	32	18	11	183
Hagupit 2008	139	34	23	13	209
Ketsana 2009	30,028	117,818	60	4,306	152,213
Megi 2010	31,994	22,923	4,748	3,978	63,643
Nesat 2011	6,408	3,307	837	531	11,083
Washi 2011	573	1,554	67	110	2,305
Vicente 2012	21	37	0.22	4.8	63
Bopha 2012	11,468	20,714	1,237	1,029	34,448
Haiyan 2013	105,626	87,981	7,370	11,847	212,824

**Table 9. Modeled insured losses for historical typhoons – The Philippines (PHP millions)**

Modeled Insured Losses (PHP Millions)					
Event Name	Residential	Commercial	Agricultural	Auto	Total
Joan 1970	8,300	33,903	77	3,811	46,091
Rose 1971	0.61	0.43	0.047	0.74	1.8
Hope 1979	3.6	13	0.71	12	30
Ellen 1983	35	49	3.9	33	121
Mike 1990	566	5,650	23	419	6,659
Angela 1995	1,712	8,070	6.9	806	10,594
Vicki 1998	159	422	6.4	126	713
Sam 1999	0.24	0.11	0.015	0.35	0.72
Toraji 2001	0.12	0.31	0.0087	0.27	0.70
Xangsane 2006	2,340	11,922	14	1,396	15,672
Durian 2006	378	1,757	13	191	2,339
Sepat 2007	0.090	0.23	0.0084	0.21	0.54
Fengshen 2008	339	1,862	5.2	237	2,444
Nuri 2008	3.6	4.2	0.36	3.3	11
Hagupit 2008	4.1	4.5	0.46	3.9	13

Modeled Insured Losses (PHP Millions)					
Event Name	Residential	Commercial	Agricultural	Auto	Total
Ketsana 2009	2,457	17,817	1.2	1,766	22,041
Megi 2010	1,016	3,123	95	1,219	5,454
Nesat 2011	191	431	17	156	794
Washi 2011	15	174	1.3	33	223
Vicente 2012	0.55	4.2	0.0045	1.4	6.2
Bopha 2012	328	2,583	25	292	3,228
Haiyan 2013	2,922	14,224	147	2,960	20,254

**Table 10. Modeled insurable/insured losses for historical typhoons – Saipan (USD millions)**

Modeled Insured Losses (USD Millions)				
Event Name	Residential	Commercial	Auto	Total
Mireille 1991	6.6	2.4	0.065	9.1
Winnie 1997	0.50	0.089	0.0071	0.60
Paka 1997	0.48	0.058	0.0064	0.54
Pongsona 2002	2.2	0.32	0.024	2.6
Chaba 2004	13	2.6	0.13	16
Nabi 2005	0.091	0.025	0.0016	0.12

**Table 11. Modeled insurable losses for historical typhoons – Taiwan (NTD millions)**

Modeled Insured Losses (NTD Millions)					
Event Name	Residential	Commercial	Agricultural	Auto	Total
Nina 1975	8,122	12,797	531	1,076	22,526
Hope 1979	340	356	29	30	754
Herb 1996	11,443	39,202	816	1,324	52,784
Winnie 1997	0.15	2.1	0.042	0.083	2.3
Toraji 2001	567	1,011	64	55	1,698
Nari 2001	18,541	138,531	1,087	5,002	163,162
Haitang 2005	5,513	15,110	460	813	21,897
Bilis 2006	12,158	114,169	538	3,826	130,691
Saomai 2006	3.6	15	0.42	0.55	19
Sepat 2007	4,016	6,081	418	433	10,948
Nuri 2008	8.0	247	0.18	2.6	258
Morakot 2009	6,928	29,959	635	1,409	38,931
Megi 2010	33	519	0.22	11	563

**Table 12. Modeled insured losses for historical typhoons – Taiwan (NTD millions)**

Modeled Insured Losses (NTD Millions)					
Event Name	Residential	Commercial	Agricultural	Auto	Total
Nina 1975	94	1,218	5.3	217	1,534
Hope 1979	3.8	51	0.29	5.9	61
Herb 1996	148	4,995	8.2	349	5,501
Winnie 1997	0.0016	0.10	0.00042	0.025	0.13
Toraji 2001	6.6	150	0.64	12	169
Nari 2001	283	12,210	11	1,442	13,946
Haitang 2005	70	1,941	4.6	210	2,226
Billis 2006	191	10,204	5.4	1,124	11,524
Saomai 2006	0.043	1.6	0.0042	0.16	1.8
Sepat 2007	50	769	4.18	87	910
Nuri 2008	0.13	32	0.0018	0.52	32
Morakot 2009	95	3,125	6.4	374	3,601
Megi 2010	0.51	74	0.0022	2.1	76

**Table 13. Modeled insurable losses for historical typhoons – Vietnam (VND millions)**

Modeled Insured Losses (VND Millions)					
Event Name	Residential	Commercial	Agricultural	Auto	Total
Hope 1979	75,663	137,091	2,140	15,593	230,486
Billis 2006	1,481	1,050	326	498	3,356
Xangsane 2006	2,051,287	4,893,510	63,981	268,256	7,277,034
Durian 2006	79,152	76,640	2,956	12,025	170,773
Hagupit 2008	312,585	576,144	66,918	85,142	1,040,789
Ketsana 2009	3,279,001	3,574,862	392,273	446,188	7,692,324
Nesat 2011	391,740	969,124	33,054	77,198	1,471,116
Vicente 2012	590,948	1,245,941	74,857	122,707	2,034,453
Haiyan 2013	5,816,507	24,309,993	896,909	1,211,013	32,234,422

**Table 14. Modeled insured losses for historical typhoons – Vietnam (VND millions)**

Modeled Insured Losses (VND Millions)					
Event Name	Residential	Commercial	Agricultural	Auto	Total
Hope 1979	3,557	32,571	11	2,559	38,698
Billis 2006	15	53	1.6	75	144

Modeled Insured Losses (VND Millions)					
Event Name	Residential	Commercial	Agricultural	Auto	Total
Xangsane 2006	32,729	763,448	320	40,238	836,735
Durian 2006	2,943	16,368	15	1,812	21,138
Hagupit 2008	1,897	28,944	335	12,771	43,947
Ketsana 2009	49,913	726,851	1,961	66,928	845,654
Nesat 2011	9,591	131,647	165	11,581	152,983
Vicente 2012	22,859	222,249	374	19,527	265,009
Haiyan 2013	147,949	3,139,733	4,485	181,705	3,473,871

**See Also**

[Significant historical Southeast Asia typhoons](#)  
[Policy conditions](#)

## Modeled losses for Extreme Disaster Scenarios

Four Extreme Disaster Scenarios (EDS) are available in the World Scenarios event set for the Verisk Typhoon Model for Southeast Asia in Touchstone and CATRADER. [Table 16](#) and [Table 15](#) provide the names and modeled insurable and insured losses for the EDS. In addition, the motivation for including EDS events in the software, and for selecting these specific EDS, is described in Section 3.

**Table 15. Modeled insurable losses for Extreme Disaster Scenarios available in Touchstone and CATRADER**

Modeled Insurable Losses (local currency in millions)					
Event Name	Residential	Commercial	Agriculture	Auto	Total
EDS SE Asia Philippines Typhoon	991,329	1,327,390	14,659	86,878	2,420,256
EDS SE Asia Taiwan Typhoon	52,175	451,274	4,651	14,150	522,250
EDS SE Asia Hong Kong Typhoon	12,348	12,747	-	144	25,239
EDS SE Asia Vietnam Typhoon	23,419,694	114,934,790	968,850	3,626,812	142,950,145

**Table 16. Modeled insured losses for Extreme Disaster Scenarios available in Touchstone and CATRADER**

Modeled Insured Losses (local currency in millions)					
Event Name	Residential	Commercial	Agriculture	Auto	Total
EDS SE Asia Philippines Typhoon	55,485	196,547	293	27,966	280,292

Modeled Insured Losses (local currency in millions)					
Event Name	Residential	Commercial	Agriculture	Auto	Total
EDS SE Asia Taiwan Typhoon	783	47,788	47	3,713	52,331
EDS SE Asia Hong Kong Typhoon	9,445	11,030	-	58	20,533
EDS SE Asia Vietnam Typhoon	1,635,299	32,211,808	4,844	623,798	34,475,749

**See Also**  
[Extreme Disaster Scenarios \(EDS\)](#)

### 1.11 Navigating the document

[Figure 38](#) illustrates the components of the Verisk model and how they are related.



**Figure 38. Components of the Verisk model**

# 2 Typhoons in Southeast Asia

## 2.1 Typhoons: An overview

There are six essential elements for typhoon formation. First, the sea surface temperature (SST) must be at least 27°C, and many scientists believe that this temperature must persist to a depth of at least 50 m below the ocean surface. Warm water provides the necessary heat energy for typhoon development. Second, vertical wind shear, which is a measure of how much wind speed and direction vary with height, must be weak. Weak wind shear will not interfere with the structure of a typhoon and thus allows deep, vertical clouds to develop. Over time, as strong thunderstorms develop, the air pressure will drop at the ocean's surface. Warm ocean temperatures and weak wind shear are critical to the formation and intensification of typhoons.

Third, the atmosphere must have some degree of instability for a typhoon to form. In a stable atmosphere, air does not rise and water vapor in the air will not condense into cloud droplets and precipitation. Fourth, there must be a high level of relative humidity from the ocean surface up to at least the mid-levels of the atmosphere, allowing deep clouds to form without being diluted by surrounding dry air. Fifth, a developing typhoon has to be far enough away from the equator so that the Coriolis force can impart spin towards the center of the storm's circulation. Finally, even if all of the conditions previously mentioned are met, a typhoon may not develop unless a pre-existing disturbance allows air to start rising. Disturbances of low air pressure periodically arrive in an area and can trigger the formation of tropical depressions and tropical storms, which can evolve into typhoons.

Many typhoons actually begin as tropical disturbances, which can form without the six elements necessary for typhoon development. Tropical disturbances can arise when other weather features, such as fronts or easterly waves, move across tropical ocean waters. The underlying ocean surface provides a source of heat and moisture, thereby destabilizing air and forcing it directly above the disturbance. Cold fronts act like snow plows, lifting warm, moist air upward ahead of the front into an unstable environment. Lifting air in an unstable atmosphere allows for the formation of clouds and showers, but without an organized cyclonic circulation at the surface. Multiple tropical disturbances exist in the tropics at any given time.

Storm intensification depends on environmental conditions, just as storm genesis does. Depending on the characteristics of the environment into which a tropical disturbance moves, intensification may occur over several hours or several days. A typhoon is usually named when it reaches tropical storm strength. At this stage, there is a well-defined cyclonic circulation at the surface with maximum sustained winds exceeding 63 km/h (39 mph), and the sea level pressure at the center of the tropical storm is typically lower than 1,000 mb.

Further intensification into a typhoon with sustained winds greater than 119 km/h (74 mph) may occur if the environment permits deep, moist clouds to form an eyewall surrounding the center of circulation. The formation of an eyewall and a cloud-free eye typically indicates

that the maturing storm has achieved typhoon intensity. The eyewall is a region of very heavy precipitation, with rainfall rates often exceeding 5 cm/h. The eye of a typhoon represents a region of relatively calm weather because the air is actually sinking, not rising as in more unstable parts of the storm. As the air sinks, it becomes warmer and less dense, which further reduces the surface pressure in the center of the storm.

Wind speeds are intensified by the difference between the lower-than-normal surface pressure and the higher pressure of the ambient air around the storm. Air at the periphery of the storm responds to the reduced pressure in the storm center. As the air moves inward, it is deflected to the right by the Coriolis force, resulting in an inward cyclonic counter-clockwise spiral of air. In the southern hemisphere, the Coriolis force deflects inwardly moving air to the left, resulting in an inward clockwise cyclone spiral. Just like an ice skater pulling in his or her arms, the spiraling winds in a typhoon spin faster as they approach the storm's center. The strongest winds are typically at the edge of the eye, just prior to being forced up within the most intense thunderstorm cells that encompass the eyewall.

## Classifying typhoons and hurricanes: The Saffir-Simpson hurricane wind scale

Since the early 1970s, typhoon or hurricane-strength tropical cyclones have been categorized according to the Saffir-Simpson hurricane wind scale (SSHWS). The scale is a useful tool for indicating the potential destruction a typhoon (or hurricane or tropical cyclone) could cause when it makes landfall, and is intended to serve as a warning of the expected threat posed by an approaching storm. The scale uses maximum sustained wind speed, the single best predictor of potential danger and damage due to wind from a hurricane. According to the NOAA's National Hurricane Center (NHC), the SSHWS places typhoons into five categories of increasing intensity, as presented in [Table 17](#). The NHC revised the scale in 2010 to better suit its purpose of warning people and again in 2012, this time to mitigate rounding errors in wind speeds during unit conversions.

**Table 17. The Saffir-Simpson hurricane wind scale**

Saffir-Simpson Category	Maximum Sustained Wind Speed <sup>3</sup>			Potential Damage
	(km/h)	(mph)	(knots)	
Tropical Depression <sup>4</sup>	≤62	≤38	≤33	Minimal
Tropical Storm <sup>4</sup>	63 - 118	39 - 73	34 - 63	Minimal
Category 1	119 - 153	74- 95	64 - 82	Minimal
Category 2	154 - 177	96 - 110	83 - 95	Moderate
Category 3	178 - 208	111 - 129	96 - 112	Extensive

<sup>3</sup> The mean of multiple wind speed measurements taken over one-minute time periods at a height of 10 meters above the ground.

<sup>4</sup> Related classification. Not part of the SSHS.

Saffir-Simpson Category	Maximum Sustained Wind Speed <sup>3</sup>			Potential Damage
	(km/h)	(mph)	(knots)	
Category 4	209 – 251	130 – 156	113 – 136	Extreme
Category 5	≥252	≥157	≥137	Catastrophic

## 2.2 Southeast Asia typhoon risk

### The hazard

The Northwest Pacific Basin produces more typhoons each year than anywhere else in the world as shown in [Figure 39](#). On average, this basin spawns 29 typhoons each year—20 of which reach typhoon status. In contrast, the North Atlantic basin generates only 10 or 11 typhoons per year on average, of which just 6 reach hurricane status. The primary reason for this ocean basin's propensity to spawn intense storms is the extremely large expanse of very warm water. Sea surface temperatures in the Northwest Pacific Basin often exceed 30 °C (86 °F). The average number of typhoon formations per year by ocean basin is presented in [Figure 39](#).<sup>5</sup>

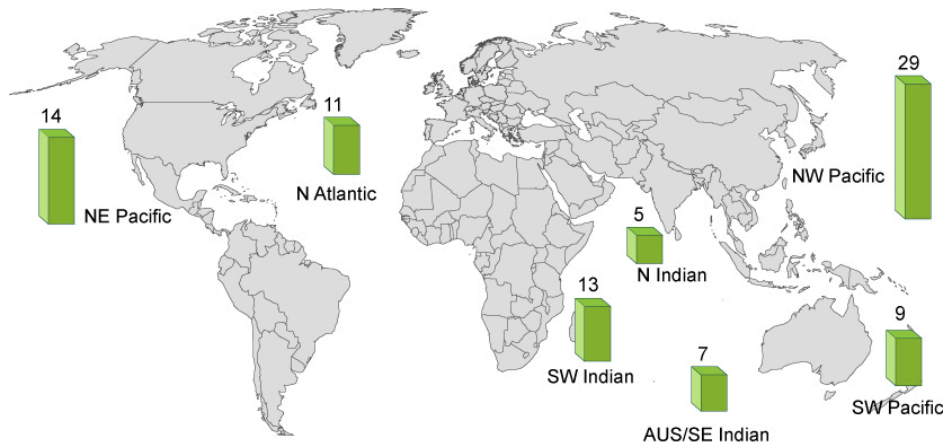


**Figure 39. Average number of typhoon formations per year by ocean basin**

<sup>3</sup> The mean of multiple wind speed measurements taken over one-minute time periods at a height of 10 meters above the ground.

<sup>5</sup> For the North Atlantic Ocean, the average is based on data from the National Oceanic and Atmospheric Administration (NOAA) and the North Atlantic Hurricane Database (HURDAT) from approximately 1950-2006. For the southeast Indian and southwest Pacific Oceans, the average is based on data from the Australia Bureau of Meteorology, the National Climatic Data Center (NCDC), and the Global Tropical/Extratropical Cyclone Climatic Atlas (GTECCA), from approximately 1945-2006. The average for the Northwest Pacific Ocean is based on information from the Japan Meteorological Agency (JMA), the Shanghai Typhoon Institute (STI), and the Japan Meteorological Business Support Center (JMBSC) from about 1951-2005. For the northeast Pacific Ocean, the average is based on information from the NOAA and the HURDAT East Pacific Storm Database from roughly 1949-2006. For the southwest and north Indian Oceans, the averages are based on information from the Joint Typhoon Warning Center from roughly 1945 to 2006 and 1949 to 2006, respectively.

Figure 40 shows the number of typhoon landfalls for Guam, Hong Kong, Macau, the Philippines, Saipan, Taiwan, and Vietnam between 1951 and 2008.

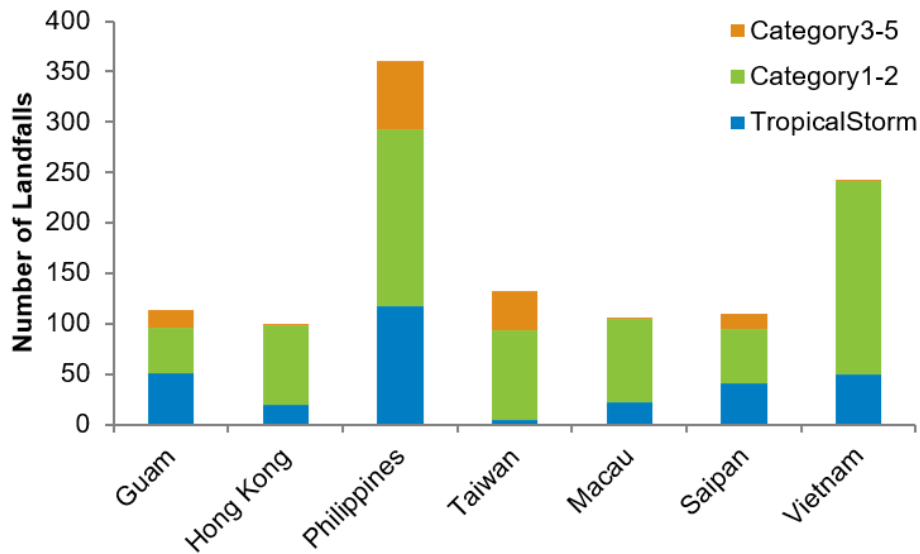


**Figure 40. Typhoon landfall counts in Southeast Asia by intensity**

While high winds typically cause the most typhoon damage in other parts of the world, rain-induced flooding often causes the most damage in the Northwest Pacific Basin. Depending on the country's orientation, location, and terrain, typhoons will have different impacts. Some countries at mid-latitudes have their coastline roughly parallel to a fairly typical path for typhoons—which in turn means that large swaths of the country can be affected by numerous events and for extended periods. Also, storms tend to have a greater chance of interacting with other weather systems as they turn northward and weaken in cooler ocean conditions, which increases precipitation. Typhoons also may undergo extratropical transition as they move northward, which can enhance the asymmetry of the storm and increase the size of the precipitation footprint. Even systems that do not come ashore can cause significant flood damage because their precipitation footprints can extend hundreds of kilometers from the storm track.

During landfall, the effects of coastal mountains and the transition between winds traveling over water to traveling over land forces air to rise, causing clouds and precipitation. This enhanced precipitation can linger even after the typhoon has moved back offshore. A country's mountainous terrain can also cause water to be continuously on the move, flowing downhill into streams that then fill rivers. Rivers that are short and steep can reach peak discharge quickly, causing water to overflow. The low-lying plains onto which water flows are home to many residents, as well as many of the country's buildings, infrastructure, automobiles, electrical goods, computer facilities, and other assets. Increasing property concentrations in flood-prone areas means that the risk of flood damage is high—despite the presence of flood control structures. A more detailed description for each of the countries modeled in the Verisk Typhoon Model for Southeast Asia is presented below.

### *Guam*

Since Guam is so small, it almost never experiences an actual landfalling typhoon. However, an average of nearly two tropical storms or typhoons each year come within 100 km of Guam – close enough to cause some damage, which is almost exclusively from wind. Typhoon Dolphin in May 2015 was the most recent storm to impact Guam and Saipan, with winds of approximately 150 km/h according to the Japan Meteorological Agency (JMA). Prior to then, on 8 December 2002, Typhoon Pongsona, with winds of 175 km/h, came very close to making landfall as it passed between Guam and Saipan. Major typhoons impact Guam once every three to four years, on average.

### *Hong Kong*

An average of one typhoon makes landfall in Hong Kong every two to three years, while one typhoon passes close enough to cause loss annually. Like Taiwan, the most active period for typhoons is May through October, with a peak in August and September. Typhoon landfalls are extremely rare, with no direct landfall in the historical record (1951-2008). Hong Kong is sheltered by the coastal mountains; therefore, the wind risk in the region is relatively low. The flood risk is also quite low because of the very sophisticated flood defense system which has been implemented in and around Hong Kong.

### *Macau*

Typhoon activity for Macau is very similar to that for Hong Kong, given their mutual proximity to one another.

### *The Philippines*

An average of six typhoons make landfall in the Philippines annually with another four passing close enough to cause a loss. Unlike Taiwan and Hong Kong, the Philippines have experienced typhoon activity in every month, with peaks in July and November. Like Taiwan, most of these occur along the relatively unpopulated eastern coast and thus wind risk, from a country perspective, is relatively low. Because of weak steering currents, storms tend to move slowly across the Philippines. As a result, heavy precipitation is very common and thus flood dominates the risk in the Philippines. It is not uncommon for more than 500 mm of precipitation to fall across a large area, with more than 1,000 mm having been observed across the mountains of Luzon.

### *Saipan*

Typhoon activity for Saipan is very similar to that for Guam, given their mutual proximity to one another.

### *Taiwan*

An average of two typhoons make landfall in Taiwan every year with another three coming close enough to land to cause loss. The most active period for typhoons is June through

October, with a peak in August and September. Category 5 strength typhoons are rare, having made landfall only once during the historical record (1951 to 2008). Because typhoons typically weaken rapidly upon interaction with the central mountain range and because the eastern coast of Taiwan is relatively unpopulated, heavy wind losses tend to be restricted to the east coast of Taiwan. As a result the country faces a serious threat from flooding. The central mountain range rises quickly from sea level to elevations as high as nearly 4,000 m within 50 km of the coast. During Typhoon Morakot (2009), extreme orographic lifting resulted in precipitation approaching three meters, over a period four days, in Alishan, Taiwan.

### Vietnam

The climatology of typhoon activity for Vietnam is influenced by the fact that it is at the western edge of the Northwest Pacific Basin. Almost four typhoons make landfall in Vietnam on an annual basis, but they tend to be mainly tropical storms or very weak typhoons and activity decreases towards the south. There has only been one Category 3 landfall in the entire historical record (from Typhoon Ketsana in 2009) dating back to 1951, and nothing stronger. The relatively frequent but weak activity is the result of warm water from the South China Sea being able to support typhoon genesis. But in almost all cases there is either not enough space or insufficient dynamics (because of its southwestward location) to allow significant intensification prior to landfall. Despite the lack of strong winds, there is typically a lot of precipitation. Damage from flood is the primary threat from typhoons for Vietnam. Typhoon Peipah 2007 made landfall with a central pressure of 1006 mb but generated nearly two meters of precipitation.

### The exposure

---

Typhoon activity poses a risk of damage to nearly all of Southeast Asia. The greatest risk, however, is from the occurrence of a landfall event in densely populated and commonly insured areas. Such high concentrations of people make the risk of loss of life and destruction of property relatively high.

The population density for the modeled countries/territories of the Verisk Typhoon Model for Southeast Asia is presented in [Figure 41](#), followed by a more detailed population density map and exposure description for each modeled country/territory in subsequent sections.

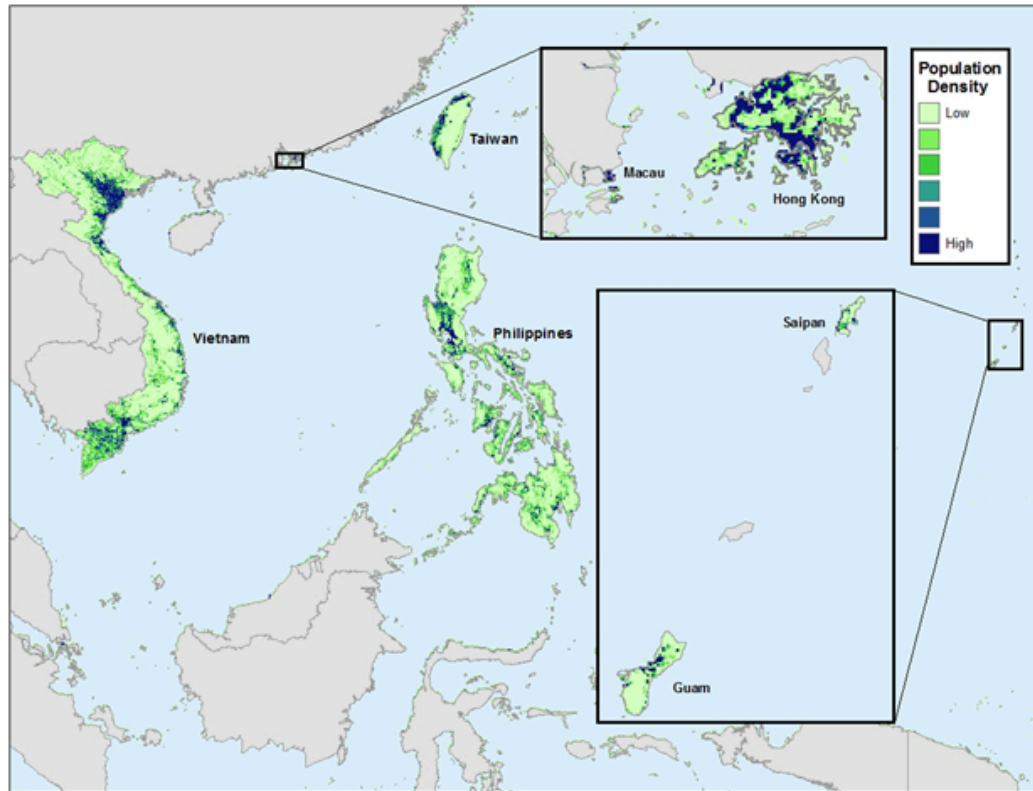


**Figure 41. Population density in the modeled countries of Southeast Asia**

### *Guam*

Guam is part of the area called “typhoon alley”, a typhoon-active area bounded by Guam, the Philippines, and Japan, and the island experiences an average of four to five storm threats each year, and one super typhoon (Category 4 or more) every 10 years.

Most of the commercial and residential buildings are located in Hagatna, Tumon Bay, Pago Bay, and Mana Bay areas, and most of them are made of reinforced masonry or concrete, which are quite wind resistant. Wood frame, which is susceptible to wind, is rare in Guam through all occupancies.

The population density for Guam and Saipan is presented in [Figure 42](#). Guam had an estimated population of 161,785 people as of July 2015. The capital city of Hagatna has a population of 143,000 (2014 estimate).

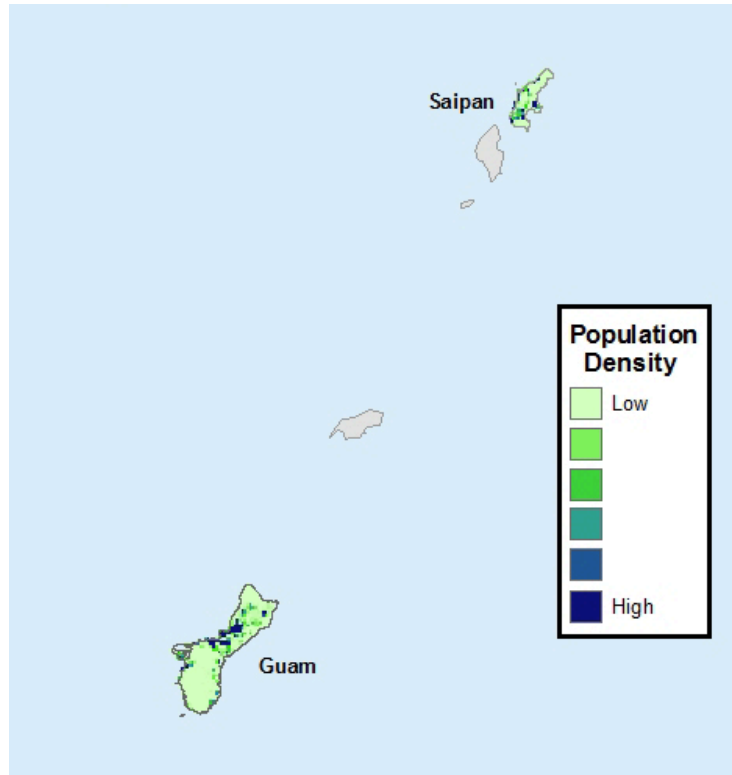


**Figure 42. Population density in Guam and Saipan**

### *Hong Kong*

The areas in Hong Kong that have the highest wind risk are generally along the South China Sea coast. Hong Kong's complex topography acts to shelter areas from the full force of typhoons and thus the wind risk in many areas of Hong Kong is much lower than it is in the surrounding South China Sea coastal areas. Hong Kong also has high construction standards with strong enforcement, which makes wind damage to be relatively normal.

The highest inland flood risk is along the coastal mountains due to orographic lifting. Hong Kong has invested heavily into flood mitigation and has a very mature flood defense system. Thus, heavy inland flood damage is relatively rare in the city but is common in the surrounding areas, particularly in the mountainous regions.

Storm surge is an increasing concern recently, because of the reclamation of lands, large areas of Hong Kong are below approximately 6 m (20 ft) above sea, and the narrowing of Victoria Harbor due to reclamation increases the possibility of amplifying effect that could cause significant storm surge during typhoon events.

In Hong Kong, most of the single-family houses are made of reinforced masonry or concrete. Meanwhile, condominiums, commercial and industrial buildings are mainly made of reinforced concrete or steel. These are quite wind resistant. Also, mid-rise and high-rise buildings are common for condominiums, commercial and industrial in Hong Kong, whose structure damage due to wind is rare. On the other side, many high-rise buildings have

basements where service equipment is located; these kinds of equipment are expensive and vulnerable to water.

Consequently, wind and flood are the dominant sub-perils in Hong Kong. But generally, wind dominates the losses for all return periods. Storm surge also has some appreciable contributions to the loss from typhoon.

The population density for Hong Kong is presented in [Figure 43](#). Hong Kong had an estimated population of 7,141,106 people as of July 2015.

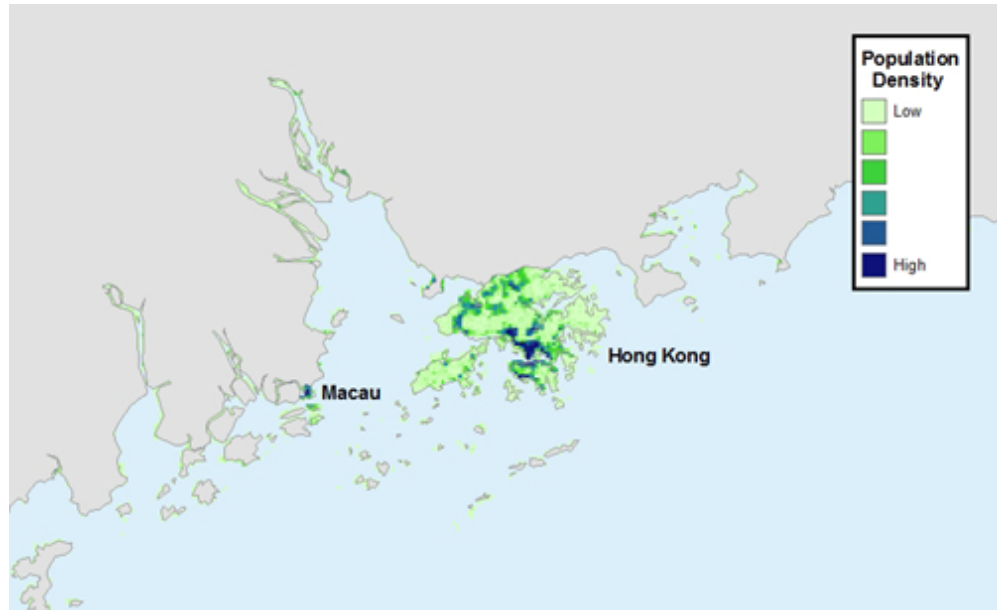


**Figure 43. Population density in Hong Kong and Macau**

### *Macau*

Macau is very close to Hong Kong, and similar to its neighbor, it also has strong construction standard with majority of the buildings are made of concrete or steel through all occupancies, and mid-rise to high-rise buildings are very common in condominium, commercial and industrial. The typhoon damage is driven by wind through all return periods, but flood contributes a relative big portion at the tail.

The population density for Macau is presented in [Figure 44](#). Macau had an estimated population of 592,731 people as of July 2015.

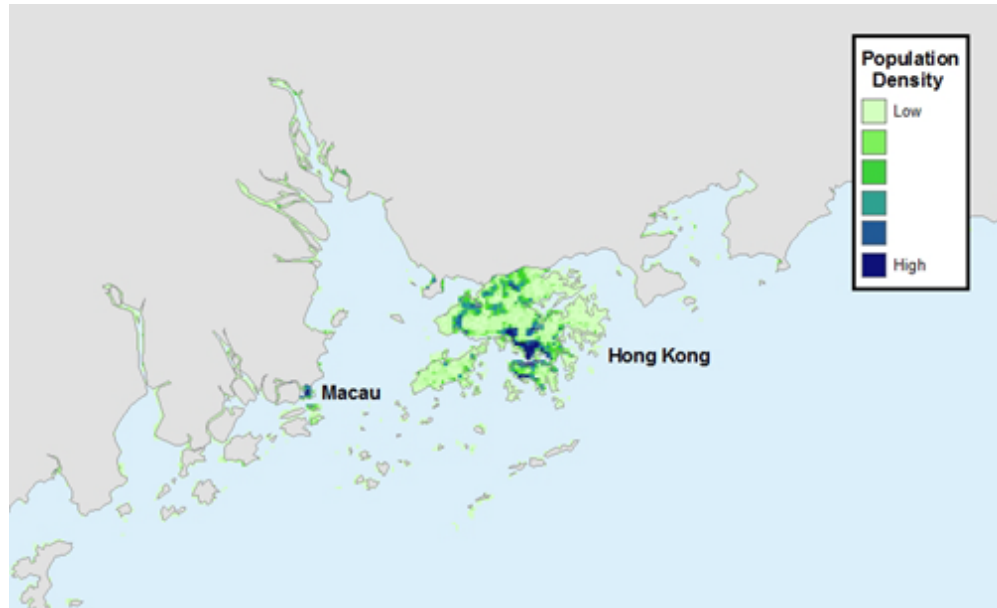


**Figure 44. Population density in Hong Kong and Macau**

### *The Philippines*

In the Philippines, the areas with the highest wind risk are along the northeast Philippine Sea coast. Because the southern half of the Philippines is so near to the equator, typhoons are rare and therefore there is a marked risk gradient extending from north to south. While it is common for storms to maintain their intensity while crossing the Sibuyan Sea, storms tend to dissipate as they move from east to west and therefore the wind risk along the South China Sea coast is relatively lower. The highest flood risk is in the mountainous regions of northern Luzon, owed to high frequency of events as well as orographic lifting.

Building materials are more diverse in the Philippines, but still the majority of the insurable properties are made of reinforced masonry, concrete and steel. They perform relatively well under moderate winds, but still vulnerable to extreme strong winds. Metro-Manila area concentrates approximately 70% of the insurable properties of the Philippines, and the loss could be significant if a super typhoon directly hit this area. In addition, flood defense system in the Philippines is generally not as good as in Hong Kong, there could be some significant flood in the Philippines, like Typhoon Ketsana (2009). Storm surge is mainly focus on the east coastline of the Philippines, but it still can cause significant loss, such as Typhoon Haiyan (2013). It is also noted that there are a lot of property in the Philippines are uninsurable.

Overall, damage to property in the Philippines is evenly distributed between wind and flood plus a notable portion from storm surge at low return periods. But at high return periods, wind is generally the dominant sub-peril. This is because at low return periods, it is generally a weak event, and the wind is not strong enough to cause huge loss to the buildings, which majority of them is wind resistant, but still many of them could be flooded by precipitation-induced flood. Therefore, at low return periods, flood losses can contribute significantly. While at high return periods, it is generally a strong event, which usually can affect a large

area, and surge could also have some appreciable contributions but it is still limited along the coastline.

The population density for the Philippines is presented in [Figure 45](#). The Philippines had an estimated population of 100,998,376 people as of July 2015.

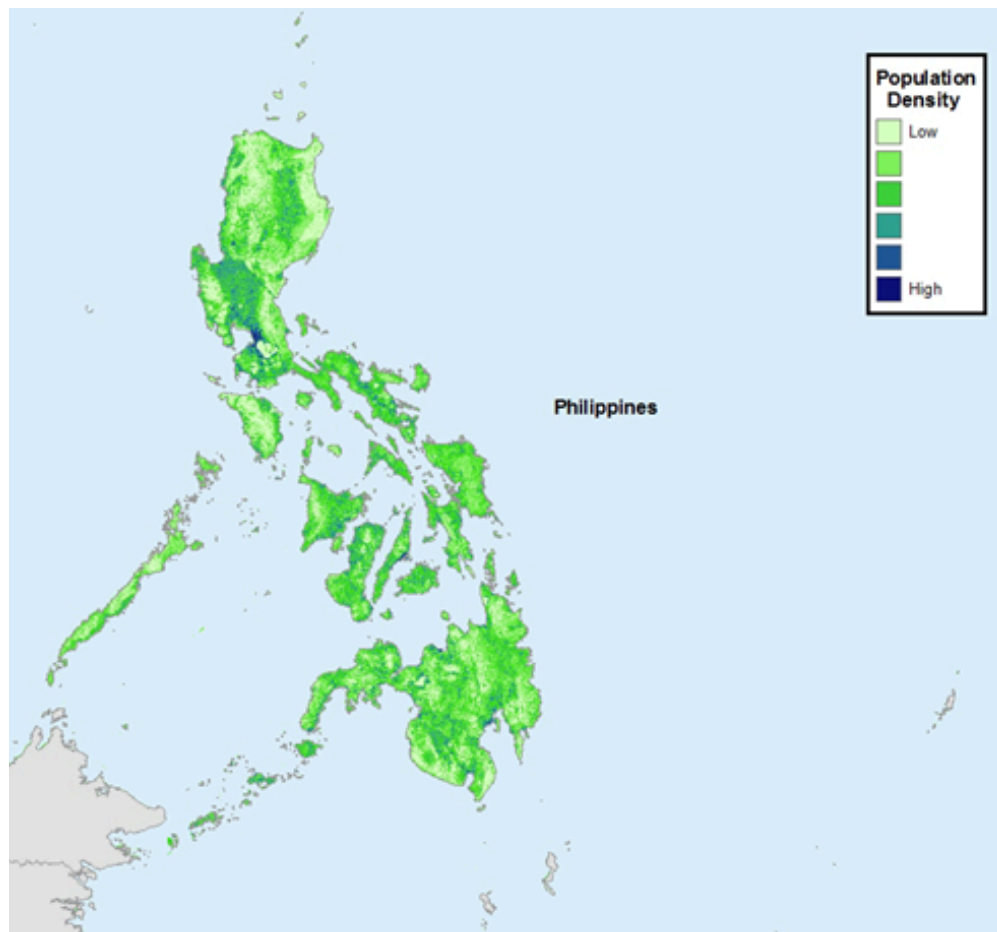


**Figure 45. Population density in the Philippines**

### *Saipan*

Most of the buildings in Saipan are made of reinforced masonry, concrete, and steel, which perform relatively well to wind. However, it still has a good chance to experience a Category 2 typhoon every five years. Besides, water can easily go to the ocean that surrounding Saipan. Therefore, it is hard to accumulate water to inundate property and the flood risk in Saipan is low.

The population density for Saipan is presented in [Figure 46](#). Saipan had an estimated population of 48,220 people as of April 2010.

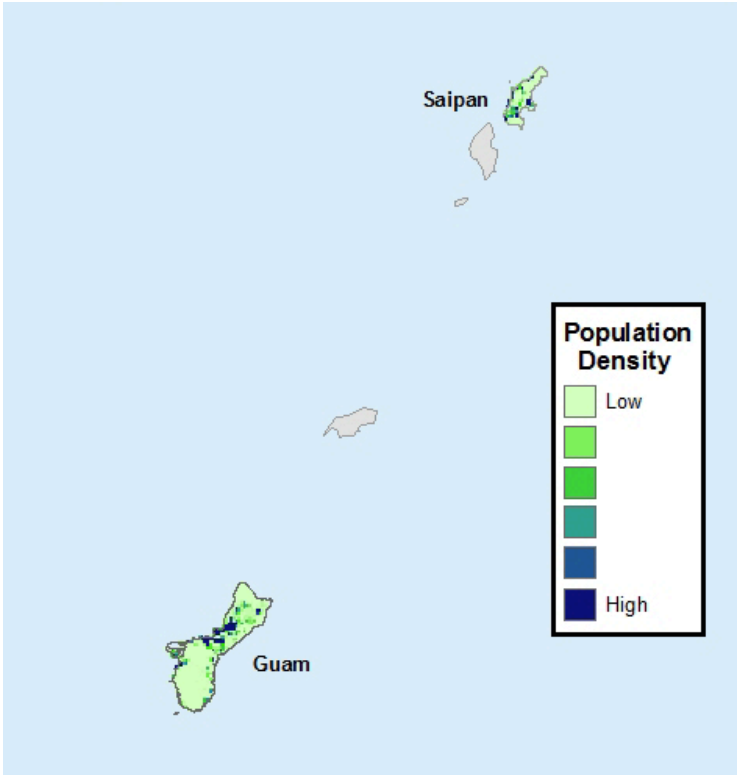


Figure 46. Population density in Guam and Saipan

Taiwan

The eastern coast of Taiwan, including the areas of Taitung and Hualien, are most affected by high winds during typhoons. The central mountain range is a formidable obstacle to landfalling typhoons, typically destroying the low-level circulation, resulting in rapid dissipation. Thus, wind risk is lower along the western coast. The highest flood risk is along the southwestern mountains, due to orographic lifting combined with occasional South China Sea monsoon-scale influences. It is not uncommon for more than 1,000 mm of precipitation to fall during the passage of a typhoon. Additionally, in Taiwan, given their strict building code and relatively good enforcement, their building is generally wind resistance, and wind damage is generally concentrated on the non-structural component.

The heavily urbanized areas of Taipei and Kaohsiung have sustained heavy flood damage during typhoons in the past, recent examples being Nari (2001) and Morakot (2009). Typhoon Nari dumped more than 800 mm of precipitation on Taipei and Typhoon Morakot produced a similar amount over Kaohsiung within, in both cases, a 48- to 72-hour time period, causing unprecedented levels of flooding.

Storm surge can be significant on the west coast of Taiwan, and could heavily affect the Taipei and Kaohsiung areas via the Tamsui and Love rivers. The east coast is not exposed to severe storm surge risk because of the deep bathymetry.

Damage to property in Taiwan is generally distributed equally between wind and flood, but storm surge also has some appreciable contributions. But generally, flood is still considered as the most destructive sub-perils in Taiwan.

The population density for Taiwan is presented in [Figure 47](#). Taiwan had an estimated population of 23,415,126 people in July 2015.

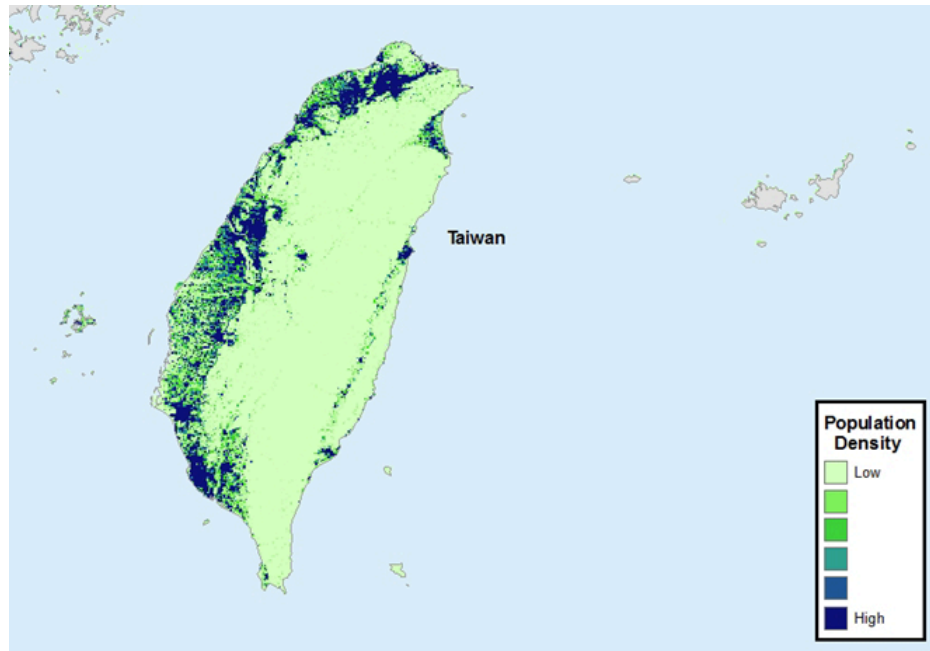


**Figure 47. Population density in Taiwan**

### *Vietnam*

Vietnam is exposed to typhoons and the entire coastal region is susceptible to storms, with mainly affected areas are regions between Hanoi and Haiphong in the North, Da Nang in the center, and Vung Tau in the south of the country. The storms are generally weak while making landfall, but usually accompanied by extensive precipitation.

Most of the insurable properties in Vietnam are made of reinforced masonry, concrete or steel, which has relatively good wind resistance. However, unreinforced masonry or wood frame is still commonly used in single family houses, and they are quite vulnerable to wind. Flood defense system is relatively poor in Vietnam as well, even in the urban areas. They have experienced several significant flood events in the past few years, such as Xangsane (2006) and Ketsana (2009).

The majority of the insurable properties concentrate in the areas mentioned above, which are affected significantly by typhoons. Therefore, even many insurable properties can resist relatively high wind pressure, they are still susceptible to flood and the flood related damage dominates through all return periods.

The population density for Vietnam is presented in [Figure 48](#). Vietnam had an estimated population of 94,348,835 people as of July 2015.

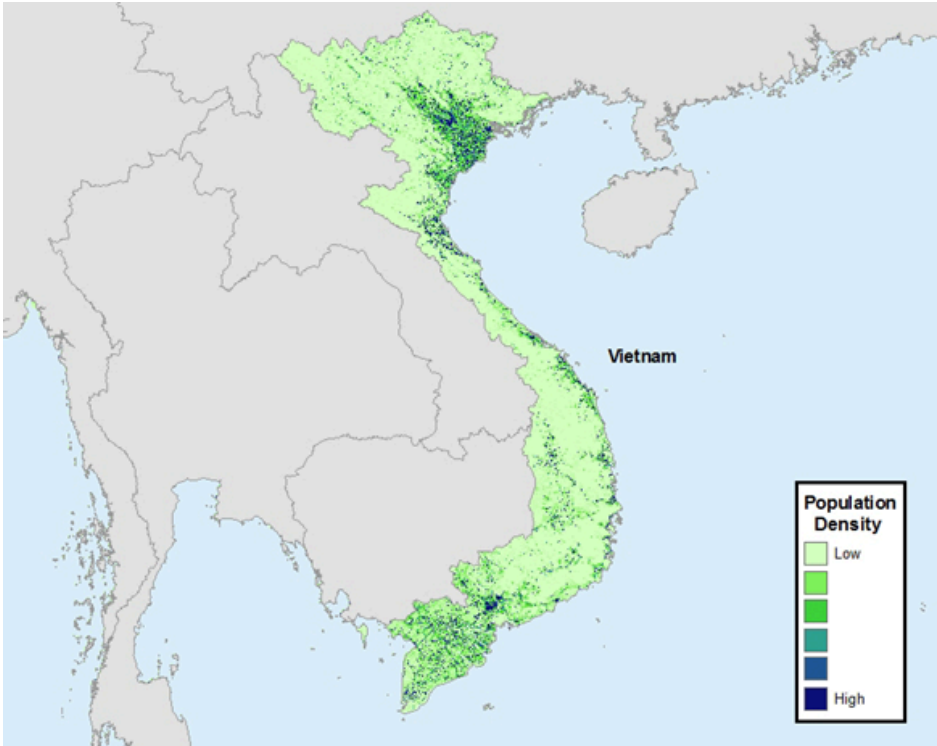


Figure 48. Population density in Vietnam

### 2.3 Significant historical Southeast Asia typhoons

The Verisk Typhoon Model for Southeast Asia’s stochastic catalog is supplemented by the historical events set, which includes 40 Southeast Asia loss-causing events. These events are listed in [Table 18](#).

Table 18. Historical event set for the Verisk Typhoon Model for Southeast Asia

Year	Event Name	Year	Event Name	Year	Event Name
1958	Ida	1997	Winnie	2007	Seplat
1959	Sarah	1997	Paka	2008	Fengshen
1962	Karen	1998	Vicki	2008	Nuri
1970	Joan	1999	Sam	2008	Hagupit
1971	Rose	2001	Toraji	2009	Morakot
1975	Nina	2001	Nari	2009	Ketsana
1976	Pamela	2002	Pongsona	2010	Megi
1979	Hope	2004	Chaba	2011	Nesat
1983	Ellen	2005	Haitang	2011	Washi

Year	Event Name	Year	Event Name	Year	Event Name
1987	Thelma	2005	Nabi	2012	Vicente
1990	Mike	2006	Bilis	2012	Bopha
1991	Mireille	2006	Saomai	2013	Haiyan
1995	Angela	2006	Xangsane		
1996	Herb	2006	Durian		

Further details about 13 of the significant historical typhoons are provided in the following subsections.

**See Also**

[Modeled losses for historical typhoons](#)

## Joan (1970)

One of the most destructive typhoons to ever reach the Philippines, Joan claimed nearly 800 lives and left about 80,000 people homeless. The storm formed on October 8, 1970, near the Caroline Islands and moved westward for three days along the southern periphery of a subtropical high, gradually intensifying until reaching typhoon status on October 11. By the following day, the typhoon intensified into a Category 5 major hurricane and a weakness in the ridge of high pressure shifted Joan to the northwest, aiming the storm directly at Luzon.

On October 13, Joan made landfall in the Lagonoy Gulf region with sustained winds estimated at 280 km/h. Sustained winds of 170 km/h with gusts above 200 km/h were recorded at the Loran U.S. Coast Guard station, about 50 km north of landfall.

Closer to landfall, a minimum sea level pressure of 950.7 mb and wind gusts exceeding 275 km/h were estimated at Virac. Joan weakened while traversing southern Luzon, passing 30 km south of Manila on the morning of October 14. Wind gusts as high as 155 km/h and a minimum pressure of 976.9 mb were recorded at the Ninoy Aquino International Airport with the observed sustained winds of 139 km/h.



**Figure 49. Track of Typhoon Joan (1970)**

Joan was followed a week later by another major hurricane, Typhoon Kate, which also affected the Philippines exacerbating an already dire situation.

### Ellen (1983)

In September 1983, Hong Kong experienced the strongest typhoon since Hope in 1979 and Wanda in 1962. The storm was Ellen, which formed near the Marshall Islands on August 29 and moved westward during the next six days while intensifying, reaching typhoon strength on September 4. Maximum intensity was reached on September 6, when a reconnaissance aircraft recorded a minimum sea level pressure of 928 mb and sustained winds at nearly 205 km/h. Ellen continued moving west-northwest and made landfall on September 9 about 50 km west of Hong Kong, near Macau, with estimated 1-minute sustained wind speeds of 170 km/h.

Maximum hourly winds of 160 km/h were observed at Stanley, with gusts as high as 248 km/h. Nearly all of the observatory stations in Hong Kong reported wind gusts exceeding 160 km/h. The substantially higher winds were a result of channeling effects due to the extreme orography in and around Hong Kong. The duration of typhoon force winds resulting in extensive wind damage throughout the region. More than 20 people were killed and as many as 22 ships ran aground.



Figure 50. Track of Typhoon Ellen (1983)

### Angela (1995)

Angela was the worst typhoon to strike the Philippines since Joan struck the area 25 years earlier. Initially taking form on October 25, 1995, about 500 km south of Guam, Angela slowly intensified while moving westward. On November 1, Angela rapidly intensified to a peak intensity of 287 km/h and a minimum sea-level pressure of 872 mb, the second lowest pressure ever observed in the Pacific basin. Angela maintained this peak intensity for the next 36 hours before striking the northern Bicol region of Luzon on November 2 with estimated 1-minute sustained wind speeds of 226 km/h.

Wind gusts of 260 km/h and 205 km/h were recorded at the Catanduenas Island radar site and Virac, respectively. Angela weakened while traversing southern Luzon, and on November 3, the storm passed directly over Manila, where the Ninoy Aquino International Airport reported a minimum sea-level pressure of 975.6 mb. The storm emerged into the South China Sea and continued moving west-northwest before weakening and finally dissipating west of Hainan Island.



**Figure 51. Track of Typhoon Angela (1995)**

The typhoon affected Manila, Calabarzon, and Bicol and claimed over 900 lives, destroyed more than 96,000 homes, and left a third of the country without power. The northern Bicol region was the worst hit; in Calauag a dam failure caused extensive damage and cost around 100 lives.

### Paka (1997)

An area of convection approximately 2,000 km southwest of Hawaii began moving north-northeastward, and organized into a tropical depression on November 28, 1997, about 465 km west-northwest of Palmyra Atoll. It turned west on December 1, and was upgraded to Tropical Storm Paka on December 2 about 1,000 km south-southeast of Johnston Atoll. It halted and moved, and weakened and intensified on its long path westward due to a mix of warm water and dry air. Paka crossed the International Date Line on December 7, moved through the Marshall Islands on December 10, and officially obtained typhoon status on December 11 when winds reached a recorded 120 km/h (Category 1 equivalent). By December 12, 1-minute sustained winds were recorded at 215 km/h (Category 4 equivalent), and the unofficial ranking of super typhoon was granted while over the open Pacific on December 14. The center of Paka passed about 8 km from the northern tip of Guam when it made landfall there on December 16. It continued to intensify as it brushed the Mariana Islands, reaching its peak 1-minute sustained winds of 295 km/h (Category 5 equivalent) on December 18 to the west-northwest of Guam. PAGASA gave Paka the local name of Rubing on December 19, when it began its degeneration due to increasing wind shear. It eventually dissipated on December 23.

Paka drenched both Guam and Saipan as it passed; Guam recorded 533 mm of rainfall in 48-hours (about 89% of its average monthly rainfall), and Saipan reported excess rainfall sending monthly totals 10% above normal. The strong winds from Typhoon Paka destroyed around 1,500 buildings in Guam, of which 1,160 were single-family homes. About two-thirds of the homes on the island reported major damage, and 10,000 buildings sustained damage to some degree. All of Guam suffered a power outage, and damage to the electrical transmission and distribution system were estimated at USD 16 million. Roads, infrastructure, and marine craft were damaged due to storm surge, and operations were interrupted across the island.



**Figure 52. Track of Typhoon Paka (1997)**

## Sam (1999)

Typhoon Sam, which was to become the wettest typhoon on record for Hong Kong, formed off the eastern coast of the Philippines on August 17, 1999. Over the next two days, Sam moved north-northwest around a subtropical ridge to the north, before turning west-northwest. On August 20, Sam struck northern Luzon in the Philippines and, on the following day, reached the South China Sea where it progressed to typhoon strength. On August 22, Sam made landfall in Hong Kong with 1 minute sustained wind speeds estimated at 125 km/h. The storm quickly dissipated once it moved over the mountains of southern Guangdong, China, but precipitation lingered over the region through August 25.

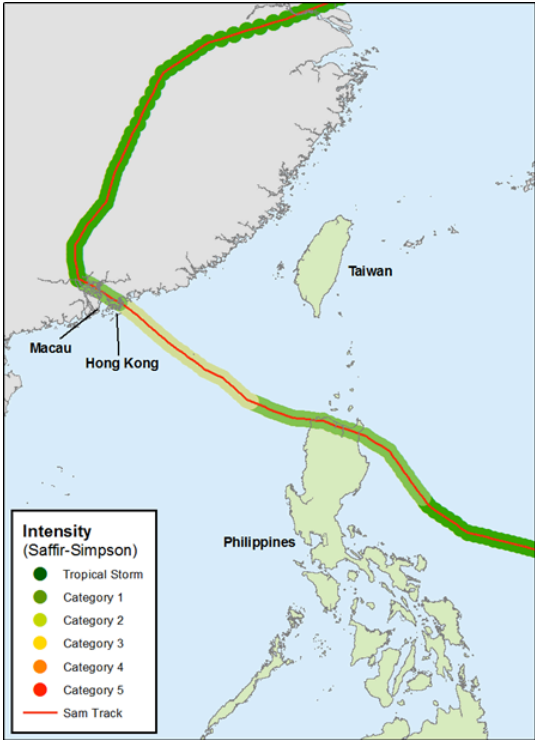


**Figure 53. Track of Typhoon Sam (1999)**

In Hong Kong, wind gusts as high as 148 km/h were observed at Waglan, while Tap Mun reported wind gusts of 115 km/h. Only minor wind damage was reported, mostly to signage and trees. Precipitation across Hong Kong was record-breaking, with over 600 mm recorded at the Hong Kong Observatory. The heavy rains caused more than 200 landslides, mostly in the northern New Territories where flood depths of up to two meters were reported. Because the 600 mm occurred over the course of five days, flooding in the city was minimal. As many as 20 people were killed, including three in an airplane crash at Hong Kong International Airport during the height of the storm.

### Nari (2001)

Nari formed east of Taiwan on September 5, 2001 and over the next two days, moved to the northeast while intensifying into a typhoon. Between September 7 and 14, due to weak steering currents, Nari made three cyclonic loops to the west of Okinawa. Eventually, Nari turned to the southwest and made landfall in northeastern Taiwan on September 16 with 1-minute sustained wind speeds estimated at 150 km/h.

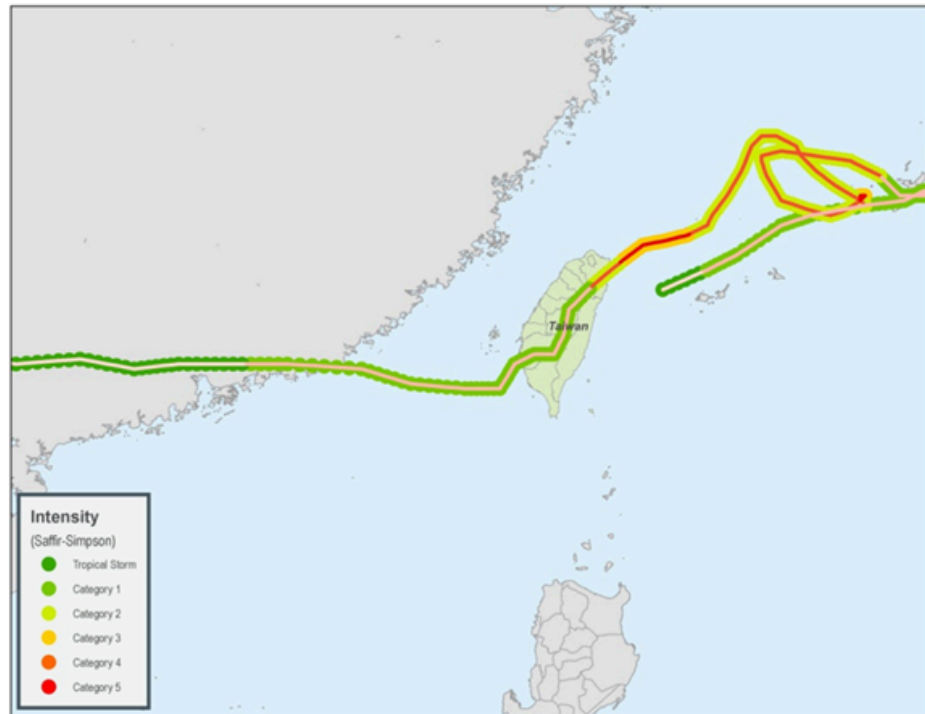


**Figure 54. Track of Typhoon Nari (2001)**

Due to the unusual track and the slow forward speed, both of which were caused by the weak steering currents, Nari caused unprecedented levels of flooding in the Taipei metropolitan area. Taipei received more than 800 mm of precipitation over a period of three days, which is the equivalent to about four months of precipitation in that area. Mountainous regions just to the south received as much as 1,200 mm of precipitation, leading to many rivers overflowing their banks. Southern and eastern Taiwan were relatively unscathed as orographic lifting cooled the air and condensed out most of the moisture in and around Taipei, while the central mountain range disrupted the low-level circulation, quickly dissipating the storm as it moved southward.

As many as 66 people died, with power and water outages affecting 650,000 households. The subway system was severely damaged by the flooding and the streets of downtown Taipei were transformed into rivers.

### Haitang (2005)

In July 2005, Taiwan was struck by Typhoon Haitang, which had formed west of Marcus Island, Japan, on July 12. By July 16, Haitang had rapidly intensified into a typhoon and made landfall two days later near Hualien, Taiwan, with 1-minute sustained wind speeds estimated at 170 km/h. While crossing Taiwan's central mountain range, Haitang weakened but regained strength after reaching the Taiwan Strait. On July 19, Haitang made landfall northeast of Fuzhou, China with 1-minute sustained winds estimated at 125 km/h. After landfall, Haitang quickly dissipated over the mountains of Fujian.

In Taiwan, the eastern coastal city of Hualien, as well as interior mountainous villages, suffered damage to trees and windows. Precipitation along the central eastern coast exceeded 600 mm and amounts as high as 1,200 mm were reported in the central mountains. Localized flooding and landslides were reported in the mountainous areas, and more than 40,000 homes were without electricity.

In China, wind gusts as high as 130 km/h were observed in eastern Fujian province causing damage to more than 20,000 homes. Precipitation exceeded 600 mm near the Fujian/Zhejiang provincial border with more than 400 mm observed along most of the Zhejiang coast, damaging more than 100,000 hectares of crops, and breaching 19 levees.

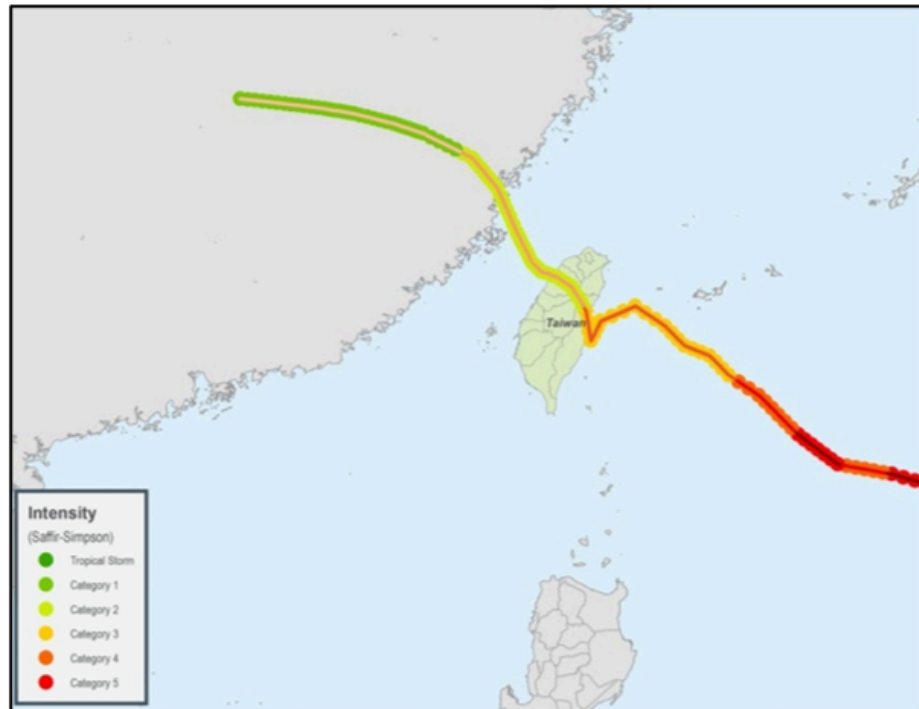


**Figure 55. Track of Typhoon Haitang (2005)**

## Durian (2006)

Durian formed southeast of Chuuk, Micronesia, on November 25 and slowly intensified over the next few days while moving west-northwest until reaching typhoon strength on November 28. The storm rapidly intensified over the next 24 hours and reached typhoon status on November 29 while approaching southern Luzon in the Philippines.

Durian made landfall on November 30, with 1-minute sustained winds estimated at 207 km/h, making it the fourth typhoon within a period of four months to make landfall in the area. The storm then crossed the Lagonoy Gulf and continued westward, making landfall on the Bondoc Peninsula, on Marinduque Island, and again on Mindoro Island before reaching the South China Sea. Once over the sea, the storm weakened temporarily, but regained strength

before causing additional damage when it struck Vietnam on December 5 as a tropical storm before degenerating to a tropical depression.

About 2,500 were evacuated from the Philippines in advance of the storm. As Durian reached the region, it uprooted trees and destroyed homes and while drenching some areas with 457 mm of rain. In Alby province, a dyke break caused by excess rain inundated nearby areas with 1.5 m of floodwaters. Thousands of people were stranded for days due to transportation disruptions. The death total from storm was reported to be at least 720 by mid-December. At the Mayan Volcano, which had erupted a few months earlier, the rain and wind combined with loosened rock and mud, resulting in massive landslides that destroyed three villages; total known deaths from the mudflows at the volcano stood at 800 to 1,000, although a final total may never be known as some areas cannot be excavated.

In Vietnam, marine vessels suffered large losses; 820 boats sank in Bình Thuận Province alone, and 896 fishing boats sank throughout the country. Strong winds and torrential rains destroyed property throughout the region, ripping off roofs and washing away structures. Approximately 34,000 homes were lost to Durian across Vietnam, and another 166,000 were damaged. Around 1,700 people were injured, and almost 100 were killed by the storm.



**Figure 56. Track of Typhoon Durian (2006)**

## Fengshen (2008)

Fengshen formed on June 18, 2008, about 100 km northwest of Palau and tracked west-northwest, intensifying into a typhoon in just 24 hours. The storm was poorly forecasted by all reporting agencies (as evidenced by the wide range in final best track intensity estimates), with no indication of a potential impact on the Philippines. However, Fengshen tracked

westward and made landfall on Samar Island on June 20 with a central pressure of 970 mb and 1-minute sustained winds estimated at between 132 km/h and 172 km/h. The storm intensified by 20 mb while crossing the Sibuyan Sea and on June 21, abruptly turned north-northwest.

The eye of Fengshen passed over Manila, where a sudden albeit brief calm was reported, with 1-minute sustained winds estimated at between 132 km/h and 172 km/h. Fengshen continued moving northwest for the next few days, making landfall near Hong Kong on June 25, glancing Macau as it went, and ultimately dissipated over the mountains of southern Guangdong, China, on June 27.

In the Philippines, Fengshen killed more than 1,300 people, the majority of whom were on the Princess of the Stars ferry, which sank off the coast of San Fernando, Romblon, located in the Visayas. According to the Philippine National Disaster Coordinating Council (NDCC), more than 155,000 houses were damaged, more than 50,000 were completely destroyed, and 109,837 were partially destroyed. In Iloilo City, tens of thousands found their homes completely submerged when a nearby reservoir burst. In Manila, power outages occurred throughout the city and surrounding areas. Across the region, Fengshen affected about 4.8 million people.

The storm caused much less damage in Hong Kong as it escaped a direct hit, although torrential rain caused minor flooding that blocked roads and downed trees and signs. Business operations were disrupted in some places by strong winds, including the delay of hundreds of flights at Hong Kong International Airport. Macau experienced minor flooding.



Figure 57. Track of Typhoon Fengshen (2008)

## Nuri (2008)

Nuri formed several hundred kilometers to the northwest of Guam on August 17, 2008, and intensified into a typhoon over a period of 24 hours. On August 20, Nuri passed through the Babuyan Islands, missing northern Luzon by less than 50 km, with 1-minute sustained winds estimated at between 150 km/h and 172 km/h. The storm maintained its intensity and continued moving to the west-northwest, before it finally started to weaken before making landfall in Hong Kong on August 22. At landfall, Nuri had 1-minute sustained winds estimated at 115 km/h and by the following day had quickly weakened and dissipated over the mountains of southern Guangdong.

In the Philippines, at least 12 people were killed with nearly 300,000 people in nine provinces adversely affected by the storm. According to the NDCC the most damage occurred across extreme northern Luzon, with agriculture impacted the most.

Nuri caused 100-150 mm of precipitation in Hong Kong, and wind gusts as high as 157 km/h were recorded at Waglan Island. Damage was reported to roofs and scaffolding, and parked cars were crushed under downed trees. Businesses were disrupted and over 500 flights cancelled at Hong Kong International Airport. In nearby Shenzhen, more than 40,000 trees were toppled by the wind.

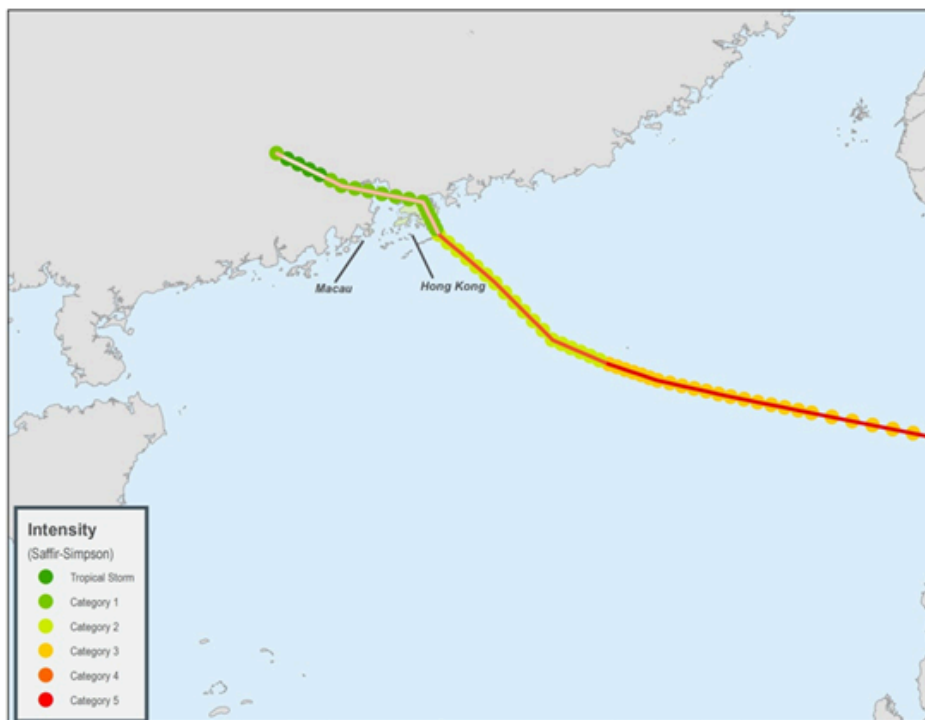


**Figure 58. Track of Typhoon Nuri (2008)**

## Morakot (2009)

One of the most devastating catastrophic events ever to strike Taiwan, Morakot initially formed 600 km southeast of Okinawa on August 2, 2009, and slowly intensified over the next 48 to 72 hours while moving westward. After reaching typhoon strength on August 5,

the storm continued westward and made landfall two days later in east-central Taiwan with 1-minute sustained winds estimated at between 150 km/h and 161 km/h. While crossing Taiwan's central mountain range, Morakot weakened before reemerging in the Taiwan Strait on August 8. Morakot then turned abruptly to the north and made a second landfall near the Fujian/Zhejiang provincial border on August 9 with 1-minute sustained winds estimated at between 125 km/h and 138 km/h. Morakot continued moving to the north-northeast, finally transitioning extratropically and dissipating over South Korea on August 12.

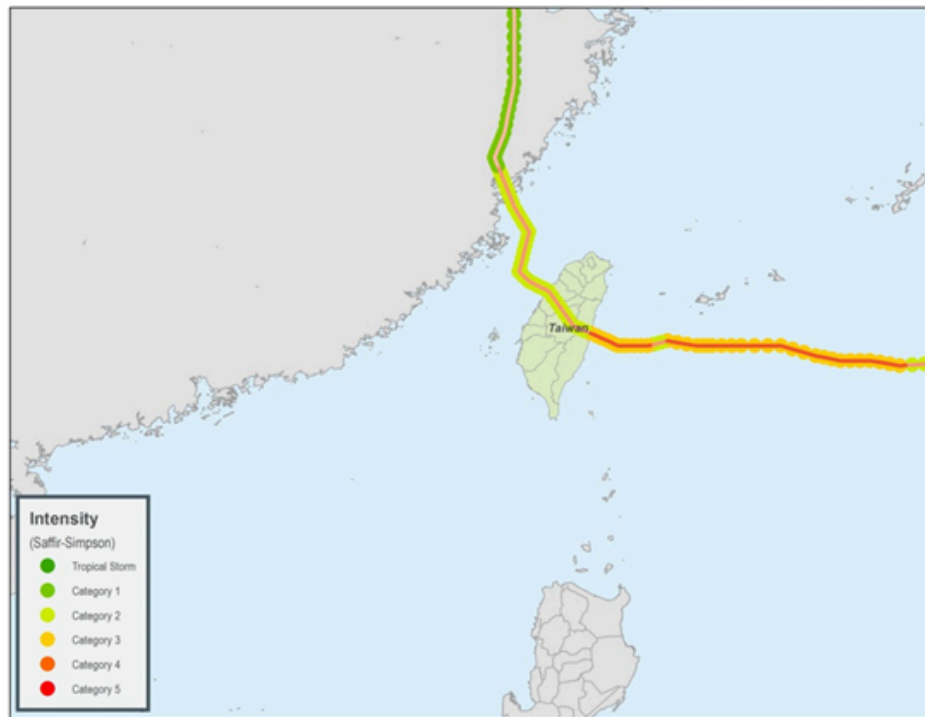


**Figure 59. Track of Typhoon Morakot (2009)**

Morakot produced record-breaking amounts of rainfall, with as much as 2,327 (2,965) mm falling in a 48 (96) hour period in Alishan. For comparison, the 48 hour world rainfall record is 2,467 mm. This amount shattered the previous typhoon record of 1,736 from Herb (1996), also observed in Alishan. Similarly, Kaohsiung recorded 723.5 (835.5) mm of precipitation in a 48 (96) hour period while Pingtung, just to the north, received more than 1,000 mm of precipitation.

Mudslides and river flooding were observed across nearly the entire southern portion of Taiwan, with the mountain village of Xiaolin completely buried by a mudslide, killing 118. In Zhiben, the Jinshuai Hotel fell into the Zhiben River, while 51 homes were swept into the Pacific Ocean in Taitung County. The extreme rainfall in southern Taiwan is attributed to the slow storm translation speed, a cyclonic monsoon gyre (South China Sea monsoonal influence), orographic lifting, and continuously-forming mesoscale rainbands.

The amount of rainfall and subsequent damage in China was much less than in Taiwan, but significant nonetheless. Most of coastal Fujian and Zhejiang provinces reached 200-300 mm of precipitation, with isolated reports as high as 1,000 mm. Eleven million people were

affected throughout eastern China, with nearly four million reporting damage to their homes from flooding or landslides, and more than 1 million acres of farmland was inundated by floodwaters.

## Nesat (2011)

---

A disturbance first reported on September 21, 2011, about 360 km southeast of Palau, gradually developed into a tropical depression on September 23. It was further upgraded and named Nesat on September 24. Above-average sea surface temperatures aided intensification to a severe tropical storm on September 25, with a further classification as a typhoon (Category 1 equivalent) later that day. Banding became clearer, and an eye-like feature was identified at about 417 km east-northeast of Manila, Philippines, which rapidly expanded to a diameter of 56 km. Originally projected to reach Category 5 wind speeds, cooler sea surface temperatures restricted Nesat's genesis to Category 4 equivalency, with peak 1-minute sustained winds of 213 km/h. It made landfall in Luzon, Philippines, on September 27, which decreased its 1-minute sustained winds to 176 km/h (Category 2 equivalent) and eroded the eye wall. Land interaction and vertical wind shear further diminished the system to a Category 1-equivalent, although it maintained a large area of gale force winds and expanded in size. Nesat brushed Hong Kong and Macau to make landfall in Hainan, China, on September 29, maintaining its strength. It continued along its path to make landfall in northern Vietnam on September 30 with 1-minute sustained winds of 102 km/h. Convection around the system and land interaction further disrupted its structure and caused rapid weakening. It was downgraded to a tropical low over land later that day.

Prior to making landfall, about 110,000 people had been evacuated from flood-prone areas of the Albay Province in the Philippines, and numerous flights had already been cancelled. Nesat—locally named Pedring—slammed the Philippines, primarily the Luzon region, with torrential rains, flash floods, severe winds, and storm surge that reportedly dwarfed palm trees. Houses, bridges, and roads were washed away, flood waters were cited as neck-deep, huge trees were toppled, and millions of people were without power. A state of calamity was declared in Luzon. Rivers swelled necessitating the release of the Magat Dam in Isabela province, causing thousands to flee and flooding 55 villages in the capital of Ilagan. As of October 3, 2011, the National Disaster Risk Reduction and Management Council reported 55 deaths and 65 injured, and announced Nesat once of the costliest typhoons to have impacted the Philippines with total infrastructure and agricultural losses estimated at USD 202 million.

Hong Kong, Macau, and China launched preparations prior to Nesat's arrival as well; ships were recalled, operations of schools and businesses were ceased, flights were cancelled, and public transportation was suspended. Hong Kong's stock market, along with all courts, was also closed. Further flights were cancelled, trees were toppled, and some structures collapsed on the island nations when Nesat passed by. In China, more than 100,000 people were forced from their homes in Hainan due to strong winds. Trees were uprooted, billboards destroyed, roofs were damaged or destroyed, and thousands lost power. Reports indicate that floods from Nesat affected 2.49 million people in the Guangxi Zhuang Autonomous Region, and economic losses were estimated at USD 328 million in China.

Significant property losses were reported in the Vietnam's northern regions of Quảng Ninh and Hai Phong because of Nesat. Almost 300 houses had lost their roofs to wind, marine vessels were destroyed, and 1,700 hectares of crop land were under water. In the south, severe flooding in the Mekong Delta displaced thousands, and total losses were estimated at USD 2.4 million.



**Figure 60. Track of Typhoon Nesat (2011)**

## Vicente (2012)

Vicente was formed from a tropical disturbance that developed when the large area of convection from Tropical Storm Khanun split on July 17, 2012. It became a tropical depression on July 20, and was given the local name of Ferdie by PAGASA as it passed through the Philippines. The international name Vicente was assigned on July 21 when the system was upgraded to a tropical storm and it moved westward into the South China Sea. Above-normal sea surface temperatures and weak vertical wind shear allowed for further genesis, and Vicente became a Category 1-equivalent typhoon on July 23 as it continued westward toward China. It underwent rapid intensification after developing two “hot towers”, and went from Category 1 to Category 4 equivalency in just six hours before making landfall in Guangdong, China, with winds of 213 km/h. It came within 111 km of Hong Kong and 40 km of Macau. Vicente began to degenerate over land, and passed into northern Vietnam on July 27 before dissipating.

As the depression pass by the Philippines, it caused torrential rains reported at rates of 40 mm/h and gusty winds. Flooding left people stranded in offices and residents were

encouraged to evacuate. Roads were rendered impassable, flights were cancelled, and operations of schools, businesses, and public transportation were suspended.

Between July 23 and 24, Vicente brought heavy rains and storm surge to Hong Kong; more than 200 mm of rain was recorded and storm surge reached 1.51 meters. Strong winds damaged or destroyed billboards, felled more than 8,500 trees, and sent dangerous debris hurtling toward people and structures. Many vehicles were damaged and some roads were rendered impassable, leaving hundreds stranded as public transportation was suspended due to winds and flooding. Hundreds of flights were cancelled, and business operations were interrupted, including the closure of schools, ports, and stock exchange. Marine vessels and cargo also suffered damage and loss.

The more than 9-meter waves kicked up by Vicente are likely to have caused coastal erosion and low land flooding in Macau and China. Significant rainfall was reported in Macau and China, with parts of China recording 300–350 mm of rainfall accumulation and a rainfall rate of 25 to 35 mm/h. Both Macau and China reported storm-force winds, which destroyed 500 homes and damaged 13,600 hectares of crops in Guangdong Province, China. About 115,000 trees were damaged in Shenzhen, of which 30,000 were downed. Some 800 properties were damaged, along with a minimum of 2,770 automobiles, the costs of which were estimated at USD 2.1 and 7.9 million, respectively. An estimated 500,000 people in were affected by Vicente in Guangdong Province, and total economic losses there were estimated at USD 28.2 million. Heavy rains in Guangxi Province triggered damaging floods that destroyed 1,886 homes and damaged 18,690 hectares of crops, generating an estimated USD 14.4 million in economic losses there. Ongoing floods in nearby Guizhou Province were worsened by Vicente; 400 homes were destroyed, 17,800 hectares of crops were damaged.

The remnants of Vicente caused heavy rain in northern Vietnam, with rainfall totals from 20 to 363 mm that triggered landslides and flooding in the Red and Thai Binh rivers. Around 479 homes and 2,492 hectares were damaged and some evacuations were conducted.



Figure 61. Track of Typhoon Vicente (2012)

# 3 Event Generation

The Verisk Typhoon Model for Southeast Asia is based on data for over 1,644 historical typhoons that took place in the Northwest Pacific Ocean from 1951 to 2008. Verisk relies on information from agencies that gather historical data in the form of barograph traces from land stations and ships, actual wind records from weather service stations, aircraft reconnaissance flight data, radar data, precipitation data, and other pressure and wind reports.

The stochastic catalog is based on historical data from a variety of sources, the most important of which are:

- The Japan Meteorological Agency (JMA)
- Shanghai Technical Institute (STI)
- Tropical Rainfall Measuring Mission (TRMM)

In addition, Global Summary of the Day (GSOD) data from the National Climate Data Center, as well as data from the Hong Kong Observatory (HKO), the Philippines Atmospheric, Geophysical, and Astronomical Services Association (PAGASA), the Central Weather Bureau (CWB) of Taiwan, and the Joint Typhoon Warning Center (JTWC) were used for hazard validation. The historical typhoon catalog on which the model's stochastic catalog is based was constructed by blending track information from the JMA and the STI. Even weak, but hydrologically-significant, historical typhoons that have affected Southeast Asia were identified, even those that did not make landfall on the mainland. The full storm track was captured to account for all precipitation associated with an event, even after the official track was terminated because winds dropped below tropical storm strength. The STI provided Verisk with invaluable information in this particular area.

The main environmental parameters needed to assess typhoon losses are wind speed, accumulated runoff from precipitation, and storm surge depth. Wind duration, or the number of hours in which wind speed is above a certain threshold at a given location, is computed based on a storm's intensity, size, distance and direction to the location, forward speed and direction, and underlying terrain and land-use conditions.

The model's inland flood module uses model generated precipitation at each hour as well as surface information about terrain slope, friction, and soil characteristics. Soil data for the flood sub-peril came from the Harmonized World Soil Database (HWSD). The native resolution of the soil data is 1 km.

Storm surge depth is calculated using the coupled numerical model of Surge, WAve and Tide (SuWAT), and is a function of storm parameters, coastal bathymetry, and land elevation. Modeled wind velocities and the coastal bathymetry are used to determine the primary component of the storm surge from wind stress. Waves from the coupled SWAN (Simulated Waves Nearshore) wave module are used to modulate the surface wind stress. The special distribution of pressure is used to compute the contribution from the inverse barometer effect.

Additional model parameters describing a typhoon event are:

- location at landfall (latitude and longitude)

- landfall segment
- landfall hour
- intensity at landfall measured as central pressure in millibars (mb)
- track angle at landfall
- forward speed
- precipitation rate
- outer storm radius
- radius of maximum winds (Rmax)
- day of year
- storm duration
- time of extratropical transition

### 3.1 Annual frequency and location

Because the model accounts for precipitation-induced flooding as well as wind damage, the domain over which typhoon-related hazards and losses are modeled needs to be considerably larger than it would be if only wind damage were modeled. Because the precipitation footprint of typhoons can extend over thousands of square kilometers, and because little correlation exists between typhoon wind speed and precipitation intensity, even weak storms several hundred kilometers offshore can cause flood damage on land.

Furthermore, local flooding is often due to precipitation that occurred upstream, so the flood damage footprint may be considerably larger than the wind or precipitation footprint. In addition, to account for the fact that it may take several days for peak flood levels to travel along a river network, typhoon track, intensity, and size must be accurately modeled for several days after landfall.

The catalog for the Verisk Typhoon Model for the Northwest Pacific Basin has been developed using historical typhoon data from 1951 to 2008. This catalog is used for the Verisk typhoon models for Southeast Asia, China, Japan, and South Korea, enabling companies to reliably assess typhoon risk to portfolios that span multiple countries.

The catalog accounts for seasonality, extratropical transitioning, and events that impact multiple countries. Modeled frequency, meteorological data, and track information are analyzed in the geographical domain depicted in [Figure 62](#).

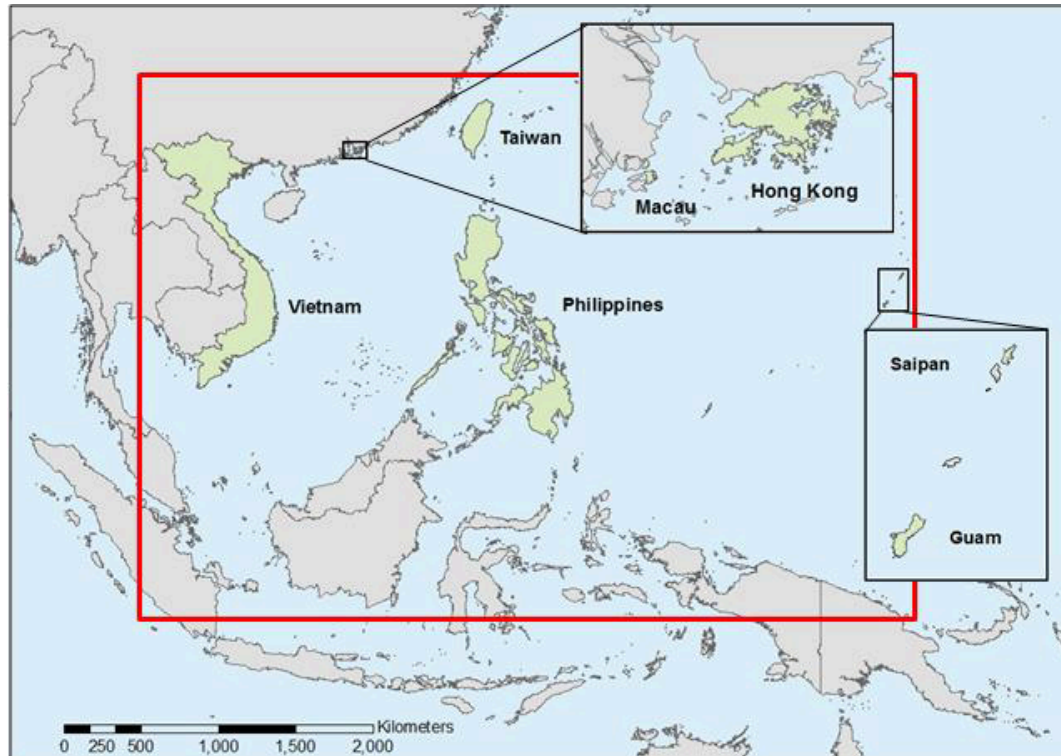


**Figure 62. Domain of the Verisk Typhoon Model for the Northwest Pacific Basin, highlighting the countries modeled in the Verisk Typhoon Model for Southeast Asia**

In addition to landfalling storms, bypassing storms are also modeled, as their precipitation may extend significantly inland.

### Annual storm frequency

The Northwest Pacific Basin is the most active area in the world in terms of typhoon activity. Not only are typhoons more frequent in this ocean basin, but they are also more intense than in other parts of the world. On average, about 29 typhoons with wind speeds exceeding 63 km/h form in this basin each year. Roughly two thirds of these events develop into severe typhoons, with wind speeds of 119 km/h or higher.

Annual frequency over the entire Northwest Pacific Basin is modeled as a Poisson distribution as shown in [Figure 63](#).

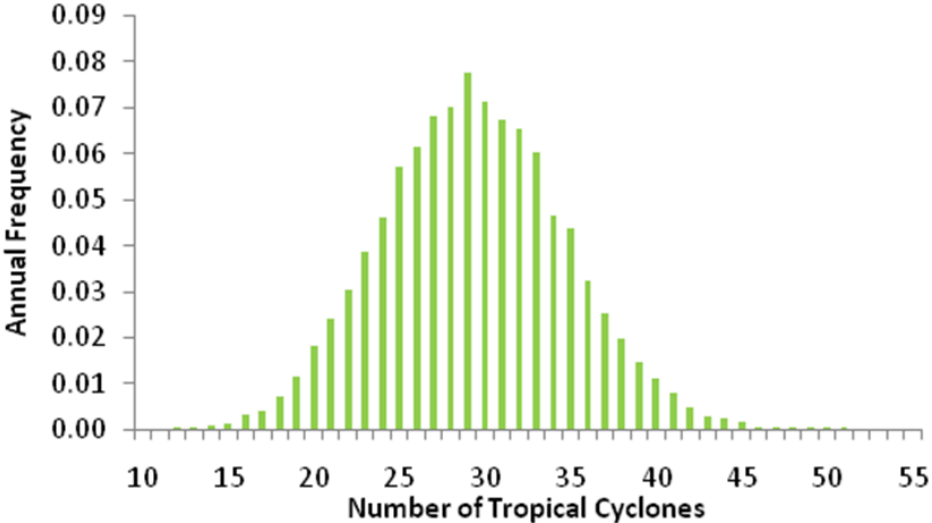


**Figure 63. Annual frequency (Poisson) distribution of simulated typhoons in the Verisk Typhoon Model for the Northwest Pacific Basin domain**

However, annual landfall frequency in Southeast Asia (and other Verisk-modeled countries in the basin) is not an imposed distribution, but rather one that naturally results from the dynamics of the track-generation process. [Figure 64](#) shows the modeled distribution of annual typhoon landfalls in Southeast Asia alone. Note that a single storm may make multiple landfalls.

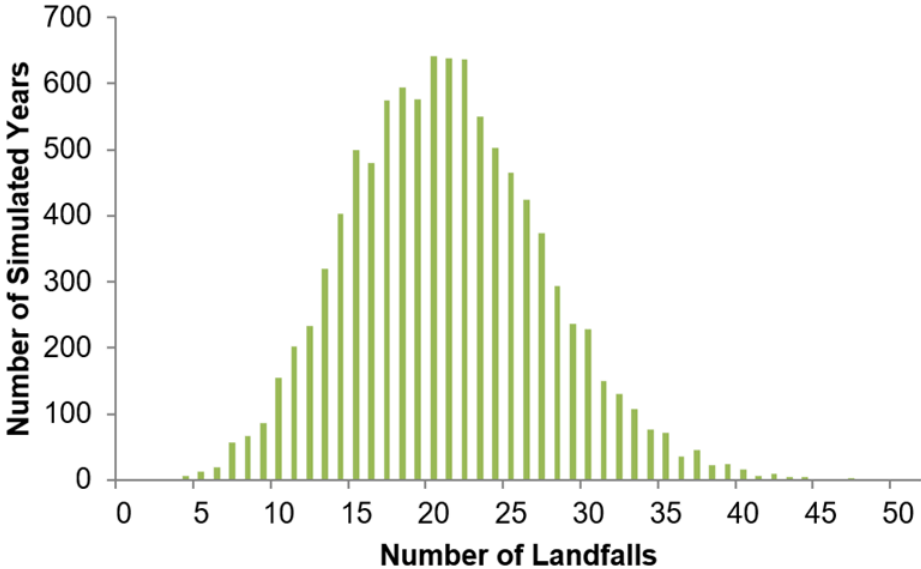


**Figure 64. Annual frequency distribution of simulated typhoon landfalls in the Verisk Typhoon Model for Southeast Asia domain**

Late summer and early fall are the most active times for typhoon formation, and there is a clear seasonal cycle that peaks in August. The Northwest Pacific Basin is unique in that

typhoon formation has been observed in all months of the year. [Figure 65](#) shows the monthly distribution of simulated typhoons in the entire model domain.

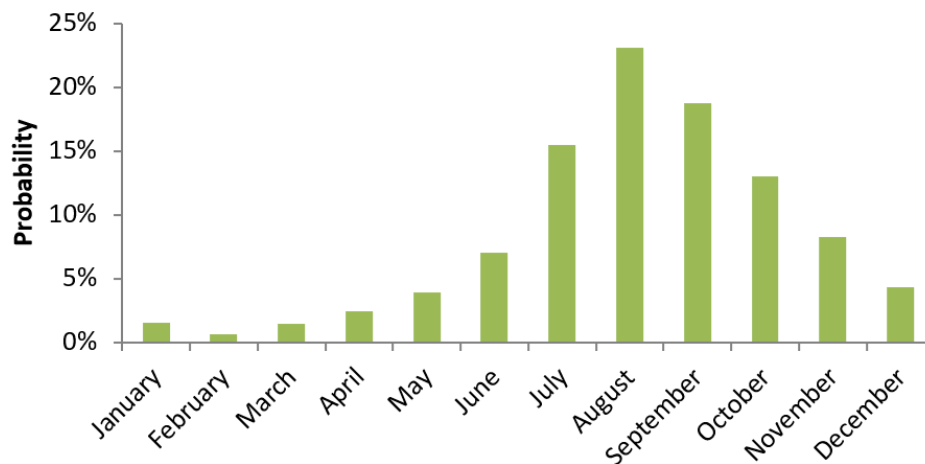


**Figure 65. Distribution by month of simulated events in the model domain from the 10,000 year catalog**

#### See Also

[Storm tracks](#)

## Storm genesis location

For each simulated storm, a corresponding historical storm is drawn at random from the set of all historical storms for the period 1951 to 2008. All genesis aspects of the simulated storm, such as storm day, starting location, track angle, forward speed, and central pressure are determined by stochastically perturbing the corresponding historical variables of the historical storm that was drawn. The perturbation is achieved by adding Gaussian “noise” to each historical value.

By using the same seed storm to determine both storm day and starting location, the correlation between the two variables—or the seasonality of the starting location—is preserved.

Future evolution of the stochastic storm is determined by using the autoregressive time series models as described in the sections that follow.

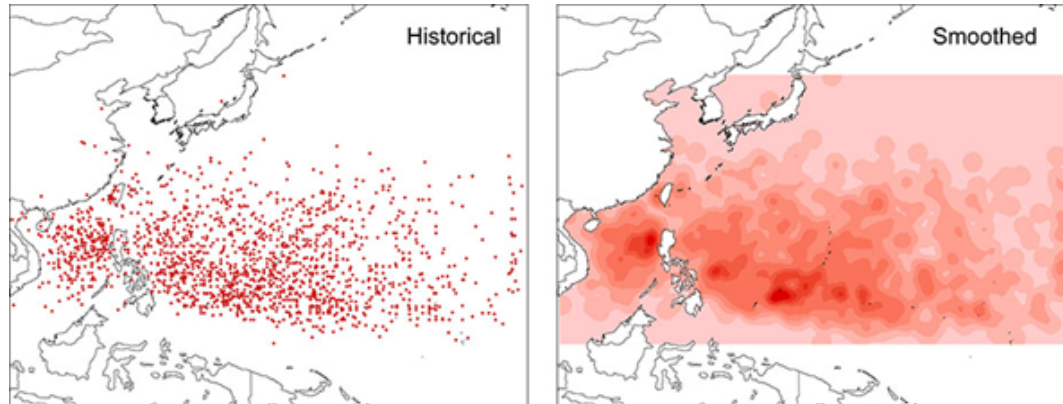


**Figure 66. Historical storm genesis locations and smoothed historical genesis locations**

## 3.2 Storm tracks

Track direction at any given point in time is a function of storm track direction at previous times. The dependence from one time period to the next can be measured by computing the auto-correlation function for historical storms. The analysis indicates that a random walk model describes the dependence well. That is, the next storm track direction equals the current storm track direction plus a random perturbation drawn from a probability distribution that is allowed to vary spatially over the model domain.

The simulation is implemented using six-hour time steps and conditional probability distributions estimated for  $1.25^\circ \times 1.25^\circ$  grid cells using the historical data available for each grid cell (see [Figure 67](#)).

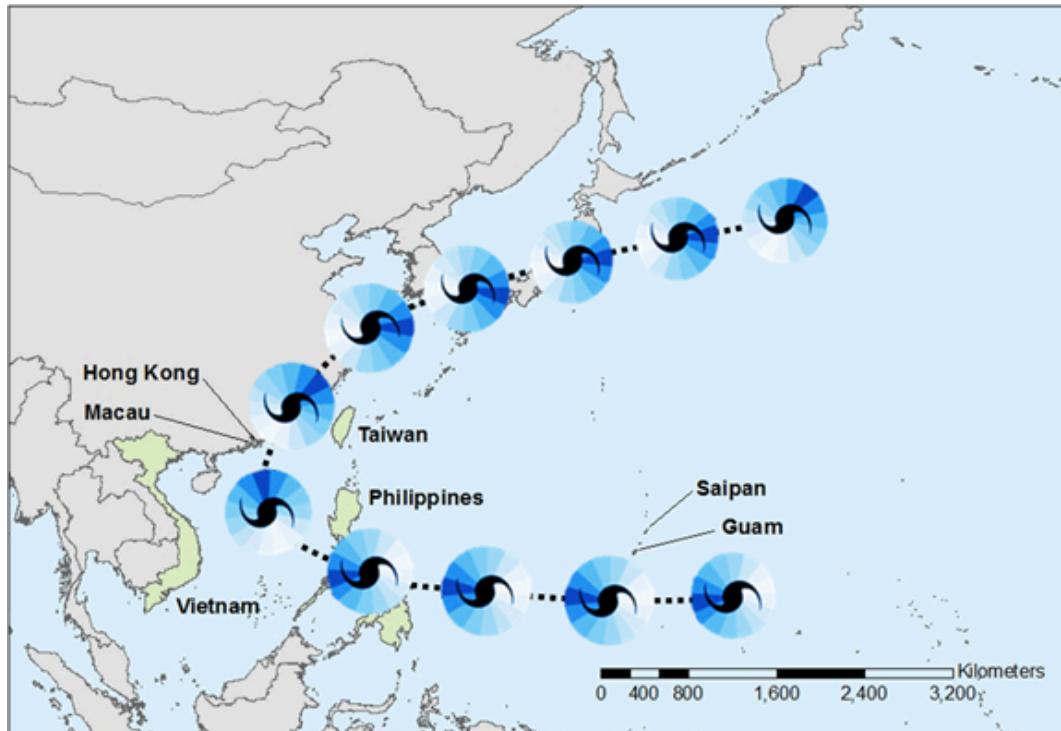


**Figure 67. Storm track generation in the Verisk Typhoon Model for the Northwest Pacific Basin**

The advantage of this probabilistic approach to storm track generation is that the tracks of simulated typhoons resemble the curving of historical tracks. Furthermore, the fact that they are fully probabilistic means that any possible storm track can be generated, not just those that have been observed historically.

### Multiple-landfalling storms

A single typhoon may comprise several landfalls or bypasses. In the model, a bypassing storm is defined as one that does not make landfall but passes sufficiently close to cause ground-up losses from combined wind and flood in excess of USD 40,000. As the Verisk Typhoon Model for Southeast Asia follows each simulated storm from inception to dissipation, multiple landfalls and bypassing typhoons are part of the simulation. The simulated frequency of multiple landfalls and bypassing storms is consistent with the historical frequency of these storms.

#### See Also

[Validating stochastic event generation](#)

### 3.3 Forward speed, central pressure, and radius of maximum winds

For each simulated storm, forward speed, central pressure, and radius of maximum winds (Rmax) are also allowed to vary along the storm track, as illustrated in [Figure 68](#).

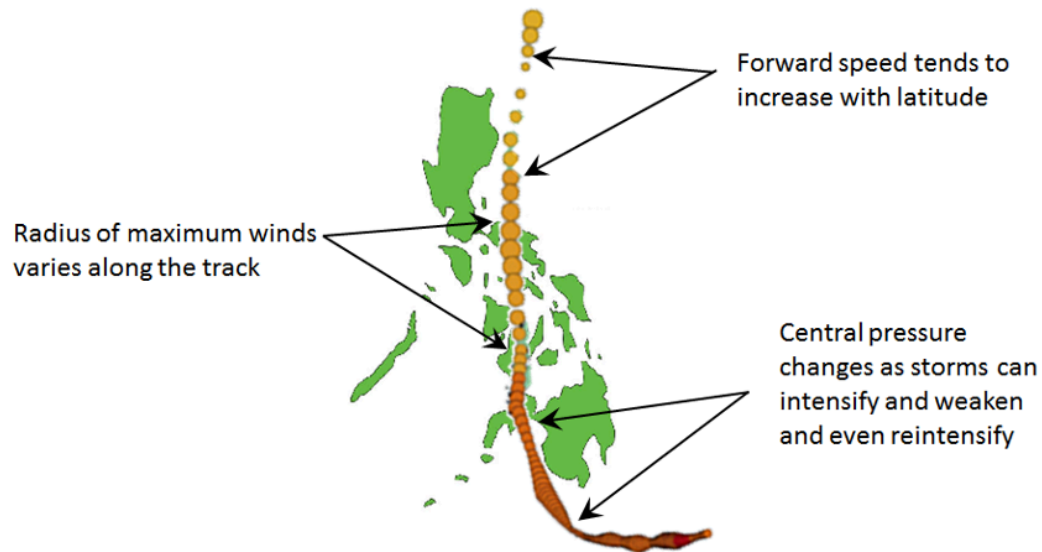


**Figure 68. Storm parameters vary along the storm track**

#### Forward speed

Forward, or translational, speed is the rate at which a typhoon moves from point to point along its track. In general, the higher the latitude of a typhoon, the faster the forward speed. Forward speed varies along the storm path, and the values observed at each time step are again correlated with the values observed at previous time periods.

An analysis of the auto-correlation function for historical storms shows that the dependence in forward speed can be represented by a first-order autoregressive model:

$$Fs_t = a_{f0} + a_{f1} Fs_{t-1} + \varepsilon_t$$

Where:

$Fs_t$  is the forward speed at time  $t$

$a_{f0}$  and  $a_{f1}$  are parameters estimated from the historical data

$\varepsilon_t$  is a noise or disturbance term

To capture the spatial variation in forward speed, the model domain is divided into 13 5°-latitude bands, in which the parameters  $a_0$  and  $a_1$  are estimated for each latitude band.

The combination of the simulated forward speed and storm direction determines the location of each simulated storm at successive time steps. This methodology yields smooth transitions in forward speed as the storm latitude changes.

## Central pressure

Central pressure is the primary determinant of typhoon wind intensity. To develop a procedure for simulating central pressure along the storm path, Verisk has performed a time-series analysis of all historical storms to determine the dependence structure present in the data between consecutive six-hour time intervals. This dependence was measured by computing the auto-correlation function for each storm. The pattern of the computed auto-correlation function indicates that the dependence over time can best be described using a second-order auto-regressive model. According to this model, the central pressure  $Cp_t$  at time  $t$  can be represented as:

$$Cp_t = a_0 + a_1Cp_{t-1} + a_2Cp_{t-2} + \varepsilon_t$$

Where:

$Cp_{t-1}$  and  $Cp_{t-2}$  are the central pressures at time  $t-1$  and  $t-2$ , respectively,

$a_0$ ,  $a_1$ , and  $a_2$  are constants estimated from the data, and

$\varepsilon_t$  is a random disturbance term.

The estimation of the constants is carried out using the method of least squares. To capture the spatial variation in the coefficients, the parameters were estimated for each  $2.5^\circ \times 2.5^\circ$  grid cell in the model domain.

The modeled distribution of landfalling storms by intensity is shown in [Figure 69](#). The modeled distribution is not imposed directly, but rather results from the dynamic second-order auto-correlation procedure.

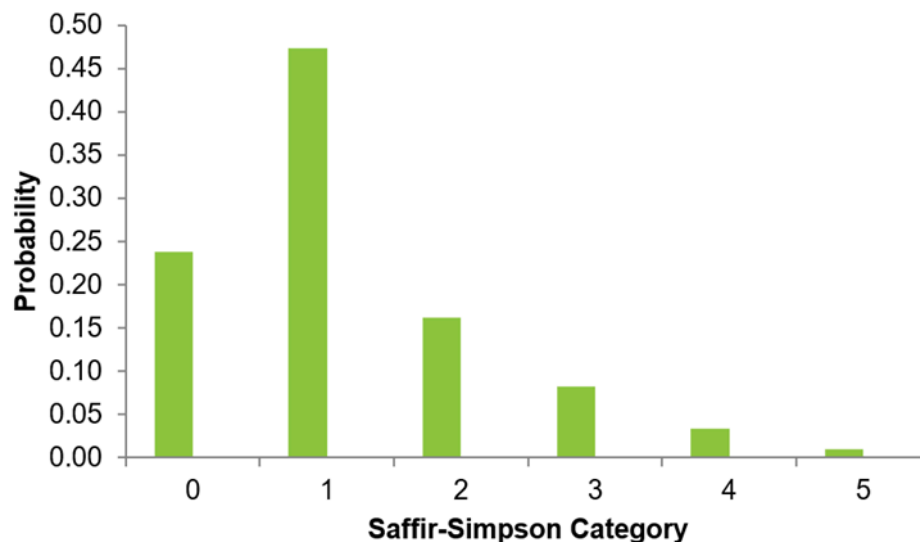


**Figure 69. Simulated storm counts by intensity category at landfall**

## Radius of maximum winds

The radius of maximum winds ( $R_{max}$ ) is the distance from the storm's center, or eye, to where the strongest winds are found. On average, the  $R_{max}$  tends to be larger at latitudes farther from the equator and smaller for more intense storms. These relationships are

explicitly accounted for in the model. While a smaller Rmax can correspond to greater storm intensity, it does not necessarily mean that losses will be greater, as a smaller radius usually results in a smaller affected area.

In the Verisk Typhoon Model for Southeast Asia, Rmax is calculated by a regression relationship dependent on central pressure and latitude, with serial correlation:

$$\ln(Rmax_t) = \beta_0 + \beta_1\varphi_t + \beta_2(Cpw_t - Cp_t)^2 + \varepsilon_t$$

Where:

Cpw<sub>t</sub> and Cp<sub>t</sub> are peripheral and central pressure at time t, respectively, and  $\varphi_t$  is the storm latitude at time t.

The disturbance term  $\varepsilon$  at time period t is a linear function of the disturbance at the previous time period t-1, and a normally-distributed perturbation  $\eta$ :

$$\varepsilon_t = \alpha\varepsilon_{t-1} + \eta$$

where  $\alpha$  is a constant.

This first-order autoregressive model captures time-series correlation in Rmax and has the effect of limiting unrealistic fluctuations in Rmax from one time period to the next.

### 3.4 Storm filling

As storms move inland, their intensity typically begins to dissipate. Central pressure rises and the eye of the typhoon begins to fill as it moves away from its energy source, the warm ocean water. The filling module in the Verisk Typhoon Model for Southeast Asia provides an abrupt decrease in intensity post-landfall, which is in line with historical observations.

The model's filling equations capture topographical effects. In addition, the equations are functions of the geographic location—particularly distance from the coastline—and time elapsed since landfall. The filling equation, which captures the rate at which the storm weakens, is:

$$Cp_t = Cp_w - \Delta Cp \cdot \exp(-at^\beta)$$

Where:

Cp<sub>t</sub> is the central pressure at hours t,

t is the number of hours since landfall,

Cp<sub>w</sub> is the peripheral pressure,

$\Delta Cp$  is the difference between the peripheral pressure and the central pressure at landfall, and

$\alpha$  and  $\beta$  are parameters dependent on the latitude and intensity at landfall.

### 3.5 Peak rainfall intensity and rainfall radius

The salient precipitation parameters for stochastic events are peak rainfall intensity and rainfall radius. The peak rainfall intensity (Pmax) is the maximum hourly precipitation rate near the center of the storm. The rainfall radius is the mean distance from the center, in all directions, to which precipitation for the event extends.

Peak rainfall intensity (in mm/h) and rainfall radius (in km) have been determined for each event in the catalog, regardless of whether extratropical transition has occurred. These two parameters are modeled as log-normal distributions based on satellite imagery and data from the Tropical Rainfall Measuring Mission (TRMM). Global Summary of the Day (GSOD) data from the National Climatic Data Center (NCDC) and data from the Korea Meteorological Administration (KMA) was used for validation purposes.

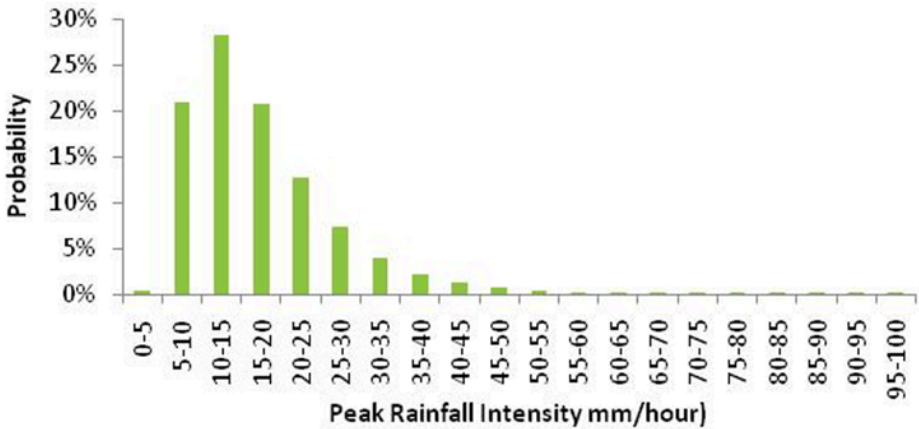


Figure 70. Peak rainfall intensity distribution

The distribution for rainfall radius intensity is shown in [Figure 71](#).

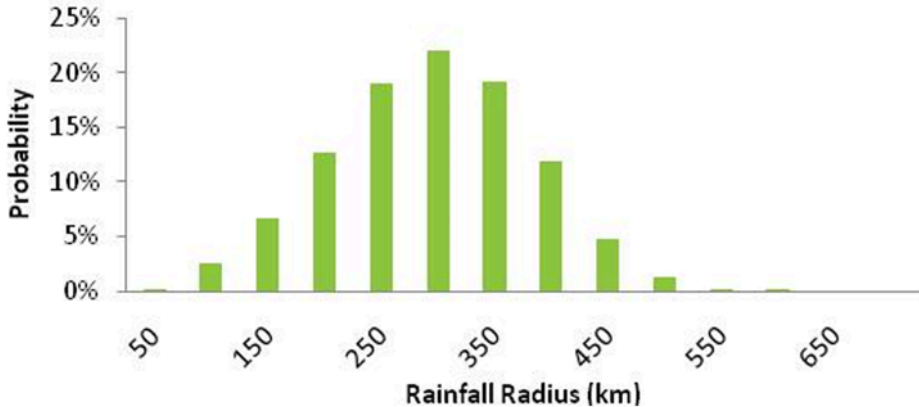


Figure 71. Rainfall radius distribution

See Also [Extratropical transition](#)

[Typhoon-induced precipitation and inland flood intensity](#)

## 3.6 Extratropical transition

While tropical and extratropical cyclones are distinctly different phenomena, it is not unusual for the former to evolve, or transition, into the latter. At some point in their predominately east-to-west track through the tropics, a typhoon may begin to move poleward, where it encounters cooler sea surface temperatures and increased vertical wind shear associated with the mid-latitude westerlies. These and other factors cause the typhoon to increase its forward speed, lose its symmetric cloud shield, and, at times, reintensify rapidly into a powerful extratropical cyclone.

Approximately 45 to 50% of typhoons in the Northwest Pacific Basin undergo extratropical transition. The resultant storm typically has a larger wind and precipitation footprint than it did as a typhoon—and it can still pose a serious threat to land and sea interests.

Because extratropical transition is a frequent and significant influence on precipitation, the hour at which transition occurs during an event is included in the model. Using six hourly data from JMA, Weibull distributions were fitted to the recorded latitude at which extratropical transition occurred, resulting in a total of twelve Weibull distributions (one for each month).

Using the genesis day for each storm, a latitude was drawn from the corresponding monthly Weibull distribution and compared to the storm's path. The first hour that the center of the simulated storm moves north of this latitude is the hour of extratropical transitioning in the model; otherwise, the storm does not transition.

[Figure 72](#) and [Figure 73](#) compare the cumulative probabilities of extratropical transition, by month and latitude, based on the 1951-2006 historical record and stochastic catalogs, respectively. The greatest inter-seasonal variability is observed in the 30 to 40 degree latitude band (indicated by the dark brown bars). During the summer months, there is a small probability that storms will have transitioned by the time they reach these latitudes. During the fall months, however, there is a strong likelihood they will have undergone transition by the time they reach these latitudes. The stochastic distribution shows good agreement with the historical.

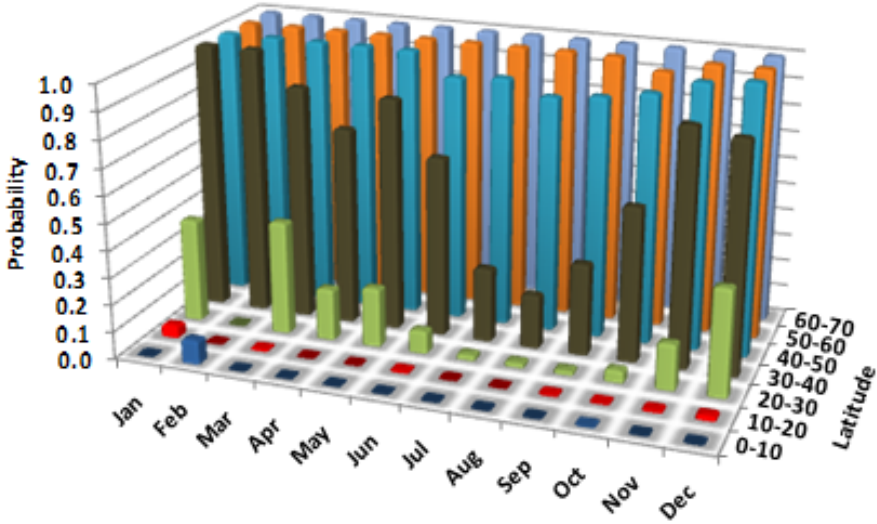


Figure 72. Extratropical transitioning by month and latitude, historical

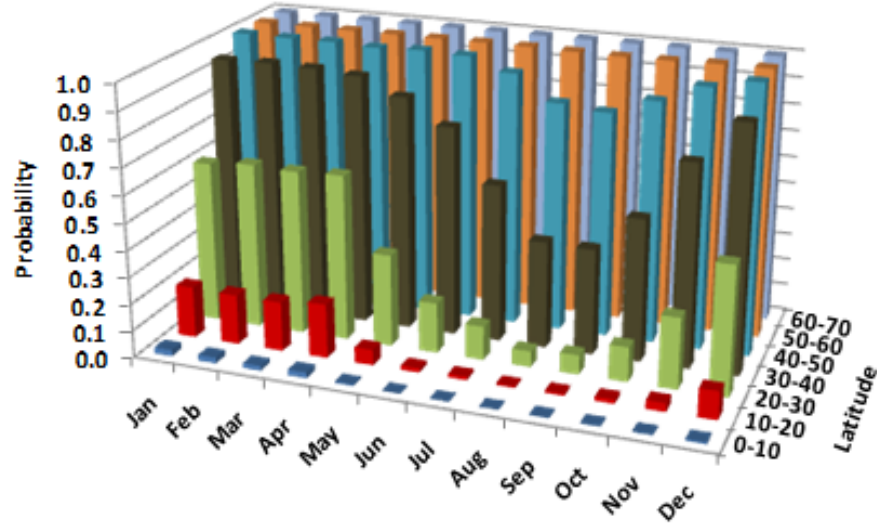


Figure 73. Extratropical transitioning by month and latitude, simulated

### 3.7 Stochastic catalog statistics

The Verisk Typhoon Model for the Northwest Pacific Basin has a 10,000-year catalog containing more than 293,000 simulated events in the domain. Of these, 121,581 events cause loss in Southeast Asia. Of the loss causing events, 92,006 make landfall and 29,575 bypass the modeled countries/territories at a range that is close enough to still cause damage. The maximum number of landfalls in a single simulated year is 18. (Note that a

single storm can make multiple landfalls.) However, the probability of such an extreme year is very low, at just 0.01%.

## 3.8 World Scenarios event set

Verisk's Extreme Disaster Scenario (EDS) events supported in the Verisk Typhoon Model for Southeast Asia are included in the World Scenarios event set in both Touchstone and CATRADER. The World Scenarios event set is meant to provide additional touchpoints to assist in assessing large loss potential. While they represent unlikely—and in some cases extremely unlikely—scenarios, they are nevertheless scientifically plausible.

Note that these events are not included in the model's 10,000-year stochastic catalogs and no attempt has been made to assign an associated probability of occurrence or return period. They should be seen as deterministic scenarios. The losses from some World Scenarios events may lie beyond the 0.01% exceedance probability (10,000 year return period). Others may be much further down the exceedance probability curve, but may be events that impact concentrations of exposure characterized by high take-up rates. They are events that standard stochastic modeling techniques are unlikely to capture, either because of the relative scarcity of historical data or because a full scientific consensus on their likelihood has not yet been reached.

The names and brief descriptions of the EDS supported in the Verisk Typhoon Model for Southeast Asia are provided in the following subsection and their associated modeled loss estimates are available in Section 1.

### See Also

[Modeled losses for Extreme Disaster Scenarios](#)

## Extreme Disaster Scenarios (EDS)

The Verisk Typhoon Model for Southeast Asia supports four Extreme Disaster Scenarios (EDS), listed in [Table 19](#).

**Table 19. Extreme Disaster Scenarios in the World Scenarios event set for the Verisk Typhoon Model for Southeast Asia available in CATRADER 18.0 and Touchstone 4.0**

World Scenarios Event ID	Event Name	Modeled Country/Territory Affected
6	EDS SE Asia Typhoon Philippines	Philippines
7	EDS SE Asia Typhoon Taiwan	Taiwan
8	EDS SE Asia Typhoon Hong Kong	Hong Kong
9	EDS SE Asia Typhoon Vietnam	Vietnam

All four EDS are variations of events in the model's historical event set and are comprised of realistic and scientifically sound and would inflict a very high degree of damage on Southeast Asia, if they were to occur. Important characteristics of these EDS are provided below.

**EDS SE Asia Typhoon Philippines** is a wind event based on Typhoon Haiyan (2013), but passing over Manila with a more intense central pressure at the time it passes over Manila.

**EDS SE Asia Typhoon Taiwan** is a flood event with landfall along the western coast of Taiwan, near the more highly populated areas. This storm is based on Typhoon Thelma (1956) with a shifted track and a stronger central pressure. The forward speed of the storm was slowed down and the Pmax was intensified greatly.

**EDS SE Asia Typhoon Hong Kong** is a strong wind event where the path was taken from Typhoon Rose (1971) with a more intense central pressure.

**EDS SE Asia Typhoon Vietnam** Vietnam is a flood event based off a typhoon from the stochastic catalog. It was one of the more highly ranked losses for the country. The Pmax was reduced and path changed to have a more direct landfall.

### 3.9 Validating stochastic event generation

Verisk catastrophe models are extensively validated. Every component of the model is carefully verified against data obtained for historical events. This section provides a few exhibits illustrating the results of the validation process.

#### Validating frequency

Annual typhoon frequency of occurrence in the model domain is represented by a Poisson distribution. [Figure 74](#) shows a comparison between historical and simulated frequency while [Figure 75](#) shows a comparison between simulated and historical seasonality at genesis.

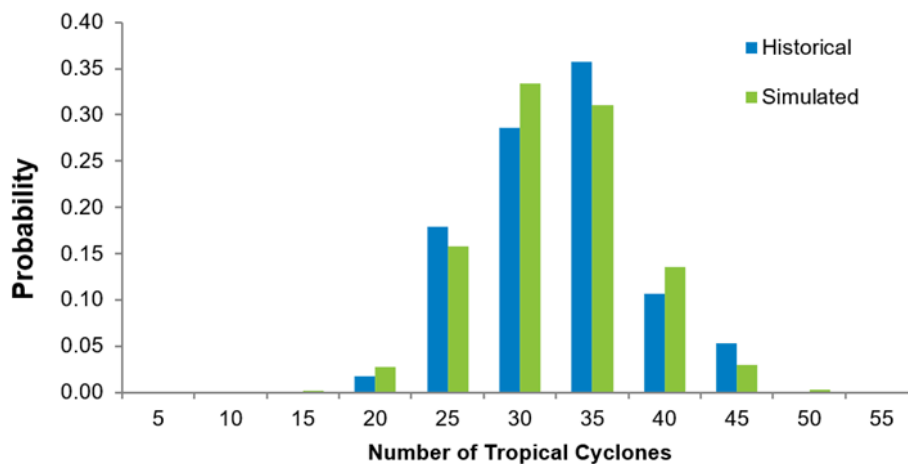


**Figure 74. Historical vs. simulated annual frequency of typhoons in the model domain**

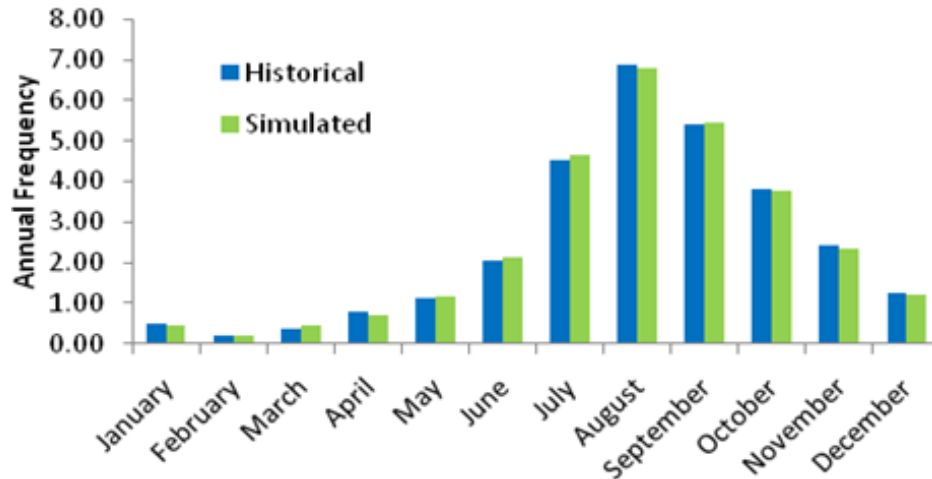


**Figure 75. Comparison of historical and simulated annual frequency at genesis for typhoons in the model domain**

Figure 76 shows a comparison between the historical and simulated frequency of landfalling typhoons in Southeast Asia while Figure 77 shows a comparison between the historical and simulated number of landfalls per event. Note that the stochastic distribution is not imposed. Rather, it results naturally from the underlying dynamics of the storm track generation procedure, providing further validation of that procedure. Apparent anomalies in the historical frequencies—such as years in which 10 typhoons make landfall—are the result of the relative sparseness of historical data.

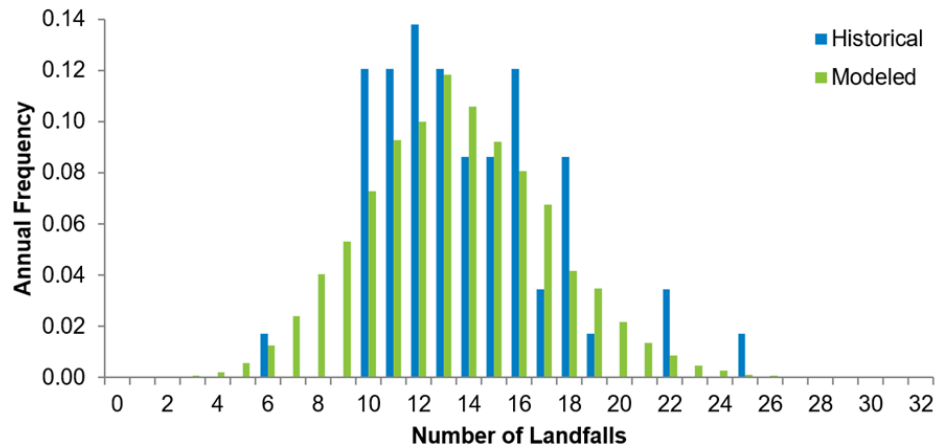


**Figure 76. Historical vs. simulated annual frequency of landfalling typhoons in Southeast Asia**

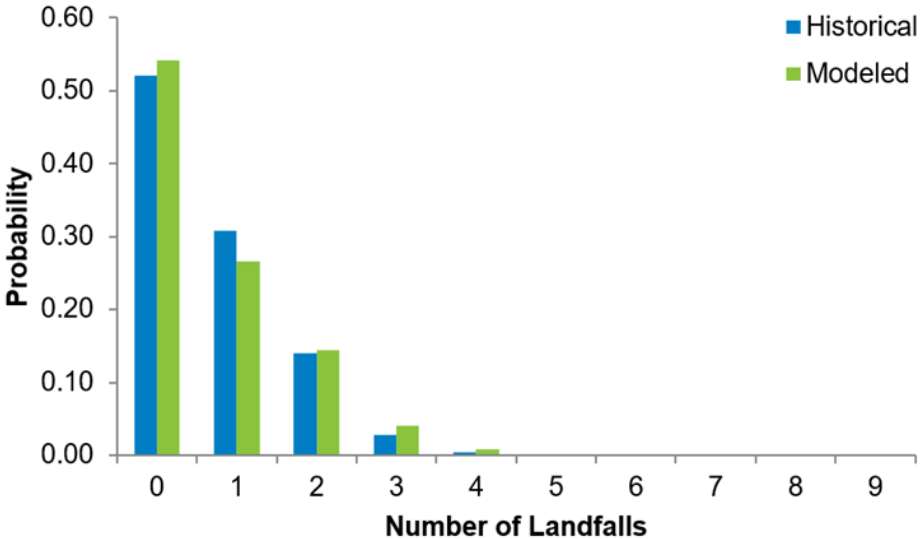


Figure 77. Historical vs. simulated number of landfalls per event in Southeast Asia

### Validating storm tracks

Figure 78 shows historical (blue) and simulated (red) storm tracks for a sample 25-year period. The simulated tracks appropriately capture the tendency for storms to move first in a westerly direction and then to curve to the northeast.

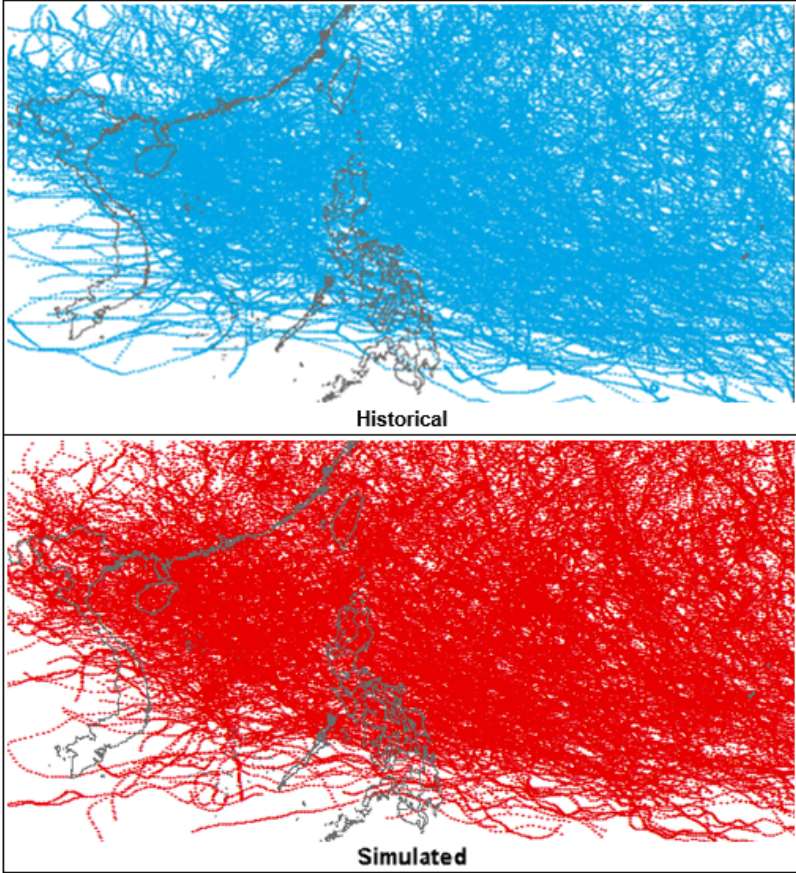
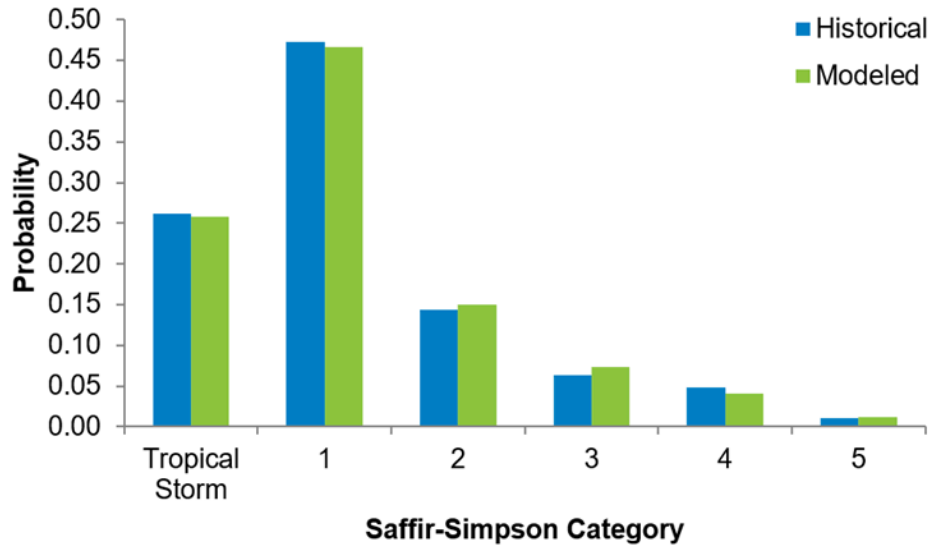


Figure 78. Historical and Verisk-simulated typhoon tracks for a 25-year period

### Validating meteorological parameters at landfall

A comparison between the historical and simulated typhoon intensity at landfall is presented in [Figure 79](#). Note that the distribution is not imposed, but rather results from the dynamic second-order auto-correlation procedure described above, further validating that procedure.



**Figure 79. Historical and Verisk-modeled typhoon intensity category at landfall**

Modeled and observed frequencies by intensity compare favorably but are different because many simulated events that result in very low levels of loss are excluded from the stochastic catalog, in order to optimize computational efficiency.

A comparison between the average values at landfall of historical and Verisk-modeled central pressure, Rmax, and forward speed is provided in [Table 20](#). The good agreement between historical and stochastic mean values is further demonstrates the validity of the 10,000-year catalog.

**Table 20. Historical vs. simulated typhoon variable values at landfall**

Typhoon Variable	Historical Typhoons (1951-2008)	Verisk-Modeled Typhoons (10,000-year catalog)
Average Central Pressure (mb)	986	985
Average Radius of Maximum Winds at Landfall (km)	28	28
Average Forward Speed at Landfall (km/h)	23	24

## Validating storm density

All storms generated for the stochastic catalog are used to validate the number of storms that affect the model domain per season. To determine the storm density across the region, the number of storms whose track passes through a one-degree grid cell was determined for the historical data, and compared to the stochastic catalog. [Figure 80](#) shows excellent agreement between the seasonal storm track density for historical and stochastic seasons.

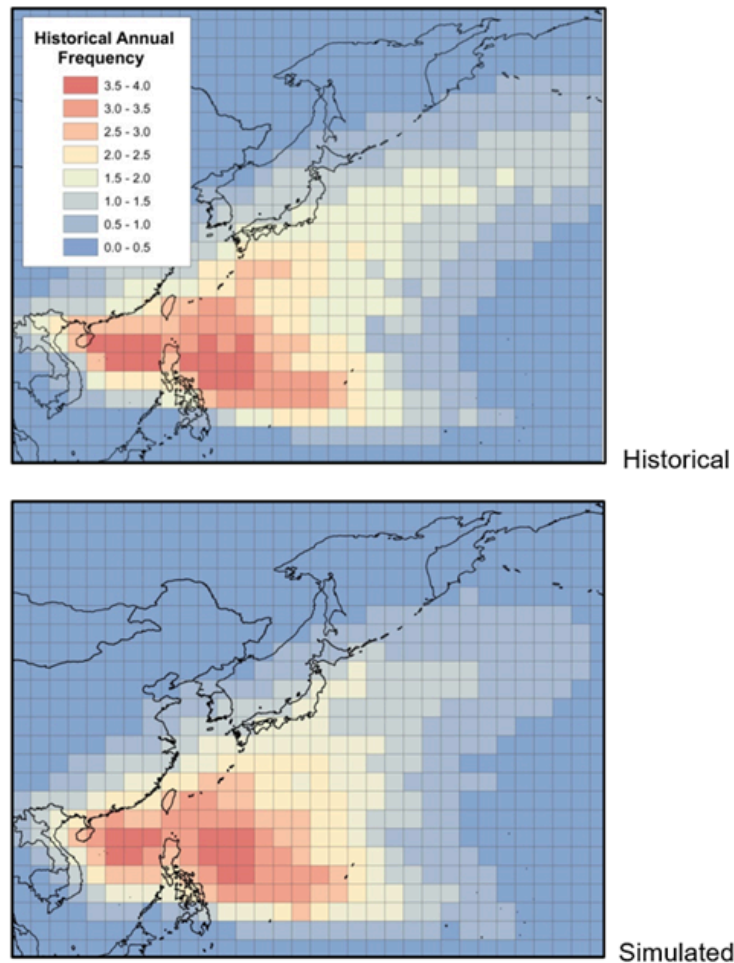


**Figure 80. Comparison between historical and simulated annual storm track density**

## Validating regional distribution of events

It is common for Northwest Pacific typhoons to impact more than one country due to the geography of the region and the dominant tracks there of typhoons. In fact, approximately 60% of loss-causing events cause loss to multiple countries. Therefore, an important consideration when modeling typhoons in the Northwest Pacific Basin is ensuring that the country or countries affected by individual stochastic storms make geographic and meteorological sense.

To analyze the regional distribution of storms in the catalog, Verisk researchers examined the other countries that incurred losses from each individual storm that caused loss in Southeast Asia. For each storm, researchers looked at which countries had ground-up losses that were at least USD 40,000. Countries with losses below this amount were not included.

[Figure 81](#) illustrates the stochastic results for Southeast Asia. For each storm that caused ground-up losses exceeding USD 40,000, the figure shows the combinations of countries that also incurred losses exceeding that amount from one storm. Note that combinations including other countries that are not part of the Verisk Typhoon Model for Southeast

Asia (i.e., China, Japan, and South Korea) are not included in the analysis. A comparison with historical storms from a loss causing standpoint is not included because not all of the historical storms are calibrated from a wind and precipitation standpoint in order to accurately generate loss and hence exceed the threshold in order to be counted.

However, from a stochastic standpoint, the results as shown in [Figure 81](#) make sense. That is a significant number of events impact only the Philippines as they are in many instances the first and only target from storms with genesis at tropical latitudes. The next most frequent occurrence is storms impacting only Vietnam, followed by Taiwan, Philippines-Vietnam, and Philippines-Taiwan. Once again, a comparison of the genesis locations in a previous section and the expected WNW trajectories of the storms in the latitude ranges of the countries mentioned support the results shown in [Figure 81](#).

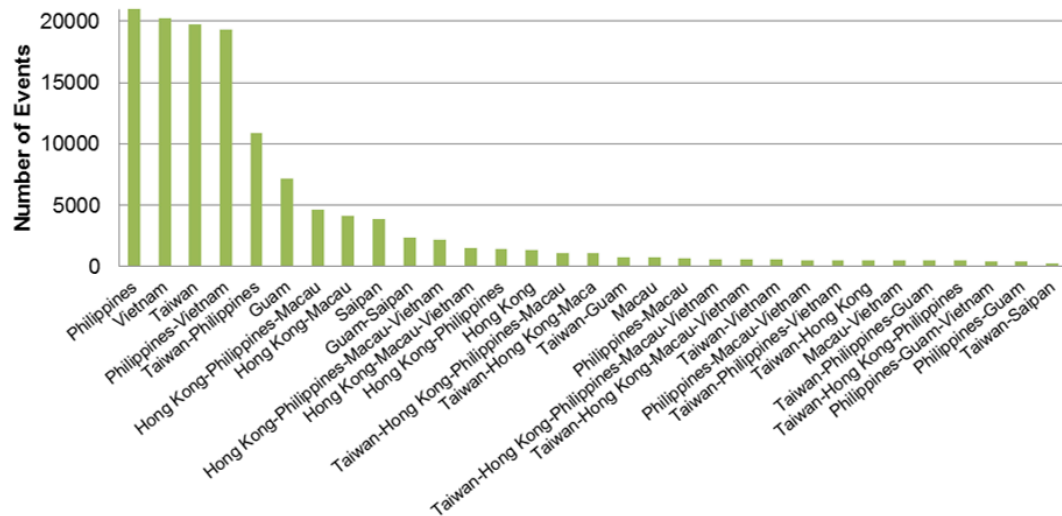


**Figure 81. Simulated multi-country loss-causing events for Southeast Asia**

### 3.10 Generating simulated storm surge events

The Verisk Typhoon Model for Southeast Asia allows explicit estimation of damage and loss from the storm surge sub-peril. Not all typhoons making landfall produce a sufficiently large storm surge to cause loss, as strong winds are required to produce a large storm surge. Other factors influencing the storm surge threat include bathymetry and tide. A given typhoon will typically produce a larger storm surge along a coastline with shallow sloping bathymetry than one with steep bathymetry. Background astronomical tide level—that is, the water height that would have been observed in the absence of a storm—influences the total water level seen during a typhoon event.

Therefore, not all events in the 10,000-year stochastic catalog produce storm surge loss. Because SuWAT, the dynamical model used to calculate storm surge, is computationally intensive, it is preferable to run the model at high resolution only for events that produce

significant storm surge. To determine whether an event of the stochastic catalog can produce large storm surge at the coast, a two step process is employed:

- Events that pass within 50 miles of the coastline of Southeast Asia with a central pressure of less than 985 mb are simulated with SuWAT at a coarse resolution (either 2.5-km or 5.0-km).
- Then, if the sum of the maximum storm surge plus the event tide is greater than a threshold value, the event is simulated with SuWAT at high (250-m or 500-m) resolution.

## Storm surge model domain

In the Verisk Typhoon Model for Southeast Asia, storm surge hazard is calculated at high resolution within the Philippines (500-m grid spacing), Taiwan (250-m grid spacing), and Hong Kong (250-m grid spacing) using 47, 4, and 1 nests, respectively. These high-resolution, or “specific location,” domains are nested within larger, region resolution (2,250-m) domains, which are nested within country resolution (6,750-m) domains, nested within the lowest resolution domain, which covers the entire region of interest. Presented in [Figure 82](#) is an example of a 500-m grid centered on Manila, nested within the two coarser grids. The medium and low resolution domains provide the boundary conditions for the higher resolution nest that they contain, and are sufficient in size to accurately capture the characteristics of the storm surge as the events approach the coast.

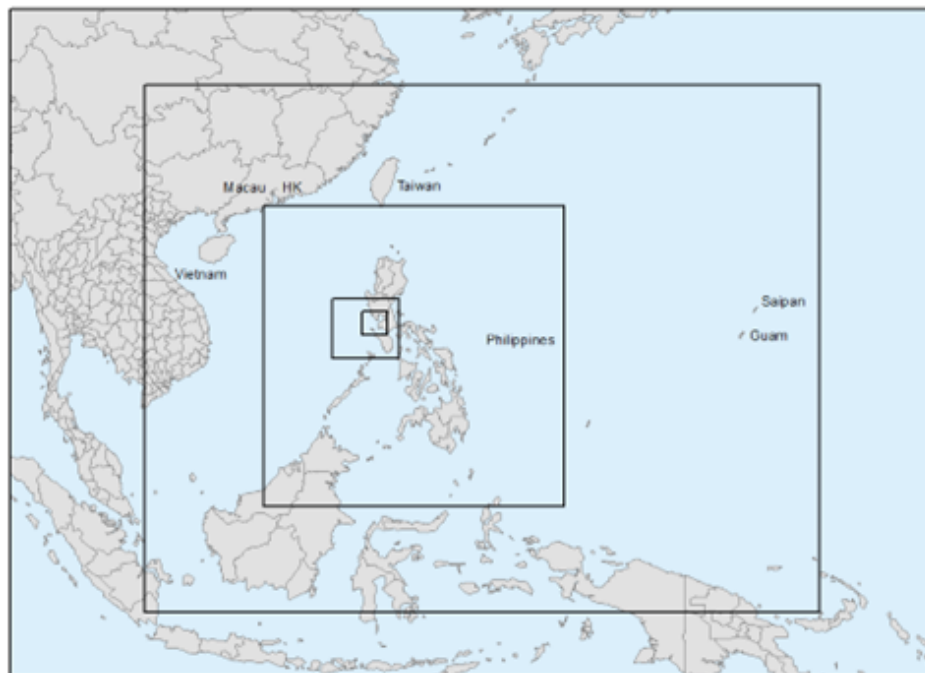


**Figure 82. Specific location (500-m resolution) grids, nested within region grids (2,250-m resolution), nested within country grids (6,750-m resolution), nested within the model domain**

### See Also

[Storm surge intensity](#)

# 4 Local Intensity Calculation

The measures of intensity used in the Verisk Typhoon Model for Southeast Asia are:

- 10-m, 1-minute sustained winds
- Flood depth (accumulated runoff) in mm
- Storm surge depth (m) and water velocity (m/s)

Their derivation and implementation in the model are described below.

## 4.1 Local wind intensity

The generation of the local wind field involves first computing the gradient wind at each model domain point as a function of central pressure, Rmax, latitude, distance from the storm center, and forward speed and direction—and then downscaling the gradient wind to the surface.<sup>6</sup> In the model, gradient wind speed is calculated based on the work of Willoughby et al. (2006).

This gradient wind profile is empirically derived and is defined by three equations: one for the region inside of the eyewall, one for the eyewall region, and one for the region outside of the eyewall. The formulation uses two tunable parameters ( $X_1$ ,  $X_2$  in the equations below) for defining the rate of decay of winds outward from the eyewall. This approach provides a high degree of flexibility to better match the observed rapid wind decay rate near the eyewall and the more moderate decay further away from the eyewall. The result is a gradient wind profile that compares well with observational data.

The gradient wind profile incorporated in the Verisk model is as follows:

$$\begin{aligned}V_{gr}(r, Rmax, \theta, V_{gr\_max}) &= V_{gr\_inner} = V_{gr\_max} (r/Rmax)^n \quad (0 < r < R_1) \\(r, Rmax, \theta, V_{gr\_max}) &= V_{gr\_inner}(1-w) + V_{gr\_outer}(w) \quad (R_1 < r < R_2) \\V_{gr}(r, Rmax, \theta, V_{gr\_max}) &= V_{gr\_outer} \\&= V_{gr\_max} [ (1-A) \exp(- (r-Rmax)/X_1) + A \exp(- (r-Rmax)/X_2) ] \quad (R_2 < r)\end{aligned}$$

Where:

$V_{gr}$  is the gradient wind speed of a stationary typhoon,

$V_{gr\_max}$  is the maximum gradient wind speed of a stationary typhoon,

$V_{gr\_inner}$  is the gradient wind speed of a stationary typhoon inside Rmax,

$V_{gr\_outer}$  is the gradient wind speed of a stationary typhoon outside Rmax,

$r$  is the distance from the storm center,

Rmax is the radius of maximum winds,

$\theta$  is the latitude,

$w$  is the ramp function for smooth transition from inner to the outer profile,

<sup>6</sup> Gradient wind is the flight-level wind, or the wind at the top of the planetary boundary layer, which is the point at which the earth's surface no longer imparts any effect on the wind. That is, gradient wind is the large-scale wind field balanced between the pressure gradient force and the Coriolis and centrifugal forces, in the absence of friction effects.

$R_1$  is the inner eyewall radius,

$R_2$  is the inner eyewall radius,

$A$  is the parameter to proportion the two exponentials in the profile,

$X_1$  and  $X_2$  are decay length parameters, and

$n$  is the exponent for the power-law dependence within the eye.

$X_2$  is a fixed distance equal to 25 km, and  $w$  is a function of  $R_1$  and  $R_2$ .  $X_1$ ,  $n$ , and  $A$  are functions of  $V_{gr\_max}$ ,  $R_{max}$ , and  $\theta$  as follows:

$$X_1 = 287.6 - 1.942V_{gr\_max} + 7.799(\ln(R_{max})) + 1.1819\theta$$

$$n = 2.1340 + 0.0077V_{gr\_max} - 0.4522(\ln(R_{max})) - 0.0038\theta$$

$$A = 0.5913 + 0.0029V_{gr\_max} - 0.1361(\ln(R_{max})) - 0.0042\theta \quad (A > 0)$$

## The relationship between central pressure and wind speed

The maximum gradient wind speed,  $V_{gr\_max}$  (m/s), is calculated from a  $C_p$ -wind relationship derived from JMA best track data from 1977 to 2012, as follows:

$$V_g = (-0.004843085345 \times \Delta P^2 + 1.418892505994 \times \Delta P + 23.6528) \div 0.9, \quad \Delta P \leq 60 \text{ mb}$$

$$V_g = (0.775 \times \Delta P + 45) \div 0.9, \quad \Delta P > 60 \text{ mb}$$

Where:

$$\Delta P = P_{env} - C_p$$

$P_{env}$  = peripheral pressure = 1006 mb, and

$C_p$  = central pressure.

This relationship is derived by Verisk meteorologists using data specific to the Northwest Pacific Basin ([Figure 83](#)). In the figure, the JMA best track data is compared to the relationship used in the Verisk Typhoon Model for Southeast Asia. Verisk's relationship is in good agreement with the data.

As the tropical Pacific Ocean is much larger than the tropical Atlantic Ocean, sea surface temperatures are warmer and thus typhoons that occur in the Northwest Pacific Basin typically experience lower environmental pressures and are larger than their North Atlantic Basin counterparts. It has been observed that for the same central pressure, Northwest Pacific typhoons tend to have lower wind speeds than North Atlantic hurricanes. It is therefore important to use a region-specific  $C_p$ -wind relationship.

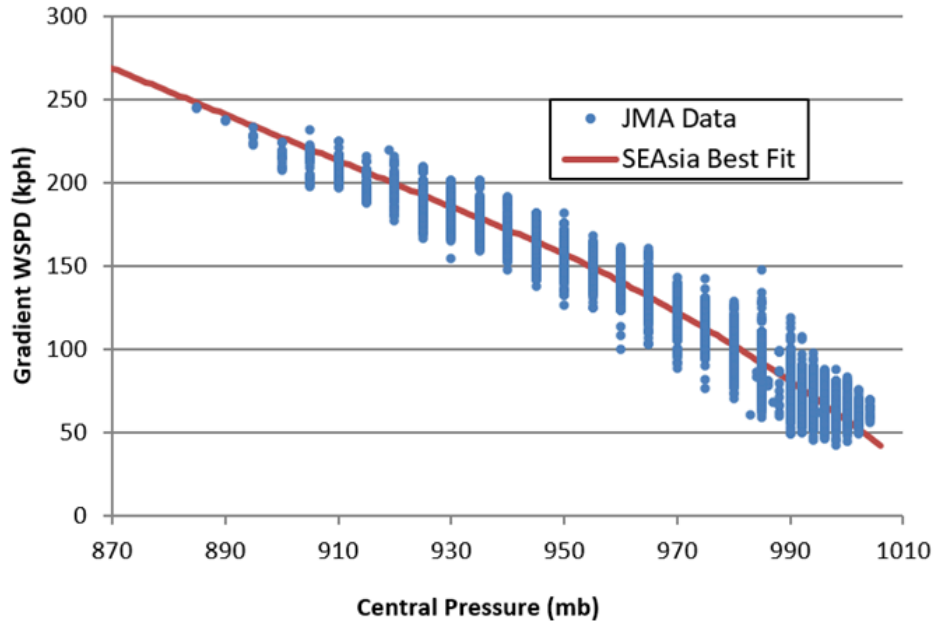


**Figure 83. Relationship between central pressure and wind speed**

## Peripheral pressure

The peripheral, or environmental, pressure ( $P_{env}$ ) is the sea level pressure at the last closed isobar of the typhoon circulation. Because the radius to the outer closed isobar typically ranges between 500 and 1000 km, another definition is the azimuthally-averaged sea level pressure at a fixed distance from the storm center. It is important to note that Northwest Pacific typhoons are the largest, on average, in the world (perhaps 50% larger than North Atlantic typhoons) and therefore a larger radius is required.

Scientists at Verisk analyzed the NCEP-NCAR Reanalysis Project (NNRP) 2.5° global dataset (1951-2008) and calculated the azimuthally-averaged sea level pressure at 750 km and 1000 km from the blended STI and JMA historical best track data (6-hourly) storm centers. An average of those values for all points within 10° of mainland Southeast Asia resulted in a peripheral pressure value of 1010 mb. This result is very similar to that of Knaff and Zehr (2007) who used a fixed distance of approximately 1000 km, resulting in a value of 1006 mb, but for the entire Northwest Pacific Basin.

## Asymmetry effect

In the Northern Hemisphere, typhoon winds rotate counterclockwise. The combined effects of typhoon winds and forward motion (or translational speed) will produce higher wind speeds on the right-hand side of the storm. The model captures this via the term  $F_{asym}$  in the equation below (from NOAA Technical Report NWS-23). In doing so, the model accounts for the dynamic interaction of translational and rotational speeds, as well as the inflow angle.

$$F_{asym} = 1.5(T^{0.63})(T_0^{0.37}) \cos\beta$$

Where  $T$  is the forward speed in knots,  $T_0$  is the conversion from knots to kilometers per hour, and  $\beta$  is the angle between the track direction and the surface wind direction.

## Topographical effects

Wind speeds increase on the windward slopes of mountains, hills, and escarpments because of amplification. Such features restrict the passage of wind, causing a compression of the streamlines, or the areas through which wind must travel. As wind speed is inversely proportional to the spacing of streamlines, wind accelerates as it moves uphill (Figure 84).

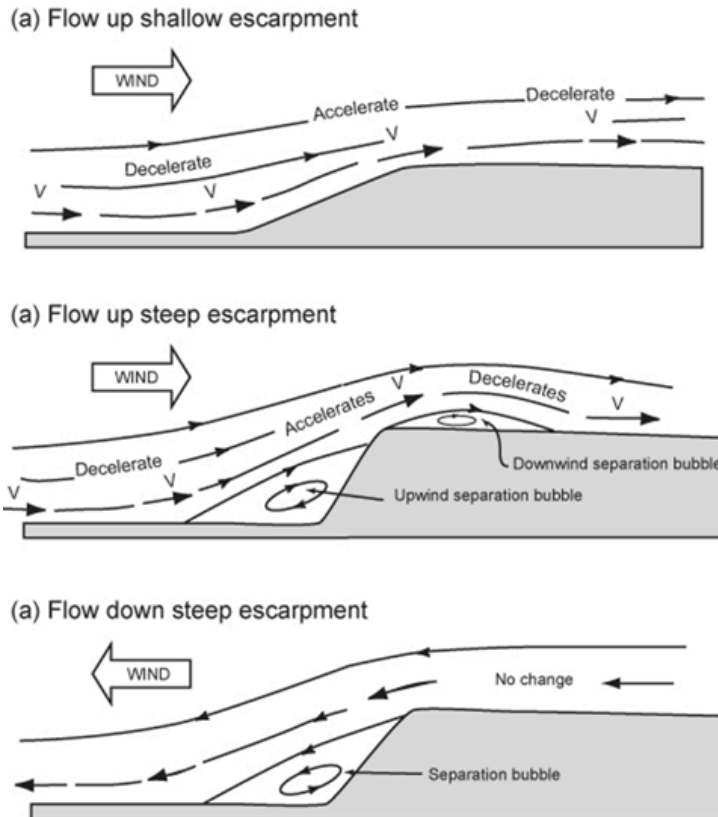


**Figure 84. Effects of topography on wind**

The slope of the incline determines the degree of compression, so the amplification effect is accentuated on steeper hills. In addition, if the angle of incline is sharp, wind flow separates because momentum near the ground is insufficient to overcome the pressure gradient at the top. A turbulent "separation bubble" is established, which causes local vortices and high suction loads/stresses, increasing potential damage.

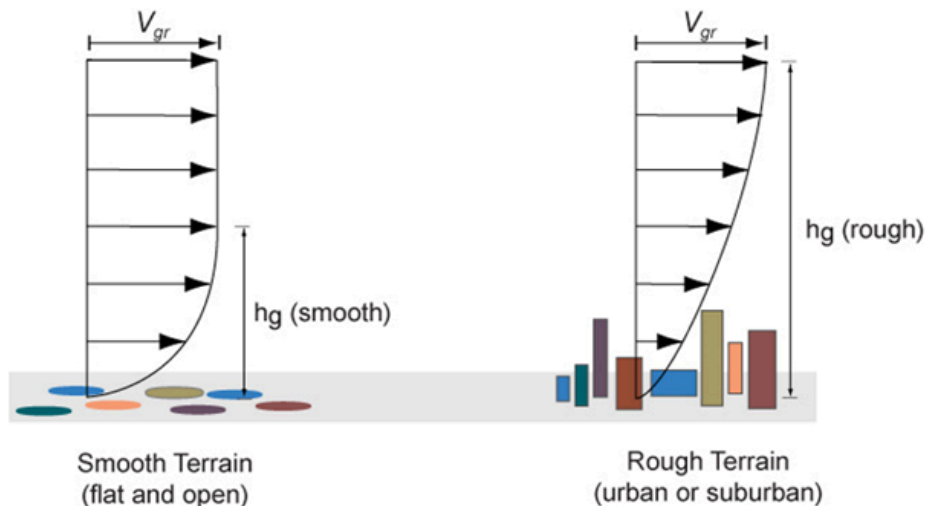
In the case of downhill winds, the leeward slope provides protection. If, however, the slope is sharp, a similar separation bubble manifests itself downwind and counteracts, to some degree, the protection provided by the hill or escarpment.

Using high-resolution topographic data, which is derived from elevation data, the Verisk Typhoon Model for Southeast Asia calculates gust, friction, and topographic values for each

grid cell. The slope angle and distances between each cell centroid are computed and wind amplification and turbulence factors are assigned. The elevation data is based on Southeast Asia's latest digital national land information, which has a native resolution of 100 m. The data was aggregated to 1-km resolution for application in the model.

## Surface friction effects on wind speeds

Differences in surface terrain on a smaller scale also affect wind speeds. Wind velocity profiles (Figure 85) typically show higher wind speeds at higher elevations. Winds travel more slowly at ground level because of the horizontal drag force of the earth's surface, or surface friction. Obstacles such as buildings will further reduce wind speed.



(Source: adapted from Cook 1985)

**Figure 85. Terrain effects on wind velocity profiles**

The gradient wind occurs 1-2 km above ground level and is therefore independent of the underlying surface conditions, except for the fact that storm intensity after landfall does account for the filling effect. Generation of the local wind field continues by modulating the gradient wind for elevation, sheltering, frictional, and gust effects. The model applies a friction coefficient at each location of interest to reflect estimates of surface roughness derived from digital land-use/land-cover (LULC) data (Figure 88). The LULC data used in the model is based the Moderate Resolution Imaging Spectroradiometer (MODIS) retrieved courtesy of the NASA EOSDIS Land Processes Distributed Active Archive Center (LP DAAC) and USGS/Earth Resources Observation and Science (EROS) Center, Sioux Falls, South Dakota, at a 1-km resolution. As this dataset contains only one urban classification, three urban categories were developed based on work by Grimmond et al. (1999), and on Verisk's Industry Exposure Database. Also, the fetch is 10 km. Fetch is the distance wind travels in a single direction over a relatively smooth surface before reaching a given location. The higher the fetch over water for example, the longer the wind will take to slow down upon reaching the shore. Thus, fetch affects wind speed at a given location.

In practice, wind has to blow over a certain distance before the planetary boundary layer (PBL)<sup>7</sup> is in equilibrium with the underlying surface. Downwind of a change in terrain roughness, such as the edge of an urban area, a new boundary layer begins to grow. Within this new layer the flow is not in equilibrium, and the wind profile adjusts.

The boundary-layer adjustment is accounted for by adjusting the friction factor according to an effective roughness, which is defined as the average surface roughness for an area out to a radius of 10 km (6.2 miles) from the location of interest—and is representative of the mean land surface acting on the wind field at that location.

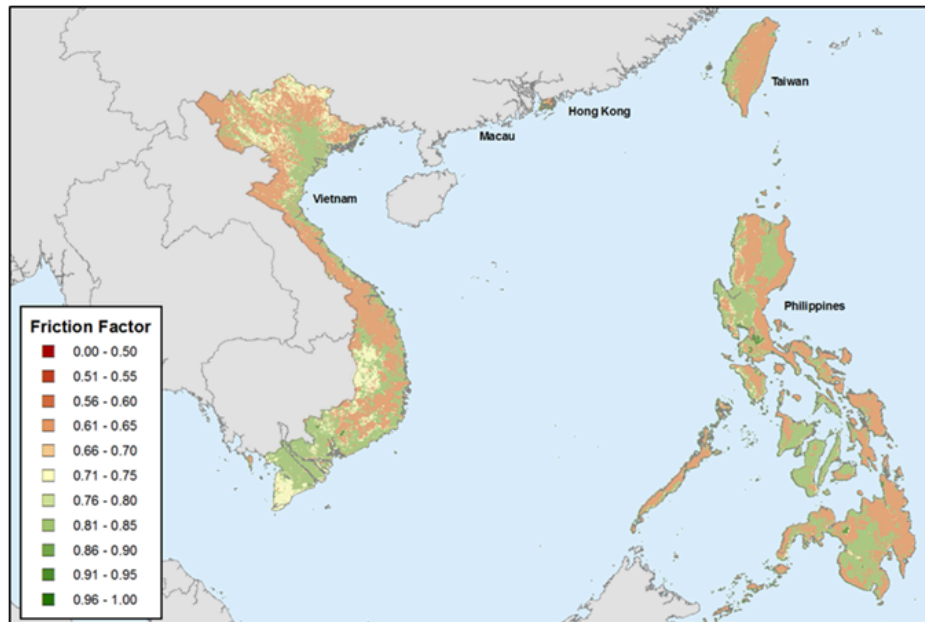


**Figure 86. Verisk friction factors used in the Verisk Typhoon Model for the Northwest Pacific Basin – the Philippines, Taiwan, and Vietnam**

<sup>7</sup> The PBL is the lowest layer of the atmosphere—extending vertically from the surface to between 305 and 610 m— within which surface roughness has an effect on wind speeds. This height, beyond which surface roughness no longer affects wind speeds, is referred to as the gradient height.



**Figure 87. Verisk friction factors used in the Verisk Typhoon Model for the Northwest Pacific Basin – Guam and Saipan**

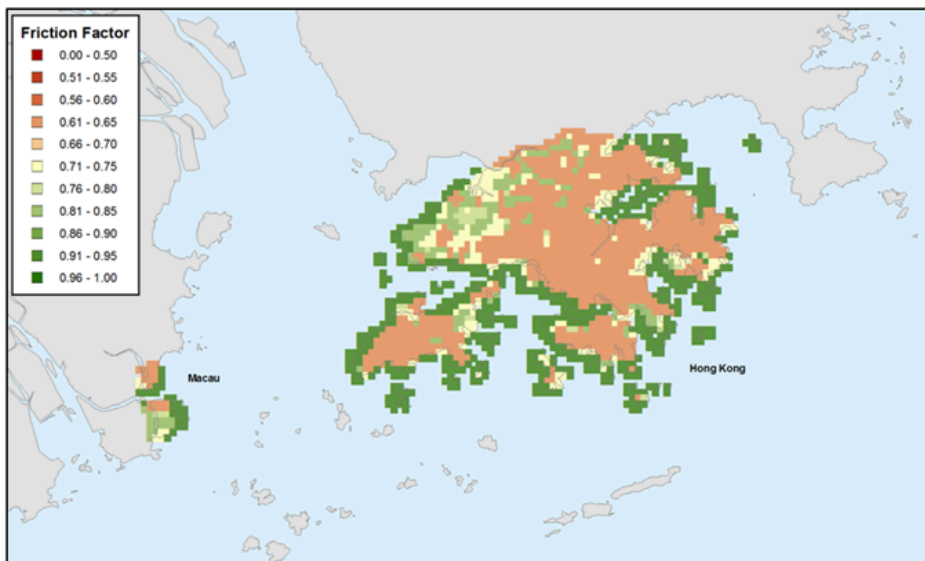


**Figure 88. Verisk friction factors used in the Verisk Typhoon Model for the Northwest Pacific Basin – Macau and Hong Kong**

## Gust effects on surface winds

Just as surface roughness exerts a frictional drag on the winds near the surface, so too can surface roughness enhance gustiness, which is a measure of how the wind speed near the surface varies as a function of time. Generally speaking, winds near the surface—even those in a typhoon that is neither intensifying nor weakening—undergo oscillations that are the

result of eddies of different sizes, which are generated from different land-use and land-cover and can cause temporary increases and decreases in wind speed.

The many eddies that exist at any given time result in different strengths and durations of gusts. These gusts range from very extreme ones that last only several seconds, to weaker ones that can last for several minutes. Typically, very rough surfaces can increase the gustiness, while smooth surfaces tend to be associated with low levels of gustiness. Scientists at Verisk have accounted for the gust effects on typhoon winds not only across different types of surfaces, but also from different directions across those surfaces ([Figure 91](#)).

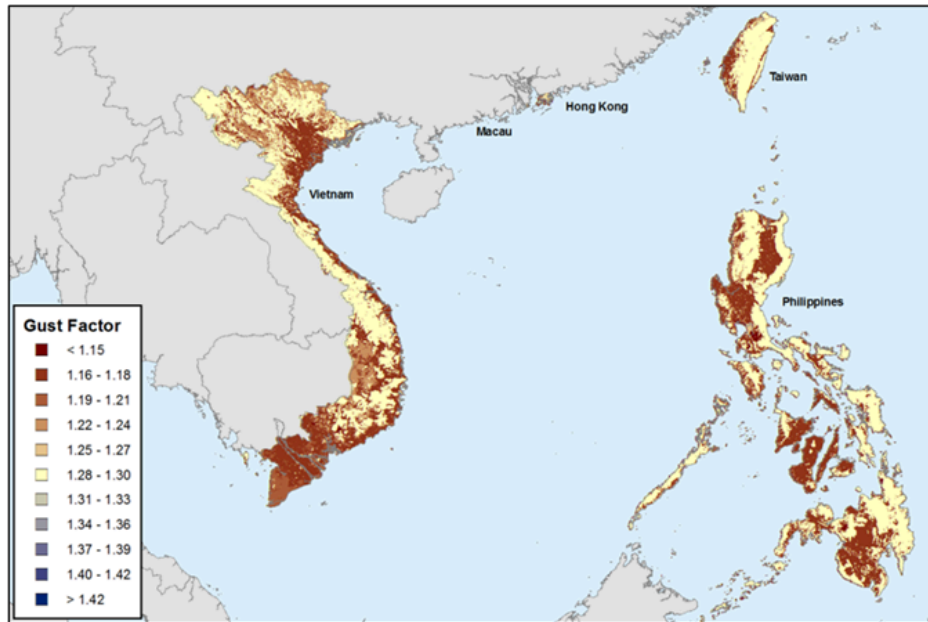


**Figure 89. Verisk gust factors used in the Verisk Typhoon Model for the Northwest Pacific Basin – the Philippines, Taiwan, and Vietnam**



**Figure 90. Verisk gust factors used in the Verisk Typhoon Model for the Northwest Pacific Basin – Guam and Saipan**

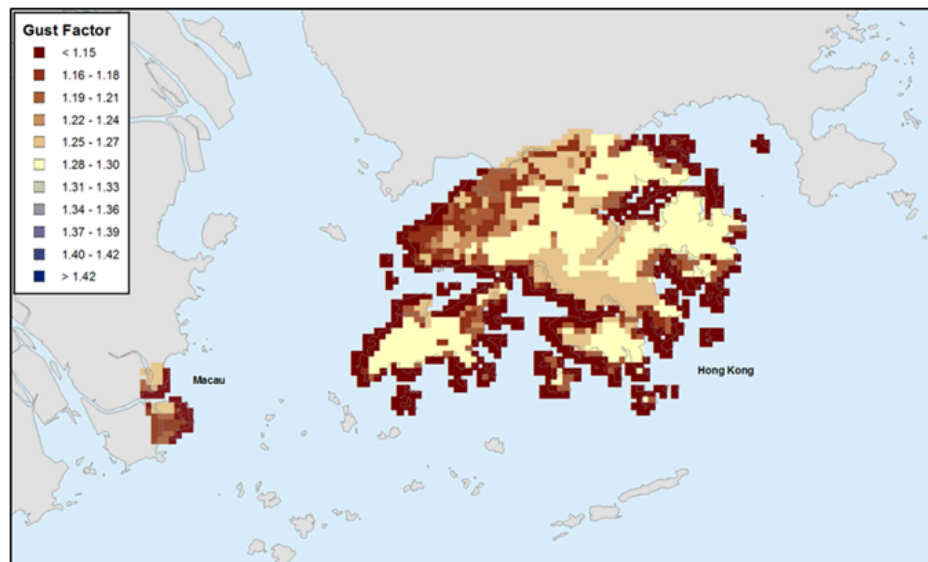


**Figure 91. Verisk gust factors used in the Verisk Typhoon Model for the Northwest Pacific Basin – Macau and Hong Kong**

[Figure 92](#) shows the storm track and modeled wind field for Typhoon Haiyan (2013) moving from east to west across the Philippines. Note that the strongest winds are on the right-hand side of the track, and are a result of the superposition of the forward motion of the storm and the counterclockwise rotating winds around its center. The strongest winds along the coast, on the right-hand side of the figure, are also a result of the fetch effect, in which winds blowing from a smooth surface (water) will take some time to slow down as they travel over

the rougher land surface. Finally, the small-scale variations of wind speed farther inland are the result of either changes in land surface roughness or terrain (elevation).

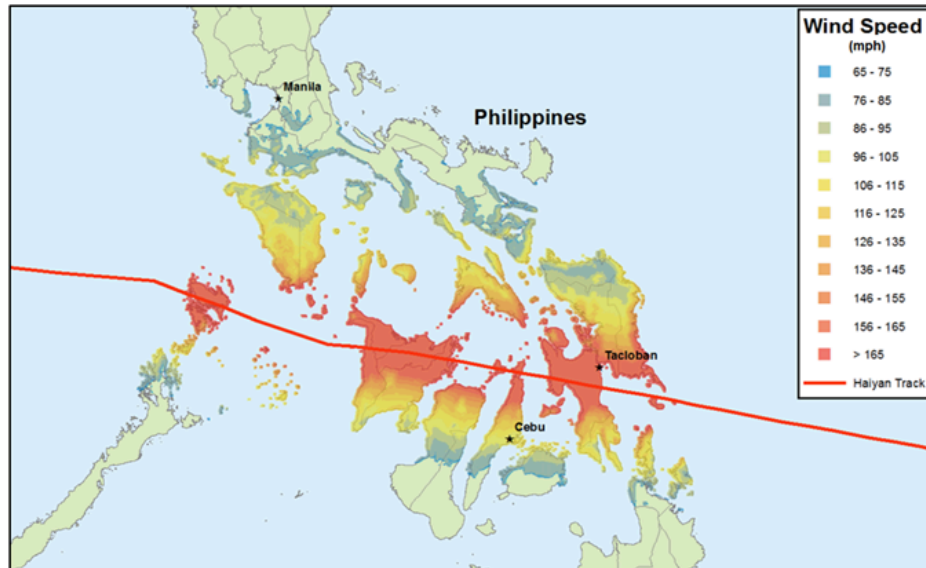


Figure 92. Storm track and modeled wind field of Typhoon Haiyan (2013)

## Wind field directionality

The model explicitly includes directional effects of surface friction on locally estimated wind speeds. Rather than using a single friction adjustment that takes into account the average land surface surrounding a location, the wind-field model uses land use/land cover data to estimate the roughness in eight wind directions: north, northeast, east, southeast, south, southwest, west, and northwest.

A wind coming from the Northwest Pacific Ocean will be relatively unobstructed. On the other hand, a wind from over land will undergo wind-reducing adjustments. In the Verisk model, the influence of the maritime environment on the wind transition is explicitly quantified, which yields a realistic wind field at a local level for the duration of the event.

## Complete specification of the wind field

The generation of local wind fields is a complex procedure requiring the use of many variables, as indicated throughout this section. As described above, once the relationship between central pressure and wind speed is established, many other aspects of the wind field are taken into consideration. The gradient wind profile is determined, and adjustments are made for asymmetry effects, surface friction, and topographical effects. A time profile of wind speeds is then developed and the effects of gusts are taken into account. The following expression takes these variables into consideration, and can be used to calculate the wind velocity at a specific site.

$$V_{10m,1min}(lat, t, r, z_0, \varphi) = ff(z_0, \varphi) \cdot Adj_{elev} \cdot Adj_{terrain} \cdot \{V_{gr\_MAX}(C_p(t, t_{LF})) \cdot Adj_{10m} \cdot Adj_{rad\_decay} \cdot gf(z_0, \varphi) + F_{asym}(\varphi, r)\}$$

Where:

$V_{gr_{r_{MAX}}}$  = gradient wind speed at  $r_{MAX}$ ,

$Adj_{elev}$  = adjustment factor for elevation

$Adj_{terrain}$  = adjustment factor for terrain

$ff(z_0, \varphi)$  = friction factor for wind direction  $\varphi$

$gf(z_0, \varphi)$  = gust factor for wind direction  $\varphi$

$Adj_{10m}$  = adjustment factor to 10 m (surface)

$Adj_{rad\_decay}$  = adjustment factor for wind away from  $r_{MAX}$

$F_{asym}$  = effect of forward speed of motion

## 4.2 Typhoon-induced precipitation and inland flood intensity

Unlike typhoon winds, which generally decrease as storms move inland, the intensity of typhoon-related precipitation and accumulated runoff can actually increase in inland regions. Thus typhoon losses in Southeast Asia are not restricted to coastal provinces, especially when extratropical transitioning is taken into account (Sousounis and Butke, 2010; Sousounis and Desflots, 2010).

### Modeling extratropical transitioning

---

Extratropical transitioning is a frequent occurrence for typhoons in the Northwest Pacific Basin. The strong dependence on latitude that is exhibited by extratropical transition is correlated to the poleward increase in baroclinicity (horizontal temperature gradient) combined with an increased likelihood of interaction with upper-level troughs or shortwaves in the Westerlies, as well as decreased sea surface temperatures (SSTs). Seasonality is also important and is correlated to the movement (poleward or equatorward) of the baroclinic zone during the beginning or end of the typhoon peak season.

The Verisk Typhoon Model for Southeast Asia explicitly accounts for extratropical transition by modifying the storm morphology from a circularly symmetric storm to a quasi-comma-shaped extratropical cyclone. Most of this morphology change occurs during the first 12 hours of the transition period, which typically lasts about 24 hours. The modeled transformation of the storm morphology is based on satellite imagery and TRMM data.

[Figure 93](#) compares TRMM average precipitation prior to and after the beginning of the extratropical transition process. The results demonstrate that the precipitation that occurs during both of these time periods is equally important for Southeast Asia precipitation risk.

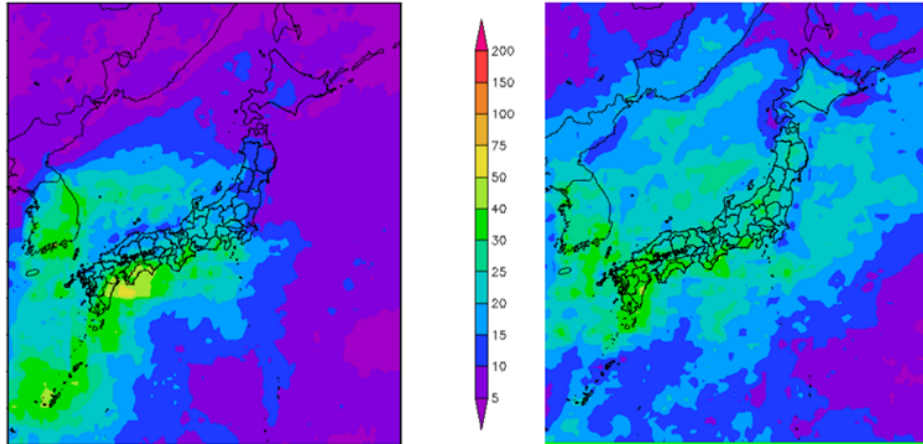


**Figure 93. TRMM average pre-extratropical transition (left panel) and post extratropical transition (right panel) precipitation 24 hours before JMA extratropical transition hour, for 2000 to 2008**

## Modeling the precipitation hazard

As typhoons approach Southeast Asia, the conceptual model of a circularly symmetric storm and its associated precipitation shield breaks down, and the typhoon takes on a more complicated and asymmetric shape. The precipitation intensity associated with the storm also changes. This evolution is spurred by several factors, including terrain, other approaching weather systems, and extratropical transitioning.

Coastal mountains enhance precipitation on the north and east sides of typhoons approaching Southeast Asia from the south. This precipitation boost occurs because the counterclockwise flow of air around this sector of the storm is onshore. As the air is forced over the mountainous terrain, it cools in its ascent, forming clouds and precipitation.

Storms can also be re-energized by cold fronts as they move inland. Sometimes, an approaching weather system can be so powerful that a typhoon's structure will begin to change after landfall, transforming from a tropical to an extratropical system. This transition also enhances precipitation.

[Figure 94](#) shows Verisk's modeled accumulated precipitation for Typhoon Nari in 2001. With a central pressure of 980 mb at landfall, Kathleen was a relatively weak typhoon, but rainfall amounts of 400 to 800 mm were common within its precipitation shield. The metro system in Taipei was flooded and inoperable for months afterward.

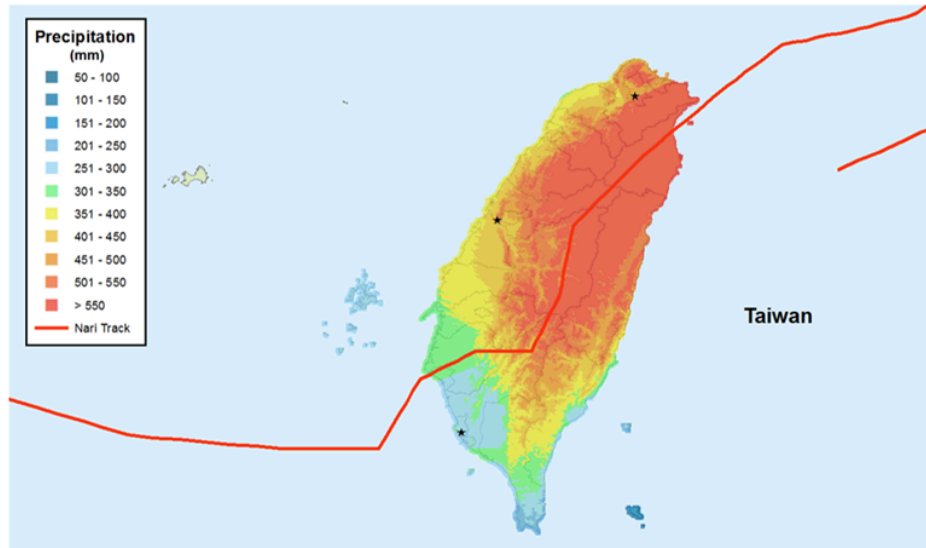


**Figure 94. Storm track and modeled accumulated precipitation levels for Typhoon Nari (2001)**

[Figure 95](#) shows Verisk’s modeled accumulated precipitation for Typhoon Ketsana in 2009. Ketsana made landfall as a weak tropical storm but precipitation amounts ranged from 200 to 400+ mm in the metro Manila area which remain the highest amounts reported in history.

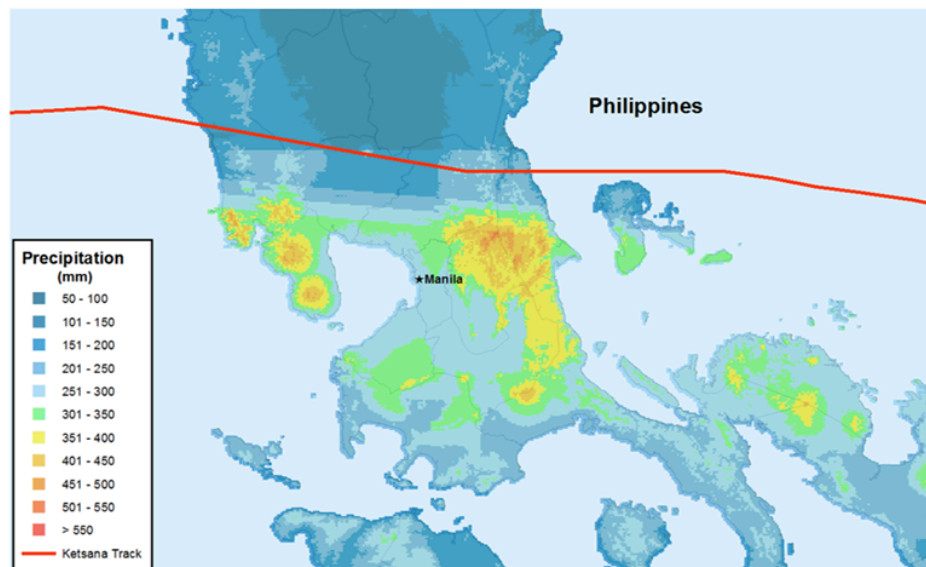


**Figure 95. Storm track and modeled accumulated precipitation levels for Typhoon Ketsana (2009)**

## Modeling the flood hazard

To model the flood hazard, a time-dependent numerical hydrological model, CASC2D, which was developed at Colorado State, was implemented into the Verisk modeling framework. This

model has been used in many research studies and provides a robust platform for calculating typhoon induced flooding. CASC2D is a sophisticated model that solves the equations of conservation of mass, energy, and momentum in order to model flood in a physically-realistic manner.

The main input to the flood model is hourly precipitation, but soil type, surface friction, and terrain slope influence where that water goes. Soil data for the flood model came from the Harmonized World Soil Database (HWSD). The native resolution of the soil data is 1 km. The soil data provided percentages of clay, sand, and loam which were used along with an algorithm developed by Saxton and Rawls (2006) for determining hydraulic conductivity, a key parameter for determining run off in the model. The surface friction was incorporated via Manning Coefficients, which were determined (see [Table 21](#)) based on the vegetation class that was obtained from the Moderate Resolution Imaging Spectroradiometer (MODIS) data at a 1-km resolution that was used for computing the friction and gust factors.

**Table 21. Manning coefficients assigned by Verisk to LULC categories in Southeast Asia**

LULC Category	Manning Coefficient	Definition
0	0.025	Water
1	0.20	Evergreen Needleleaf Forest
2	0.20	Evergreen Broadleaf Forest
3	0.20	Deciduous Needleleaf Forest
4	0.20	Deciduous Broadleaf Forest
5	0.20	Mixed Forest
7	0.05	Closed Shrubland
8	0.05	Open Shrubland
9	0.05	Woody Savannas
10	0.05	Grasslands
11	0.05	Permanent Wetlands
12	0.05	Croplands
13	0.05	Urban and Built-Up
14	0.05	Cropland/Natural Vegetation Mosaic
15	0.01	Snow and Ice
16	0.05	Barren or Sparsely Vegetated

For each typhoon event, hourly-modeled precipitation was input to the flood model for the life of the event. The flood model redistributes water over the model domain based on soil type, vegetation, and terrain slope. These factors determine what fraction of the falling precipitation is absorbed by the soil. For example, more rain water will percolate in sandy soil than in clay soil and in forest land than in an urban environment. Finally, all else being equal, a sloped surface will absorb less water than a horizontal one. A schematic of the flood model is presented in [Figure 96](#).

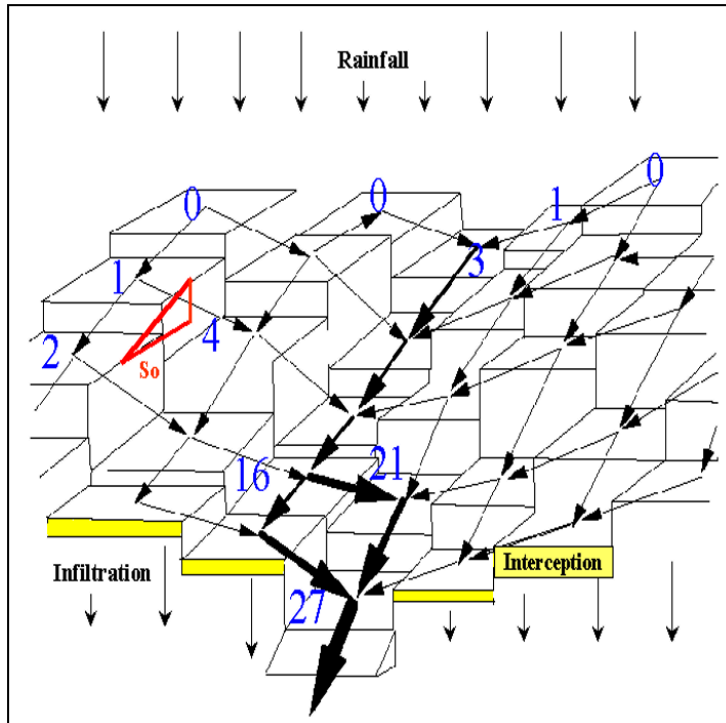


**Figure 96. Schematic of CASC2D showing how a fraction of rainfall at each grid cell is absorbed and the rest runs off to the next cell**

The flood module in the Verisk Typhoon Model for Southeast Asia provides realistic information at a high resolution within the precipitation footprint to identify which areas are at high risk of flood. [Figure 97](#) and [Figure 98](#) show Verisk’s modeled accumulated runoff for typhoons Nari (2001) and Ketsana (2009), respectively.



**Figure 97. Storm track and modeled accumulated runoff for Typhoon Nari (2001)**



**Figure 98. Storm track and modeled accumulated runoff for Typhoon Ketsana (2009)**

### 4.3 Storm surge intensity

The Verisk Typhoon Model for Southeast Asia uses a modified version of the Surge, Wave, and Tide (SuWAT) model developed by scientists of Tottori University and Kyoto University in Japan. The SuWAT model uses depth-integrated nonlinear shallow water equations and the Simulating Waves Nearshore (SWAN) model, in order to more accurately determine the impact of waves on storm surge. The SuWAT model employs a set of nested model domains, whose resolution and placement are fully customizable; this approach yields more accurate estimation of storm surge height and water velocity (see Kim et. al. 2008), and is also computationally efficient.

SuWAT requires the input of several data files to calculate storm surge. Specifically, for a given event, gridded wind speeds are calculated at 10-minute intervals using the methodology described previously; these wind speeds are then read by SuWAT. The wind speed information provides the primary contribution to storm surge through wind stress. In addition to wind speed, sea level pressure is calculated and read by SuWAT at the same 10-minute interval. Reduced sea level pressure contributes to storm surge by allowing the water level to rise. This effect is known as the inverse barometer effect and contributes approximately one centimeter per millibar of reduced atmospheric pressure. SuWAT also requires water bathymetry and terrain elevation files—the methodology for creating these data files is described in the following subsection. Finally, SuWAT utilizes spatially-varying Manning coefficients, to more accurately model the effects of land friction on storm surge. Development of the model’s Manning coefficients is also described in the following subsection.

**See Also**[Local wind intensity](#)[Bathymetry, elevation, and levees](#)

## Bathymetry, elevation, and levees

When a typhoon approaches the coast, the coastal bathymetry strongly influences the amount of storm surge. As the surge approaches the coastline, the decreasing ocean depth and the increasing effects of friction along the ocean floor slow its speed and increase its amplitude. As the surge travels inland, it passes over a variety of surfaces and its flow becomes more complex. Therefore, to accurately model storm surge intensity, high resolution bathymetry, elevation, and land use land cover (LULC) data are all required.

To model coastal bathymetry accurately, Verisk researchers used General bathymetric chart of the oceans (GEBCO) data with a resolution of 30 arc-second (~925 m). GEBCO data consists of quality-controlled ship depth soundings with interpolation between sounding points guided by satellite-derived gravity data. Data sets from other methods are included to create continuous terrain model for ocean and land. The resulting bathymetry for the region is shown in [Figure 99](#).

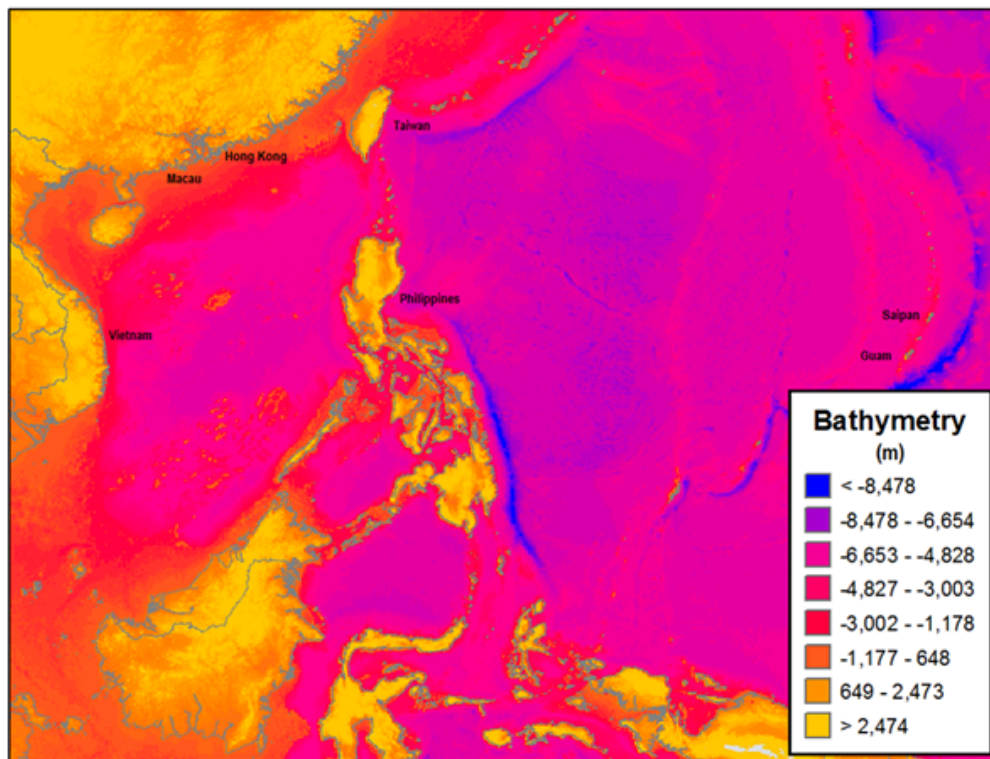


**Figure 99.** Water depth and land elevation for the model domain, produced using 30 arc second GEBCO data for bathymetry and a combination of SRTM90 and InterMap Data products for terrain height

For onshore terrain heights, 90-m resolution SRTM (Shuttle Radar Topography Mission) data was mainly used but augmented in key locations with InterMap Data. Two different DEM

products were used based on availability: NEXTMap World 10 (10-m resolution) DTM, and NEXTMap World 30 (30-m resolution) DSM.

Because the height of levee structures is likely underrepresented in the 90-m elevation data, a separate levee height database was used to supplement the 50-m elevation data. Levee information from Southeast Asia's government was augmented by Verisk analysts and then used in the model to better represent the presence of levee structures. Specifically, where levee height information was available, SuWAT land elevations were changed to be consistent with levee height.

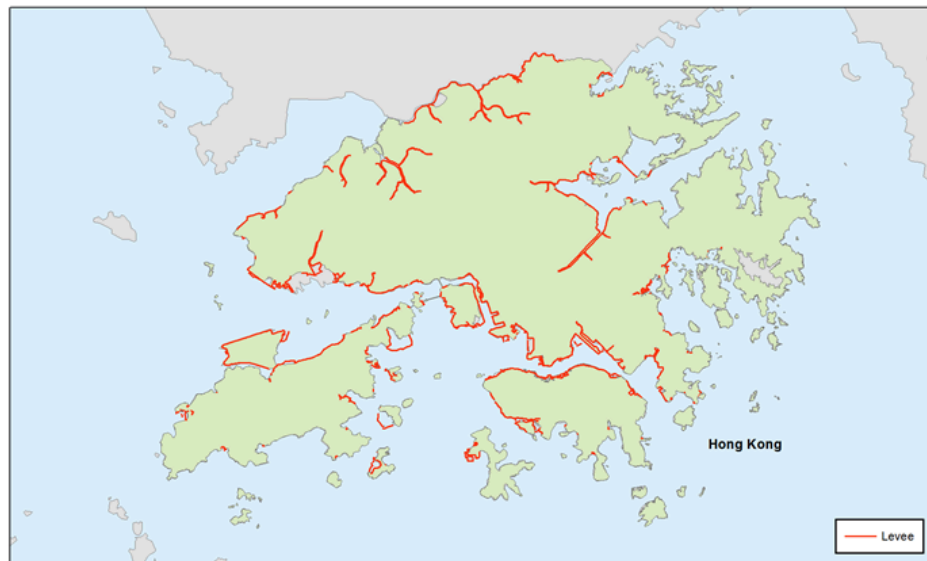


**Figure 100. Location of levees in Hong Kong**

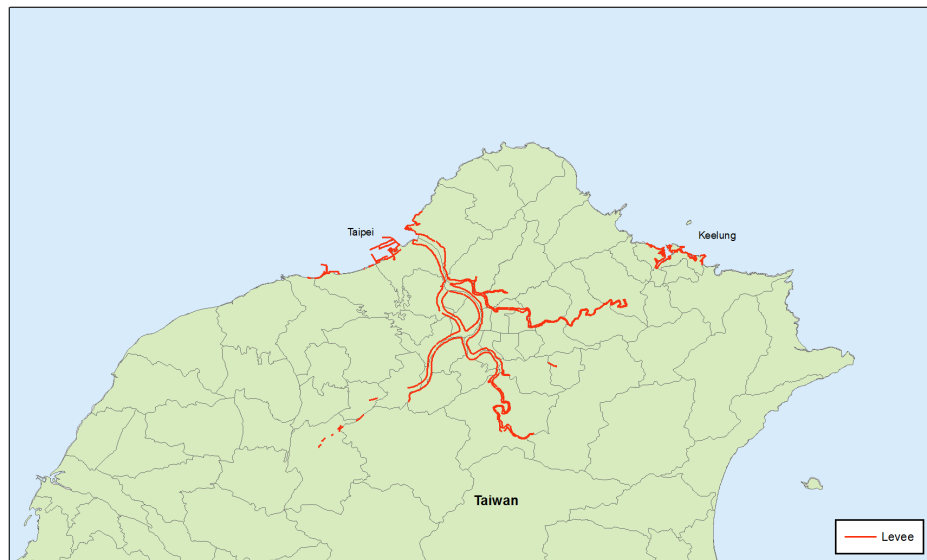


**Figure 101. Location of levees in Taipei and Keelung, Taiwan**

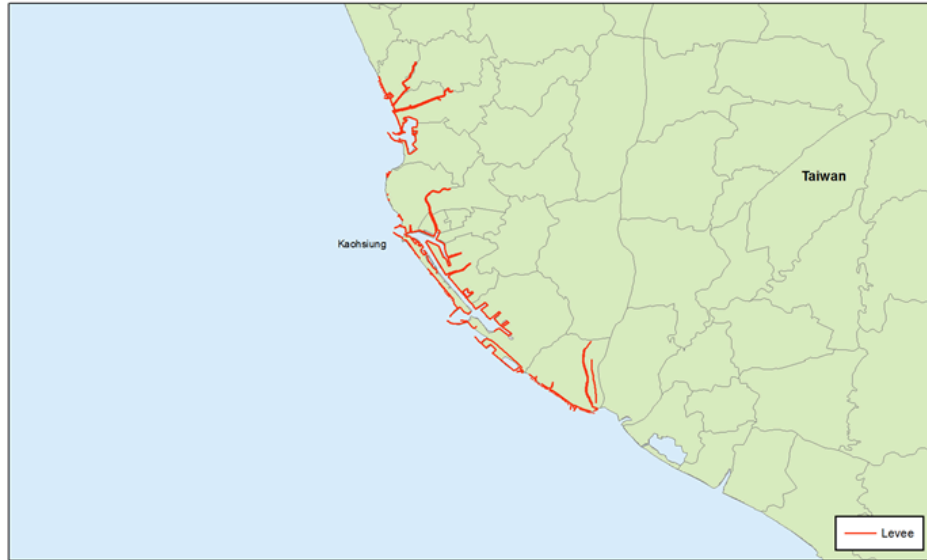


Figure 102. Location of levees in Kaohsiung, Taiwan



Figure 103. Location of levees in Tacloban, Philippines



**Figure 104. Location of levees in Manila, Philippines**



**Figure 105. Location of levees in Cebu, Philippines**

## Friction and Manning's Roughness Coefficients

Over the open ocean, the friction coefficient is used to determine the effects of the ocean floor on the storm surge propagation. Once inland, land friction in addition to terrain elevation influences how far inland surge waters are able to propagate.

To determine the effects of friction, the model uses the Manning Coefficient  $n$ :

$$n = \sqrt{\frac{fD^{1/3}}{2g}}$$

Where  $D$  is the total depth and  $f$  is the friction coefficient defined as:

$$f = \frac{2gn^2}{D^{1/3}}$$

Verisk researchers developed grid-specific Manning Coefficients using the MODIS data used for creating the Physical Properties and for creating the Manning Coefficients used for the inland flood model.

**See Also**

[Modeling the flood hazard](#)

## The effect of astronomical tides on storm surge inundation

A storm surge event's inundation depth at a given location can be significantly affected by the phase of the astronomical tide at that location. Given that typical tidal amplitudes in the Philippines range from 0.5 m–2.5 m (and even higher in portions of the Inland Sea), a high tide could potentially turn an otherwise minor storm surge into a loss-causing event. The same storm surge at low tide, however, would probably not cause any damage.

To account for tides in the storm surge portion of the Verisk Typhoon Model for Southeast Asia, Verisk researchers specified a background tide value for each 250- or 500-m resolution model domain along the coastline that depended on the Julian day and hour of the event. In this manner, for a given portion of the coastline there are stochastic events making landfall over a wide range of astronomical tide values. The specified tide values for a given event across adjacent domains reflect observed phase differences (that is, it typically isn't high tide at exactly the same time for two locations that are hundreds of kilometers apart.). These tide values were calculated using the Oregon State University (OSU) tidal prediction software, and are designed to represent an appropriate range within the entire area covered by the SuWAT model domains.

The observed tidal ranges (astronomical high tide minus low tide) used for the 250 and 500-m computational domains for the Philippines are presented in [Figure 106](#).

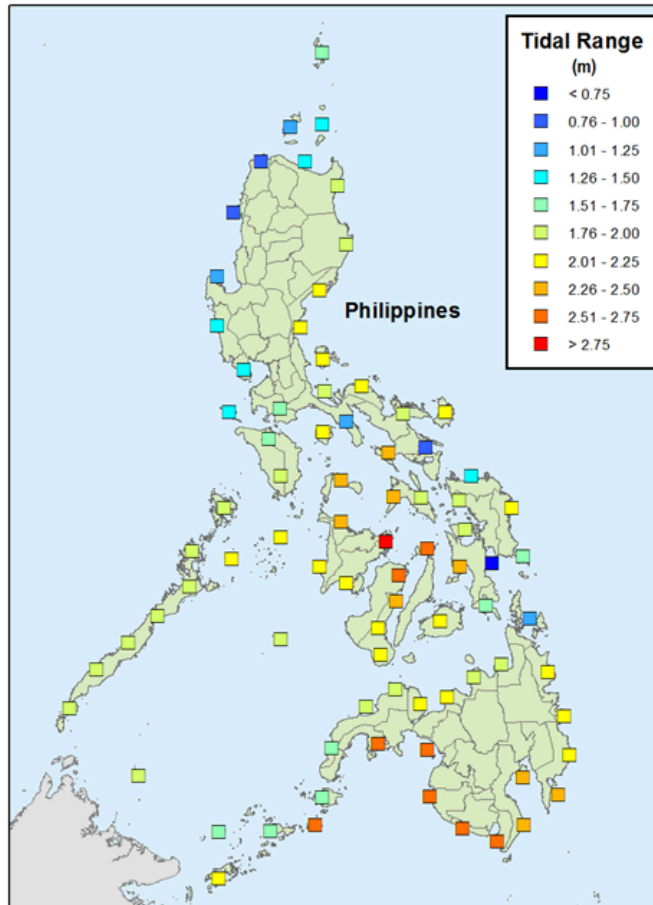


Figure 106. Modeled astronomical tidal range for each 250-m computational domain

## 4.4 Validating local intensity

The local intensity module of the Verisk Typhoon Model for Southeast Asia has been extensively validated against observational data. Modeled wind speeds have been compared with information from the Hong Kong Observatory (HKO), the Philippines Atmospheric, Geophysical, and Astronomical Services Association (PAGASA), the Central Weather Bureau (CWB) of Taiwan, and the Joint Typhoon Warning Center (JTWC). Modeled precipitation totals have been compared with information from the Global Summary of Day (GSOD) and Tropical Rainfall Measurement Mission (TRMM) data. Validating modeled flood depths was more challenging given the relative unavailability of such observations although for two significant events, Typhoon Nari (2001) and Typhoon Ketsana (2009) there were sufficient observations to support the quality of the modeled result. To validate modeled storm surge intensities, Verisk researchers compared modeled maximum surge heights for historical typhoons to actual buoy observations from HKO and from measurements that were taken by a joint Philippine-Japan Survey Team immediately following Typhoon Haiyan (2013).

In the following subsections, text and exhibits for wind speed validation, precipitation validation, and storm surge validation are provided separately.

## Wind speed validation

Although isolated wind speed reports from stations can be found regarding typhoons impacting the Philippines (e.g., in peer reviewed journals, storm reports, etc.), finding complete sets of station data for an event in that area as well as in the other Southeast Asian countries is exceedingly difficult. An alternative strategy is to compare our maximum modeled wind speeds for each of the historical events to those estimated by the JMA at the time of landfall. That comparison is shown in [Figure 107](#). Agreement is very good, especially considering that the modeled wind speed corresponds to a point on land and the JMA wind speed corresponds to a point over open water. Note that two typhoons that affected Hong Kong, Hagupit (2008) and Vicente (2012), were bypassing events, so the maximum JMA wind speed, even though it was taken at the time of closest approach, is still higher than what those storms actually generated over a land point on Hong Kong.

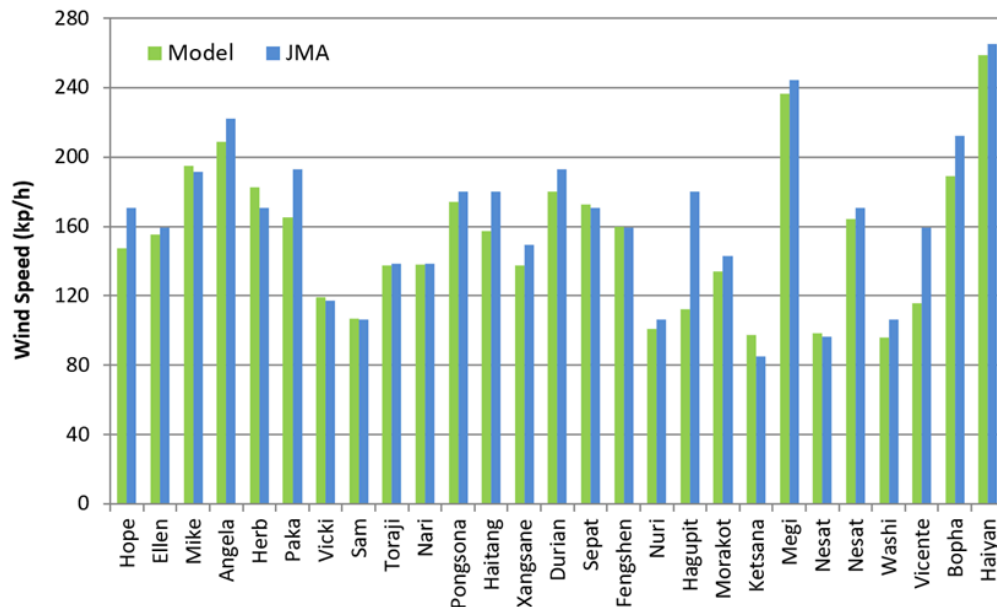


**Figure 107. Verisk-modeled and JMA-estimated maximum wind speeds at landfall for historical events**

**Note: Typhoons Hagupit and Vicente were bypassing events for Hong Kong, so JMA wind speeds are notably higher than those modeled.**

For storms affecting Hong Kong, the station data recorded by the Hong Kong Observatory (HKO), which has been operational since 1884, are very reliable. [Figure 108](#) shows maximum modeled wind speeds for Cheung Chua, an island 10 km southwest of Hong Kong. The observed wind speeds are converted to 1-minute sustained winds, because they are measured as 3 second gusts, using a conversion factor of 1.49 as was recommended by the WMO (World Meteorological Organization).

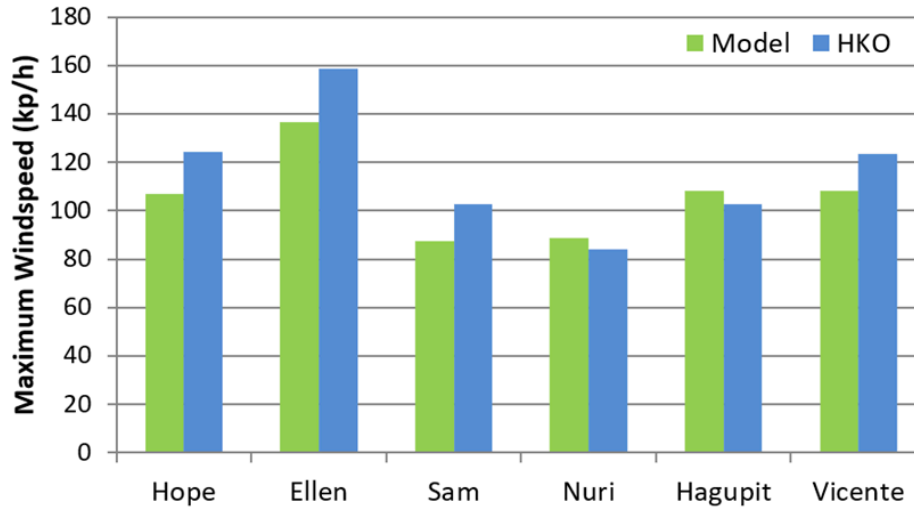


**Figure 108. Maximum modeled and observed wind speeds for historical typhoons affecting Hong Kong**

Station observations outside of Hong Kong, but within Southeast Asia, are difficult to obtain. However, for the purpose of validating the wind speed model (formulation), it is just as useful and important to validate a parameter like the return period wind speed. To that end, [Figure 109](#) compares the modeled 100-year return period wind with that calculated by PAGASA for the Philippines. While modeled and PAGASA wind speeds compare well, the PAGASA wind speeds are slightly higher than the modeled wind speeds in some locations, like Panay Island along the east coast. Not knowing exactly how PAGASA conducted their analysis, which was likely augmented by some extrapolation of the data that exists for only a fraction of the 100 year period, it is difficult to ascertain exactly why this is, but it is likely that the PAGASA winds represent those over an open fetch. That said, the modeled result does capture the expected behavior that the PAGASA result does not, such as the higher wind speeds along the coast in selected locations.

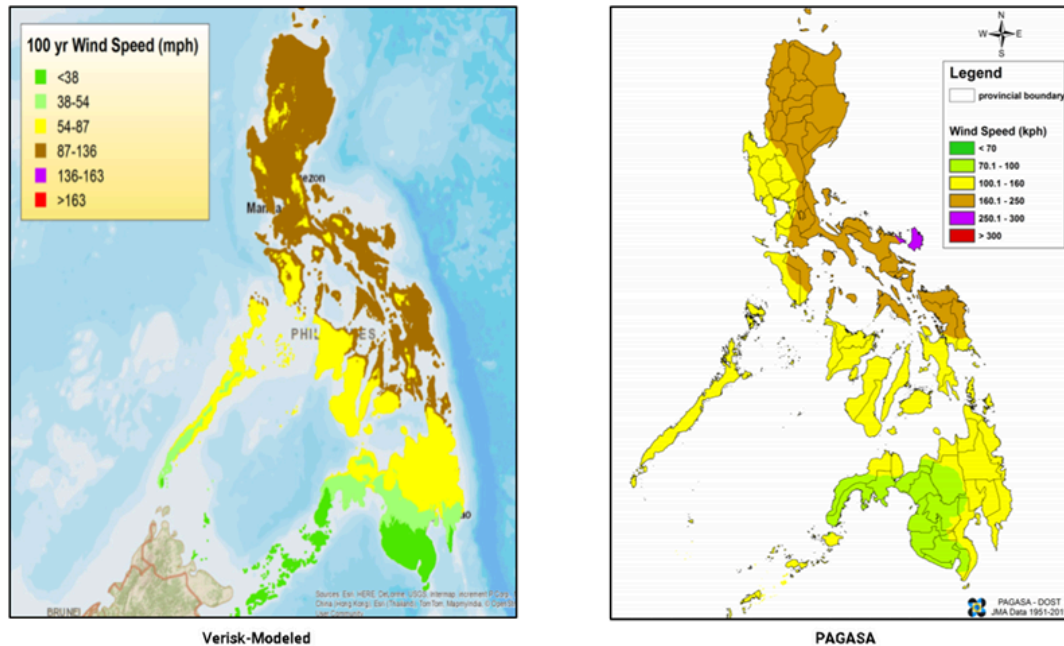


**Figure 109. Verisk-modeled 100-year return period wind speeds for the Philippines (left) and a similar analysis as determined by PAGASA (right)**

A similar result is shown for Taiwan in [Figure 110](#) except the basis for comparison is from an engineering study by Jang and Lee (1997). The study used the method of moments and exceedance probability theory owing to the fact that only 40 years of observed data was used ending in 1990. It is therefore missing data from some significant storms that affected Taiwan. Regardless, the agreement is reasonably good, especially on the windward (east) side of the island, where wind speeds are most significant.

An additional wind validation exhibit is [Figure 111](#), which presents a comparison of maximum wind speeds for typhoons affecting Guam. The source of the observations for these storms is from reports published by the JTWC.

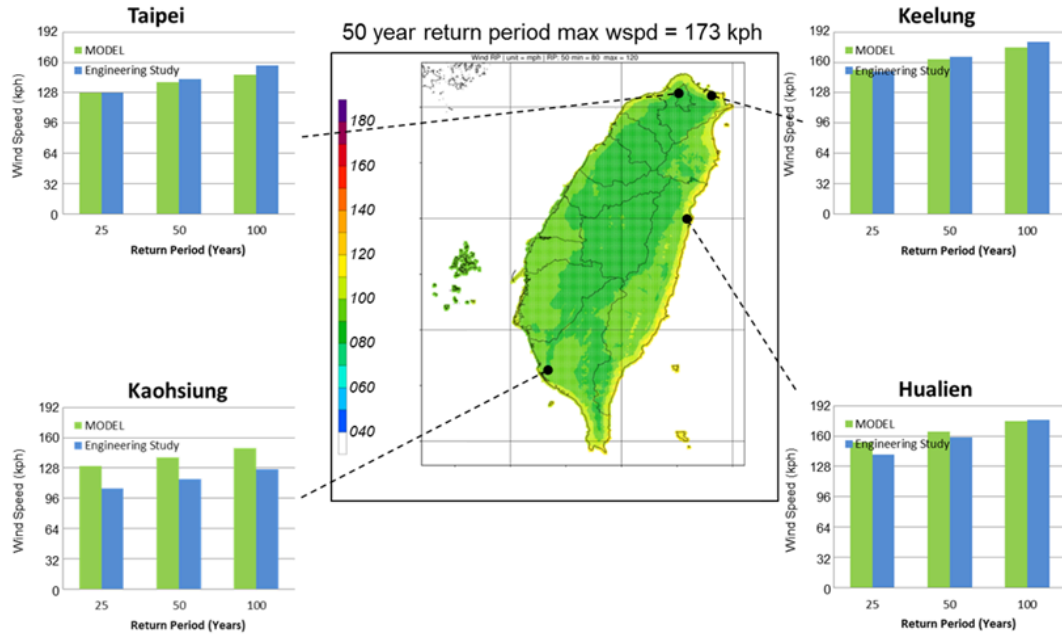


Figure 110. Verisk-modeled 100-year return period wind speeds for Taiwan and similar analysis from a wind engineering study

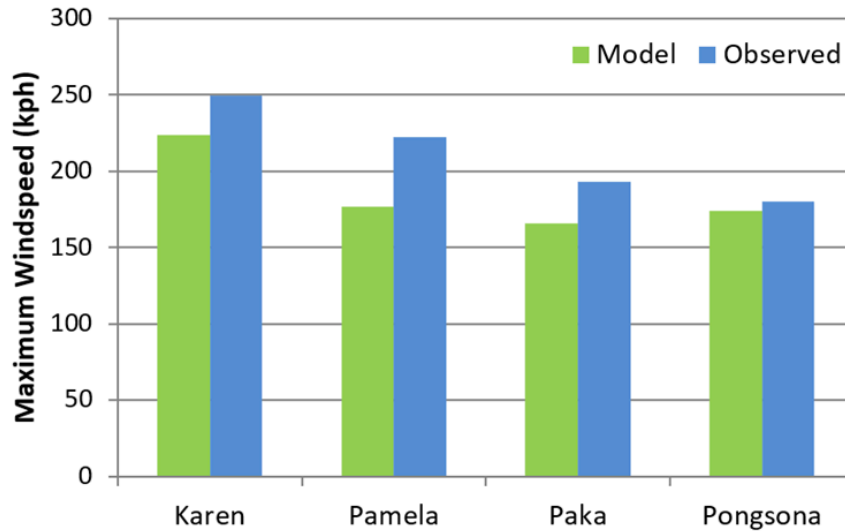
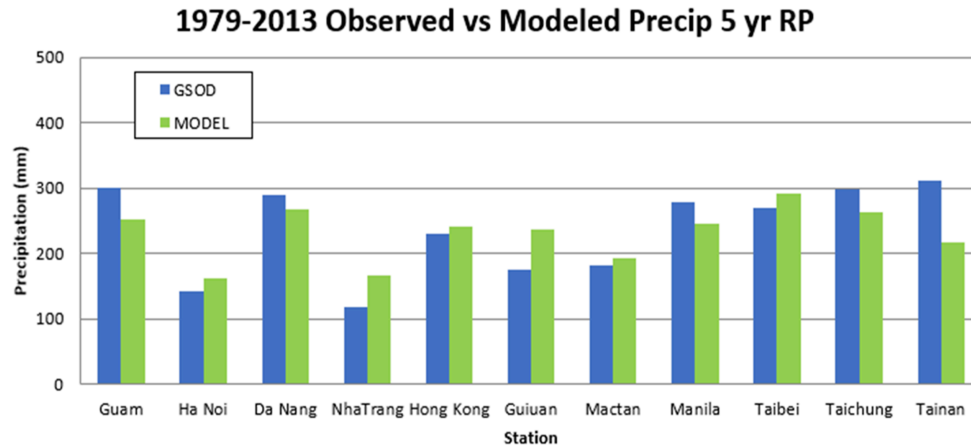


Figure 111. Maximum modeled and observed wind speeds for historical typhoons affecting Guam

## Precipitation and flood validation

The flood depth is the quantity used for calculating damage from flood but validating this quantity can be challenging because of severe limitations in data availability. Because precipitation is the main input to the flood model, it is relevant to therefore evaluate performance of the precipitation model. However, the same limitations that were noted

for wind data also apply to precipitation. The best source of precipitation observations is available from the National Climatic Data Center’s Global Summary of the Day (GSOD) dataset. Even still, data is available by station by day – there is no distinction between non-typhoon and typhoon-based precipitation amounts. Therefore, a strategy was employed to extract precipitation for a given day for a given station if it was within 3.5 degrees of the typhoon track on that day. There was no finer extraction made based on the fraction of the day for which that held true. Most of the stations in Southeast Asia have useable data over a 20-year period or so. [Figure 112](#) shows a comparison of model generated 5-year return period (occurrence based) precipitation and that obtained from GSOD.



**Figure 112. Verisk-modeled and observed 5-year (occurrence) return period typhoon related precipitation amounts. Observed values are computed from the National Climatic Data Center’s Global Summary of the Day data.**

Despite the challenges of flood measurements, two events have been widely studied. [Figure 113](#) shows the modeled flood footprint from Typhoon Ketsana 2009 as it compares to a 100-year flood map generated by PAGASA. In the Figure, the modeled result shows areas outside Manila that also flooded but they are not included in the PAGASA result that is shown. The modeled result captures the three main regions that were flooded – near the shores of Manila Bay through the downtown area, farther east along the San Juan River, and still farther to the east along the Marikina River fanning out (southward) into a triangular shape approaching the Laguna de Bay. Amounts typically ranged from less than a meter to upwards of two meters and those amounts are faithfully captured by the model. The excellent agreement between model and observation for this high profile case is a testament to the accuracy of the model in general, especially given the fact that its resolution is 1 km.

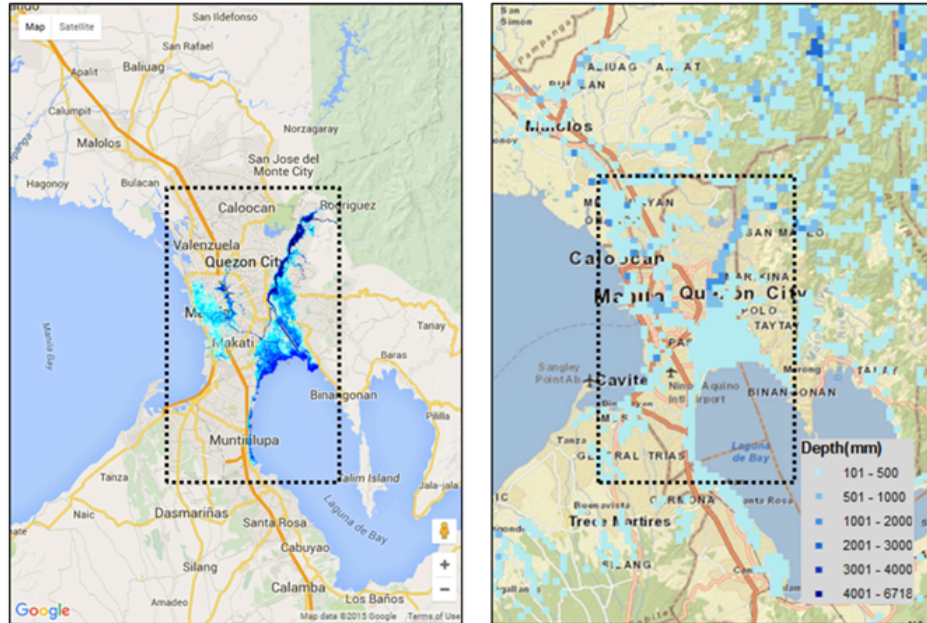


**Figure 113. Verisk-modeled 100-year return period flood footprint (right) and flood footprint from PAGASA (left) (Ketsana was considered to be a 100 year event for the Manila region; dashed rectangle on PAGASA analysis shows only the flood in the Manila region, which is also identified in the modeled result)**

Another high profile flood event was typhoon Nari in 2001. The event prompted many to consider what a 200-year flood for Taipei would look like. [Figure 114](#) presents the result from Hsu et al (2012)<sup>8</sup> along with the Verisk model-generated 250 year flood footprint. The flooding along three rivers that cross/border Taipei is once again accurately represented by the model – especially considering the 1-km resolution.

<sup>8</sup> Flood Damage Assessment in Taipei City Taiwan - Scientific Figure on ResearchGate. [https://www.researchgate.net/257164403\\_fig1\\_Figure-1-Flood-potential-map-of-200-year-return-period-in-Taipei-city](https://www.researchgate.net/257164403_fig1_Figure-1-Flood-potential-map-of-200-year-return-period-in-Taipei-city)

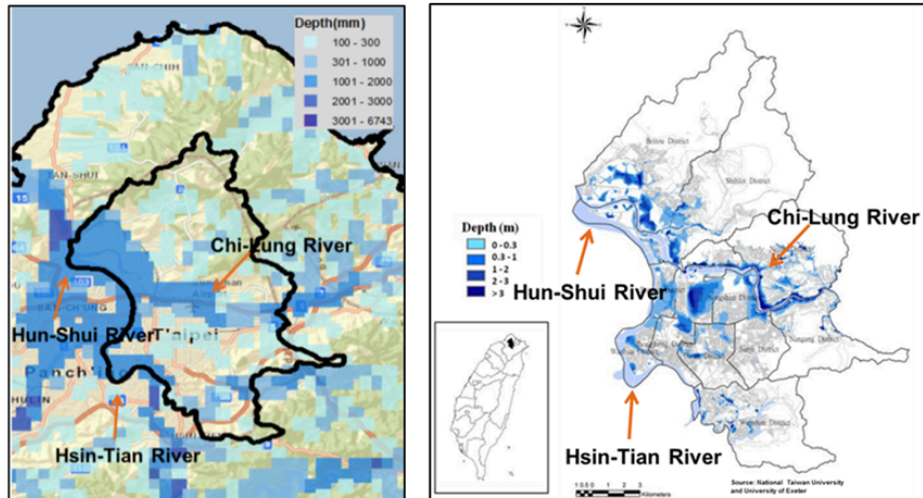


**Figure 114. Verisk-modeled 200-year return period flood footprint (left) and Taiwan Government Agency 250-year flood footprint (right) for Taipei Region (Taiwan)**

## Storm surge validation

SuWAT has been used in many peer-reviewed publications, and has been shown to predict both water levels and waves with reasonable accuracy (Kim et. al., 2008). To further validate SuWAT, Verisk researchers compared modeled maximum surge heights for historical typhoons to actual buoy observations. [Figure 115](#) compares maximum observed surge height to the modeled surge height for several historical typhoons affecting Hong Kong. The observations are from available buoy reports and do not necessarily capture the maximum storm surge heights for each event, which may be one possible explanation for why the modeled values tend to be higher than the observed ones. Despite the constraint on the buoy data, there is good correlation between modeled and observed surge heights across the range of typhoon intensities.

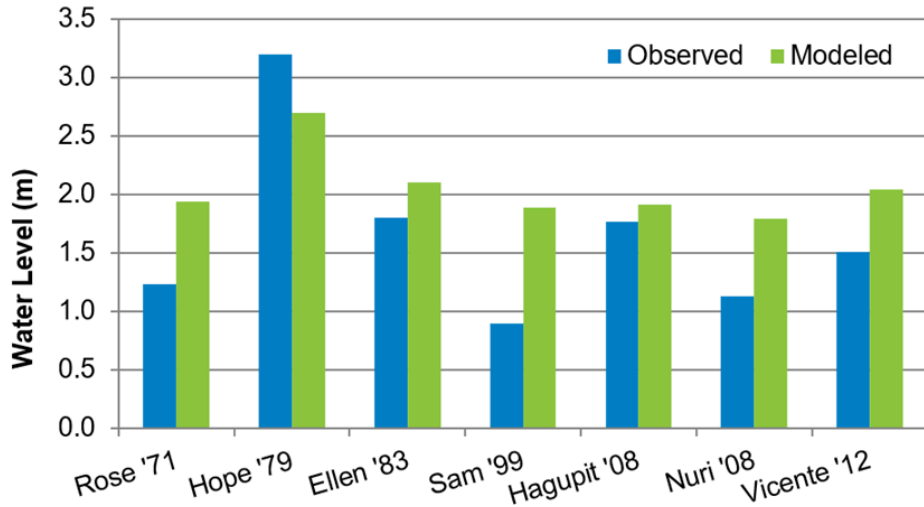


**Figure 115. Verisk-modeled maximum and observed storm surge heights for selected historical events for Hong Kong**

The highest profile storm surge event for perhaps the entire Northwest Pacific Basin is still Haiyan 2013. Immediately following the event, a joint Philippine-Japan Survey team was dispatched to document the storm surge heights in over 100 different locations. Some of those observations are shown – superimposed on the modeled storm surge footprint for the Leyte Gulf region extending into Tacloban (Figure 116). Maximum modeled storm surge heights approached 6 m, which was very close to the maximum observed values that were slightly above 6 m. Some reports may have exceeded that but they were likely including splash up from waves and/or seiche that the storm surge model does not capture.

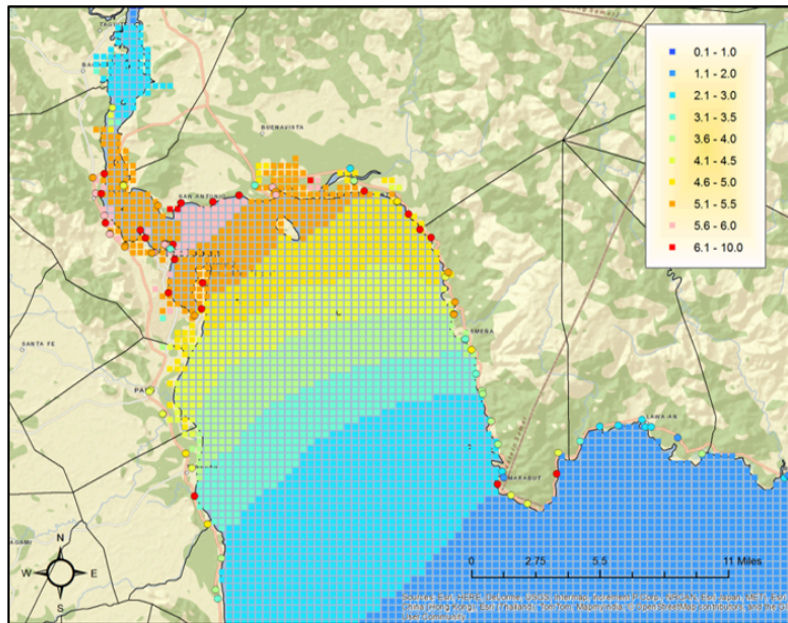


**Figure 116. Verisk-modeled maximum storm surge heights (m) for Typhoon Haiyan (2013) and selected observations (color-filled circles)**

# 5 Damage Estimation

The Verisk Typhoon Model for Southeast Asia uses the vulnerability module to estimate the losses incurred by a property for a given hazard intensity parameter. The parameter used for the wind sub-peril is the one-minute sustained wind speed at a height of 10 m, the parameter used for flood is the total accumulated run-off (also referred to as flood depth), and the parameter for storm surge is effective inundation depth (referred to as effective surge depth). Detailed building inventory information is used to develop wind, flood, and storm surge damage functions for various combinations of occupancy, construction, and height classes. Buildings, contents, and business interruption losses, from wind, flood, and storm surge, are calculated by applying the appropriate damage function to the replacement value of the insured property.

## 5.1 Building classifications

This section discusses some of the most prominent of these classes, and how each is affected by typhoons. For more information regarding construction and occupancy classes in Southeast Asia, refer to the Industry Exposure Documentation, [Verisk Industry Exposure Database for Southeast Asia](#), on the [Client Portal](#), and the UNICEDE Documentation ([www.unicede.com](http://www.unicede.com)).

The building characteristics in the modeled countries/territories of Southeast Asia vary significantly depending on several factors including the hazard exposure, the socioeconomic conditions of each country/territory, and the availability of construction materials, the types of building codes and their enforcement.

For example, wood frame is rarely found in residential buildings through the region, but still widely used in agricultural buildings in the Philippines, Taiwan, and Vietnam. The primary materials for commercial use buildings are reinforced concrete and steel, although there is still a significant portion using masonry in the Philippines, Taiwan, and Vietnam. Compared to other country/territories in the region, Hong Kong and Macau have a larger percentage of high-rise and tall buildings.

These and other differences in building classifications in each country/territory were studied when developing the model's damage functions. This section provides descriptions of the buildings in each of the modeled countries/territories along with construction percentages in the Verisk Industry Exposure Database.

### **See Also**

[Construction and occupancy classes, year built and height bands, and relative vulnerabilities](#)

## Engineered and non-engineered buildings

The model captures the difference between engineered and non-engineered buildings, which has a great effect on their vulnerability to typhoon related sub perils. How well a building is

engineered, what key building features it contains, and if it is enforced to follow the building code when constructed, vary according to its occupancy, construction, and height. For example, the roof-to-wall connection is an important determinant of vulnerability in a low-rise building, whereas for a high-rise building—which is assumed to be better engineered—the roof-to-wall connection is not as important as other features (e.g., the percentage of the building that is glass, and the glass type). [Table 22](#) summarizes the definitions of engineered and non-engineered buildings in the model, based on construction, occupancy, and building height.

**Table 22. Definition of engineered and non-engineered buildings**

Occupancy Codes	Construction Class	Building Height	Engineered or Non-engineered
All	101-104, 112-115, 152	All	Non-engineered
All	111, 116-120	All	Engineered
All	131-140, 151, 153-159	All	Engineered
300-307	100	1-3 stories	Non-engineered
300-307	100	> 3 stories	Engineered
300-305, 307	100	Unknown	Non-engineered
306	100	Unknown	Engineered
311-384	100	All	Engineered
All	200 Series	All	N/A
400 Series	All	All	N/A

## Residential buildings

In Hong Kong and Macau, the majority of residential structures are reinforced concrete high-rise and tall buildings (Campbell, 2005), with some steel high-rise and tall buildings as well. These structures are well-engineered and have to conform to Hong Kong and Macau's building code requirements. The design wind speed specified in Hong Kong and Macau's codes is quite conservative; therefore, the engineered structures have good wind-resistance. Most masonry buildings are older and relatively rare, as they are being replaced with more durable construction types.

In the Philippines, lighter materials, such as wood frame with galvanized iron or aluminum roofs are often used for residential buildings in rural areas. In contrast, urban residential structures are generally made of concrete block with metal roofs, although hollow concrete is also used. Masonry residences can be found in the cities, which also have many high-rise apartments made of reinforced concrete. The use of lighter roof materials, together with unsupported roof overhangs, makes the residential construction more vulnerable when compared with Hong Kong or Taiwan.

In Taiwan, low- to mid-rise buildings usually have reinforced concrete frames with brick infill walls. Some masonry residential buildings can also be found, although these are usually built prior to 1950 and are often designed in a Japanese style. In recent years, these residences have given way to mid- and high-rise apartment buildings and three-story street houses (*tow tien*), with both types generally made of reinforced concrete or steel. Moreover, most of the buildings in Taiwan are fairly new and recent residences tend to be high-rise complexes built in clusters. These are predominantly reinforced concrete structures, many with ceramic facades, although some are steel (Su, 2002). Taiwan's residential buildings usually have commercial establishments on the first floor, while the upper stories are used for residential purposes.

In Vietnam, the majority of residential structures are reinforced concrete low- to mid-rise buildings. However, there is still a large portion of residential structures that are unreinforced masonry buildings, especially for those that are low-rise. These masonry buildings usually fail to follow local building codes and are constructed without proper supervision (Duy et al., 2007), which makes them vulnerable to natural hazards, such as typhoons.

In Guam and Saipan, most of the residential structures are low-rise buildings constructed with reinforced masonry or reinforced concrete (Axco, 2002). These buildings usually follow the local building code properly, which is one of the strictest sets of requirements in Asia. Thus, compared to other regions in the Verisk Typhoon Model for Southeast Asia, the vulnerability of residential buildings in Guam and Saipan is considered to be relatively low. However, this does not mean that typhoon risk is low in these two territories - though the buildings are considerably strong, the hazard in these regions is high and the effects of devastating events can still be substantial.

The distribution of construction types used for residential buildings in each of the modeled regions of Southeast Asia, from the Verisk Industry Exposure Database, is presented in [Figure 117](#).

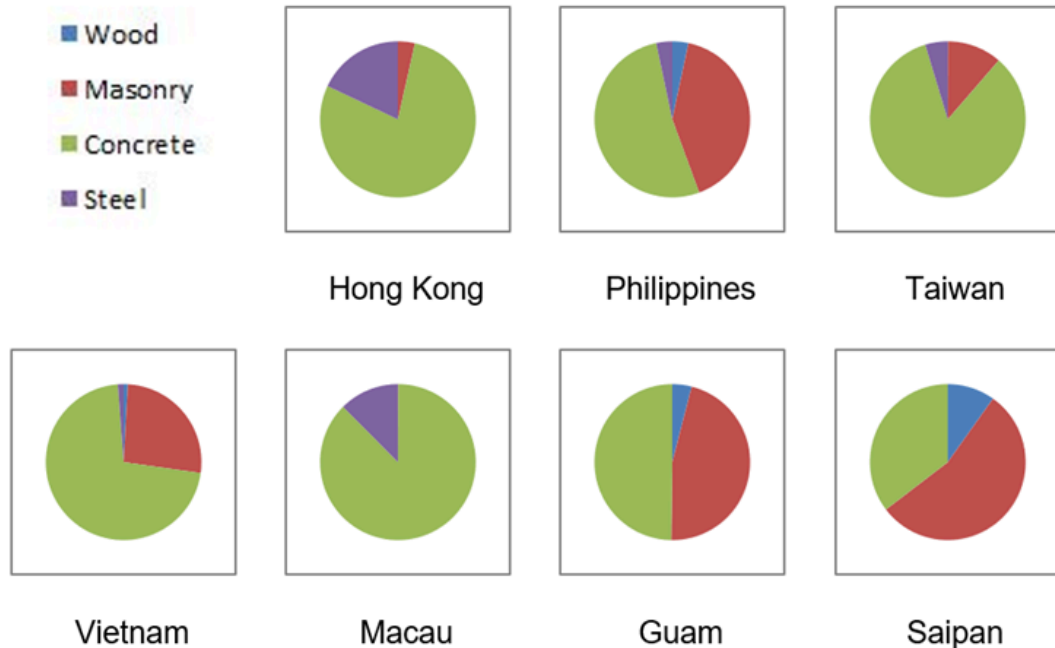


**Figure 117. Construction type distribution for residential buildings in Hong Kong, the Philippines, Taiwan, Vietnam, Macau, Guam, and Saipan**

## Commercial and small industrial buildings

Commercial and small industrial buildings in Southeast Asia have a different distribution of construction types than residential buildings. Here, wood is only used for a small percentage of commercial building stock while steel and concrete are the dominant construction types. An even smaller percentage of the commercial building stock is made of light metal - these are usually warehouses or some other manufacturing buildings. In contrast, a significant portion of industrial buildings are made of light metal.

In Hong Kong and Macau, commercial and industrial buildings are either reinforced concrete or steel. Similar to the high-rise residential buildings in Hong Kong, the commercial and industrial buildings are well-engineered and conform to Hong Kong and Macau's strict building code practices. The design wind speed specified in the Hong Kong and Macau codes are quite conservative; therefore, the engineered structures are wind-resistant.

In the Philippines, masonry is often used for smaller commercial establishments although the majority of all commercial and industrial buildings are reinforced concrete or steel. The use of masonry, along with less stringent building codes and enforcement, lead to lower wind resistance in these buildings than found in Hong Kong.

In Taiwan, the commercial and industrial building stock is similar to the stock in Hong Kong. The buildings in Taiwan usually date to 1970 or later, since before that time the territory relied more heavily on agriculture. These buildings are therefore generally built to better structural standards (Su, 2002). Most of Taiwan's commercial and industrial stock is made of reinforced concrete, while the rest is mostly steel, and some masonry. As described under

the residential structures, the vulnerability of Taiwan’s commercial and industrial buildings is similar to residential, due to the prevalence of mixed-occupancy buildings.

In Vietnam, reinforced concrete and steel are common building materials for commercial and industrial buildings; masonry, especially unreinforced masonry, is still popular for low-rise commercial buildings. Similar to the Philippines, the use of masonry with less attention paid to the building code and enforcement, resulted in the construction of buildings with less wind resistance. There is also a large portion of industrial buildings built with light metal, which is vulnerable during typhoon events.

In Guam and Saipan, most of the commercial and industrial buildings are made of reinforced concrete and steel, following strict building code with good construction supervision. It is reasonable to consider that they perform well when facing strong wind and other sub-perils related to typhoon. However, a portion of the Guam and Saipan’s building stock is light metal industrial buildings (mainly warehouse). The light metal buildings are more easily damaged under strong wind events, comparing to reinforced concrete or steel.

Low-rise, non-engineered commercial and industrial buildings usually perform similarly to single-family homes under typhoon conditions. In contrast, damage to engineered buildings is usually confined to nonstructural components, such as mechanical equipment, roofing, cladding, and windows. Complete structural collapse of engineered buildings due to typhoons is extremely rare.

The distribution of construction types used for commercial and industrial buildings in each of the Southeast Asia modeled countries/territories (Guam, Hong Kong, Macau, the Philippines, Saipan, Taiwan, and Vietnam), from the Verisk Industry Exposure Database, is presented in [Figure 118](#).

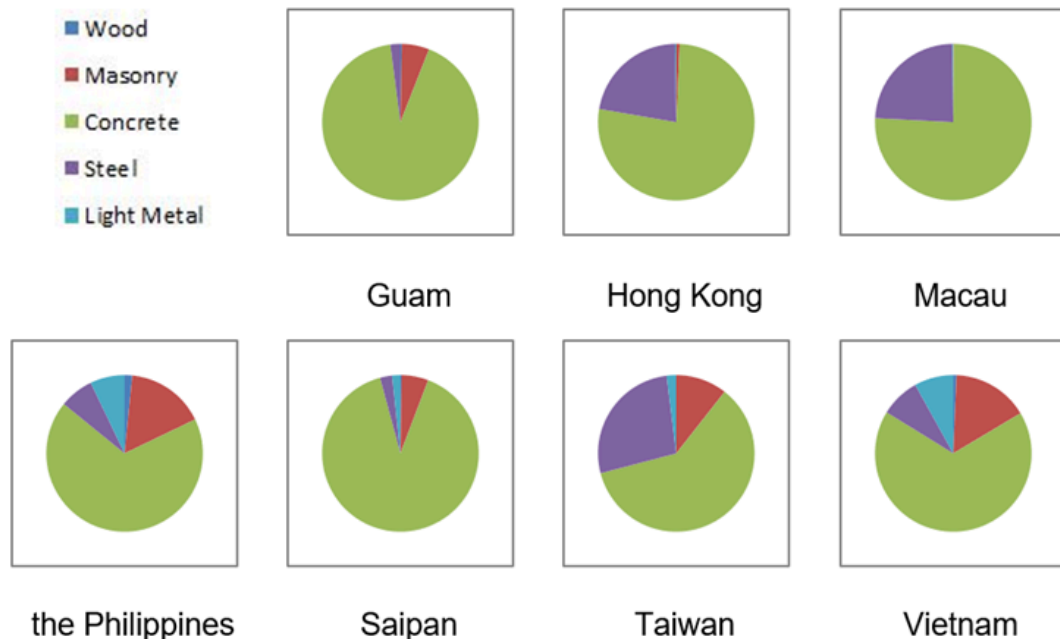


**Figure 118. Construction type distribution for commercial and industrial buildings in Guam, Hong Kong, Macau, the Philippines, Saipan, Taiwan, and Vietnam**

## Agricultural buildings

In the Verisk Industry Exposure Database, agricultural buildings are distinguished by a separate line of business for the Philippines, Taiwan, and Vietnam. The distribution is similar among these three countries/territories. Most of them are light metal, which is quite vulnerable to wind as discussed before. The second most widely used material is wood, which is also not very resilient against high wind. There are also some unreinforced masonry buildings, which perform better than light metal or wood, but are still considered as non-engineered buildings.

The distribution of construction types used for commercial and industrial buildings in each of the Southeast Asia modeled countries/territories (Guam, Hong Kong, Macau, the Philippines, Saipan, Taiwan, and Vietnam), from the Verisk Industry Exposure Database, is presented in [Figure 119](#).

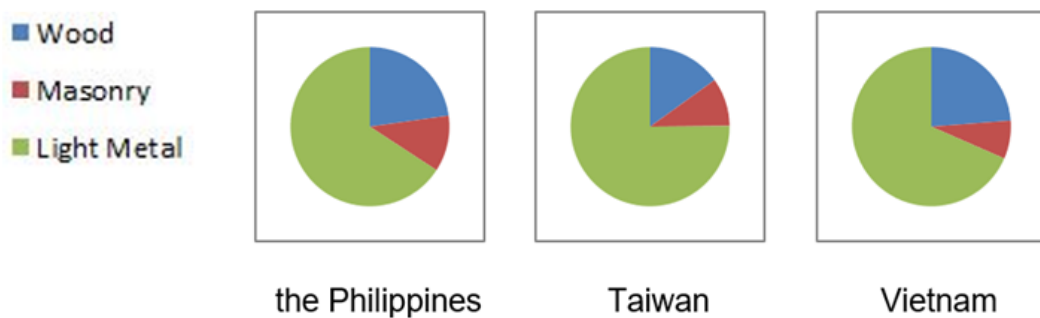


**Figure 119. Construction type distribution for agricultural buildings in the Philippines, Taiwan, and Vietnam**

## Large industrial facilities

Large industrial facilities have diverse classes of structures or components, including stacks, cooling towers, pipes, and tanks located in a widespread open area. All of these different classes of structures, or industrial facility components, have different vulnerabilities when subjected to wind, precipitation-induced flooding, and storm surge. Examples of types of large industrial facilities and industrial facility components, respectively, are shown below.



**Figure 120. Examples of large industrial facilities**  
**Top left to lower right: steel mill,<sup>9</sup> wastewater treatment plant,<sup>10</sup> paper mill,<sup>11</sup> hydroelectric power plant,<sup>12</sup> aluminum plant,<sup>13</sup> electric substation,<sup>14</sup> chemical plant,<sup>15</sup> petroleum refinery,<sup>16</sup> and cement plant.<sup>17</sup>**

<sup>9</sup> Source: [Kobe Steel, Ltd-Kakogawa Works 1172657](#) by Matsuoka Akiyoshi, [CC BY-SA 3.0](#)

<sup>10</sup> Source: [Marlborough East Wastewater Treatment Plant Aerial](#) by Nick Allen, [CC BY-SA 4.0](#)

<sup>11</sup> Source: [Rumford paper mill 2](#) by Alexius Horatius, [CC BY-SA 3.0](#)

<sup>12</sup> Source: [Özbaht Hydroelectric power plant](#) by Josef Moser, [CC BY-SA 3.0](#)

<sup>13</sup> Source: [Bogoslovsky aluminum plant](#) by Kostya Wiki, [CC BY-SA 2.5](#)

<sup>14</sup> Source: [MLGW electric substation Person Ave Memphis TN 01](#) by Thomas Machnitzki, [CC BY-SA 3.0](#)

<sup>15</sup> Source: [Polymer plant along the Ohio River near the settlement of Apple Grove in Mason County, West Virginia](#) by Carol M. Highsmith, Library of Congress Prints and Photographs Online Catalog

<sup>16</sup> Source: [Anacortes Refinery 31911](#) by Walter Siegmund, [CC BY-SA 3.0](#)

<sup>17</sup> Source: [Lafarge, ZI Horizon Sud, Frontignan, Hérault 01](#) by Christian Ferrer, [CC BY-SA 3.0](#)



**Figure 121. Examples of large industrial facility components**  
**Top left to lower right: buildings,<sup>18</sup> open frame structures,<sup>19</sup> cooling towers,<sup>20</sup> processing towers,<sup>21</sup> distillation towers,<sup>22</sup> flare towers,<sup>23</sup> tanks,<sup>24</sup> conveyors,<sup>25</sup> pipe racks,<sup>26</sup> transformers,<sup>27</sup> high voltage circuit breakers,<sup>28</sup> and transmission towers.<sup>29</sup>**

In the Verisk model, these different components are considered when developing facility-level damage functions. Accordingly, the total value of these physical assets should be entered as the total replacement value of the facility in the model. This includes large, ground-bolted

<sup>18</sup> Source: [Volkswagen factory in Wolfsburg, Germany](#) by Andreas Praefcke, [CC BY 3.0](#)

<sup>19</sup> Source: [Modular, portable GTL plant outside Houston Texas](#) by Serge Zolotukhin, [CC BY-SA 4.0](#)

<sup>20</sup> Source: [Industrial cooling towers for a power plant](#) by CenK Endustri, [CC BY-SA 3.0](#)

<sup>21</sup> Source: [Petroleum refinery in Anacortes, Washington, United States](#) by Walter Siegmund, [CC BY 2.5](#)

<sup>22</sup> Source: [A double effect distillation plant](#) by Luigi Chiesa, [CC BY 3.0](#)

<sup>23</sup> Source: [Gas flare, PetroChina Jabung field, Jambi, Indonesia](#) by Darmawan Kwok, [CC BY-SA 4.0](#)

<sup>24</sup> Source: [Spherical gas tank farm in the petroleum refinery in Karlsruhe MiRO](#) by Michael Kauffmann, [CC BY 2.0](#)

<sup>25</sup> Source: [Large sulfur pile at North Vancouver, B.C., Canada](#), by Leonard G., [CC SA 1.0](#)

<sup>26</sup> Source: [Pipe rack constructing](#) by Pbjair, [CC BY-SA 4.0](#)

<sup>27</sup> Source: [Trafostation Alter Hellweg](#) by Rainer Knäpper, [CC BY-SA 2.0](#)

<sup>28</sup> Source: [Circuit Breaker 115 kV](#) by Wtshymanski, [Public Domain](#)

<sup>29</sup> Source: [High voltage switchgear at a transmission substation](#) by Dingy, [CC BY-SA 3.0](#)

machinery as well. The model also supports separate damage functions for the supplies and finished products as part of the content vulnerability.

## Infrastructures

The Verisk Typhoon Model for Southeast Asia supports broad types of infrastructures, such as bridges, railroads, dams, tunnels, tanks, pipelines, electrical transmissions, towers, etc. The damage assessments for these infrastructures are challenging, because different types of infrastructure respond to different typhoon sub-perils. For example, modern bridges that are constructed mainly out of concrete or steel are quite resistant to wind, but relatively vulnerable to storm surge, due to the buoyancy force and the lateral force from the storm surge. Railroads and highways are also more vulnerable to water than wind, but for different reasons. Scour and inundation, which destroy them or make them impassable, are the main threats to these types of infrastructure. Compared to bridges, towers such as electrical transmission and broadcast towers are vulnerable to wind, but relatively resilient to flood and surge. Examples of typical infrastructures are presented in [Figure 122](#).



**Figure 122. Examples of typical types of infrastructures**  
**Top left to lower right: Golden Gate bridge,<sup>39</sup> trees down on roadway,<sup>40</sup> Glen Canyon concrete dam on the Colorado River in Arizona,<sup>41</sup> fuel storage tank,<sup>42</sup> industrial pipeline,<sup>43</sup> industrial chimneys - Big Bend Power Station near Apollo Beach, Florida,<sup>44</sup> tornado-damaged transmission lines,<sup>45</sup> tornado-damaged cell phone tower,<sup>46</sup> and computer servers.<sup>47</sup> Images cropped by Verisk.**

<sup>39</sup> Source: [GoldenGateBridge-001](#) by Rich Niewiroski, Jr., [CC BY 2.5](#)

<sup>40</sup> Source: [Birmingham tornado 2005 damage](#) by User Oosoom on en.wikipedia, [CC BY-SA 3.0](#)

<sup>41</sup> Source: [Glen canyon dam](#) by Agunther, [CC BY 3.0](#)

<sup>42</sup> Source: [Fuel tank gnangarra](#) by Gnangarra, [CC BY 2.5 AU](#)

<sup>43</sup> Source: [Ammiakoprovod NS](#) by Антон Оболенский (Azh7), [CC BY-SA 2.5](#)

<sup>44</sup> Source: [Big Bend Power Station](#) by Wknight94, [CC BY-SA 3.0](#)

<sup>45</sup> Source: [Crumpled transmission towers after 2011-04-27 tornado IMG 0952](#) by Samt2565393, [CC 1.0](#)

<sup>46</sup> Source: [PlainviewTXEF2](#) by NWS Lubbock, TX, Public domain

<sup>47</sup> Source: [IBM Blue Gene P supercomputer](#) by Argonne National Laboratory's Flickr page, [CC BY-SA 2.0](#)

## 5.2 Wind damage functions for residential, commercial, and small industrial buildings

The Verisk wind damage functions represent the relationship between 1-minute sustained wind speed at a height of 10 m and the mean damage ratio (MDR). The model also explicitly accounts for the duration of extreme winds in damage estimation. Damage functions are available for buildings and contents, as well as for time-element coverage. The MDR is defined as the ratio of the repair or replacement cost of the damaged part of building or contents to their replacement value. The time element is the loss related to the expected days that the part or the entire building is uninhabitable (residential building) or unusable (commercial building).

### Building damage

---

Buildings respond differently to wind loads, depending on characteristics such as construction and occupancy class and their height. The vulnerability also changes by year-built of construction and depending on its location as the design considerations generally change in time and by region. The wind damage functions for the Verisk Typhoon Model for Southeast Asia have been developed based on engineering considerations learnings from past damage and loss data from Southeast Asia and other regions. The damage functions have been modified to account for labor and materials costs, building construction practices, and claims adjustment practices in Southeast Asia.

Wind damage is primarily from the nonstructural elements for residential properties, such as different components of the building envelope. Failure of houses with wood frame roofs often occurs first at the roof, and often because of improper fastening between the roof sheathing and building frame. For example, a common failure initiation point on roof systems occurs where the roof membranes are attached to edges and corners; failure is often attributable to the lifting and peeling of metal edge flashings.

Uplift of the roof edges allows the wind to penetrate underneath the roof membrane, resulting in pressure rise beneath the membrane and subsequent removal of the roof covering. At high wind speeds, the integrity of the entire structure can be compromised, particularly in cases where the roof provides the lateral stability by supporting the tops of the building's walls.

Thus, three damage regimes can be identified for residential buildings: (a) a low damage regime generally corresponding to wind speeds of less than about 145 km/h, where damage is limited to roof covering and cladding; (b) a medium damage regime where damage propagates to roof sheathing, connections and openings, and; (c) a catastrophic damage regime generally corresponding to wind speeds in excess of 210 km/h, where the roof framing is severely damaged, resulting in lateral instability of walls, possibly causing their collapse and ultimately the complete destruction of the building.

The effects of different wind speed levels on residential buildings are illustrated in [Figure 123](#). At wind speeds below 145 km/h, the mean damage ratio remains low, but increases rapidly at higher wind speeds, particularly for wood-frame residential buildings.

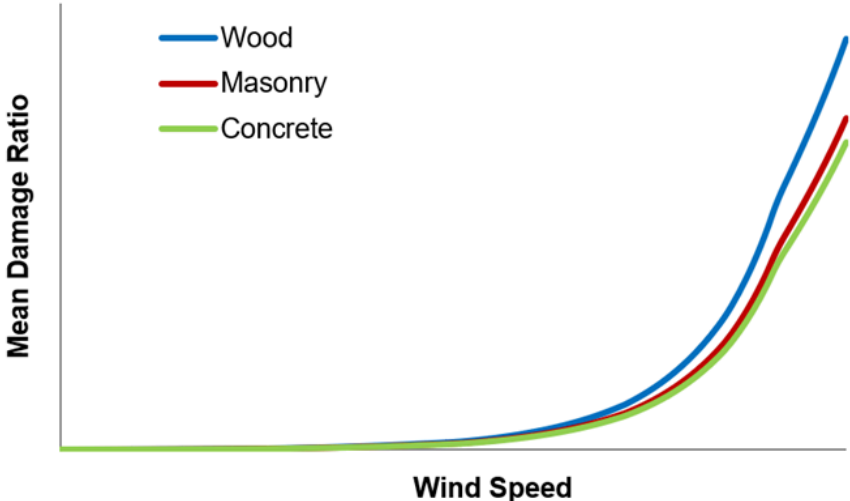


Figure 123. Wind building damage functions for selected construction types, including unknown, for a single-family home in Southeast Asia

Apartment buildings and commercial structures typically receive extensive degree of engineering attention during construction. From a structural viewpoint, therefore, commercial construction and apartment buildings are quite similar and perform quite well against wind. Nevertheless, apartments have some components that make them more susceptible to wind damage than commercial construction, including balconies and double-sliding glass doors. These components are less engineered at the design and construction stages, and contribute to a greater structural vulnerability than commercial construction.

Figure 124 shows an example of relativities for Verisk wind building damage functions for various apartment construction types in Southeast Asia, including “unknown” construction.

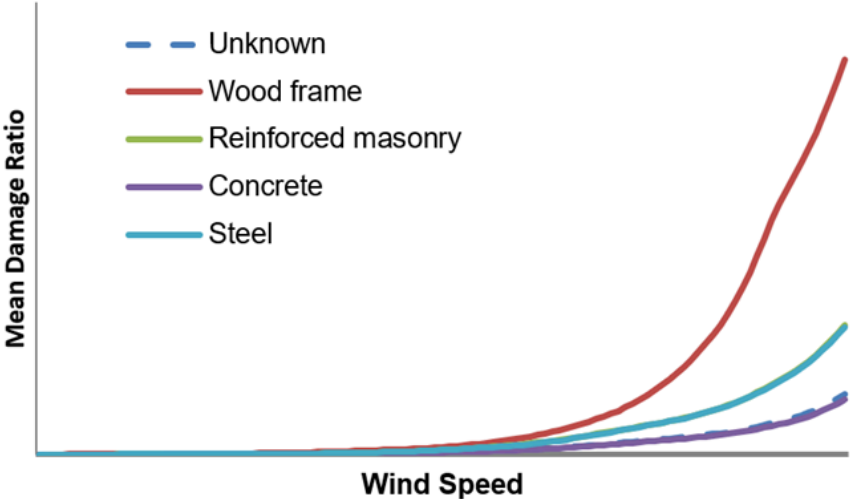


Figure 124. Wind building damage functions for selected construction types, including unknown construction, for unknown-height apartment in Southeast Asia

Damage functions in the Verisk Typhoon Model for Southeast Asia incorporate engineering research and damage survey results. Model losses have been validated using actual losses from several typhoons in Southeast Asia.

Damage functions for buildings with unknown characteristics, including unknown occupancy, construction, and height, are developed using the damage functions of the buildings with known characteristics and Verisk's Industry Exposure Database for Southeast Asia, which is described in a subsequent section.

#### See Also

[Validating modeled losses](#)

[CRESTA-level damage functions for unknown construction, occupancy, or height classes](#)

## Effects of wind duration on building damage

The damage estimation module develops a complete time profile of wind speeds at each location affected by an event, thus capturing the effects of wind duration and peak wind speed on structures. Design loads are routinely exceeded in even moderate intensity typhoons. With no reserve strength, a fastener or connector that has been pulled out or pulled through, as a result of uplift, load can compromise the integrity of the building envelope. Wind damage manifests itself at the weak links in a structural system. As each connector is overwhelmed, loads are transferred to the next point of vulnerability. The longer the duration of high winds, the longer this process continues, and the greater the resulting damage.

[Figure 125](#) (left) shows a sample time profile of wind speeds at a particular location. Note that the wind speed peaks at  $w_4$ , and then diminishes as the storm recedes. [Figure 125](#) (right) shows the corresponding damage function for the given wind speed profile. The building damage ratios ( $d_1$  through  $d_5$ ), corresponding to each wind speed as shown in the wind speed profile and appear on the vertical axis.

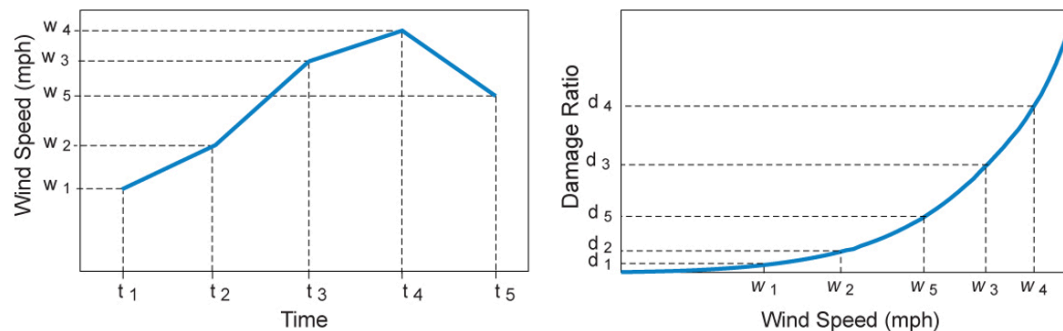


**Figure 125. Wind speed profile and corresponding damage ratios**

The *cumulative* effects of winds on damage can be examined using a dynamic approach. In order to estimate damage to a property at any point in time, it is important to take into account the extent of the damage that occurred in the preceding period. Each damage ratio is applied in succession to the undamaged portion of the exposure remaining from the preceding period. [Figure 126](#) illustrates this process.

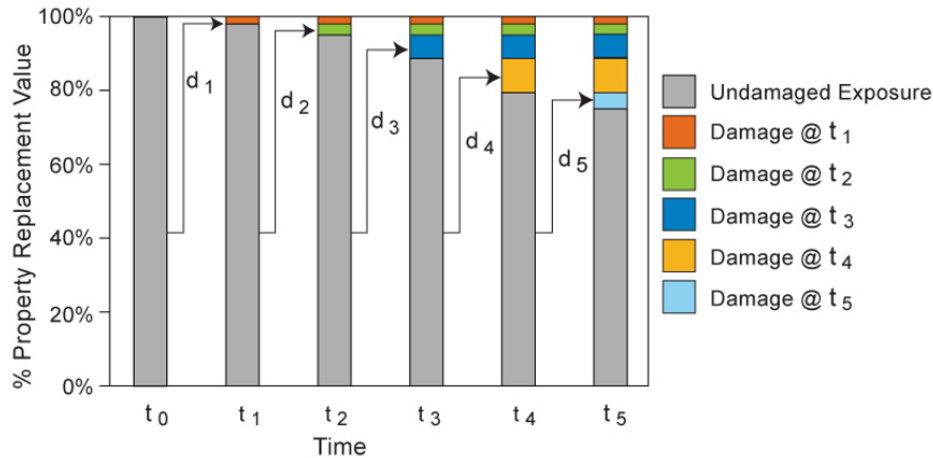


**Figure 126. Measuring the cumulative effects of winds**

At  $t_0$ , before even tropical storm force winds have reached the site, there is zero or negligible damage. At time  $t_1$ , the damage ratio  $\delta_1$  is calculated as a percentage of the full replacement value. At  $t_2$ , the damage ratio  $\delta_2$  is applied to the percentage of the property that was left undamaged in the previous period. This process continues until wind speeds once again fall below tropical storm strength.

Calculating damage only when winds are at their maximum,  $t_4$ , and applying a single damage ratio,  $\delta_4$  to the full replacement value would not capture the cumulative effects of prolonged winds. Therefore, the Verisk damage estimation module captures the effect of storm at each location.

## Contents damage

The contents damage ratio is defined as the monetary loss to the contents divided by the replacement value of the contents. The Verisk model calculates contents damage separately from building damage.

Damage to contents caused by wind is a function of building damage; the main cause of content damage is wind driven rain after the building envelop has been breached. Therefore, damage to contents will be relatively small in comparison to building damage until the envelope of the structure is penetrated. Thus, substantial damage to contents is not likely to occur unless there is significant damage to the roof covering, loss of roof decking panels, or window failure. Thereafter, both building and contents damage will escalate with increasing wind speed, with contents damage increasing more quickly than building damage as wind speeds increase.

Occupancy, in particular, is crucial to the development of damageability of content, as it provides information on the likely contents present and their potential vulnerability. Generally, residential buildings have lower content vulnerability than apartment and commercial properties, which is opposite to their relationships in building damage. [Figure 127](#) shows an example of relationship between building mean damage ratio and content mean damage ratio for the wind sub-peril for different lines of business, including unknown.

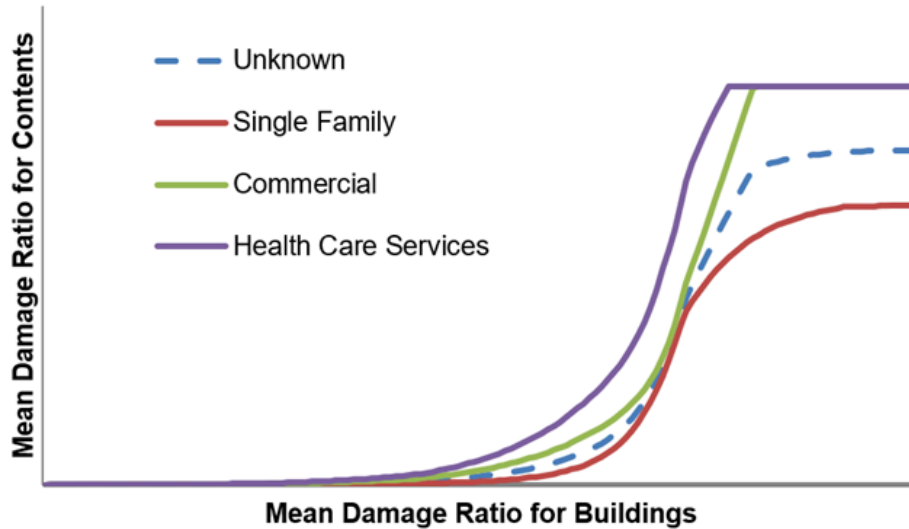


Figure 127. Relationship between wind mean building damage and wind mean contents damage for different lines of business, including unknown

**See Also**

[Building vulnerability by height](#)

### Building vulnerability by height

The Verisk model’s damage functions explicitly account for building height. Separate damage functions have been developed for each of seven height bands: unknown height, 1 story, 2-stories, 3-stories, mid-rise (4-7 stories), high-rise (7-29 stories), and tall (30+ stories). The delineation for the low-rise buildings is more important for the flood and storm surge sub-perils, rather than wind.

Analysis of wind speed profiles reveals that the wind hazard increases with height. For a given storm at a given location, a low-rise building may experience Category 1 wind speeds, while the upper floors of a 20-story building may experience wind speeds corresponding to a Category 3 storm. On the other hand, while the wind hazard increases with height, vulnerability typically decreases with height. High-rise and tall buildings are typically less vulnerable than low-rise structures because they are generally well-engineered and built to strict building code requirements. Verisk wind damage functions for commercial and apartment/condominium buildings explicitly account for building height, as shown in [Table 23](#).

**Table 23. Supported height bands for construction and occupancy classes for wind**

Occupancy Codes	Construction Class	Construction Codes	Building Height (stories)				
			Low	Mid	High	Tall	Unknown
302	All	All	Same vulnerability for all height bands				
301, 303-373	Wood Frame	101-104	Same vulnerability for all height bands				

Occupancy Codes	Construction Class	Construction Codes	Building Height (stories)				
			Low	Mid	High	Tall	Unknown
	Masonry	111-120	1-3	4-7	≥8	-	0
	Concrete	131-140	1-3	4-7	7-29	≥30	0
	Steel	151, 153-159	1-3	4-7	7-29	≥30	0
	200 Series	201-263, 2010-2286	Same vulnerability for all height bands				
	Unknown	100	1-3	4-7	7-29	≥30	0
400-482	All	All	Same vulnerability for all height bands				
300	Wood Frame	101-104	Same vulnerability for all height bands				
	Masonry	111-120	1-3	4-7	≥8	-	0
	Concrete	131-140	1-3	4-7	7-29	≥30	0
	Steel	151, 153-159	1-3	4-7	7-29	≥30	0
	200 Series	201-263, 2010-2286	Same vulnerability for all height bands				
	Unknown	100	1-3	4-7	7-29	≥30	0
All	Light Metal	152	Same vulnerability for all height bands				

**See Also**

[CRESTA-level damage functions for unknown construction, occupancy, or height classes](#)

## Regional wind vulnerability

The Verisk Typhoon Model for Southeast Asia takes into account regional variations in the vulnerability of buildings to wind from two perspectives: variations within each country/territory, as well as across countries/territories. These variations are the resultant of the different design requirements and construction practices across Southeast Asia.

Southeast Asia is subjected to a variety of perils, including typhoons, earthquakes, extreme flooding. Generally, building construction practices have adapted and responded to this unique multi-hazard environment. In the Verisk model, regional vulnerabilities for engineered buildings, like reinforced concrete commercial and steel frame buildings, were developed based on national building codes adopted within each country/territory, building code enforcement levels and the quality of construction practices. For non-engineered buildings, such as residential single family homes and light-metal frame structures, regional vulnerabilities were considered as a combination of multi-hazard and local awareness of these hazards.

The Verisk Typhoon Model for Southeast Asia supports regional vulnerability at 1-km resolution for wind, which matches the high resolution of hazard. Regional vulnerabilities for engineered and non-engineered buildings in the Philippines, Taiwan, and Vietnam, are presented in [Figure 128](#) through [Figure 130](#).

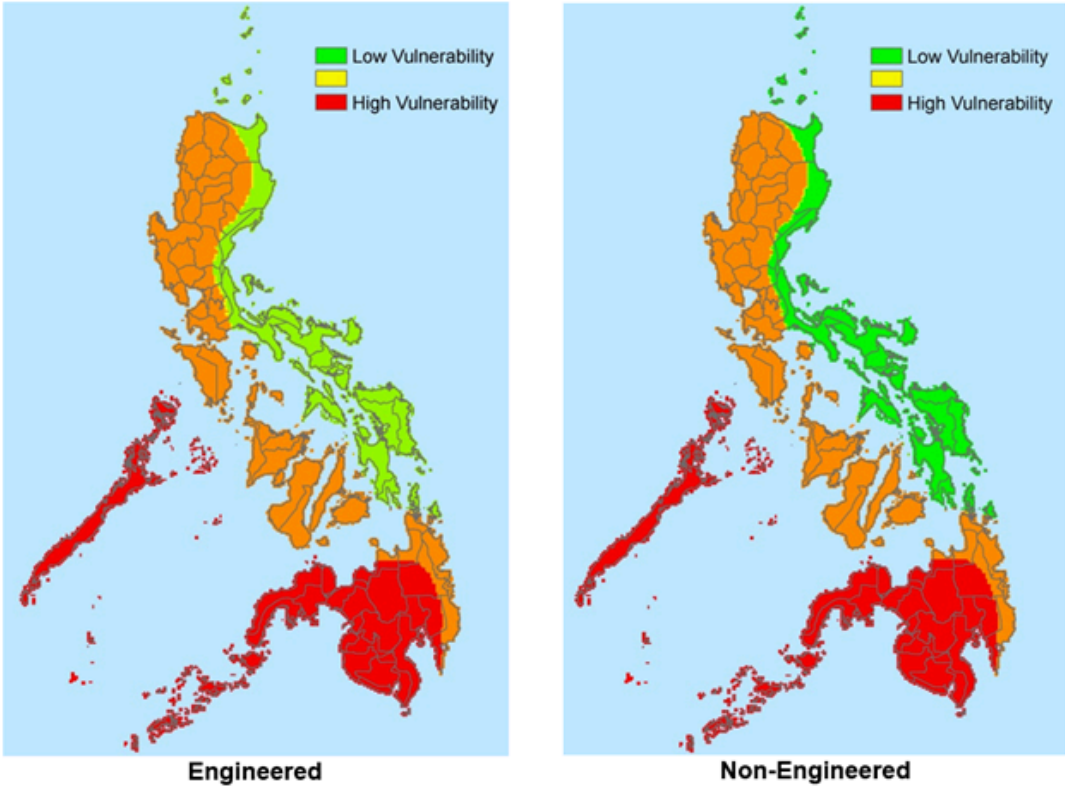


Figure 128. Regional vulnerability for engineered and non-engineered buildings in the Philippines

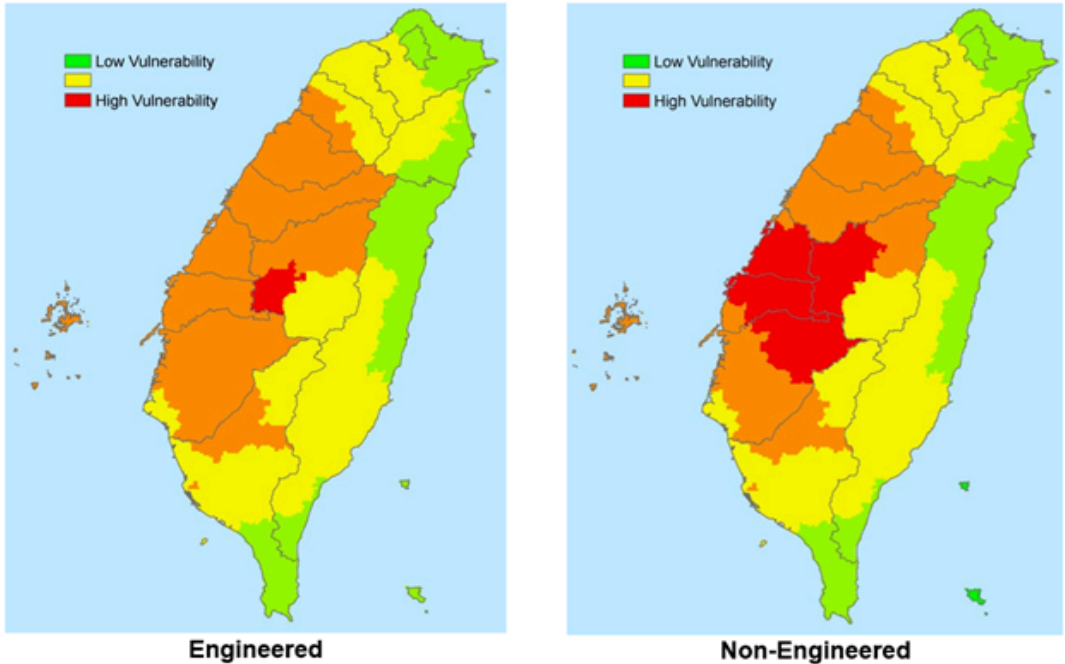
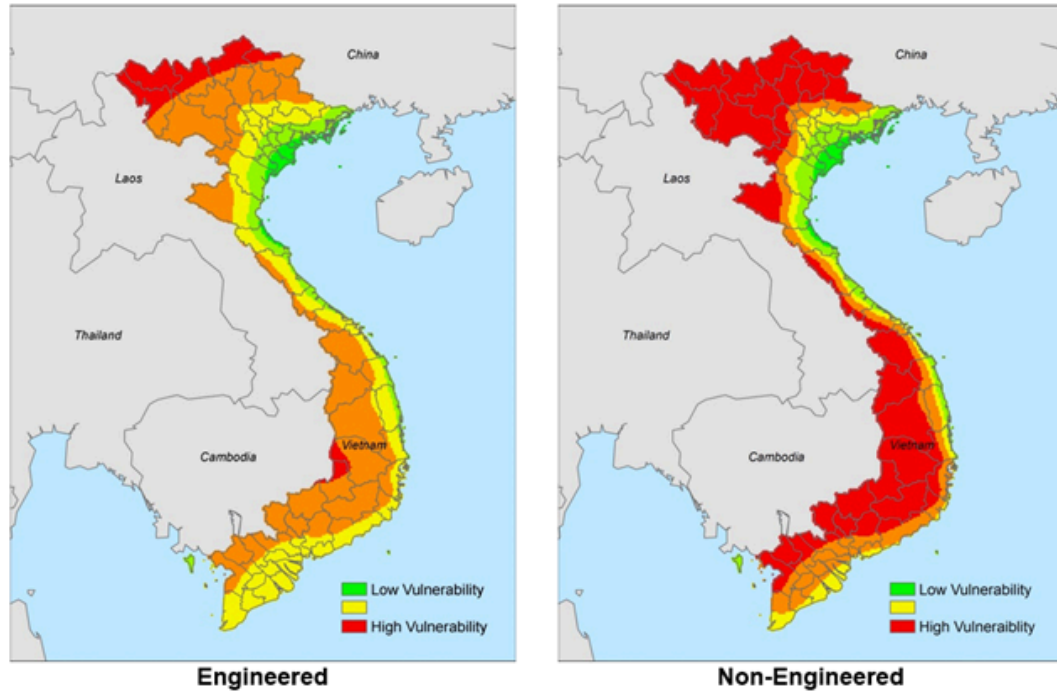


Figure 129. Regional vulnerability for engineered and non-engineered buildings in Taiwan



**Figure 130. Regional vulnerability for engineered and non-engineered buildings in Vietnam**

The vulnerability variation across countries/territories is mainly considered as a combination of building code requirement, building code enforcement, and constructing quality, based on information available in the published research papers, local reports (e.g., see Holmes, Campbell, Aquino, Pacheco, Cheng, Jang, Duy, and Giang), and engineering judgement. Generally, high wind hazard areas are expected to be low wind vulnerability, because they usually use stricter standards and better engineering, and people intend to build better wind resistant houses, and vice versa. However, this is not always true when taking enforcement and quality of constructing practice into account. [Table 24](#) lists the relative wind risk and vulnerability variations across regions in the Verisk model, considering the aforementioned factors.

**Table 24. Relative wind risk and vulnerability across regions**

Country/Territory	Wind Hazard Level	Building Design and Enforcement Level	Wind Vulnerability Level
Guam	Mid-High	High	Mid
Hong Kong	Mid-Low	High	Low-Mid
Macau	Mid-Low	High	Low-Mid
Philippines	High	Low	Mid-High
Saipan	Mid-High	High	Mid
Taiwan	High	High	Low
Vietnam	Low	Low-Mid	High

## Temporal wind vulnerability

---

Temporal vulnerability refers to how the vulnerability of a building varies by the year it was built. A building's capability to resist extreme weather deteriorates with time - older buildings have begun deteriorating and their resistance is then worse than buildings more recently constructed. Sunshine, moisture, hot/cold weather, pollution, salty water, etc. all of these factors contribute to the erosion of buildings and increase their vulnerability gradually. Building code evolution is another reason differentiating buildings constructed in different years. In general, the newer the building code, the stronger and more detailed requirements are issued and followed, especially for engineered buildings, whose construction enforcement is high.

The Verisk Typhoon Model for Southeast Asia studied all the building codes that are available in modeled regions for the past few decades, and developed temporal vulnerability variations for buildings in each region based on the two factors discussed above. The deterioration assumption is applied to all modeled regions but different for each one; this is because the overall circumstance one building exposed in one region is different than another. The model also considers building code effects along with the deterioration assumption. For regions that have multiple versions of building codes issued, their requirements are carefully studied and combined into the overall temporal vulnerability variation, especially for years that have a significant update in the requirements. For regions that only have one building code available, it is expected that change occurs around the year that the code was issued. The factor for unknown year built is the weighted average of factors for known year built, which is derived from year built information for building stock in each country/territory.

[Figure 131](#) shows the temporal changes in vulnerability for engineered building in each modeled country/territory.

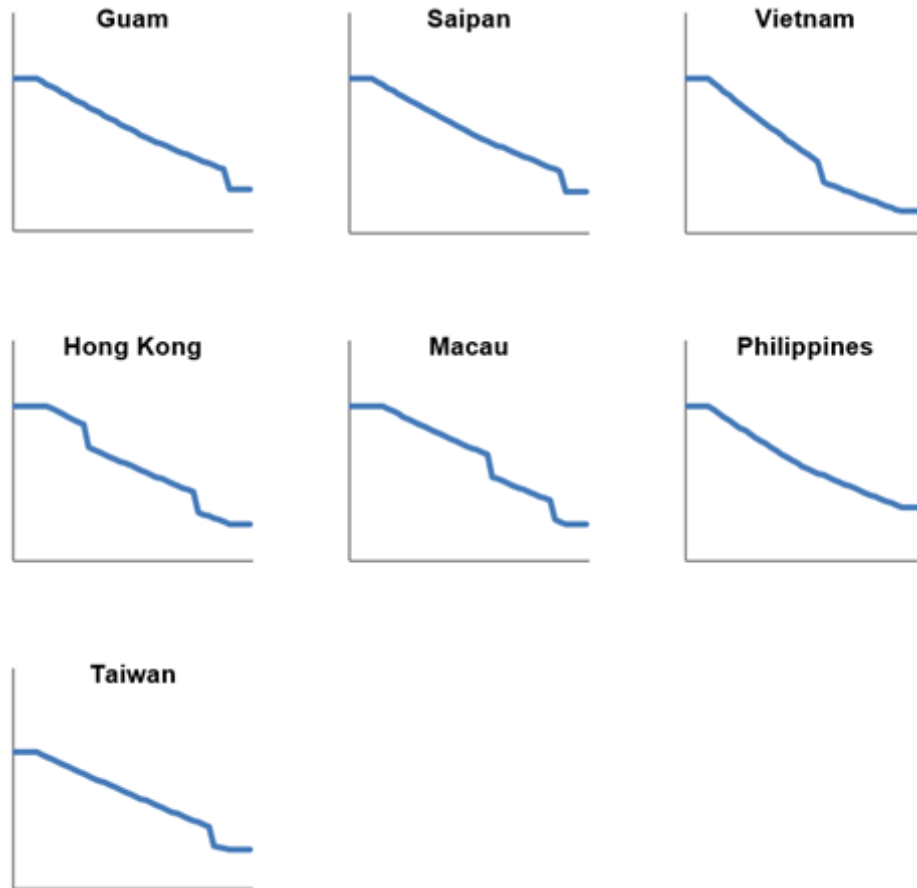


**Figure 131. Temporal modifier for engineered building in the model (x-axis represents the year built, y-axis represents the temporal vulnerability)**

### 5.3 Flood damage functions for residential, commercial, and small industrial buildings

The Verisk Typhoon Model for Southeast Asia explicitly accounts for inland flooding caused by typhoon-induced precipitation in Southeast Asia. Verisk flood damage functions represent the relationship between accumulated precipitation runoff (flood depth) and the mean damage ratio (MDR). Damage functions are available for buildings and contents, as well as for time-element coverage. As mentioned earlier, the MDR is the ratio of the repair or replacement cost of the damaged part of building or contents to their replacement value. And the time element is the loss related to the expected days that part or the whole building is uninhabitable (residential building) or unusable (commercial building).

## Building damage

The damage mechanism to a building from flood is quite different from wind. For wind, different construction materials are responsible for significant variations of resistances against wind, while for flood, these differences among construction types are not that dramatic. Occupancy type and height, however, are the driving factors considered for flood vulnerability.

[Figure 132](#) shows an example of the damage functions for reinforced-concrete, low-rise buildings for single-family, condominium, general commercial, and general industrial.

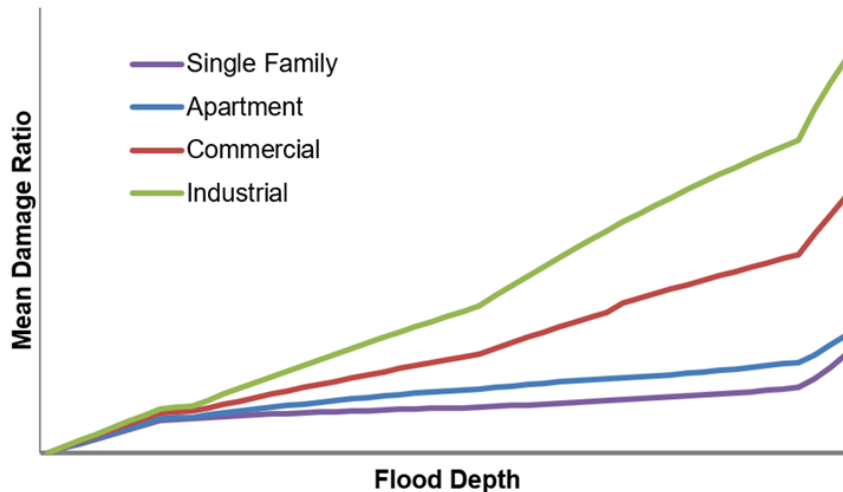


**Figure 132. Flood building damage functions for reinforced-concrete, low-rise buildings for single-family, condominium, commercial, and industrial in Southeast Asia**

From [Figure 132](#), it is suggested that in general, commercial/industrial building is more vulnerable than residential building. One of the reasons is that some high-value and vulnerable components, such as mechanical, electrical and other service equipment are more common in commercial and industrial buildings, and the replacement value from these equipment contributes appreciably to the building replacement value, even for low-rise buildings. However, for high-rise buildings, these kinds of equipment are also widely used in condominiums. Therefore, the performance for apartment and commercial are similar for high-rise building.

### Single-family building

Generally, most of the single family buildings, which are low-rise and do not have basements, are not very vulnerable to shallow water, and building repair costs are relatively low and stable for low water depth. However, with the increment of flood level, a larger portion of total building is submerged, and walls and other parts are likely to be replaced, then the cost increases rapidly. [Figure 133](#) shows an example of flood damage functions with selected construction types, for low-rise single-family building. The damage curve in [Figure 133](#) is relatively flat at the beginning, where flood depth is low, and increases sharply after a certain depth, usually as a large portion of the building is underwater and will need replacement.

Variations of vulnerability among construction types are not very significant, especially at low flood depth.

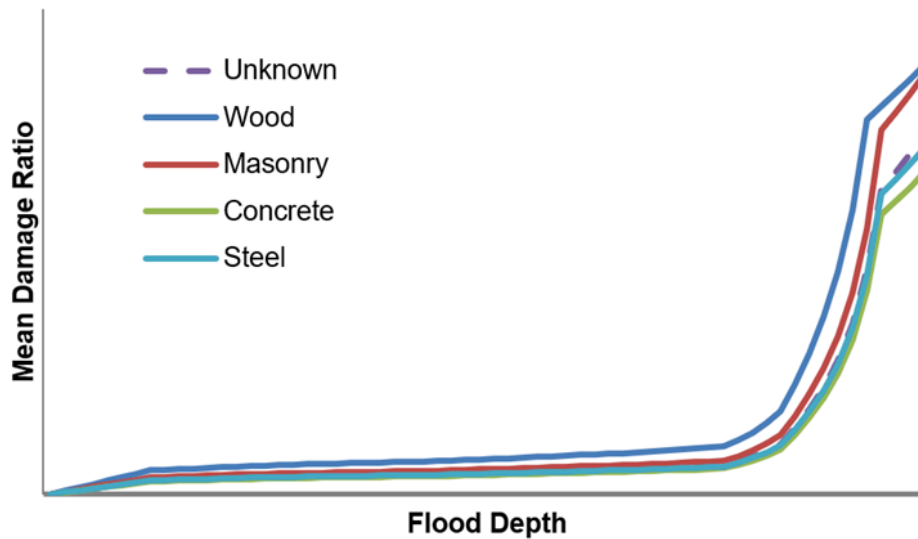


**Figure 133. Flood building damage functions for selected construction types, including unknown, for low-rise single-family buildings in Southeast Asia**

#### *Apartment and condominium building*

Apartment and condominium buildings, which are possible in all height bands and usually have underground parking garage or service equipment located in the basement, turn out to be more vulnerable than single family buildings at relatively low flood depth. [Figure 134](#) shows an example of flood damage functions with selected construction types for 3-story condominium building. Compared to single-family buildings, condominium buildings are more vulnerable at relatively low flood depths; this is mainly because of the damage from underground facilities, which are usually valuable and associated repair or replacement costs are high. The damage curves tend to be flat toward very high flood depth; this is because even if the flood depth is quite high, some structural components survive and reusable after the water has been extracted, especially in concrete and steel buildings.

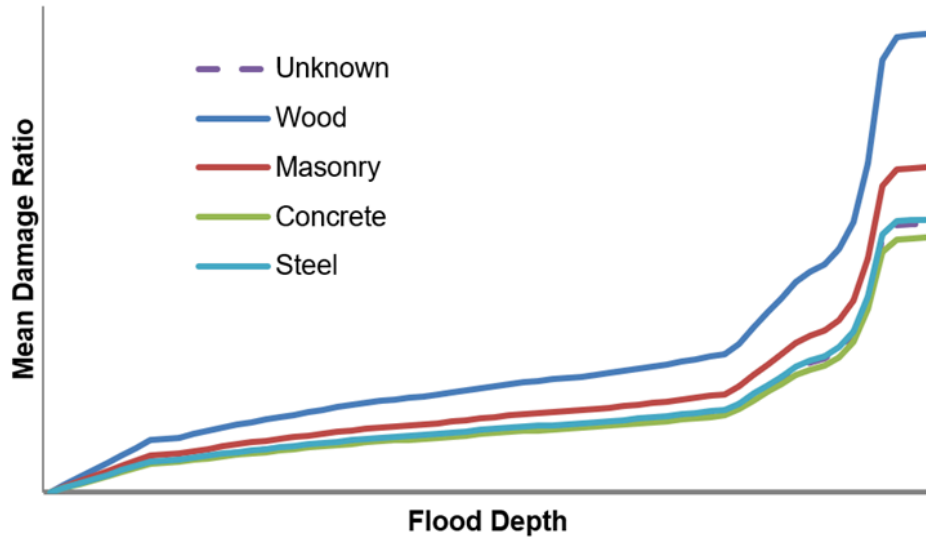


**Figure 134. Flood building damage functions for selected construction types, including unknown, for 3-story condominium in Southeast Asia**

#### *Commercial and small industrial building*

The vulnerability of commercial and small industrial buildings is more complex than apartment buildings. Fixture and fitting such as partition and cabinet, which is common in commercial and small industrial buildings, is vulnerable to water and usually needs to be replaced if inundated. Carpet, which is commonly used in these types of buildings, is vulnerable to water damage, even at low water depths. Generally, carpet that is flooded needs to be replaced. These buildings also have service equipment such as generator and heater located at lower floor or basement, if exist. If they are damaged, the repair costs are quite high because of the high value and complexity of the equipment. Construction material and building frame is also important for buildings. For example, comparing to masonry, concrete is generally less penetrable and more resistant to erosion. Presented in [Figure 135](#) is an example of flood damage functions with selected construction types, for a 3-story commercial building.

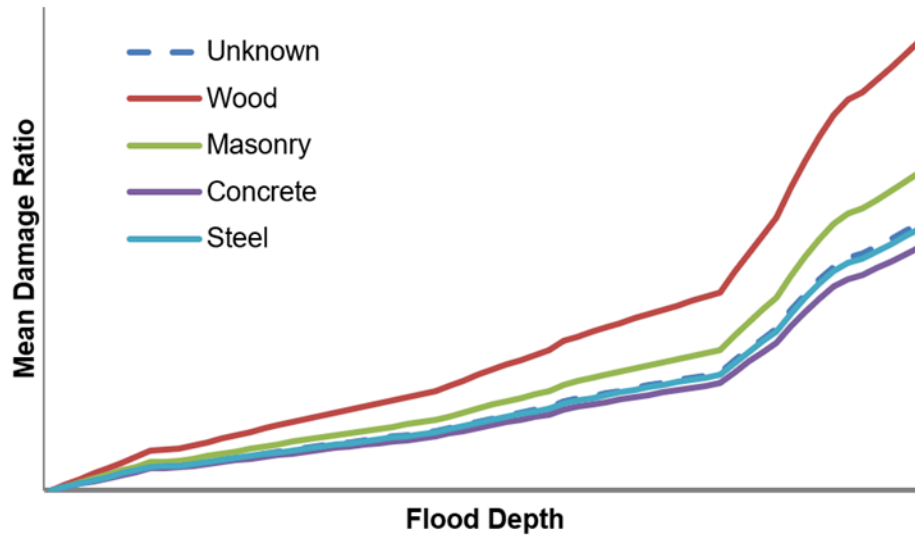


**Figure 135. Flood building damage functions for selected construction types, including unknown, for 3-story commercial in Southeast Asia**

Overall, occupancy type mainly determines building vulnerability to flood, but construction type is also important as some additional information can be gathered based on building materials. For example, for a given flood depth, a wood-frame, residential building will be more vulnerable than a masonry residential building. Concrete construction is less vulnerable to flood than steel or masonry structures. Masonry is characterized by weak connections between building elements and is thus permeable to water. Steel buildings have a strong frame structure, but may experience surface corrosion and rust-induced expansion. Concrete buildings also have a strong frame structure, but may suffer from cracking and rebar expansion. Condominium and commercial buildings usually have stronger foundations than residential buildings, and are thus better able to resist flood loads. However, this does not mean their overall vulnerability is always lower than residential, because of the high value service equipment located beneath; they may be more vulnerable than residential buildings for certain water levels.

## Content damage

The contribution of content damage to the total damage from flood can be substantial. Even though content damage has a weaker tie to building damage for flood than for wind, it is highly correlated with occupancy types and height. We will discuss height in next section, and this section will cover the relationship between content damage and occupancy type.

Buildings occupied for different purpose usually contain and store things differently. For example, the valuable contents for a single family home may be appliance and furniture, and for apartments may be carpet, interior decors, etc. These are usually located on the lower floors and hard to mitigate when water comes in. Therefore, they are vulnerable to flood. An example of the relative vulnerability of contents for a residential home is presented in [Figure](#)

136. The vulnerability is not only based on the likely location of the contents, but also based on their damageability should they become flooded.

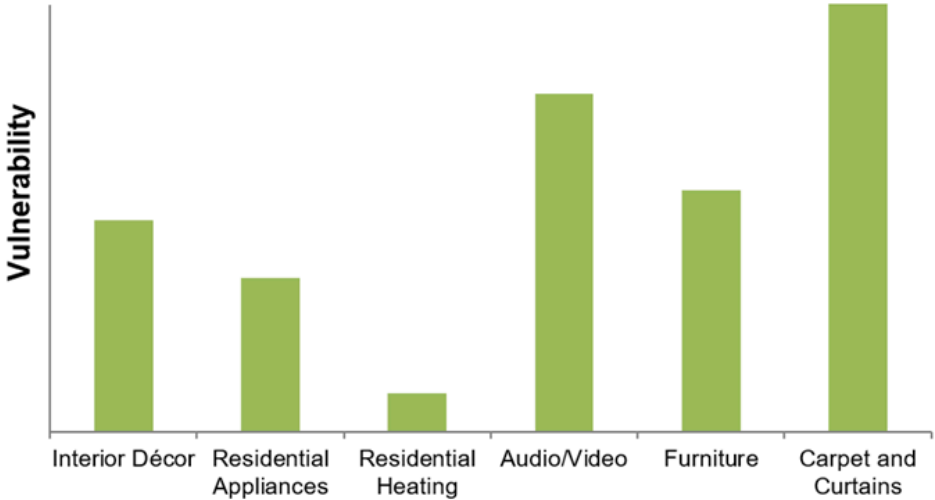


Figure 136. Relative vulnerability of contents for residential buildings

An example of flood content damage functions for reinforced concrete, mid-rise buildings for general occupancy types is presented in Figure 137. Content vulnerability for commercial buildings is higher than that of industrial buildings because most of the contents in commercial buildings are easily damaged and generally become unusable if soaked with water, such as office furniture, while some of the contents in industrial buildings are repairable, or still usable to some extent, such as industrial raw materials or finished products.

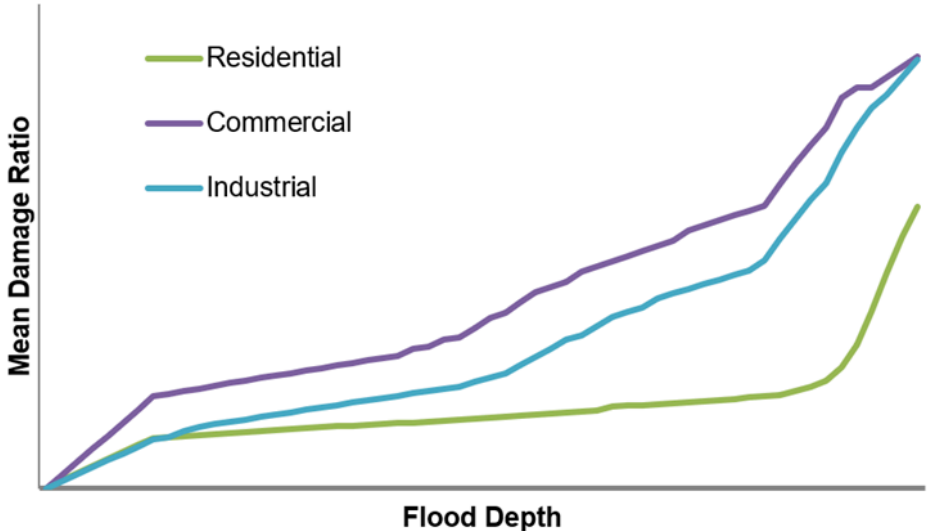
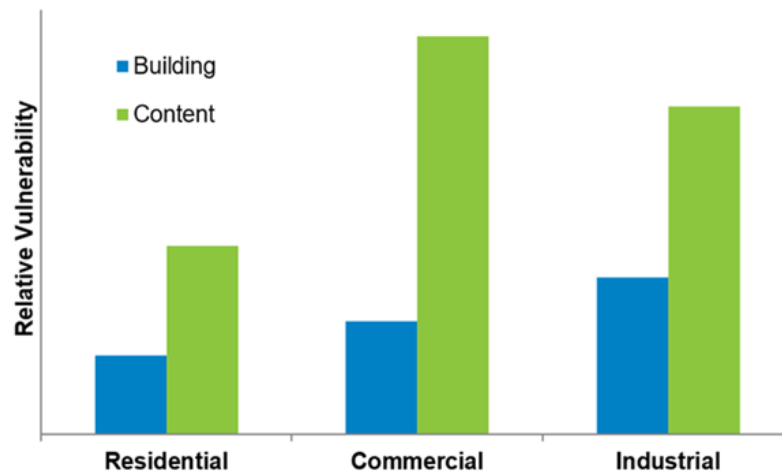


Figure 137. Flood content damage functions with reinforced concrete, mid rise building for general occupancy types in Southeast Asia

Flood, in general, is more destructive to a building's contents than to the building itself. Because most of the damage to building structures is repairable, while contents damage is usually permanent. Vulnerability of buildings and contents, for major general occupancy classes constructed with reinforced concrete, are presented as a comparison in [Figure 138](#).



**Figure 138. Relative flood vulnerability of building and content for general occupancies with reinforced concrete in Southeast Asia**

## Building content vulnerability by height

From a risk perspective, the impact of flood is usually restricted to the lower stories of a building. This means that building height is a very important determinant of both building and content vulnerabilities. Building values, including building self and content, can be reasonably assumed to be relatively distributed evenly at each story. Thus, higher buildings usually means smaller portion of values located at lower floors, which reduces their flood vulnerabilities. Meanwhile, higher building usually gets more engineering attentions, including better flood defense mechanisms. However, it is noteworthy that higher buildings, especially high-rise and tall building, are generally locate electrical and mechanical fixtures in the basement or the ground floor, which dilutes the benefits from robust engineering practices. Building height is also correlated with construction type. Construction materials that are commonly used for higher buildings, such as steel and concrete, have lower porosity and higher strength than masonry and wood, and thus have lower vulnerability.

[Table 25](#) shows the supported height categories for flood and [Figure 139](#) presents an example of flood relative vulnerability of different supported height categories for a concrete apartment building in Southeast Asia, including unknown height.

**Table 25. Supported height bands for construction and occupancy classes for flood**

Occupancy Codes	Construction Class	Construction Codes	Building Height (stories)						
			1-story	2-story	3-story	Mid	High	Tall	Unknown
302	All	All	1	2	≥3	-	-	-	0

Occupancy Codes	Construction Class	Construction Codes	Building Height (stories)						
			1-story	2-story	3-story	Mid	High	Tall	Unknown
303	All except unknown	All except 100	1	2	≥3	-	-	-	0
303	Unknown	100	1	2	3	4-7	≥8	-	0
301, 304-373	Wood Frame	101-104	1	2	≥3	-	-	-	0
	Masonry	111-120	1	2	3	4-7	≥8	-	0
	Concrete	131-140	1	2	3	4-7	7-29	≥30	0
	Steel	151, 153-159	1	2	3	4-7	7-29	≥30	0
	200 Series	201-263	Same vulnerability for all height bands						
	Unknown	100	1	2	3	4-7	7-29	≥30	0
400-482	All	All	Same vulnerability for all height bands						
300	Wood Frame	101-104	1	2	≥3	-	-	-	0
	Masonry	111-120	1	2	3	4-7	≥8	-	0
	Concrete	131-140	1	2	3	4-7	7-29	≥30	0
	Steel	151, 153-159	1	2	3	4-7	7-29	≥30	0
	200 Series	201-263	Same vulnerability for all height bands						
	Unknown	100	1	2	3	4-7	7-29	≥30	0
All	Light Metal	152	1	3	≥3	-	-	-	0

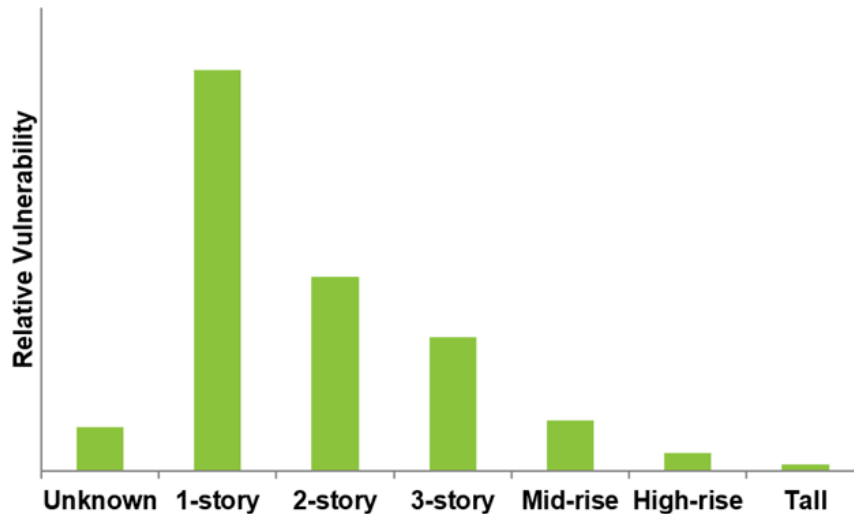


**Figure 139. Flood damage functions for supported height categories for concrete apartment building in Southeast Asia**

Verisk recognizes that building height information is not always readily available. Therefore, flood damage functions, like wind damage functions, are developed for buildings with unknown heights as a weighted average of damage functions for buildings with known heights. The weight is based on their representations in Verisk's Industry Exposure Database. The section on unknown vulnerability discusses this in further details.

## Accounting for flood defense systems

Flood defense systems, which include levee systems, sewer and drainage systems, water storage systems, and many other flood protection and reduction systems, are taken into account during the flood loss estimation within the Verisk Typhoon Model for Southeast Asia. Well established flood defense systems can significantly help manage and reduce flood loss.

Levee systems along a river can help protect against flood events for a particular magnitude. A well-designed drainage system is critical for properties and lives, especially in urban areas, because urbanization has a significant impact of drainage flows within the environment. When rain falls on impermeable artificial surfaces and is drained by a system of pipes, it passes much faster to the receiving water body than it would have in a natural environment. This causes a rapid build-up of flows and higher peak flows, increasing the risk of flooding in the receiving water body.

Water storage systems attenuate flood flows, effectively reducing peak flows. This is especially true when there is a significant volume of storage available.

The completeness and complexity of a flood defense system can vary dramatically across a region. Hong Kong pays a significant amount of attention to flood management and has invested billions of dollars in improving flood infrastructure and engineering technological solutions. The design return period of the main trunk of Hong Kong's urban drainage system is 200 years; the branch of the same system has a return period of 50 years.

Taiwan also actively manages flood by employing the use of flood defense structures and early warning systems, especially in Greater Taipei area. Taipei is located within the Tamsui River basin, a basin which has experienced many flood events in the last few decades. Since 1982, Taipei has been upgrading flood control systems, many of which were originally constructed in 1899. Taipei has developed river levees and built better drainage systems. These and other upgrades have significantly increased flood capacity and have helped managing flood risks to a great extent. However, with the explosive growth of population, demand of urbanization, a great increase in buildings had erected along the river valley, and some extreme typhoon driven flood events, such as Nari in 2001, still have the ability to cause destructive flood damages.

Flood defense systems are an important part of urban planning. Flood defense systems need to be considered and designed ahead of time and they are difficult to upgrade or enhance. Unlike Hong Kong and Taiwan's flood defense systems, which were well designed decades ago and have been carefully maintained, flood defense system construction in the Philippines and Vietnam cannot keep pace with the speed of building and infrastructure construction. This leaves many areas prone to increased potential flood risk from typhoon events.

After carefully reviewing and assessing the flood hazard and defense systems across all the territories in Southeast Asia, the Verisk Typhoon Model for Southeast Asia differentiates the flood vulnerability using the relative flood risk view, shown in [Table 26](#).

**Table 26. Relative flood risk and vulnerability for Southeast Asia modeled countries/territories**

Country/Territory	Flood Hazard Level	Flood Defense Level	Flood Vulnerability Level
Guam	Low	Low	Low
Saipan	Low	Low	Low
Hong Kong	Mid	High	Mid
Macau	Mid	High	Mid
Taiwan	Mid-High	Mid-High	Low-Mid
Philippines	Mid-High	Low	Mid-High
Vietnam	High	Low	High

## 5.4 Storm surge damage functions for residential, commercial, and small industrial buildings

The Verisk Typhoon Model for Southeast Asia explicitly accounts for flooding from storm surge in Southeast Asia (for Hong Kong, the Philippines, and Taiwan). Verisk storm surge damage functions represent the relationship between the effective inundation depth and the mean damage ratio (MDR). Damage functions are available for buildings and contents, as well as for time-element coverage. As mentioned earlier, the MDR is the ratio of the repair

cost of the building or contents to their replacement value. And the time element is the loss related to the expected days that the building is uninhabitable (residential building) or unusable (commercial building).

In the Verisk Typhoon Model for Southeast Asia, the amount of damage that a building or its contents will sustain from storm surge depends on the effective inundation depth, construction class, occupancy class, and building height. Similar to the precipitation-induced flooding sub-peril, storm surge damage to contents is based directly on the hazard intensity parameter, which is the effective inundation depth. The effective inundation depth is the combination of the hydrostatic forces (due to water depth) and hydrodynamic forces (due to the water's forward velocity). The model includes separate storm surge damage functions for buildings and contents.

Storm surge damage is broadly similar to that of precipitation-induced flooding because both are caused by water-related sub-perils. There are, however, some unique features that increase the potential for storm surge to cause greater destruction than precipitation-induced flood. The dynamic component of water velocity is one differentiator between storm surge and precipitation-induced flood. The velocity component from storm surge can generate continuous lateral force on a building, and increase the probability of damage. Water velocity can also push and move debris with significant force, making it more dangerous than floating in static water. Furthermore, storm surge is salty water, which contains salt and other minerals that can cause more corrosive damage to buildings and contents that are not specifically engineered to withstand such conditions. Therefore, for a given effective inundation or water depth, storm surge is expected to cause more damage than precipitation-induced flooding.

Similar to precipitation-induced flooding, building height also plays an important role in vulnerability to storm surge, wherein damage is also most often restricted to the lower stories of a building. This means that higher buildings usually experience lower damage ratio because the value of building and contents in lower part of the building takes a small portion of the replacement value, thus the contribution of loss in percentage from damaged stories is lower in higher building than in lower building. [Figure 140](#) shows an example of surge relative vulnerability of different supported height categories for a concrete commercial building in Southeast Asia, including unknown height.

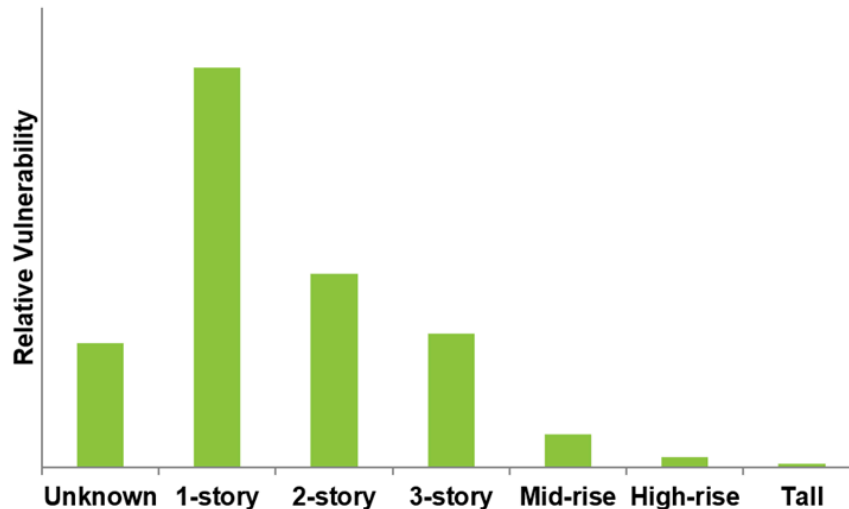


**Figure 140. Storm surge vulnerability for supported height categories for a concrete commercial building in Southeast Asia**

Verisk recognizes that building height information is not always readily available. Therefore, storm surge damage functions, like wind and flood damage functions, are developed for buildings with unknown characteristics as a weighted average of damage functions for buildings with known characteristics. The weight is based on their representation in Verisk’s Industry Exposure Database.

It is important to recognize that the levee systems is taken into account when estimating storm surge hazard intensity parameter, because the levees along the coastline is explicitly modeled during the storm surge hazard simulation process.

## 5.5 Combined damage from multiple sub-perils

With the explicit modeling of the three individual sub-perils of typhoon—wind, precipitation-induced flood, and storm surge—damage due to each sub-peril is calculated separately. This methodology provides more accurate estimations for each sub-peril. However, the ultimate monetary loss to a building should be a combination of losses from all three sub-perils, and it is not always a sum. Two main challenges of combining sub-peril loss to generate the final loss estimation are double counting and overestimating.

Double-counting is common when considering two similar sub-perils together, such as precipitation-induced flood and storm surge. At first, the areas affected by these two sub-perils infrequently overlap. Storm surge is generally focused on coastline area, and precipitation-induced flood is generally inland. Additionally, even though the same property experienced the damage from both precipitation-induced flood and storm surge, simply adding the damage from these two sub-perils together does not represent reality since the hazard is not additive and the damage mechanisms is very similar for both sub-perils. To avoid this, the Verisk Typhoon Model for Southeast Asia first calculates the mean damage

ratio for these two sub-perils separately using individual intensities, and then calculates the water-related MDR by taking the maximum MDR between precipitation-induced flood and storm surge.

Overestimating is rare but still observable, especially in extreme events where the wind MDR and water-related MDR could be very high and their summation would exceed 100%. To ensure this does not occur, the Verisk Typhoon Model for Southeast Asia always checks the reasonability of the combined MDR and caps it at 100% by reducing the MDR for each sub-peril proportionally if it is exceeded. An example of how this approach affects the final MDR for each sub-peril is provided in [Table 27](#).

**Table 27. Example of combined MDR calculation using sub-peril MDRs**

Step	Wind	Flood	Storm Surge
1. Original coverage A MDRs for all sub-perils (sum exceeds 100%)	80%	60%	40%
2. Modified coverage A MDRs for all sub-perils (combine flood and surge)	80%	60%	
3. Modified coverage A MDRs for all sub-perils (cap to 100% and reduce each sub-peril proportionally)	57%	43%	
4. Final coverage A MDRs for all sub-perils (redistribute water loss into flood and storm surge proportionally)	57%	26%	17%

Note that if the cap is exceeded, then the model distributes water-related loss to flood and storm surge based on the ratio calculated from the original MDRs for those sub perils.

Once the combined MDR is finalized, the model calculates and distributes Coverage D (time element) loss, also known as business interruption loss.

**See Also**

[Time element \(business interruption\) damage functions for commercial and small industrial buildings](#)

## 5.6 Time element (business interruption) damage functions for commercial and small industrial buildings

Business interruption (BI) functions represent per-diem expenses or business interruption losses associated with the expected number of days that the building is uninhabitable (for residential structures) or unusable (for commercial).

To estimate BI losses for commercial and small industrial buildings, the damage function uses an “event tree” approach, incorporating the latest research and findings from an extensive analysis of claims data, as illustrated schematically in [Figure 141](#). For each damage state, a probability is assigned to two possible outcomes for the exposure: continued or

ceased operations. If operations cannot continue, a probability of relocation is assigned, which varies by occupancy. For example, while relocation is feasible for an office, it is not for a hotel. As these exposures will require different paths to recovery, they will have different downtimes in the event of business interruption.

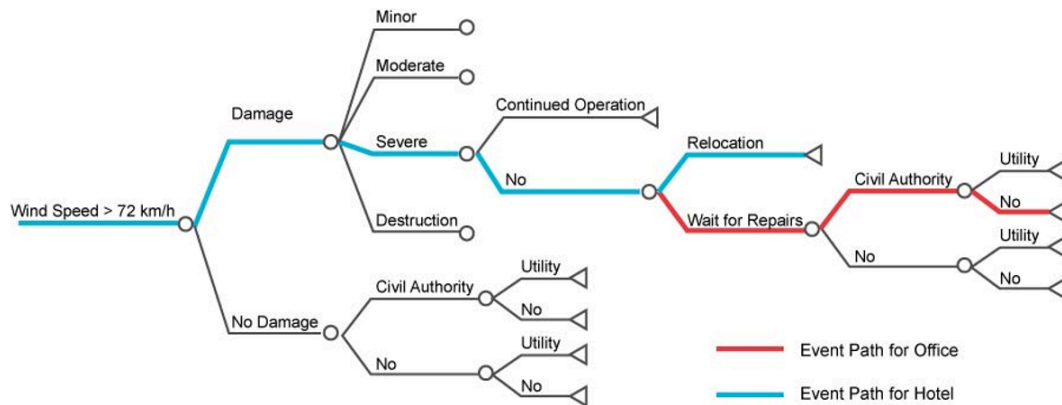


**Figure 141. Hypothetical event tree of BI estimation for an office and a hotel**

Downtime is calculated for each stage of the damage assessment and recovery process. Stage 1 is the time before repairs can begin (pre-repair), during which damage must be assessed, repair costs must be negotiated with contractors, and building permits must be obtained. Stage 2 is the repair time, during which some businesses will choose to relocate rather than wait for repairs. Not that relocation also takes time, and revenues may not immediately return to pre disaster levels even if operations have begun; it may take some time to regain market share and/or rebuild a workforce that may have been relocated.

In the Verisk Typhoon Model for Southeast Asia, the estimated number of days needed to restore the business to full operation depends on a number of key factors, including the level of damage sustained, the size of the building (as approximated by building height) and its architectural complexity (as approximated by occupancy class).

For a given damage ratio, a hotel with a 2,500 square meter hotel will take significantly longer to repair than a 450 square meter professional office building. Interior finishes must also be taken into account, as the higher quality finished often seen in hotels can take more time to repair. Since floor area is usually not directly available, it is estimated using building height. Buildings with significant architectural complexity will also take more time to repair. Although warehouses can be quite large, repairs are more likely to occur quickly because of their architectural simplicity.

Some types of businesses, such as hospitals, are more resilient than others and may be able to restart operations before repairs are complete, or may have had disaster management plans in place that allow them to relocate some operations quickly. For other businesses, such as hotels and restaurants, relocation is not an option due to existing infrastructure required for operation that is immovable. Since many parameters (such as building size, complexity, and business resiliency) critical to determining business interruption are generally not available for input into the model, occupancy class is used as a measurement proxy.

Occupancy is also used to estimate the probability of business interruption at a dependent building within the damage footprint—such as the supplier of a necessary manufacturing component—that will exacerbate BI losses at the principal building.

Damage estimation of the impact of a dependent building (or multiple dependent buildings) on a principal building requires both the location data and the degree of interdependence between the dependent and principal building(s). Logical assumptions are made based on published construction and restoration data and expert engineering judgment to estimate the impact of the dependent building(s) on the principal building’s downtime due to typically limited exposure information ([Figure 142](#)).

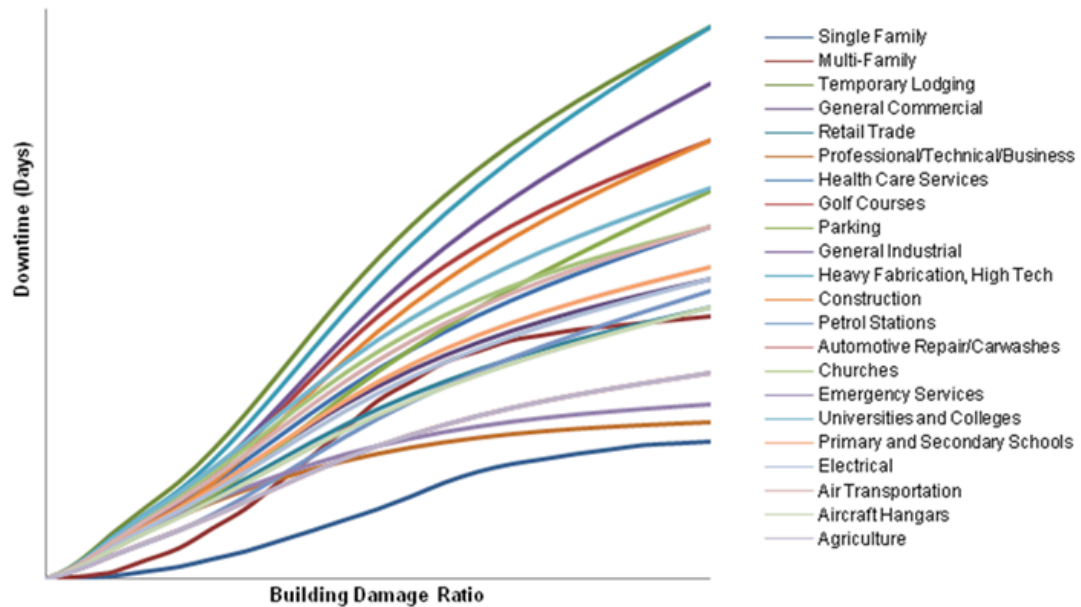


**Figure 142. Time element (BI) damage functions for different buildings of varying occupancy classes**

## 5.7 Distribution of damage: Uncertainty in damage estimation

Individual damage functions for different construction type, occupancy class, and lines of business provide estimates of the mean—or expected—damage ratio corresponding to each level of intensity. However, these estimates are sampled from full probability distributions that allow for non-zero probabilities of zero percent and one hundred percent damage ([Figure 143](#)).

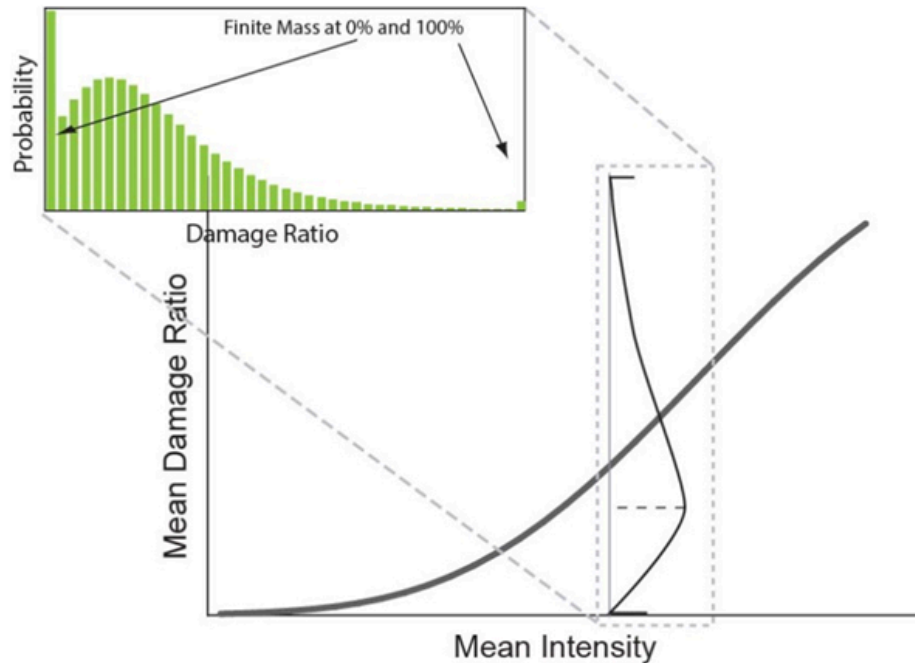


**Figure 143. Representative damage function**

As is commonly seen in the course of damage surveys conducted in the aftermath of actual events, there can be a wide range of damage to structures of similar construction for the same intensity (wind speed, flood depth, etc.), including buildings that are untouched and those that are completely destroyed. This variation in building damage can arise due to a degree of inherent randomness in building response, or differences in building characteristics, construction materials, and/or workmanship. The uncertainty in damage is captured in the model by the probability distributions around the mean damage ratio (MDR).

Verisk researchers also conducted detailed analyses of location-specific claims data by coverage type in regions where such information is available, and uncovered that these uncertainties (distributions) can vary significantly by building classification (engineered vs. non-engineered) and coverage. For this reason, the damage distributions in the model vary by building classifications and coverages.

## 5.8 CRESTA-level damage functions for unknown construction, occupancy, or height classes

The Verisk Typhoon Model for Southeast Asia supports damage functions for buildings with any combinations of features that are unknown, such as construction, height, or occupancy for each territory and within each territory. Each combination of unknown characteristics is evaluated as a weighted average of the damage functions for buildings for which these characteristics are known, with building inventory weights derived from the Verisk Industry

Exposure Database. For example, the damage function for a particular exposure of known construction and occupancy, but unknown height, would be a weighted average of the damage functions for the same construction and occupancy classes corresponding to all the different height classes that are available in the region studied. The damage function for a particular exposure of known occupancy, but unknown construction and height, would be a weighted average of the damage functions for the same occupancy class corresponding to all combinations of construction and height classes that are available in the region studied.

Based on the available client data in this region, generally, some important building characteristics, such as the construction type and height, are missing. Therefore, it is very important to introduce a more granular level unknown damage function. To more precisely capture the regional variability of building inventory distribution and better represent the regional risk, the Verisk Typhoon Model for Southeast Asia supports unknown damage functions at CRESTA level. This means that for each CRESTA in each territory, weights of known damage functions used for calculating any unknown damage functions are derived from building inventory within the CRESTA from Verisk's Industry Exposure Database. Examples of variations of building inventory distributions within two CRESTA areas in Taiwan are illustrated in [Figure 144](#).

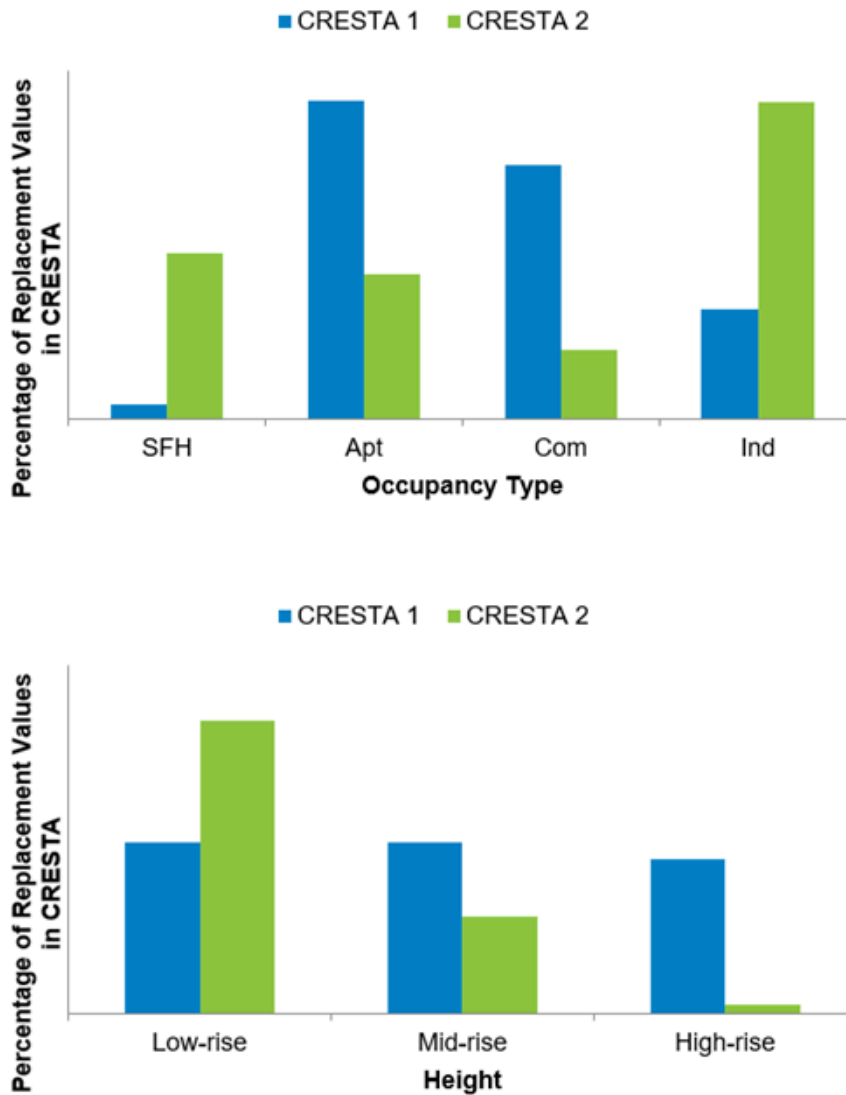


Figure 144. Comparison of building inventory with CRESTA areas by occupancy and height class in Taiwan

## 5.9 Estimating damage to large-scale industrial facilities

The Verisk Typhoon Model for Southeast Asia features the ability to assess potential property and business interruption (BI) losses to large-scale industrial facilities (IFM) from wind, flood, and storm surge. As mentioned previously, large-scale industrial facilities are defined as collections of assets, including regular buildings, cooling towers, tanks, flares, pipe-racks, and process towers that spread over a large area. Such components are essential for site operations and the vulnerability of each of these components is different from one another when subjected to different sub-perils. Therefore, more than 400 damage functions were developed for roughly 550 distinct industrial components and sub-components from

findings from detailed, site-specific, engineering-based risk assessments—conducted by Verisk through Verisk’s Catastrophe Risk Engineering (CRE) services—that encompassed engineering studies, structural calculations, materials tests, and post-disaster field surveys. By developing component-level damage functions based on engineering analyses and hard data, Verisk has created a defensible, transparent, and reproducible methodology resulting in damage functions that are realistic and robust.

This component-based approach to evaluate the damage and loss to an entire large-scale industrial facility allows the damage functions to account for the primary components intrinsic to a large-scale industrial facility and the interconnectivity between them. Primary components are categorized into classes and sub-classes to account for variations in vulnerability within each component class.

To develop damage functions for a large-scale industrial facility, some assumptions regarding the characteristics of individual components are made. Aggregated functions based on the component and sub-component damage functions were developed for each large-scale industrial facility. Each component and sub-component damage function was assigned a weighting factor based on its replacement value relative to the replacement value of the facility to determine the damage function for the industrial facility as a whole.

This approach provides damage estimates that are transparent, realistic, and consistent for a variety of facilities. Furthermore, the component-based approach is essential for reliable assessments of BI losses, which depend on the numerous interactions between the various components and lifelines at a large-scale industrial facility.

Many content-like components are considered to be part of the facility. Hence, the facility-level damage function already incorporates their vulnerability. Accordingly, significant portion of the facility replacement value should be modeled as coverage A in the model. Only “stocks and supplies” (e.g., raw material, finished product, etc.) should be modeled as coverage C. Accordingly, when modeling these facilities in the model using IFM (400-series occupancies), the replacement value entered in the coverage A field is expected to be significantly larger than the replacement value used for coverage C. If a breakdown of replacement value by coverage is not available when modeling large industrial facilities in Verisk models using IFM (400-series occupancies), it is suggested to place the full replacement value (total replacement value of the property, excluding the business interruption) as coverage A. In case the main value of the facility is from “stocks and supplies, this could suggest that this property is a small industrial facility consisting of a main building/factory with a lot of stock and supplies. In this case, we would suggest using Verisk occupancy codes 321-330 with appropriate exposure value distribution for building and content. Verisk Occupancy 320s coverage A vulnerability functions are based mainly on building damage. The following considerations can be used to decide which Verisk occupancy codes (320 series vs. 400 series) will better reflect the vulnerability of the exposures under consideration.

- If the facility mainly consists of building/factory structures and stocks and supplies, use Verisk occupancy 320s
- If a significant portion of the replacement value is from industrial components, use Verisk occupancy 400s

It should be also noted that since the Verisk's IFM damage functions represent specific facility-level vulnerability given the specific IFM occupancy type (401-482), construction code and building height fields are irrelevant and the damage functions do not change by these features. However, if Verisk Occupancy 320 series is used then building characteristics become important and should be coded properly.

**See Also**

[Large industrial facilities](#)

## Components used for the development of industrial facility damage functions

The Verisk model can be used to estimate damage to industrial components and their many associated sub-components. To develop the damage function, Verisk engineers conducted thorough analyses of the components most commonly found in industrial facilities, such as storage tanks and process towers ([Table 28](#)). The remaining components and sub-components are implicitly included in a damage estimate based on whether they are generally part of a typical type of industrial facility in the area, and their relative contribution to the total damage of the facility.

**Table 28. Industrial facility components used in the Verisk Typhoon Model for Southeast Asia**

Industrial Facility Components		
Air Handling Units	Distribution Panels	Open-Frame Structures
Baffles	Electric Power Backup	Paddles
Basins	Electric Transmission Towers	Pipe Racks
Battery Chargers	Elevated Pipes	Pipes and Pipelines
Battery Racks	Engine Generators	Potential Transformers
Boiler/Pressure Vessels	Equipment	Pressurized Reactors
Boilers	Fans	Process Towers
Buildings	Filter Gallery	Pumps
Chillers	Flares	Scrapers
Chlorination Equipment	Generators	Sediment Flocculation Equipment
Circuit Breakers	Highways/Runways/Railroads	Silos
Commercial Backup Power	Large Horizontal Vessels	Stacks/Chimneys
Compressors	Large Motor-Operated Valves	Switch Gears
Control Panels	Large Vertical Vessels with Formed Head	Tanks
Cooling Towers	Lightning Arrestors	Transformers

Industrial Facility Components		
Coupling Capacitors	Loading Structures (Cranes/ Cargo Handling/Conveyor Systems)	Tunnels
Current Transformers	Motor Control Centers	Wells
Dams	Large Motor-Operated Valves	Valves
Disconnect Switches	Motor-Driven Pumps	

## Tanks

Storage tanks are probably the most common components found in industrial facilities. Their vulnerability to wind, flood, and storm surge varies widely depending on the tank's aspect ratio (the ratio of height to diameter), its fill level, and the anchorage at its foundation.

Anchorage systems are used to prevent tanks from becoming displaced or toppled by high winds or from floating due to storm surge or precipitation runoff accumulation, which can happen if the flood depth exceeds the liquid level within the tank. This type of damage is more common among taller, narrower tanks (those with a higher aspect ratio), which are therefore usually anchored. Short, squat tanks (those with a lower aspect ratio) are usually not moved by the wind, and are usually not anchored.

Verisk engineers developed wind damage functions for tanks of different aspect ratios and three liquid levels (empty, half-full, and full). The wind damage function reflects the types of minor damage associated with insulation damage, minor deflections, and flying debris until the onset of buckling, at which point the damage ratio reaches 100%.

Buoyancy calculations were performed for a range of tank dimensions assuming an equal probability of liquid level within the tank. This analysis was performed for tanks with and without foundation anchorage. A damage ratio of 50% was assigned to unanchored tanks since most floating tanks experience minimal displacement during a typhoon and can be reused with minimal repair costs. Anchored tanks were assigned a damage ratio of 75% since most anchor failure likely results in additional repair costs for both the anchor and the tank. A damage ratio of 100% was assigned to floating tanks to reflect displacement and impact with floating debris during storm surge (or displacement during precipitation-induced flooding), which can result in extensive damage.

To simulate increasing wind loads, wind pressure distributions (based on published wind tunnel studies) were applied to the models incrementally ([Figure 145](#)), and the pressure distribution around the entire tank was observed.

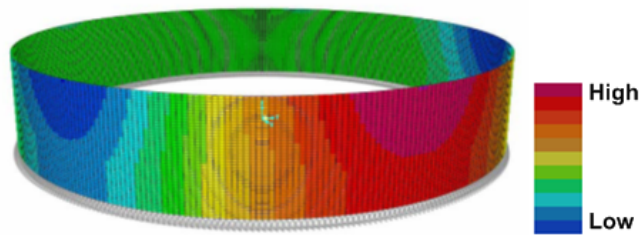


**Figure 145. Distribution of wind pressure around a tank wall**

The primary form of damage seen on shorter tanks is buckling, to which shorter tanks are more vulnerable since a larger portion of the tank wall becomes damaged. To account for buckling, the wind loading factor was increased until elastic buckling occurred, indicated by a local failure of the tank wall. The deflection of a tank wall due to elastic buckling is greater where the wall is thinner (Figure 146).

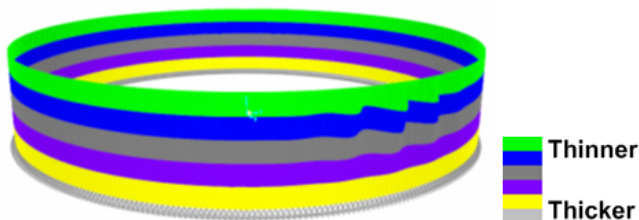


**Figure 146. Deflection of tank wall due to elastic buckling**

## Open-frame structures

Open-frame structures are used in rail and marine transport systems to support a variety of plant equipment and product-loading systems. They vary in size and bracing, and generally consist of a combination of welded and bolted steel connections that form open steel frames, with little or no exterior cladding.

The wind vulnerability of open-frame structures was evaluated using an analytical model that incrementally increases the wind loads on the structure. Loading was increased until elastic buckling occurred at a brace causing the structure to lose some of its lateral load resistance and either partial or complete collapse. The results of the analysis indicate that open-frame structures perform well when subjected to typhoon-force winds.

Due to their design, which uses a substantial amount of steel, open-frame structures exhibit low vulnerability to flooding over a large range of water depths. Damage to the bare frame is negligible at all flood depths, even when the embedded equipment sustains substantial damage.

## Cooling towers

Cooling towers are designed to release heat produced by industrial processes into the atmosphere. Damage usually starts with the loss of exterior cladding and fan cylinders.

Collapse of the tower frame is possible. Unless the damage progresses toward the interior of the tower, the interior cells may remain operational even after an extreme wind event. Smaller portable cooling towers typically sustain less damage than larger ones because they contain less equipment. An example of a cooling tower is provided in [Figure 147](#).



**Figure 147. West Ford Flat power plant geothermal cooling tower**  
Source: [West Ford Flat Geothermal Cooling Tower](#) by Rtracey, Public domain

Observations indicate that fan shroud damage is possible at wind speeds between 89 to 160 km/h. As winds speeds approach 160 km/h, minor to moderate damage to louvers, sidewall cladding, fans and fan cylinders, and shrouds can occur. There may be limited instances of partial or complete collapse of cell frame structures, which would result in the loss of tower functionality. The damage ratio for events with wind speeds between 118–199 km/h is approximately 10 to 20%. This ratio increases to 20 and 50% for events with wind speeds exceeding 200 km/h, during which louvers, sidewall cladding, fans and fan cylinders, and shrouds will experience moderate to major damage, and additional equipment, such as motors and gearboxes, will also be damaged.

Flood damage is usually minor in the case of cooling towers. They typically have a low vulnerability over a wide range of flood depths, primarily due to their substantial cross-sectional area, sound footing, and open frame structure. In contrast, storm surge is much more likely to cause damage to cooling towers due to the impact of floating debris.

## Process towers

Process towers generally consist of insulated steel cylinders that are bolted to a concrete foundation, with piping and access decks often attached at various levels ([Figure 148](#)). Damage at wind speeds of 160 km/h and greater is typically limited to the insulation. There are, however, isolated observational accounts of strong winds that cause towers to lean at an angle due to elongated anchor bolts.



**Figure 148. Example of a process tower**  
 Source: [Colonne distillazione](#) by Luigi Chiesa, [CC BY 3.0](#)

Based on historical wind damage reports, structural damage to process towers is usually associated with anchor bolt yielding or rupture. Wind pressure for different design loads (ASCE) was determined for three typical process towers with heights ranging between 24 and 42 meters. Wind pressure was increased incrementally until the first anchor bolt yielded, leading to anchor bolt elongation and subsequent leaning of the process tower. The wind pressure was then increased further until the first anchor bolt ruptured, causing the loss of lateral capacity and collapse of the process tower.

The damage functions for process towers assume no damage until the first anchor bolt yields, and complete damage at the point where the first anchor bolt ruptures. A low-vulnerability damage function, which increases with wind speed, was used to represent damage to insulation and other minor damage associated with flying debris.

Process towers exhibit low vulnerability to flooding over a wide range of flood depths, primarily due to their substantial cross sections and sound footing. Damage to process towers from storm surge events is typically inflicted by floating debris.

## Flare towers

---

Flare towers are tall structures that burn off industrial waste gas. To develop damage functions for flare towers, Verisk engineers analyzed three different types: freestanding, guyed flare, and derrick-supported, as shown in [Figure 149](#).



**Figure 149. Examples of flare tower types: freestanding (left), guyed flare (middle), and derrick-supported (right)**

**Source:** Left image: [Gas flare, PetroChina Jabung field, Jambi, Indonesia](#) by Darmawan kwok, [CC BY-SA 4.0](#); middle image: [Flare, Bayport Industrial District, Harris County, Texas](#) by Jim Evans, [CC BY-SA 4.0](#); and right image: [Shell haven flare](#), by Terryjoyce, [CC BY-SA 3.0](#)

Verisk engineers developed an analytical structural model of a derrick-supported flare tower. In a similar manner to process towers, ASCE wind pressure distributions were used to apply incrementally increasing wind loads to the structures. Loading was increased until the onset of buckling at a tower leg located approximately in the middle of the structure. Once buckling occurs ([Figure 150](#)), the capacity of the structure begins to diminish and ultimately collapses.

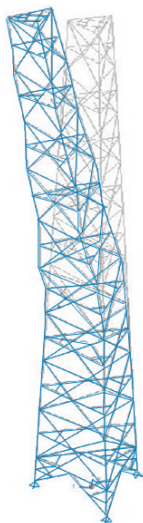


**Figure 150. Buckling of a derrick-supported flare tower**

Structure failure occurs at wind speeds upwards of 200 km/h. The wind damage functions for flare towers demonstrate a steep increase in the damage potential beginning with wind

speeds at around 90 km/h, and approach almost complete damage at wind speeds of 160 km/h.

Flare towers exhibit low vulnerability to flooding from precipitation or storm surge over a wide range of flood depths, primarily due to their substantial cross sections and sound footing. Similar to process towers, storm surge damage to flare towers is typically due to floating debris.

## Damage functions for industrial facilities

Verisk developed aggregated damage functions for each type of industrial facility based on the damage functions for the components and sub-components associated with that type of facility. The damage functions for each component and sub-component were assigned a weighting factor equal to the ratio between the replacement value of the class and the total replacement value of the industrial facility. These weighting factors are based on scientific research, the Applied Technology Council report ATC-13 1995, and HAZUS data.

To develop component-level damage functions, some reasonable assumptions are made about the typical characteristics of the sub-components. For example, Verisk assumes different percentages of anchored and unanchored tanks, and different filling levels and aspect ratios for tanks, depending on the type of facility.

[Figure 151](#), [Figure 152](#), and [Figure 153](#) show the damage ratios for selected industrial facilities for the wind, flood, and storm surge sub-perils, respectively. The facility level damage function is a weighted average of the damage functions of the individual components. Damage functions for the unknown (general) facility type, indicated with a dotted black line, are based on the weighted average of the damage functions.

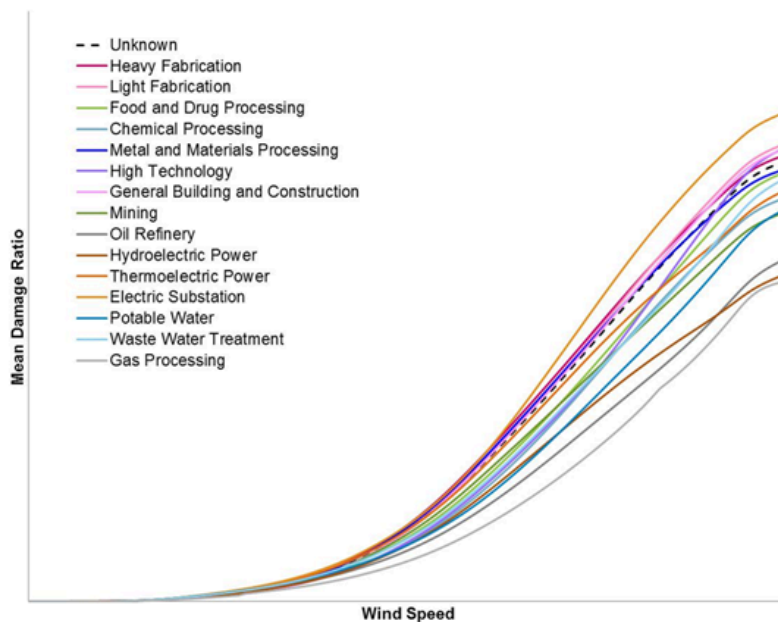


**Figure 151. Wind damage to selected industrial facilities**

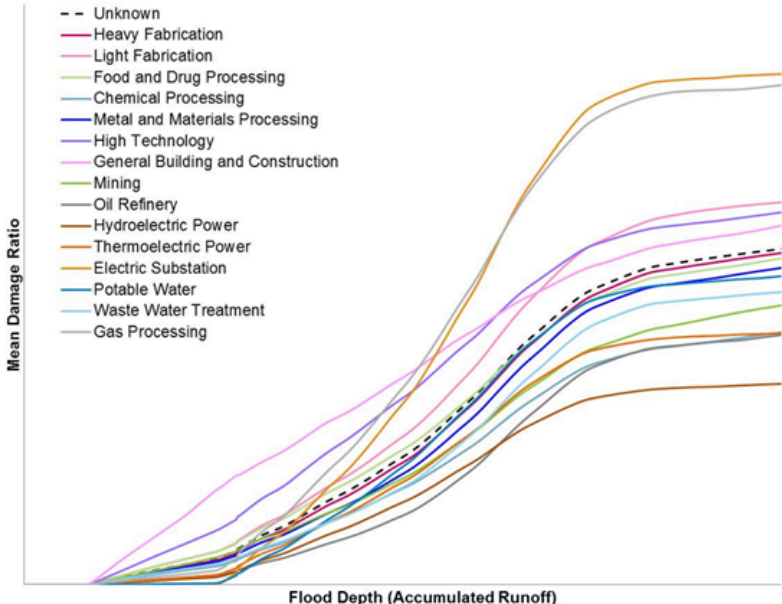


Figure 152. Flood damage to selected industrial facilities

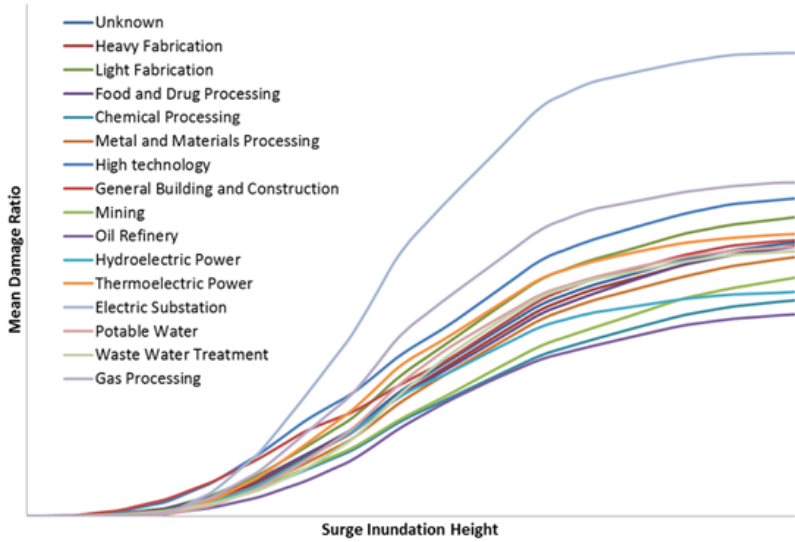


Figure 153. Storm surge damage to selected industrial facilities

### Damage functions for industrial facility components

Verisk researchers developed damage functions for some industrial facility components using damage data or available research. However, such information was not available for many components. In these cases, information from many sources, including historical typhoon damage data, scientific literature, site-specific measurements, and structural analyses was incorporated to assign mean damage ratios over a range of wind speeds

and flood depths. All analyses took into account the complexity of each component and its characteristic response to wind speeds and flood levels.

Note that the damage functions for industrial facilities are not applicable to any individual component at a particular location (e.g., a specific pump or cooling tower).

At any given hazard level, the damage ratio for a particular component may be found within a range of damage ratios corresponding to the hazard level and component class. This range reflects the fact that seemingly identical components may experience different levels of damage during a particular event. That is, one cooling tower may experience total collapse while another similar cooling tower may experience moderate damage during the same typhoon. Such variation exists due to differences in material properties, wind field patterns, construction quality, building maintenance, and the presence or absence of flying debris. The damage functions have been developed considering a range of characteristics and behaviors within any particular component class or sub-class and are intended to represent the average damage ratio for a group of many individual components.

[Figure 154](#) and [Figure 155](#) show the damage ratios for some industrial facility components for wind and flood, respectively. Note that the damage functions for storm surge depend on effective inundation depth and are very similar to the damage functions for flood, which are based on flood depth.

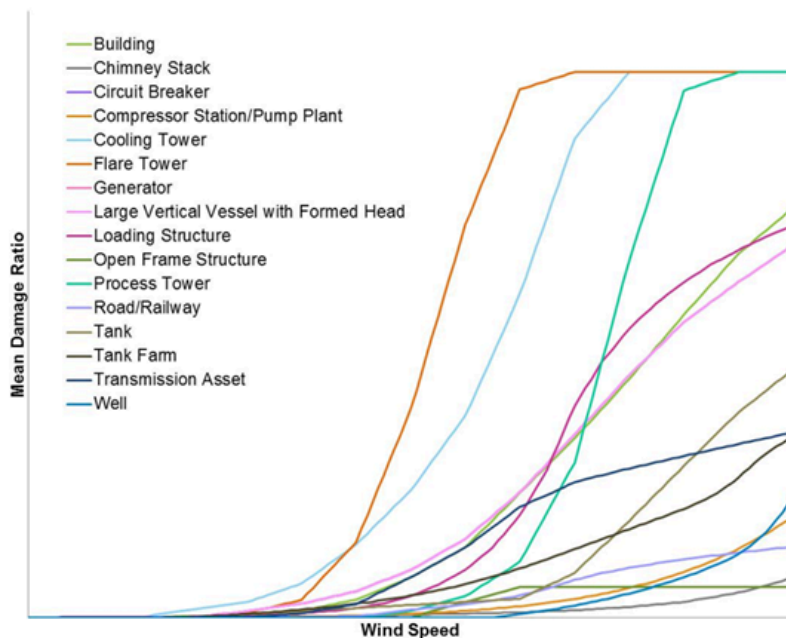


**Figure 154. Wind damage to selected industrial facility components**

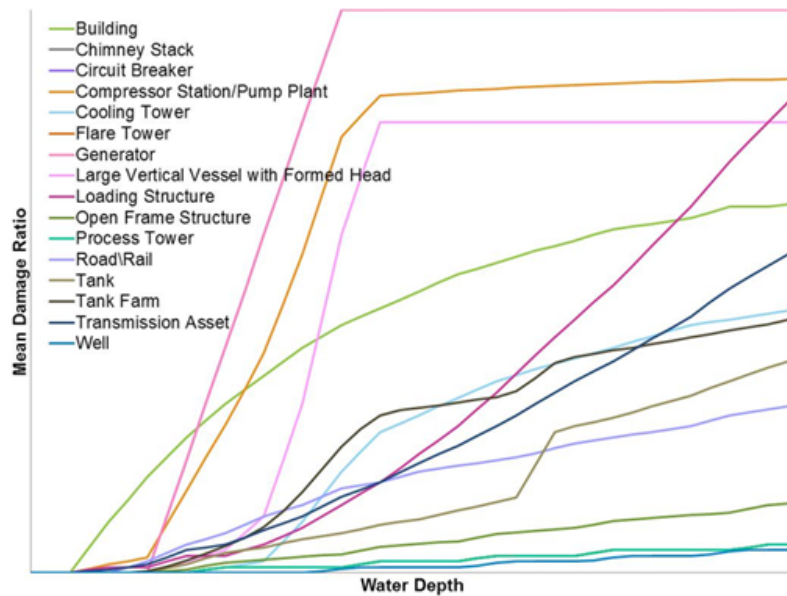


**Figure 155. Flood damage to selected industrial facility components**

## Time element (business interruption) damage functions for large-scale industrial facilities

Assessing business interruption (BI) loss for large-scale industrial facilities is complex, particularly in the case of highly integrated facilities. Product chains that are rendered completely or partially non-functional are the main contributor to BI losses, which can occur as a result of physical damage to the components, the interconnectivity between components, or lifelines such as electricity and water systems.

Downtime is the primary parameter for assessing BI losses. To assess these losses for an entire large-scale industrial facility, time element damage functions are determined for each component for each stage of the damage assessment and repair process. As in any other BI assessment, the time before repairs can begin, or pre-repair, is determined and combined with the time required for the actual repair. Once the time element functions are determined for all components, the model aggregates them via a weighted average. Since downtime is closely associated with the loss of functionality due to a damaged component, the time element damage functions are very similar for wind, flood, and storm surge, with some differences for wind due to the nature of the damage to certain components. The time element damage ratios for wind, flood, and storm surge are illustrated in [Figure 156](#) and [Figure 157](#), respectively.

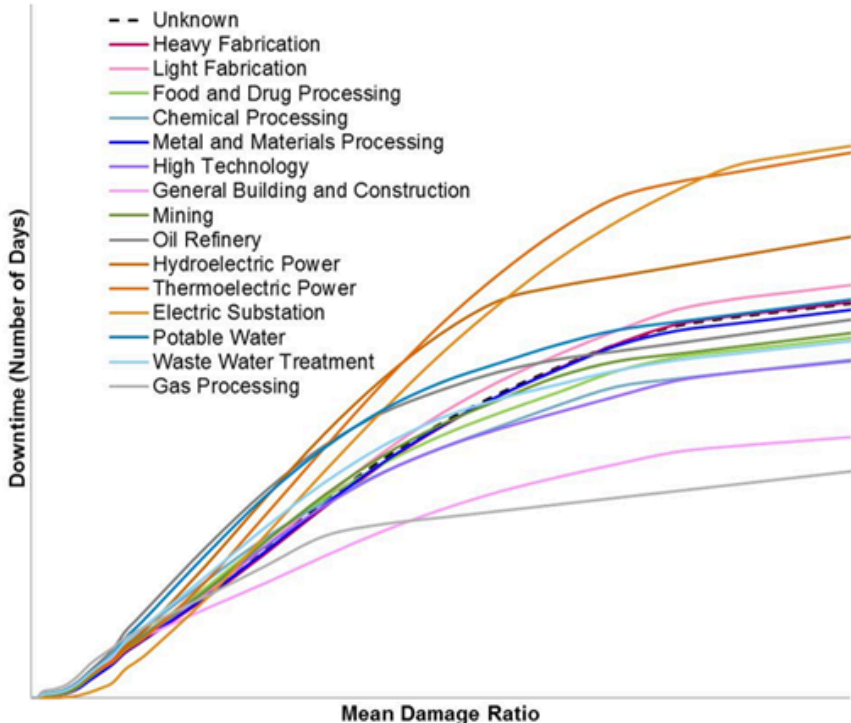


Figure 156. Time element ratios for wind damage to selected large-scale industrial facilities

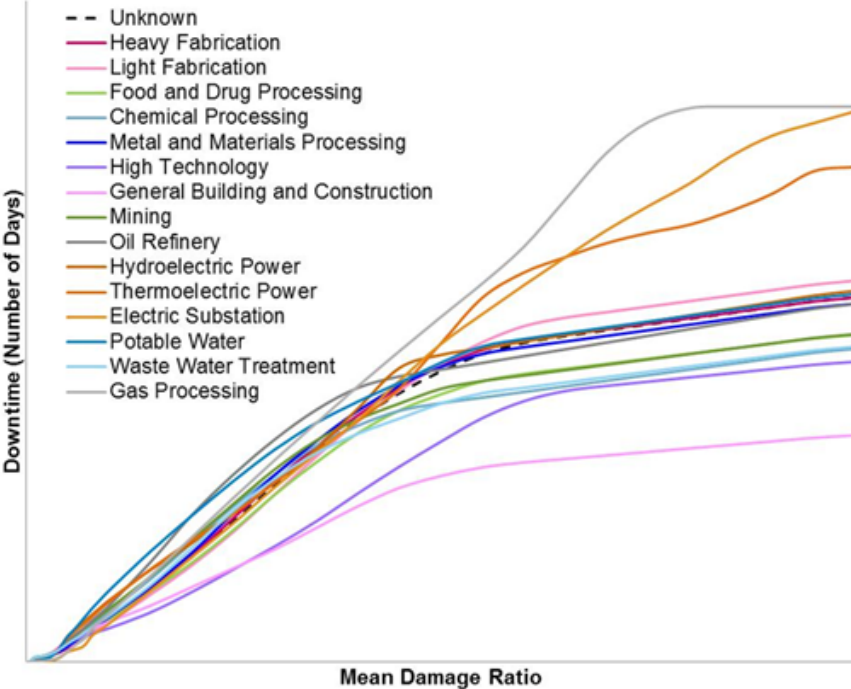


Figure 157. Time element ratios for flood and storm surge damage to selected large-scale industrial facilities

A partial correlation between components is utilized to assess modeled BI losses to large-scale industrial facilities. The analysis implicitly incorporates the numerous connections between components, lifelines, and product chains. The high degree of site-specific connectivity and the complexity of the product chains that exist at most plants make the estimation of downtime for large-scale industrial facilities challenging, requiring a multifaceted calculation involving numerous operations, including evaluations of onsite process interactions, bottlenecks and redundancies, offsite interdependencies, and revenue generators. Downtime estimation is accomplished by building a “network model” that constructs a simulation of the many interconnections between components, processes, lifelines, and product chains, and accounts for components to be idle even if undamaged or already fixed in the event that other components or lifelines remain inoperable.

## 5.10 Damage functions for additional lines of business

In the Verisk Typhoon Model for Southeast Asia, loss estimates can be calculated for a variety of specialized risks such as:

- Automobiles
- Marine cargo (including oceangoing cargo, carpool, and inland transit cargo)
- Marine hull
- Railways
- Buildings under construction

Users should note that due to a scarcity of detailed claims data and often little detail in the underlying exposure data available as input to the model, there is a higher degree of uncertainty surrounding the loss estimates for the risks included in this section.

### The automobile line of business

---

In the Verisk model, automobile damage functions have been developed for the wind, flood, and storm surge sub-perils to represent the vulnerability of automotive vehicles, including two-wheeled and four-wheeled, for passenger and commercial transport. Automobiles can be damaged during a typhoon by multiple causes, such as falling trees, airborne or floating debris, and water from precipitation or storm surge ([Figure 158](#)).



(Sources: Associated Press; Philippine Daily Inquirer)

**Figure 158. Examples of automobile damage due to water inundation**

Automobiles are especially vulnerable to water damage because the operational parts, such as the mechanical and electrical components of the engine, are positioned low to the ground, and are not useable after water inundation. In urban areas, numerous automobiles can be parked in underground garages that are at particularly high risk to water-related damages from precipitation-induced flood and storm surge due to the subterranean position of the garages, which makes them more vulnerable to inundation, more difficult to drain, and impedes evacuation. These factors can also increase the time for which automobiles are submerged and/or exposed to water, thus elevating potential losses.

## The marine cargo and inland transit lines of business

Marine cargo insurance generally covers the risks that are in transit or waiting to be shipped. There are three categories of this type of insurance: oceangoing, carpool, and inland transit cargo.

Oceangoing cargo risks in the Verisk Typhoon Model for Southeast Asia include general container cargo, heavy cargo, refrigerated cargo, dry bulk cargo, and liquid bulk cargo. General container cargo is transported in containers on ships, trains, or airplanes. These containers are usually box-shaped and approximately 240 cm (8 feet) wide x 260 cm (8.5 feet) tall x 600–1200 cm (20–40 feet) long. Electronic equipment is generally packed tightly within general cargo containers for shipment over long distances. While some forms of heavy cargo can be shipped in general cargo containers, most heavy cargo consists of machinery that does not fit into standard containers, such as construction machinery, harbor equipment, or luxury yachts. Semi-submersible heavy-lift ships, conventional heavy-lift ships, barge tows, or dock ships are used to transport these forms of heavy cargo.

Refrigerated cargo is similar to general containerized cargo, but requires additional electrical equipment to maintain temperatures to preserve the commodities stored within them. Dry bulk cargo, which refers to grains and solid materials such as coal, metal ore, and lumber, are usually stored on the ground in an open yard. Liquid bulk cargo refers to onshore tanks that store oil, liquefied natural gas, and other liquid chemicals.

Carpool cargo refers to thousands of cars that are parked in open areas near harbors before being shipped on personal car carriers, while inland transit cargo refers to risks that are in transport or in transit warehouses waiting to be distributed over land. Transit warehouses

are distribution centers that temporarily store various commodities, such as food, clothing, medicine, or construction machinery, for further dissemination. They are typically one-story buildings of light steel frame construction with high ceilings that are generally very susceptible to wind damage. The commodities stored within transit warehouses are also susceptible to wind and wind-driven rain damage, as well as flooding-related damage.

During typhoon events, oceangoing cargo risks are generally damaged due to high winds and accompanying storm surge. Crane failure, the collision of ships with docks during loading and unloading at port, and storm surge are the main causes of damage to different types of cargo. Since these types of risk mainly accumulate at ports, excessive precipitation does not cause significant damage to them, as the excess water drains directly in to the sea. For carpool cargo risks, damage patterns are similar. However, flood can be a significant cause of damage for inland transit cargo. Warehouses are generally very susceptible to wind damage due to their long spans and large doors, which can easily be damaged by large uplift and suction forces. Once the building envelope is breached, heavy precipitation can cause significant damage to the contents of the warehouse. Precipitation-induced flooding is also a major cause of damage to the cargo within transit warehouses.

*The following notes are important to consider when modeling the Marine Cargo and Inland Transit risks in the Verisk Typhoon Model for Southeast Asia in Touchstone:*

- The model requires that users enter exposure values for marine cargo at the time of an event, and not the monthly or yearly aggregates. Since cargo is constantly moving, average daily amounts (taking accumulations into account) should be used in Touchstone to estimate typhoon losses.
- Oceangoing cargo: Only Coverage A (building) is supported for occupancy 354 (Sea and Inland Waterways) and construction classes 271–276.
- Carpool: Only Coverage A is supported for occupancy 354 and construction class 270 (Carpool).
- Inland transit cargo: Both Coverage A and Coverage C (content) is supported for the combination of construction classes 100, 101–104, 111–120, 131–140, 151–159 and occupancy class 366 (Transit Warehouse). Coverage A represents the building exposure, while Coverage C represents the cargo.

**See Also**

[Construction and occupancy classes, year built and height bands, and relative vulnerabilities](#)

## The marine hull line of business

---

The marine hull line of business (LOB) includes the hull of a ship—the structure of the vessel—and the vessel machinery—the equipment that generates the power to move the vessel and control the lighting and temperature systems, such as the boiler, engine, cooler, and electricity generator. It does not include cargo. In the Verisk Typhoon Model for Southeast Asia, this risk can be modeled at a specific port location (by latitude and longitude) and a particular status of Port Risk, Builder’s Risk, or Repair Risk, depending on whether the vessel is at port, at a shipyard under construction, or at a shipyard undergoing regular maintenance.

Marine hull insurance covers loss against physical damage to the ship hull and machinery of a vessel. Marine hull Builder's Risk insurance provides coverage while the vessel is under construction when it is exposed to fire, tidal wave, capsized, failure in launch, collision, and sinking on a trial trip. The insured value is either the contract price or the estimated completed value of the vessel if there is no contract price. The period of insurance is from the time of the start of construction to the time of vessel delivery. See the notes at the end of this section regarding how to run this LOB.

In terms of exposure information and typhoon vulnerability, the marine hull risk can be analyzed in three separate states:

### **Marine hull at port**

- Damage to marine hull risks at port is primarily caused by collision with other ships or a barge, dock, or pier
- The marine hull at port risk is generally more vulnerable to wind damage compared to marine hull at shipyard due to the unprotected nature of the physical location, whereas vulnerability to flood and storm surge is typically lesser since the machinery is protected within the ship

### **Marine hull at shipyard, under repair**

- Damage to marine hull risks under repair at a shipyard is typically caused by collision with the block or pier, or flooding
- The marine hull at shipyard while under repair risk is generally less vulnerable to wind due to the protected nature of the physical location (in dry-dock) compared to marine hull on a berth, whereas vulnerability to flood and storm surge is typically greater since machinery can be damaged during repair and construction

### **Marine hull at shipyard, under construction**

- Damage to marine hull risks at shipyard while under construction has a similar mechanism to that of marine hull risks at shipyard under repair
- The value and vulnerability of marine hull risks at a shipyard under construction changes throughout the construction process, and is annually less than that of marine hull risks at shipyard under repair because the value of the marine hull is much lower during construction

Although the marine hull risk is also insured during travel at sea, damage and losses from typhoons are generally very rare as these events can be tracked quite easily with current technology enabling ships to navigate away from the hazard.

Overall, most typhoon damage to marine hull risks at ports and shipyards is mainly attributed to high winds and storm surge. Flood due to high levels of precipitation should contribute less to overall losses than wind. When developing wind and flood damage functions for these risks, engineers at Verisk primarily depend on engineering judgment and information from marine hull underwriters to understand and characterize vulnerability.

*The following notes are important to consider when modeling the Marine Hull risk in the Verisk Typhoon Model for Southeast Asia in Touchstone:*

- Similar to the marine cargo risk, the model requires that users enter exposure values at the time of an event (not the monthly or yearly aggregates) for the marine hull at port and marine hull at shipyard under repair/maintenance risks. As ships are constantly moving, the average daily amounts of exposure should be used in Touchstone to estimate losses from typhoons. Since ships are at sea most of the time, the exposure on berth time at port or at shipyard for repair and maintenance during a typhoon event is small. The following assumptions can be made to estimate the marine hull exposure at risk during a typhoon (note that ships will be traveling most of the year, at which time it is assumed that typhoon risk is zero):
  - On berth time at port:
    - Domestic ships: one out of three days
    - International ships: one out of 10 days in Southeast Asia
  - Repair/maintenance time at shipyards: four services, of six days each, in five years:
    - Domestic ships: 100% in Southeast Asia
    - International ships: 20% in Southeast Asia
- For the marine hull at shipyard under construction risk, the total replacement value should be used. Modeled losses represent an average annual loss; that is, the losses over one year for a ship under construction. Accordingly, users should enter policy start and end days as January 1 and December 31 (the equivalent of one full year) in Touchstone. This facilitates the estimation of portfolio losses on an annual basis, when other types of risks (building, automobile, etc.) coexist in a portfolio. Modeled losses can be adjusted accordingly to estimate losses for a specific marine hull builder's risk with duration of other than one year.
- When only aggregate-level exposure data is available, the user should preprocess the data and distribute it to port locations to properly capture the underlying hazard. The model has a disaggregation tool, which should not be used for disaggregating marine hull exposures, as this disaggregation is based on the underlying building exposure.
- In Touchstone, construction code 260 and Coverage A (building) should be used. Occupancy codes 300, 314, 354, and 381 are available for this LOB.

## The railway line of business

---

The Verisk Typhoon Model for Southeast Asia estimates damage and loss to railway systems, which comprises tunnels, bridges, tracks, and cables. Damage to trains and stations is not modeled explicitly, but stations can be modeled using different building construction types available in the model.

Damage reports from historical typhoons indicate that the railway LOB is very vulnerable to flood. Flash floods and landslides are the main causes of damage to railway tracks during periods of excessive rain; high water levels, debris, and scour are the main causes of damage to railway bridges over rivers during excessive rain ([Figure 159](#)). Wind damage to railway tracks and bridges is generally much less likely, as wind mainly causes damage to power

cables and train stations, although, in some cases, localized wind bursts can sometimes derail trains.



(Sources: REUTERS/Stringer; AFP/Getty Images)

**Figure 159. Damage to railway tracks and bridges**

The Verisk railway LOB represents railway assets such as tracks, cables, bridges and tunnels, but excludes trains and stations. Touchstone users should use occupancy code 352 (Railroad) in combination with any supported construction class to model railway assets.

## The CAR/EAR line of business

“Construction All Risks” (CAR)/“Erection All Risks” (EAR) represents buildings that are currently under construction. The Verisk damage functions for this line capture both damage to the partially constructed buildings themselves and to construction equipment, machinery, and other contents. To properly model CAR/EAR typhoon risk, Verisk engineers have analyzed wind, flood, and storm surge vulnerability of buildings in various phases of construction. Results from these studies were used to develop damage functions that take into account the time-dependent aspect of buildings under construction.

Wind, flood, and storm surge vulnerability can vary for a given construction phase. Building vulnerability to flood or storm surge is the highest in the earliest phases of construction, while building vulnerability to wind is the lowest during the earliest stage of construction. It is therefore important to consider all three sub-perils when determining typhoon vulnerability for CAR/EAR risks.

In addition, information regarding construction costs, equipment costs, and project timelines was analyzed to determine the building replacement value as a function of time. Cost ratios, normalized by total investment, have been developed for each construction phase for each construction type.

A replacement value time function is generated based on an assumed cost distribution during each phase of construction. By integrating the time-dependent vulnerability and the time-dependent cost functions, the wind, flood, and storm surge risk to buildings under construction can be accurately estimated over the entire period of construction.

## 5.11 Validating the model's damage functions

The Verisk Typhoon Model for Southeast Asia leverages Verisk's 20+ years of experience in developing typhoon related damage functions. These damage functions incorporate findings from published engineering research and engineering analyses, extensive building code study, and are validated based on billions of dollars of detailed claims data from windstorms around the world, as well as damage surveys conducted by Verisk engineers.

The damage relationships for different construction and occupancy classes are also validated through company exposure and loss data. Because high resolution claims data for Southeast Asia is generally very limited, Verisk worked with several local companies that provided aggregated exposure and loss data. This information has been leveraged to validate damage functions in this model. In addition, Verisk engineers leverage the extensively validated damage functions from other, more mature insurance markets and modify them to reflect local materials, labor and material costs, construction practices, and claims adjustment practices in Southeast Asia.

Additional validation is obtained through the analysis of findings from damage surveys conducted in the aftermath of typhoons. Verisk also works closely with clients in the region to analyze claims data from those events. The relative vulnerabilities of different construction/occupancy/height combinations in the Verisk damage functions are validated by observations not just from typhoons that impact Southeast Asia, but from a large number of damage surveys that Verisk has performed after typhoon events worldwide.

# 6 Insured Loss Calculation

In this component of the Verisk Typhoon Model for Southeast Asia, ground-up damage is translated into financial loss. Insured losses are calculated by applying policy conditions to the total damage estimates produced by the damage estimation module. Policy conditions may include deductibles, coverage limits, loss triggers, and risk-specific reinsurance terms.

## 6.1 Aggregating losses probabilistically

Post-disaster surveys and actual claims data reveal an inherent variability in the damage that results from a given wind speed, flood depth (accumulated runoff), or storm surge effective inundation depth. Loss estimates generated by the Verisk Typhoon Model for Southeast Asia capture this variability by accounting for both primary and secondary uncertainty. Primary uncertainty derives from the uncertainty associated with the stochastic event generation process, while secondary uncertainty describes the uncertainty in damage resulting from a given event. This secondary uncertainty captures the uncertainty in damage and in the local intensity estimation. The uncertainty in building damage arises from variations in the response of buildings of similar construction to a given intensity, resulting from non uniformities in building characteristics, construction materials, and workmanship. The uncertainty in the local intensity of the hazard can be attributed to unmodeled phenomena and local site factors.

As was discussed earlier, damage is calculated using damage functions that provide, for a given event intensity, a mean damage ratio and a probability distribution around the mean that captures the variability in damage. In the Verisk Typhoon Model for Southeast Asia, a four-parameter inflated transformed beta distribution is used to allow for non zero probabilities for damage at zero percent and at a maximum percent. In cases of very low mean damage ratio (MDR), maximum damage is not necessarily 100%, but is defined by a threshold on the cumulative probability distribution.

Damage functions are used to produce, for each event, a distribution of ground up loss by location and coverage. Limits, deductibles, and reinsurance are applied in the financial module to the ground-up loss distribution to produce gross and net loss estimates. Note that insured losses can accumulate even if the MDR is below the deductible, because some structures are damaged above the MDR and the deductible. The distributions are applicable to the analysis of a single exposure, and usually have a high degree of uncertainty. The individual distributions are combined to obtain the portfolio distribution, where the uncertainty is lower.

The financial module aggregates losses probabilistically, at various levels. To accomplish this, computational techniques have been developed for statistically aggregating nonparametric distributions. This is necessary because even though the ground-up, coverage-level damage distributions typically use parametric distributions, after the application of

location and policy terms the distributions cannot be represented in a parametric way. Further aggregations of such loss distributions are achieved using numerical algorithms. The probability density function of the sum of two independent random variables F and G with density functions  $f(x)$  and  $g(x)$ , respectively, is represented by the convolution equation:

$$(f * g)(x) = \int_{-\infty}^{\infty} f(x-t)g(t)dt$$

Where:

$t$  = a dummy variable

Verisk models employ an efficient and accurate numerical algorithm for convolving any number of nonparametric loss distributions. Extreme care has to be taken when combining distributions with differing sizes of loss. The technique used allows the correct representation of the shape of the loss distributions throughout the financial loss estimation process. Preserving the right shape is particularly important when insurance terms apply to the tails of the distributions.

The financial module within Verisk's software allows for the application of a wide variety of location, policy, and reinsurance conditions. Location terms may be specified to include limits and deductibles by site or by coverage. Supported policy terms include blanket and excess layers, minimum and maximum deductibles, and sub-limits. Reinsurance terms include facultative certificates and various types of risk-specific and aggregate treaties with occurrence and aggregate limits. Please see product-specific documentation available on the Verisk [Client Portal](#) as well as details on the industry standard UNICED data format ([www.unicede.com](http://www.unicede.com)) for additional information.

## 6.2 Demand surge

Market forces generally ensure that the availability of materials and labor in any particular geographical area is sufficient to accommodate a normal level of demand without affecting price. However, demand can increase sharply and unexpectedly after a catastrophe such as a significant typhoon. The resulting widespread property damage can cause a sharp increase in the need for building materials and labor, which in turn can cause prices to inflate temporarily. Demand for related services and resources such as transportation, equipment, and storage might also escalate in the affected area.

Scarce resources can also result in an increase in the time required to repair and rebuild damaged property, which may cause greater business interruption losses and additional living expenses. Infrastructure damage, delayed building-permit processes, and a shortage of available building inspectors also increase time-element loss. These factors can lead to insured losses exceeding expectations for a particular event and portfolio, a phenomenon known as demand surge. The greater and more widespread the damage from an event, the greater the resulting demand surge and insured losses will be.

Note that the current default Verisk demand surge function was developed using economic principles and validated based on U.S. loss levels and component cost analyses as described in demand surge documentation, which is available on the Verisk [Client Portal](#). Because

demand surge is a phenomenon seen only with especially large catastrophes, there are relatively few events with which to validate demand surge functions outside of the U.S. This scarcity of data is further complicated by the relative paucity of cost indices and detailed data.

For countries other than the U.S., clients may choose to apply the U.S. demand surge function or a user-defined demand surge function, at their discretion. Clients are also encouraged to perform sensitivity testing to better understand the scale of impact and uncertainty inherent in applying demand surge to non U.S. models and perils.

## 6.3 Validating modeled losses

Event losses account for local wind intensity, flooding from storm surge, precipitation-induced flooding, vulnerability, and industry inventory data. Validating event losses ensures a model's overall performance, and comparing historical and modeled losses is a critical component of model validation.

The loss module of the Verisk Typhoon Model for Southeast Asia has been extensively validated by comparing modeled insurable and insured industry level losses with observed insurable and insured losses from historical events. Given the difficulty in estimating reliable insurable and insured industry level losses from historical events in this region, the published reports from insurance industry and local government as well as a significant amount of data from insurance company are all used to estimate the losses. In addition, the Verisk Typhoon Model for Southeast Asia has also been validated by using a significant amount of company exposure and loss data.

### Observed losses

---

The first step in validating modeled losses is to understand the benchmarks being employed. The Verisk Typhoon Model for Southeast Asia identified and collected information for more than 40 events that affected modeled countries/territories in the last 60 years. Multiple sources are explicitly investigated and used, including reports from insurance industry, governments, loss data from local companies, and published academic papers.

Major reinsurers and brokers usually publish annual reports for global catastrophic events. The reports are representative and widely used to estimate the industry level losses for historical events. The Verisk Typhoon Model for Southeast Asia embraced reports from Munich Re, Swiss Re, AXCO, Aon Benfield, Guy Carpenter, etc., for all modeled countries/territories in the past few decades.

Government reports are another reliable source to utilize. These official reports are comprehensive and are generally available for many years. Annual reports from the Hong Kong Observatory can be found back to 1968 and Taiwan Non-Life Insurance Association reports are also available since 2001. The Philippines National Disaster Risk Reduction and Management Council (NDRRMC) has aggregated loss information from 1970 to 2003 and categorized loss information for major events after 2003. However, in general, the loss

numbers from these sources are not only for property losses as they could also include losses from crops, fishery, infrastructure, and post-disaster relief costs, etc., which are not modeled in this model. Therefore, in order to estimate the observed insurable and insured loss that can be compared to our modeled insurable and insured loss, respectively, appropriate assumptions were used.

Claims data from local companies is also valuable for benchmarking historical events. Verisk engineers worked with several active insurance and reinsurance companies who have a representative market share in the modeled territories, and used company exposure and Verisk's Industry Exposure Database to estimate the market share. However, even with a reasonable market share, there is another aspect that also needs to be carefully evaluated when using these data. The company generally writes the business with special interests, such as focusing on commercial or industrial buildings, or in specific geographical areas. Sometimes, after experiencing significant losses from an area, company may decide to stop insuring the property in that area to minimize the risk in their portfolio. These insurance preferences may sometimes lead to a biased conclusion when the latest company book is used for the validation, and these company books need to be studied more carefully.

The large volume of information from different sources made it challenging to benchmark losses for historical events in a simple and standard way. Therefore, in Verisk Typhoon Model for Southeast Asia, the losses were estimated event by event, while keeping the maximum viable amount of consistency among the assumptions. Verisk benchmarked both insurable and insured property losses, and validated the model results from both perspectives. For events with multiple sources, appropriate assumptions were used to estimate the insurable and insured loss with our best judgement. For events that only have economic loss, Verisk estimated insurable and insured property losses using information derived from similar events or company claims data in each modeled territory. For events which only insured property losses were available, Verisk used the similar information above to back calculate insurable property losses from insured ones.

## Trending observed losses

Observed losses in Southeast Asia have been trended to the most recent exposure update in the Verisk Industry Exposure Database to reflect losses as if these events were to happen today. The trending method uses real gross domestic product (GDP) per capita growth, population growth, and GDP deflator, as follows:

$$L_t = L_n \times \frac{Exch_t}{Exch_n} \times \frac{Pop_t}{Pop_n} \times \frac{GDP_{pc,t}}{GDP_{pc,n}} \times \frac{DFL_t}{DFL_n}$$

Where:

$t$  = Year of the most recent Industry Exposure Database for the territories modeled in the Verisk Typhoon Model for Southeast Asia

$n$  = Year of loss

$Exch$  = Equivalent local currency amount, per one in the reported currency

$Pop$  = National population

$GDP_{pc}$  = Fixed real gross domestic product per capita in local currency

$DFL$  = Local currency deflator

Population growth  $\frac{Pop_t}{Pop_n}$  is used to approximate the increase in the number of properties over time, under the assumption that an increase in population proportionally leads to an increase in building stock. Real GDP per capita is used to approximate the wealth increase over time, which correlates with property value. The GDP deflator accounts for inflation.

## Industry level validation

This section discusses model validation based on the Verisk Industry Exposure Database for Southeast Asia. Company book validation will be presented in the next section.

### See Also

[Company book validation](#)

### Event level validation by country/territory

Validating event level losses for each country/territory can ensure a model's overall performance and comparing historical event observed losses with modeled is a critical component of the validation process. The historical observed losses are estimated and trended to 2015 as discussed above, and the modeled losses are obtained by running the 2015 Verisk Industry Exposure Database for Southeast Asia.

Observed and Verisk-modeled insured gross losses for selected events in the modeled countries/territories are compared in [Figure 160](#) through [Figure 164](#).

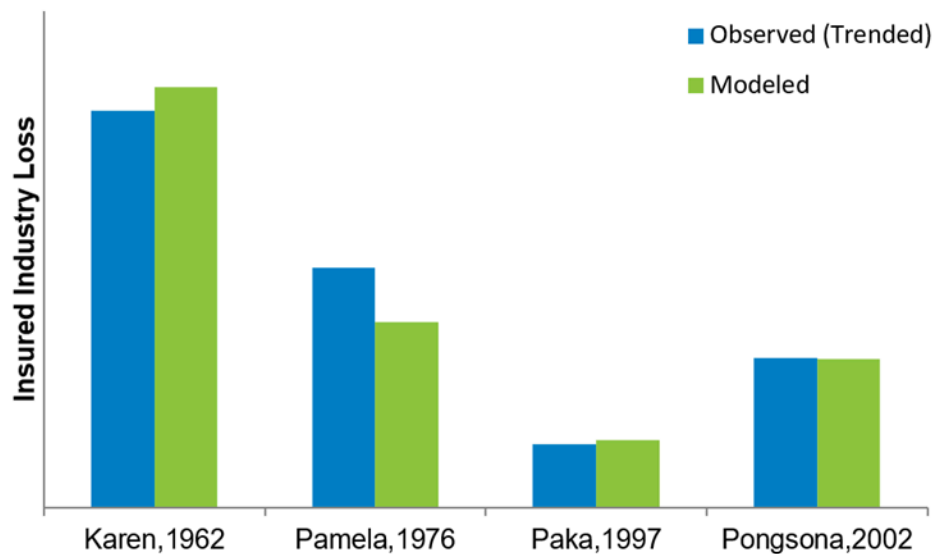


Figure 160. Observed and Verisk-modeled gross losses – Guam

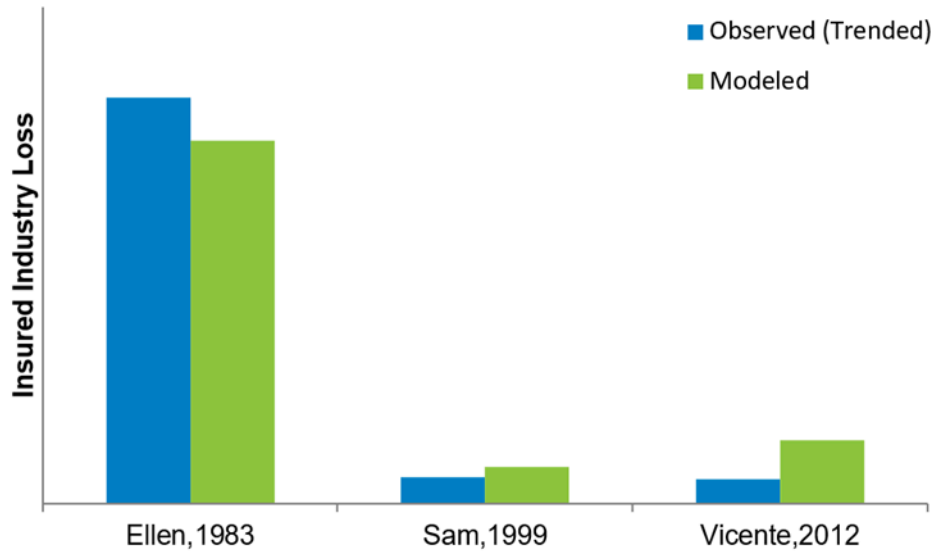


Figure 161. Observed and Verisk-modeled gross losses – Hong Kong

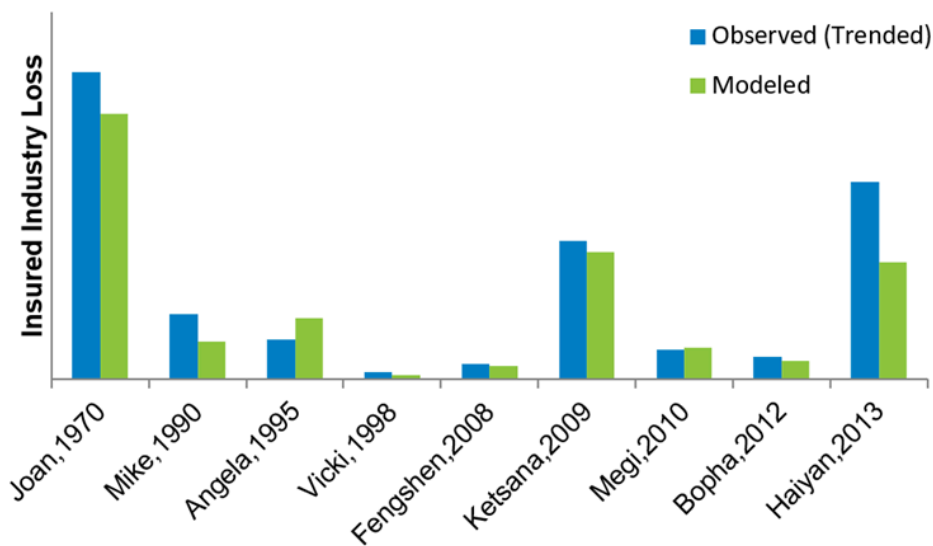


Figure 162. Observed and Verisk-modeled gross losses – the Philippines

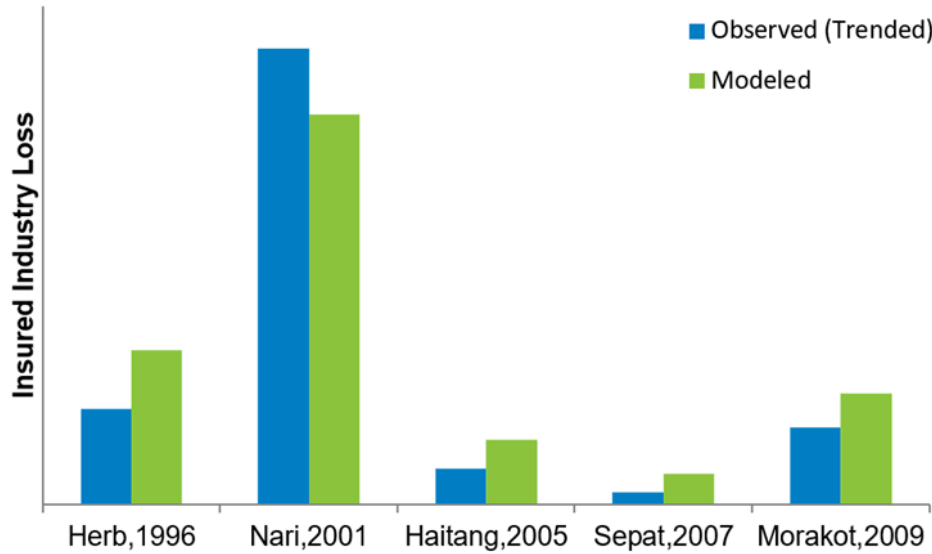


Figure 163. Observed and Verisk-modeled gross losses – Taiwan

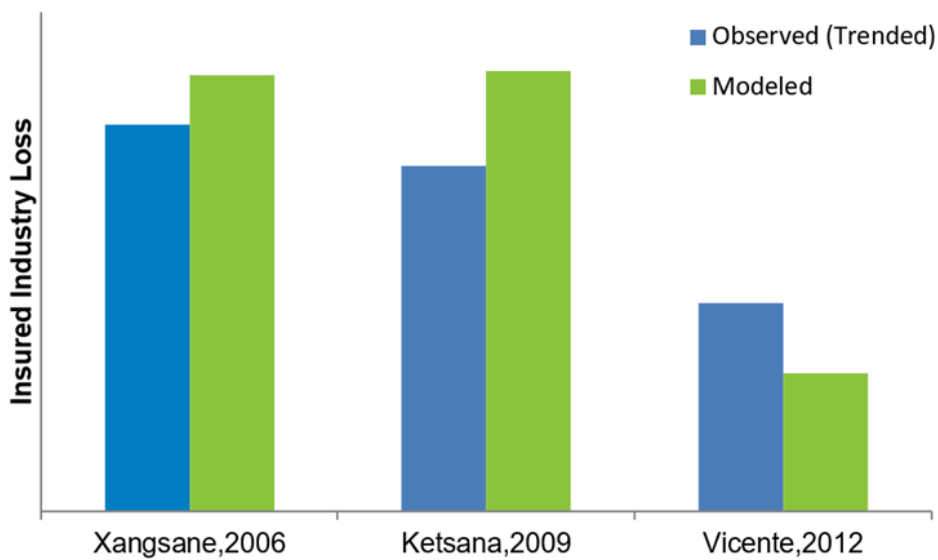


Figure 164. Observed and Verisk-modeled gross losses – Vietnam

### Exceedance probabilities

Verisk scientists and engineers benchmark the predicted frequency of losses that result from the simulated storms, as captured in the 10,000-year stochastic catalog. Since these events have not occurred, a check of the reasonability of their modeled frequency is obtained by comparing the simulated return period losses with actual loss experience.

The benchmarking of historical losses for selected events in the modeled countries/territories on Verisk’s insurable occurrence exceedance probability curve is presented below.

Insurable gross losses were obtained using the policy conditions described in the *Verisk Industry Exposure Database for Southeast Asia*.

Historical losses for Guam are benchmarked on Verisk’s insurable occurrence exceedance probability curve are presented in [Figure 165](#). Wind is the dominant sub perils in Guam; therefore, each of the selected events was characterized by notably strong winds. In the past 64 years, one event was observed to exceed the 50 year (2%) return period, three exceeded the 20 year (5%) return period, and four exceeded the 10-year (10%) return period. Thus, it is suggested that the stochastic catalog from the Verisk Typhoon Model for Southeast Asia appropriately captures the risks in Guam.

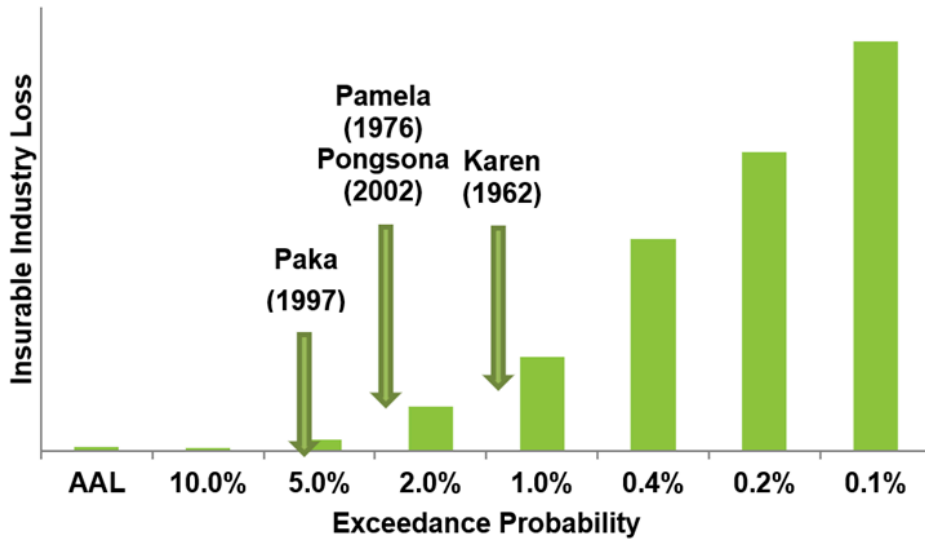


**Figure 165. Benchmarking historical losses on Verisk's insurable occurrence exceedance probability curve – Guam**

Historical losses for rest of the modeled countries/territories are benchmarked in [Figure 166](#) through [Figure 171](#).

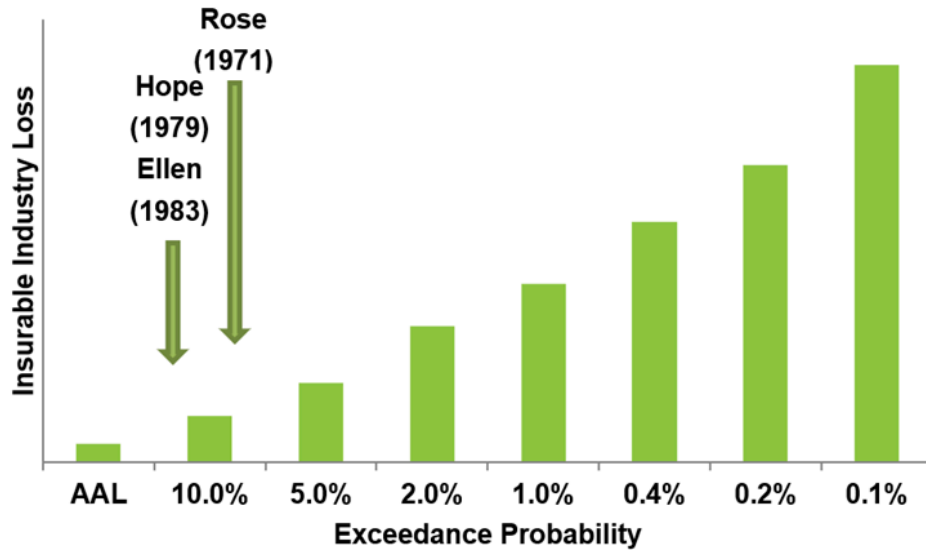


Figure 166. Benchmarking historical losses on Verisk's insurable occurrence exceedance probability curve – Hong Kong (all sub-perils)

Storm surge has been a seriously considered threat in the Philippines, especially since Typhoon Haiyan in 2013 which caused significant storm surge loss in the Tacloban area. [Figure 167](#) shows benchmarking all sub-perils combined losses in the Philippines on Verisk's all sub-peril exceedance probability curve. [Figure 168](#) shows benchmarking surge only losses from historical events on Verisk's surge only exceedance probability curve for the Philippines.

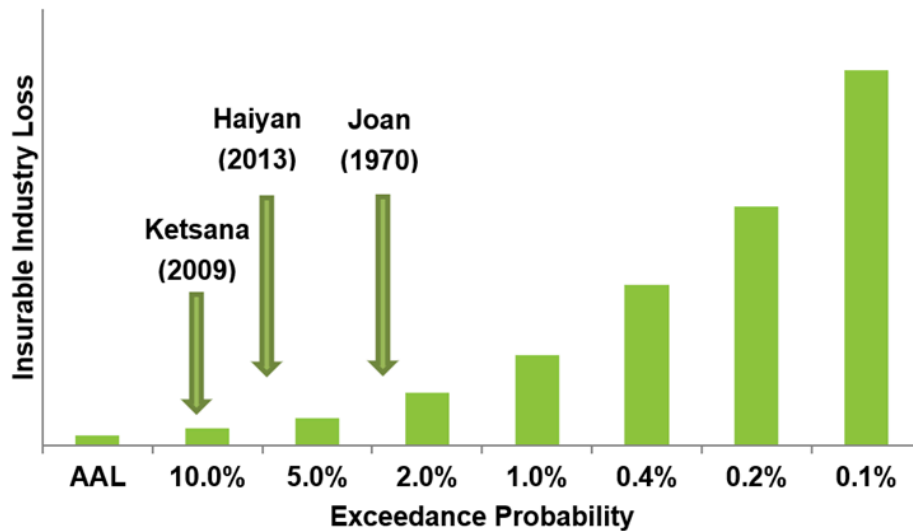
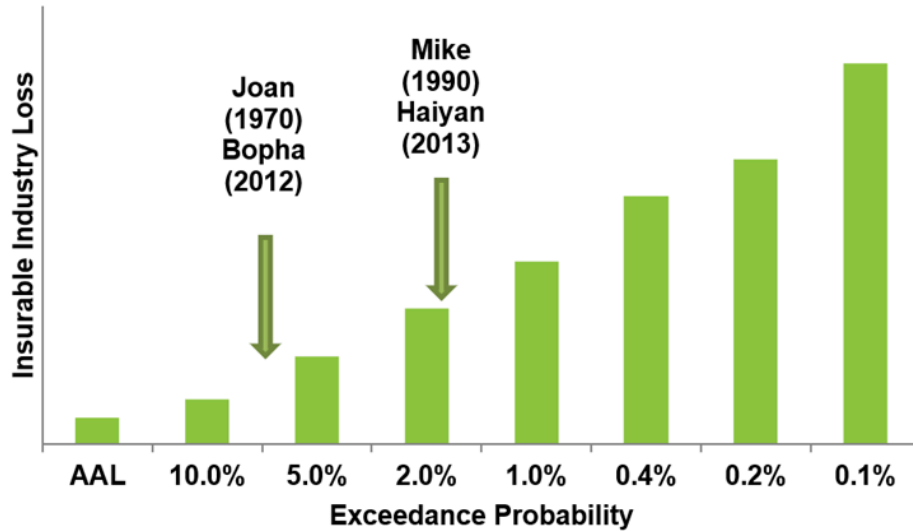
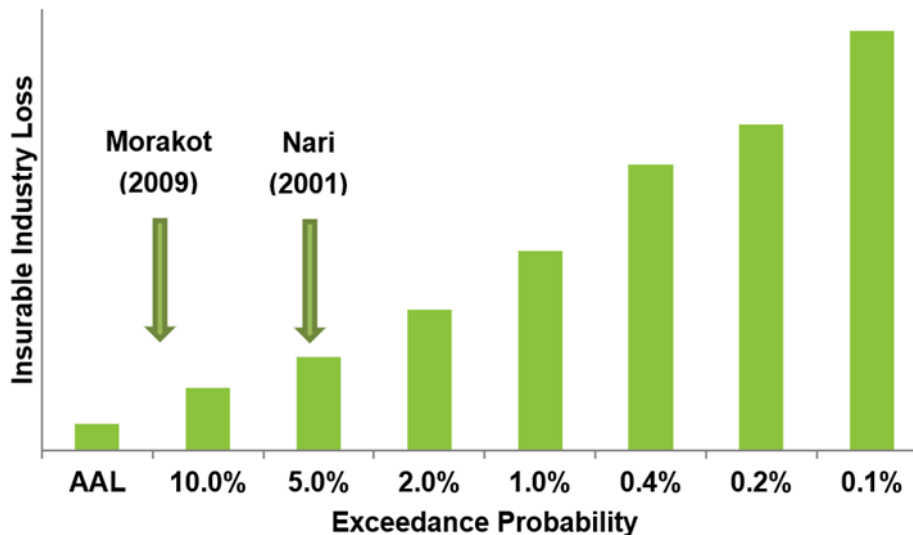


Figure 167. Benchmarking historical losses on Verisk's insurable occurrence exceedance probability curve – the Philippines (all sub-perils)



**Figure 168. Benchmarking historical losses on Verisk's insurable occurrence exceedance probability curve – the Philippines (surge only)**

In Taiwan, precipitation-induced flood contributes a significant portion of the typhoon losses. For example, Typhoon Nari in 2001 brought tremendous torrential rainfall that caused numerous rivers to overflow, and severely damaged the city of Taipei. [Figure 169](#) shows benchmarking historical events for all sub-perils combined losses in Taiwan on Verisk's all sub-perils combined exceedance probability curve, and [Figure 170](#) shows benchmarking historical events flood only losses on Verisk's precipitation-induced flood only exceedance probability curve for Taiwan.



**Figure 169. Benchmarking historical losses on Verisk's insurable occurrence exceedance probability curve – Taiwan (all sub-perils)**

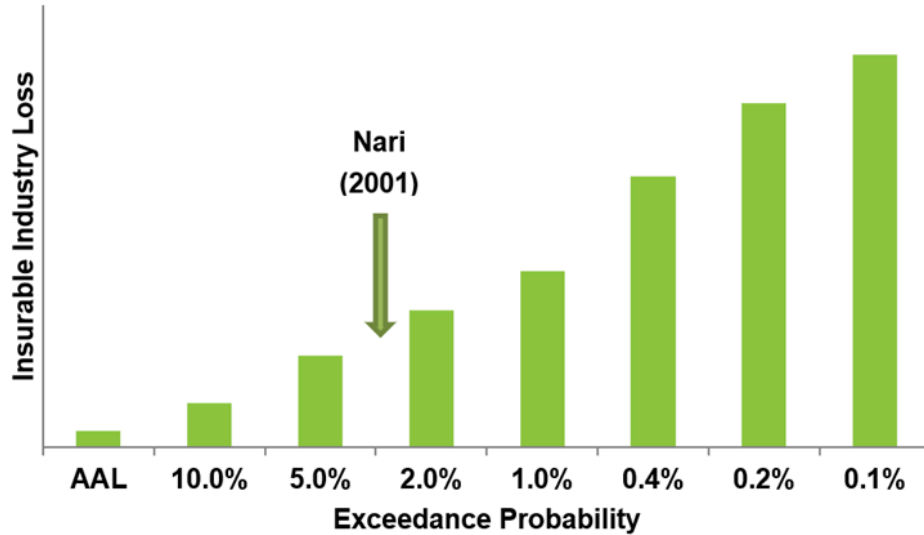


Figure 170. Benchmarking historical losses on Verisk's insurable occurrence exceedance probability curve – Taiwan (precipitation-induced flood only)

Lastly, historical events for all sub-perils combined losses for Vietnam are benchmarked in [Figure 171](#).

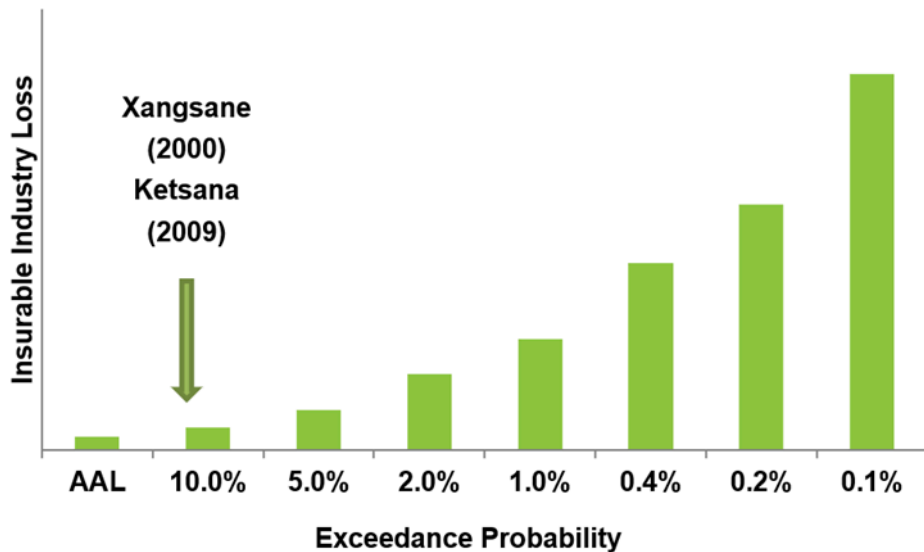


Figure 171. Benchmarking historical losses on Verisk's insurable occurrence exceedance probability curve – Vietnam (all sub-perils)

### Company book validation

Validating company books is another important step to the overall model validation process. However, given the quality of the data available in this region, appropriate study of the exposure and claims data provided by insurance client company is needed. For example, the modeled losses are not necessarily based on the exposure data provided by the client

company at the time of the event, but the claims data is the loss at the time of the event. Sometimes the latest exposure data is provided by the client company. Even though most of the time the exposure are relatively stable and does not change dramatically year to year, significant changes do occur and need to be appropriately evaluated. For example, sometimes after one significant event causes a huge loss and affects an area that has a high concentration of exposures for a client company, they may drop a significant portion of its business in that area next year. Therefore, when the latest client book is used to validate the loss for some old historical events, the results might be misleading. If the exposure and the claims data provided by the client company are not in the same vintage, Verisk engineers have conducted further investigations to check the reasonability of the gap between the modeled loss and claims data.

Another thing that might affect the company book validation is the resolution of the exposures provided by the client company. Generally, in Southeast Asia, the exposure is aggregated at different levels (e.g., CRESTA or postal level). To take advantage of location-specific hazard characteristics, based on Verisk's Industry Exposure Database, the disaggregation function in Touchstone is used in running the company exposure. However, the disaggregation process, can introduce uncertainties to some extent since the exposure from client company may not follow the same spatial distribution as the Verisk Industry Exposure Database.

A comparison of losses from client companies and the Verisk model is presented in the figures below. In the company loss data we collected, there are some big losses from large companies and strong events, but there are also some small losses from small companies and weak events. Using the linear scale may not necessarily show all the losses. The benefit of a logarithmic scale is that it is easier to observe the loss comparisons from both large and small events in one chart. Therefore, the same figure with two different scales is presented in [Figure 172](#) and [Figure 173](#), respectively. Overall, about 40% market data were used in the validation for the Philippines.

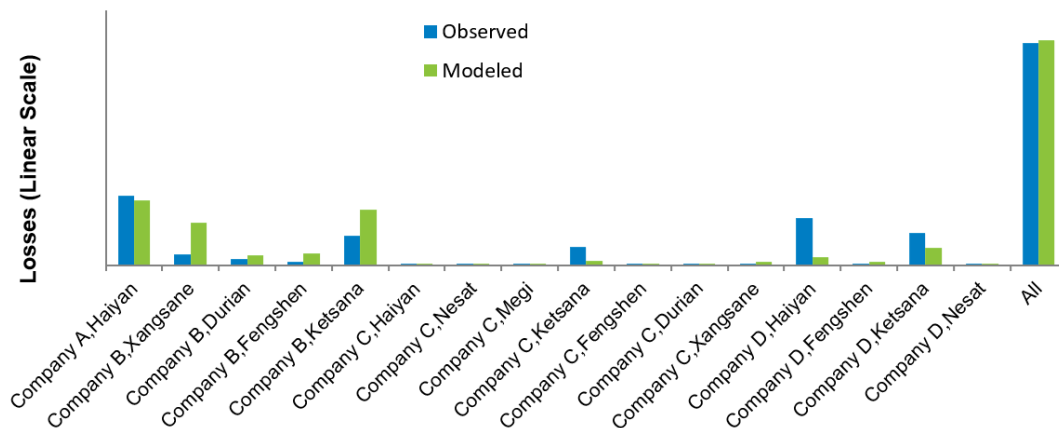


**Figure 172. Observed and Verisk-modeled gross losses by company with different events (linear scale) – the Philippines**

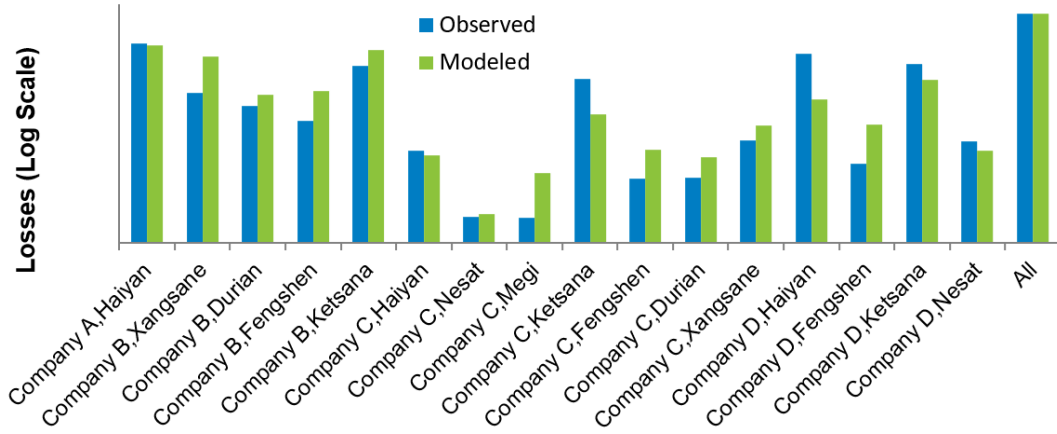


**Figure 173. Observed and Verisk-modeled gross losses by company with different events (logarithmic scale) – the Philippines**

# 7 Accounting for Climate Change

Detecting and attributing climate change impacts on various weather phenomena is a relatively new branch of climate science that is growing in demand and sophistication, but it is clear that climate change impacts extreme weather events. Attribution confidence, however, depends on many factors, including:

- whether the climate models agree with each other,
- whether there is a detectable trend in the historical data that agrees qualitatively with the modeled future result,
- how well we can physically connect and understand the modeled or observed effect on climate

Figure 174 shows the relative degree of confidence scientists have in attributing climate change impacts to individual weather events. Temperature phenomena are most confidently assessed because of the direct physical connection between increasing carbon dioxide (and other greenhouse gases) and a warming atmosphere. The temperature dependence of saturation water vapor pressure – described by the Clausius-Clapeyron equation – means that about 7% more water vapor can exist in the atmosphere for each degree Celsius increase. Therefore, as the atmosphere warms, its moisture content can increase, causing potentially heavier rainfall rates.

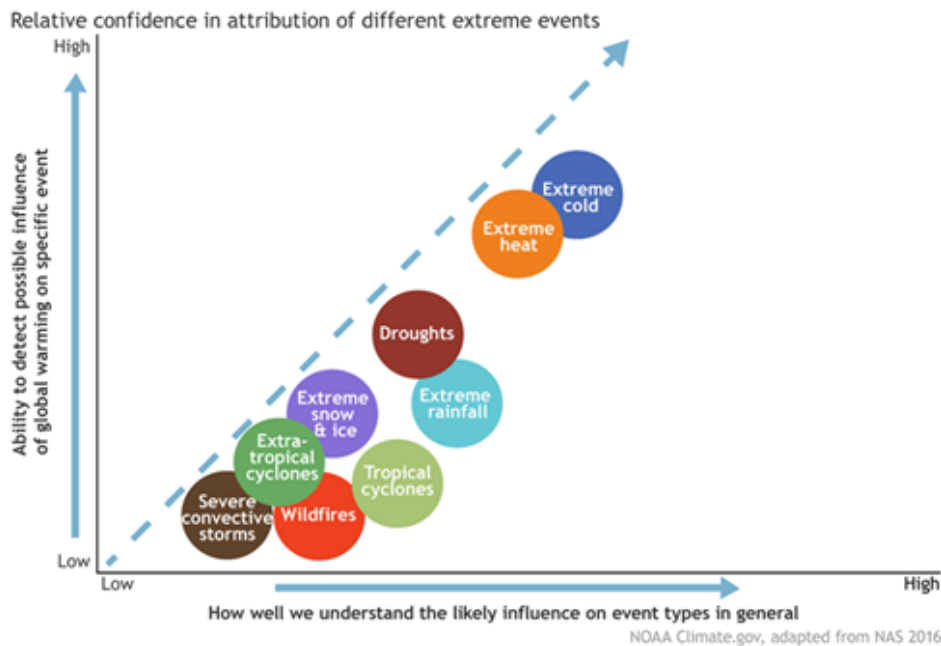


Figure 174. Relative degree of confidence that climate change is impacting various weather phenomena

source: NOAA.gov

There is less confidence that climate change is impacting tropical cyclones (including typhoons) relative to some other types of weather phenomena (such as extreme heat/cold). Reasons for this low confidence include:

- the relative infrequent occurrence,
- a historical record with changes in observational uncertainty over time,
- the inherently nonlinear physics driving these events.

Climate change is, however, expected to have a notable impact on tropical cyclone activity worldwide by later in the 21st century (Knutson et al., 2020). Analyses of global climate model projections indicate that future climate change will yield an increase in the proportion of Category 4 and 5 storms, as well as an overall decrease in the total number of tropical cyclones. Rahmstorf et al. (2018) found a global increase from 1980 to 2016 in frequency of high-intensity cyclones. See [Figure 175](#)

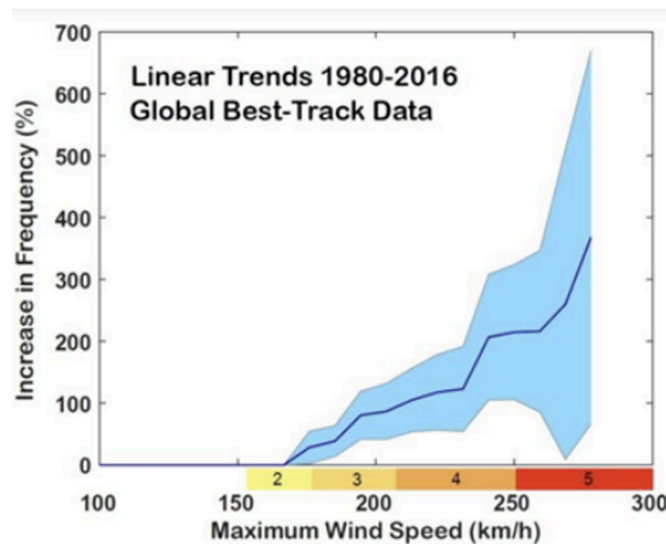


**Figure 175. Recent increases in tropical cyclone frequency by Saffir-Simpson Hurricane Wind Scale**

**Source:** *Rahmstorf et al (2018)* [realclimate.org](http://realclimate.org), ©CC BY-SA 3.0)

However, published results vary across ocean basins, as seen in [Figure 176](#).

## Tropical Cyclone Projections (2°C Global Warming)

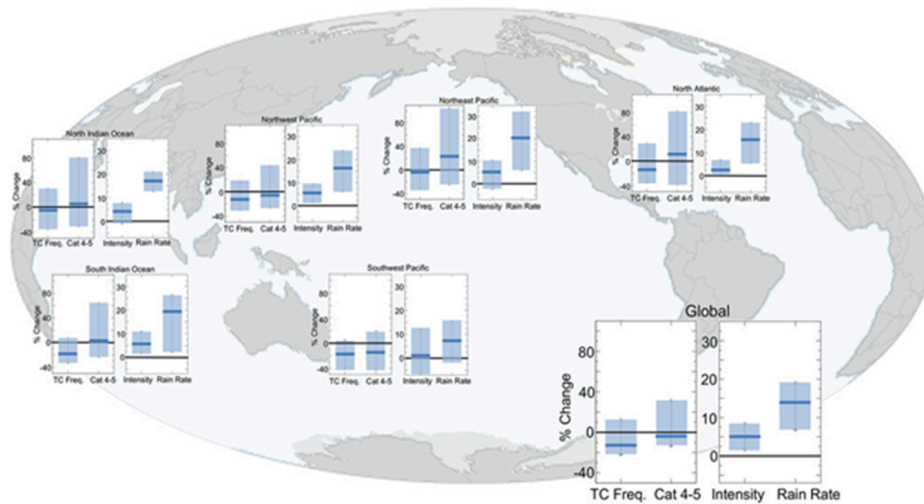


**Figure 176. Summary of tropical cyclone projections for a 2°C global anthropogenic warming**  
**Median and percentile ranges for projected percentage changes in tropical cyclone frequency, Category 4–5 frequency, tropical cyclone intensity, and near-storm rain rate are shown. For tropical cyclone frequency, the 5th–95th-percentile range across published estimates is shown. For Category 4–5, frequency, intensity, and near-storm rain rates the 10th–90th-percentile range is shown. Note the different vertical-axis scales for the combined tropical cyclone frequency and Category 4–5 frequency plot versus the combined tropical cyclone intensity and rain rate plot. The supplemental material in Knutson et al. (2020) has further details on the underlying studies used. [Source: Knutson et al. (2020), © American Meteorological Society. Used with permission.]**

While global climate modeling studies such as these provide estimates of future tropical cyclone activity, the more relevant challenge for catastrophe risk modeling is representing the current climate, including any variability that could be attributed to global warming.

The following sections include published studies and Verisk analyses that indicate:

- predicting future trends and analyzing past trends in typhoon activity over the model domain is a robust area of climate science with little consensus; in general, however, trends over the past few decades in typhoon activity over the modeled domain, where they exist at all, are not very robust.
- analyses comparing Verisk model results and current climate conditions show good agreement in typhoon frequency, intensity, and precipitation.

## 7.1 Historical trends

Through a combination of reviewing existing literature and conducting internal research, Verisk scientists have examined historical trends associated with typhoon activity across Southeast Asia.

The following sections summarize some relevant published literature and internal Verisk research on the intensity, frequency, location (poleward shift), forward speed,<sup>48</sup> and precipitation associated with typhoons in the model's domain, and globally. The Verisk analysis focuses on landfall events because those are the events likely to cause damage, whereas the scientific literature tends to focus less on landfall events.

Although these analyses and summaries are focused on the intensity, frequency, location (poleward shift), and forward speed, the impact that Super-typhoon Haiyan (2013) had on the Philippines was a stark reminder of how climate change may affect storm surge. Aside from stronger storms and more frequent strong storms, rising sea levels will further exacerbate damage and loss from storm surge (Lagmay, 2015). Some studies report a rise in the intensity of storm surges in the Northwest Pacific; Oey and Chou (2016) attribute these changes to a weakening of large-scale steering flows in the tropics.

### Published studies on trends in the intensity and frequency of typhoons in Southeast Asia

Numerous studies have focused on understanding how typhoon frequency and intensity have evolved over the historical period. Results differ across the studies but there is some scientific consensus that there has been a decrease in frequency and an increase in intensity over the Northwest Pacific basin since 1980. However, within the basin itself there is considerable variation in the overall trends as well as large interannual and interdecadal variability. Below is a summary of some key studies.

- Mei et al. (2015) found an increase in peak intensity of typhoons from 1980 to 2010 in the Northwest Pacific.<sup>49</sup>
- Wu et al. (2018) found an increase in frequency of intense (Category 4 and 5) typhoons over the Northwest Pacific (1980-2015), possibly because of deepening of ocean mixed layer (the warm layer of the ocean above an abrupt transition to cooler water).
- Kossin et al. (2020) found no change in tropical cyclone intensity in the Northwest Pacific Basin, and (at the 95% confidence level) an 8% increase globally. They analyzed global and basin-specific trends in the intensity of tropical cyclones (categories<sup>50</sup> 3 to 5) for the period 1979 to 2017. Landfall activity was not examined. The authors hypothesized that the lack of intensity trends in the Northwest Pacific may be due to poleward trends in tropical cyclone tracks into regions of lower potential intensity.<sup>51</sup>
- Lee et al. (2020) found

<sup>48</sup> All else being equal, slowly moving typhoons yield higher rainfall totals

<sup>49</sup> See Figure 1 in Met et al. 2015 <https://www.science.org/doi/10.1126/sciadv.1500014>

<sup>50</sup> Categories are based on central pressure

<sup>51</sup> Unlike many of the other studies mentioned here, Kossin et al. (2020) used an Automated Dvorak Technique (ADT) track data set.

- no statistically significant trends in Hong Kong and Macao, the only regions studied that are part of the Verisk Typhoon Model for Southeast Asia
  - a statistically significant decreasing trend in annual counts of storms of at least tropical storm and typhoon intensities from the China Meteorological Administration (1949–2017) and Hong Kong Observatory (1961–2017) data sets
  - no statistically significant trends from the Joint Typhoon Warning Center (1945–2016) or Regional Specialized Meteorological Centre-Tokyo (1951–2017) data sets
  - all datasets show a decline in tropical storm/typhoon (and above) counts for a common period across the data sets (1977–2017) – but this decline is not statistically significant at the 5% level.
- Murakami et al. (2020) used a suite of high-resolution dynamical model experiments to analyze historical tropical cyclone behavior and concluded that the different observed trends globally over the period 1980-2018 cannot be entirely explained by natural decadal variability. Instead, external forcing (such as greenhouse gases and aerosols) likely exert an important influence. See [Figure 177](#). They found significant regional variations, specifically:
    - decreased typhoon activity over the region covered by the Verisk Typhoon Model for Southeast Asia (with the exception of perhaps Vietnam). The decrease in activity over the northern Philippines is particularly noteworthy and significant with rates as high as -0.15 typhoons per year
    - increased activity in the North Atlantic and central Pacific
    - decreased frequency in the South China Sea and east of the Philippines
    - increases along the East China coast and Japan.

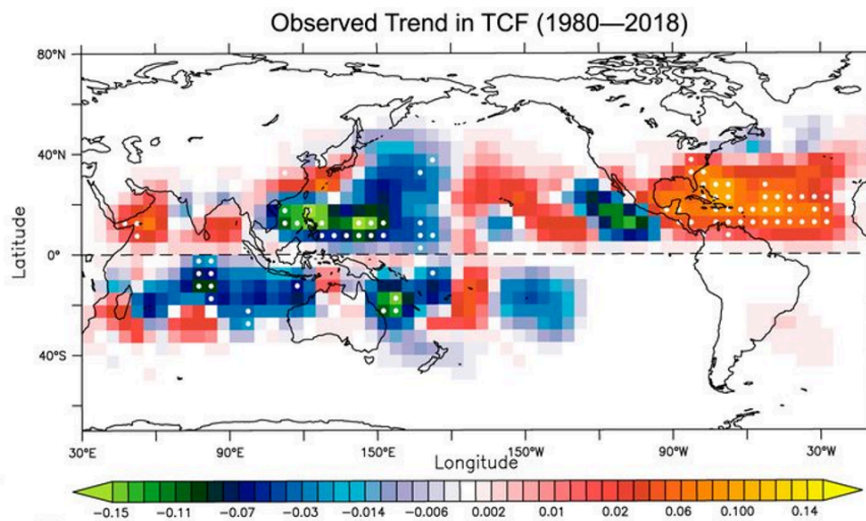


**Figure 177. Observed trends in tropical cyclone frequency (number per year) over the period 1980 to 2018**

**Source: Murakami et al., (2020) ©Murakami, Delworth, Cooke and Hsu, 2020, used with permission**

- Kubota et al., (2021) confirmed the findings of Lee et al., (2020) and others. They also examined information from various sources to extend the typhoon data time series analysis back to 1877 and up to 2019. The counts over the basin were found to agree well across various agencies (e.g., from Hong Kong, Shanghai, Philippines, and Japan) from 1960 onward and qualitatively before that. Prior to 1960 some agency data show trends, but this could be an artifact of scarce historical data and not related to climate. Key findings from the study as shown in the figure below support an oscillating basin counts hypothesis with a periodicity of 20 to 25 years.

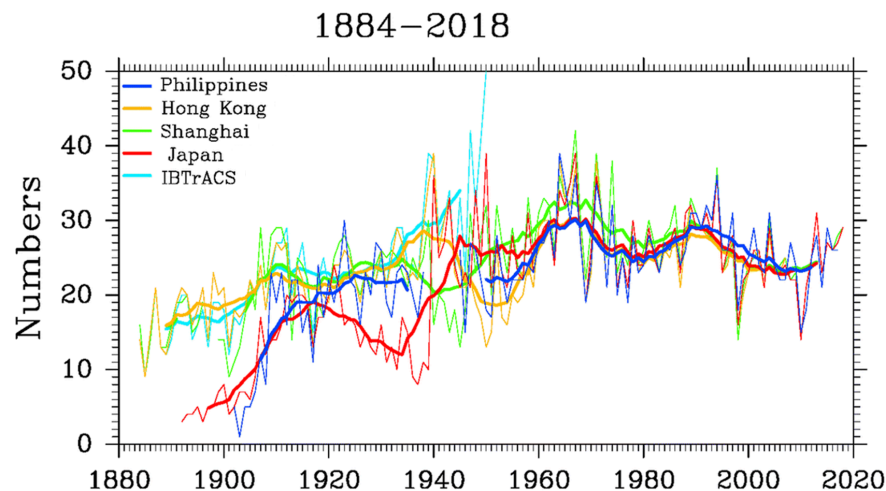


**Figure 178. Annual typhoon numbers over basin the from 1884 to 2018, for Philippines, Hong Kong, Shanghai, Japan and IBTrACS data**

**Data are merged using historical and best track data: Philippines (blue), Hong Kong (orange), Shanghai (green), Japan (red) and IBTrACS TD9636 (sky blue). Thick lines are 11-year running means. [Source: Kubota et al. (2021)] ©2021, Kubota, Matsumoto, Zaiki et al., CC by 4.0.**

- Chen et al. (2021)
  - Found that between 1979 and 2016, over east and Southeast Asian regions, storm duration increased by 2–9 hours and storms traveled 30–190 km further inland, most significantly over Hanoi and South China.
  - Projected that inland impacts from tropical cyclones in a warming future will include increased durations of almost 5 hours (56% increase), and an increased average penetration farther inland of 92.4 km (50% increase).
- Wu et al. (2022) concluded that the degree to which climate change has affected tropical cyclone intensity or when the impact of climate change on tropical cyclone intensity will be detectable in the future remain unclear because of:
  - uncertainty in the historical datasets of tropical cyclones
  - incomplete understanding of the mechanisms for the basin-wide intensity change
  - inter-dependent natural variabilities
  - considerable model bias in the projected large-scale environment

- poorly-simulated inner-core structures of tropical cyclones.

## Verisk analysis of trends in the intensity and frequency of typhoons in Southeast Asia

This section includes trend analyses performed by Verisk scientists to identify and understand changes for the period between 1951 to 2021 in:

- intensity of typhoons that make landfall
- frequency of typhoons that make landfall, for all storms, and for strong storms

These analysis differ from much of the published literature in that they focus on typhoon characteristics at landfall, rather than typhoon formation or development over a basin.

The data used in these analyses are the same as were used to create the historical and stochastic catalogs, except that data sources for these analyses extend through 2021.

In order to determine if observed trends were significant, Mann Kendall significance tests were done for trends in minimum central pressure over the two time periods 1951-1921, and 1979- 2021.

In Vietnam from the years 1951 to 2021, there is a decreasing trend (0.1mb per year – 90% confidence) in minimum central pressure of storms that make landfall, indicating that the intensity of landfalling storms in Vietnam has increased over the last 70 years. Consistent with this, there was a small increasing trend in the number of category 3 storms (0.03 storms per decade) over Vietnam for that same time period – but only at the 85% confidence level. This is consistent with Murakami et al. (2020).

The other time series do not have any significant trends.

The figures below show annual average minimum central pressure and frequency of storms that make landfall for Hong Kong, Philippines, Taiwan, and Vietnam, over the time period 1951-2021.

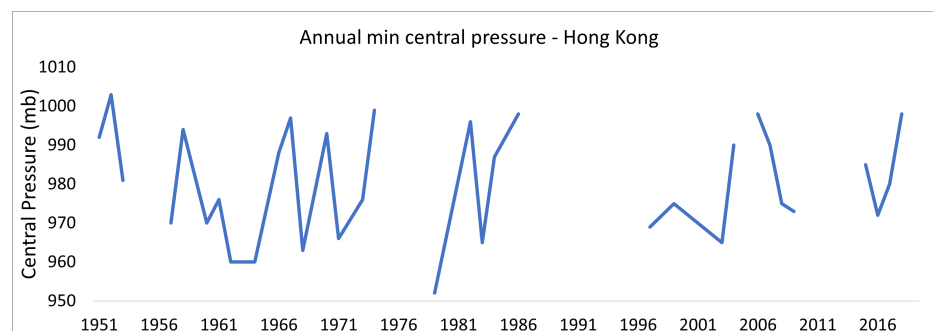


**Figure 179. Annual average minimum central pressure of storms that make landfall in Hong Kong**

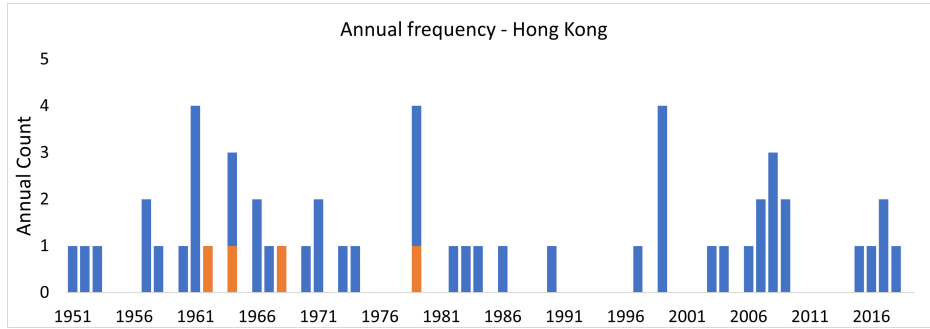


**Figure 180. Annual frequency of landfalling typhoons in Hong Kong**  
 Total storm count (blue) and category 3 and higher storms (orange)

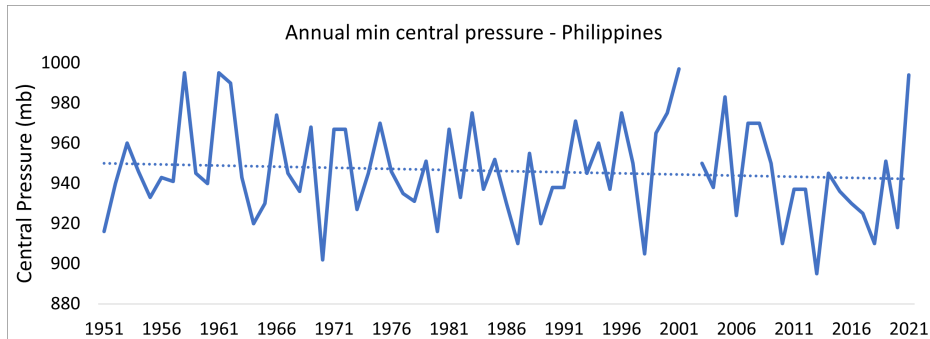


**Figure 181. Annual average minimum central pressure of storms that make landfall in Philippines**

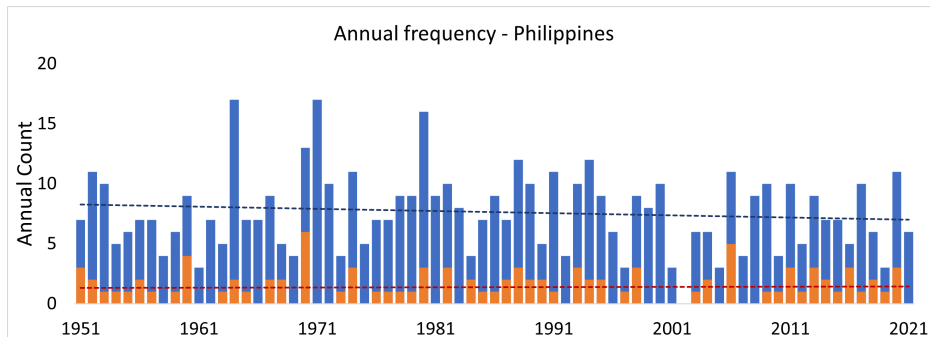


**Figure 182. Annual frequency of landfalling typhoons in Philippines**  
 Total storm count (blue) and category 3 and higher storms (orange)

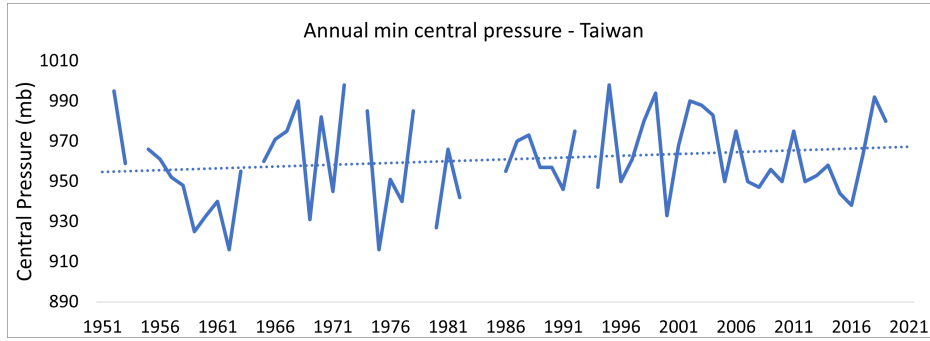


**Figure 183. Annual average minimum central pressure of storms that make landfall in Taiwan**

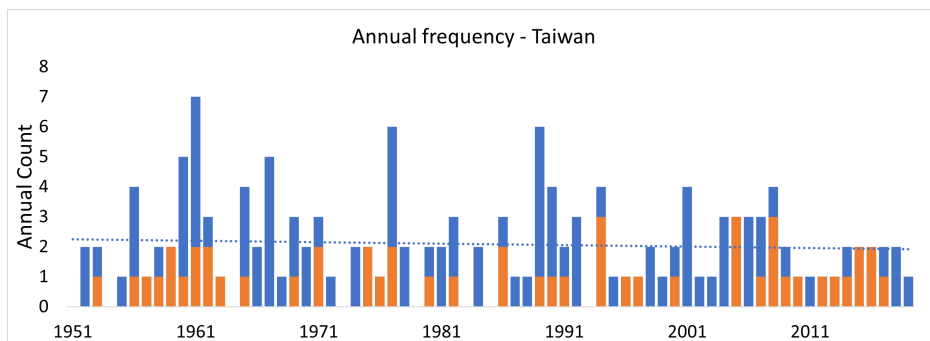


**Figure 184. Annual frequency of landfalling typhoons in Taiwan  
Total storm count (blue) and category 3 and higher storms (orange)**

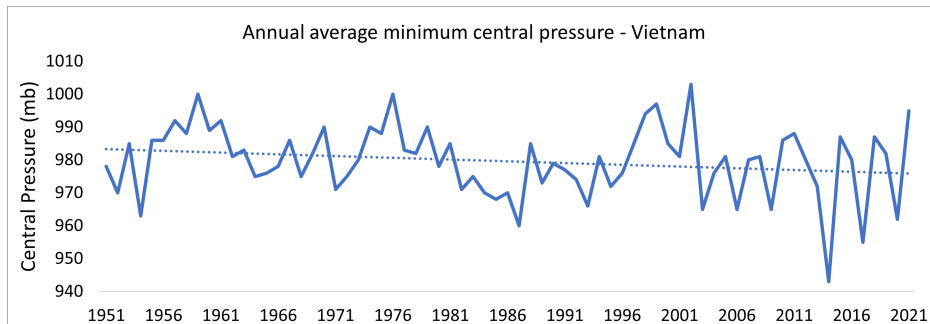


**Figure 185. Annual average minimum central pressure of storms that make landfall in Vietnam**

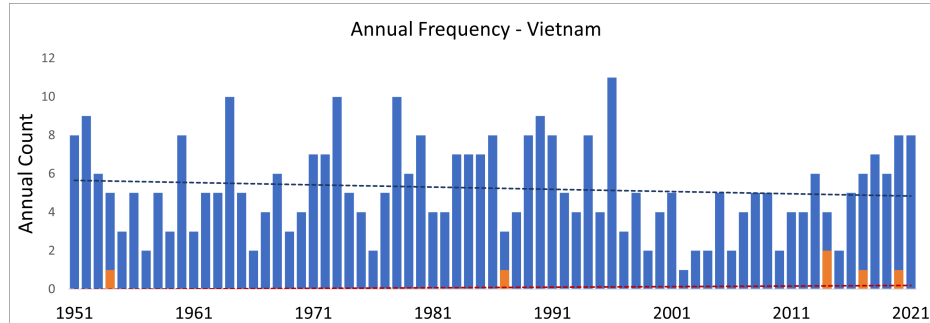


**Figure 186. Annual frequency of landfalling typhoons in Vietnam**  
**Total storm count (blue) and category 3 and higher storms (orange)**

## Published studies on poleward shift of latitude of lifetime maximum intensity

Several studies found poleward shifts in the latitude of lifetime maximum intensity (LMI) of tropical cyclones. Despite a consensus in the basic finding, there are differences in the explanation for the shifts and thus considerable uncertainty in attributing the result to climate change. Specifically:

- Kossin et al. (2014) found a shift in tropical cyclone activity away from the tropics and toward the pole of about one degree latitude per decade (accounting for poleward shifts in both hemispheres), consistent with estimates of the observed expansion of the tropics. The study suggests a connection to anthropogenic warming.
- Zhan and Wang (2017) found a significant northward shift over the period 1980-2016 for all tropical cyclones, but the greatest contributions were from tropical cyclones with maximum near-surface winds less than 33m/s ("weak" tropical cyclones), see [Figure 187](#). They attribute the result to an increase in the genesis of these weak storms farther north and a decrease in genesis farther south. They note that the shift may be related to climate change.
- Liu and Chan (2019) found a significant northward shift over the period 1960-2016 for tropical cyclones of at least tropical storm strength, but no trend for strong typhoons. Specifically, they determined the shift results from (1) a higher percentage of recurring storms with a more northward rather than eastward trajectory, (2) a northwards shift of genesis locations, and (3) an increase in latitudinal distance between genesis position and LMI location in the second period, all of which may be linked to the interdecadal Pacific Oscillation or the Pacific Decadal Oscillation.
- Wang and Wu (2019) found poleward migration due to changes in the steering subtropical high, rather than from changes in sea surface temperatures and wind shear.

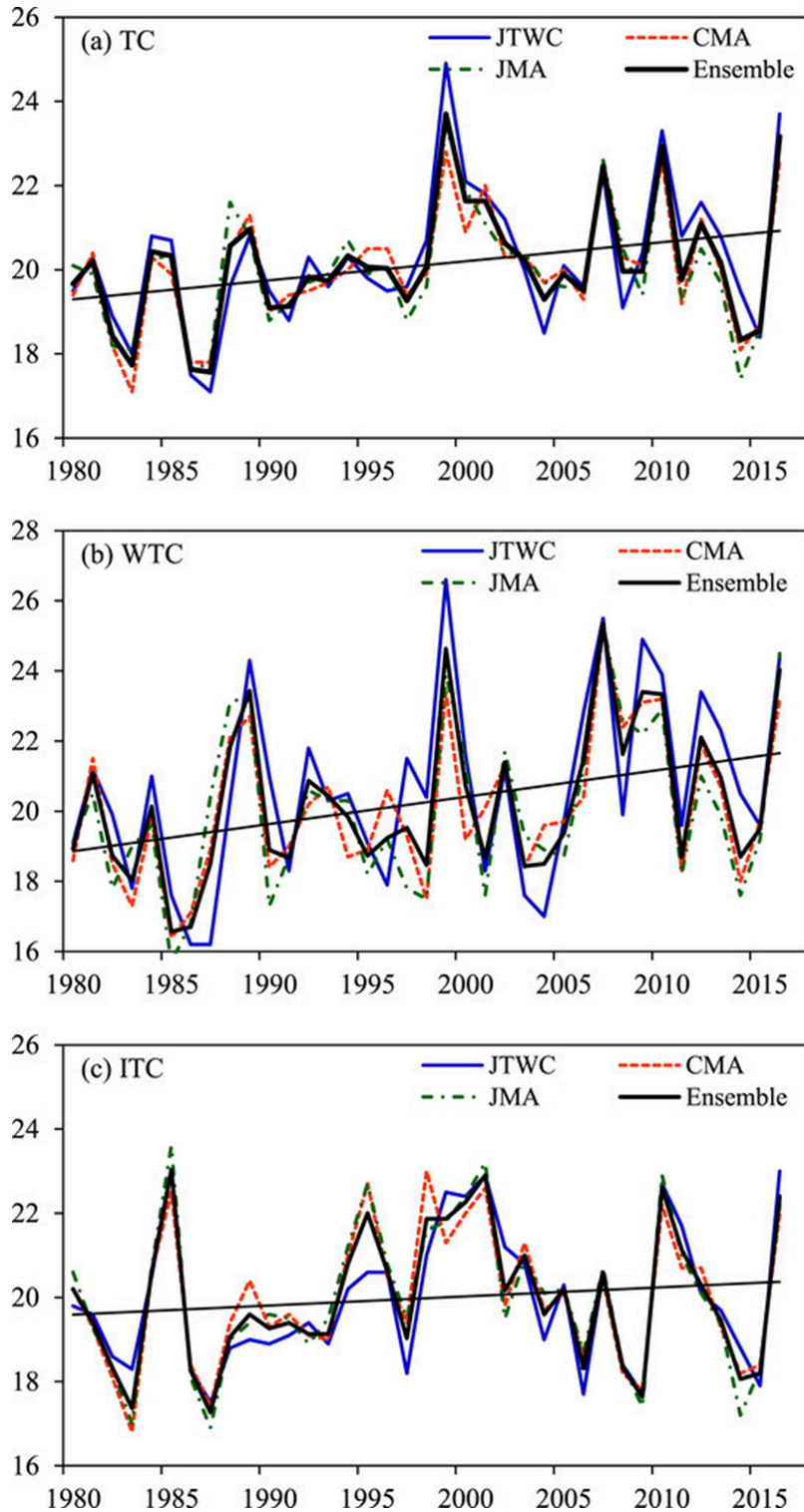


**Figure 187. Mean latitude of lifetime maximum intensity (LMI)**  
*The vertical axis is the annual mean latitude of LMI for (a) all tropical cyclones, (b) tropical cyclones with maximum near-surface winds less than 33 m/s (weak tropical cyclones) and*

**(c) tropical cyclones with maximum near-surface winds of 33m/s or more (intense tropical cyclones). Used with permission, Zhan and Wang (2017) © American Meteorological Society.**

Verisk scientists examined possible poleward shifts in landfall activity across the model domain and did not find any significant trends or variability.

## Published studies on trends in forward speed

---

Several studies have discussed the hypotheses that the reduction in the pole-to-equator temperature gradient caused by global warming has reduced the speed of the jet stream and the forward speed of weather patterns. However, the effects of Arctic warming on global climate dynamics are a complex and robust discipline of climate science (see for example Cohen et al., 2020). Whether or not there have been significant trends in the forward speed of tropical cyclones over the model domain is an area of scientific research; some studies have found significant trends and others have not, and explanations on mechanisms vary.

- Kossin (2018) found statistically significant slowdowns in forward speed: 20% over water and 30% over land, for the Northwest Pacific Basin. The author does not attribute the result to climate change noting that more research is needed.
- Moon et al. (2019) hypothesized that the statistically significant slowdowns in forward speed found by Kossin (2018) are due to the exclusion from that analysis of weak storms that typically move more slowly - especially at northern latitudes.
- Chan (2019) found smaller trends than in Kossin (2018) for the period 1970-2016 - essentially zero - and thus did not conclude that climate change was causing a slowdown. See [Figure 188](#) .

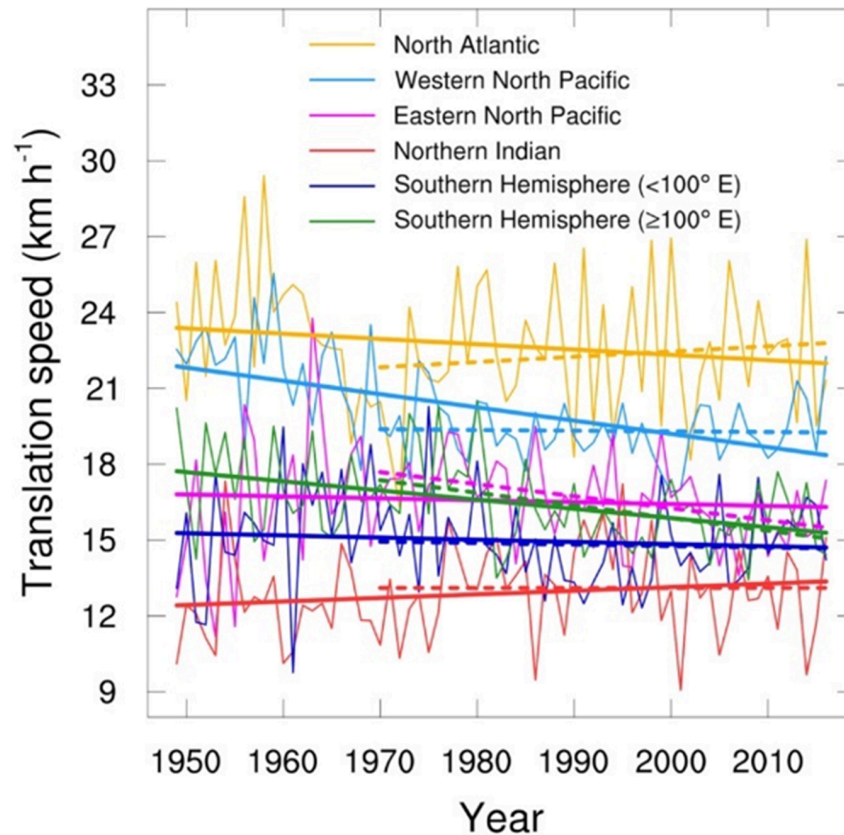


**Figure 188. Time series of annual-mean tropical-cyclone forward speed (labeled "translation speed") and their linear trends in different regions**  
**Long solid and short dashed linear trend lines indicate the corresponding trends over the periods 1949–2016 and 1970–2016, respectively. Source: Chan (2019), © CC BY 3.0**

- Zhang et al. (2020) found smaller trends as well, and although the tropical cyclone forward speed decreased during the 1949–2017 period they examined, there was no significant trend after 1981. They also found the changes in forward speed to depend on latitude and intensity.
- Kim et al. (2020) hypothesized that because of the positive correlation between forward speed and latitude, climate change may well produce faster storms if a poleward shift in tropical cyclone activity continues.
- Gong et al. (2022) found that storms progressively moved more slowly and reached lower lifetime maximum intensity (LMI) prior to 1998. After 1998, forward speed and LMI increased. This may be due to changes in low-level wind speed: the low-level winds slowed down between 1980-1999 and therefore vertical wind shear increased, this increased vertical wind shear inhibited LMI and decreased forward speed. After 1998, low-level winds increased, resulting in lower vertical wind shear, higher LMI, and faster moving storms. This interdecadal variability is not thought to be related to climate change.

## Verisk analysis of trends in the forward speed of typhoons in Southeast Asia

This section includes trend analyses performed by Verisk scientists to identify and understand changes for the period between 1951 to 2021 in the forward speed of typhoons at landfall in the model domain.

These analysis differ from much of the published literature in that they focus on typhoon characteristics at landfall, rather than typhoon formation or development over a basin.

The data used in these analyses are the same as were used to create the historical and stochastic catalogs, except that data sources for these analyses extend through 2021. Landfall points for these analyses were determined by taking the last six hourly points offshore before the storm path crossed the coastline. In the case of Hong Kong, the coastline was considered to be a circular area of 0.5 degree radius surrounding Hong Kong.

In order to determine if observed trends were significant, Mann Kendall significance tests were done for trends in forward speed at landfall over the two time periods 1951-1921, and 1979- 2021, and none of them were found to be significant.

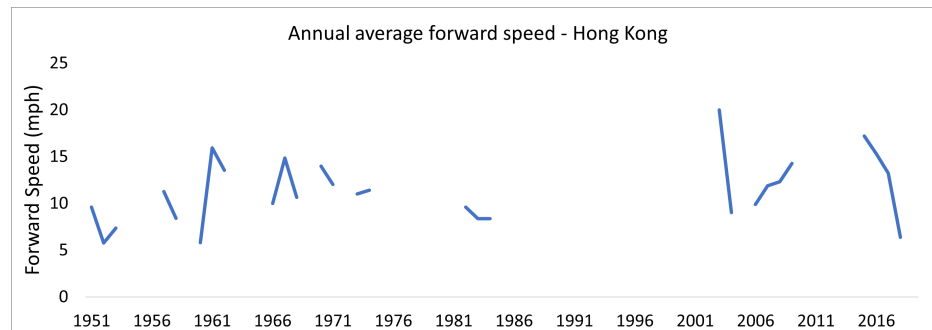


**Figure 189. Forward speed of typhoons at landfall – Hong Kong**

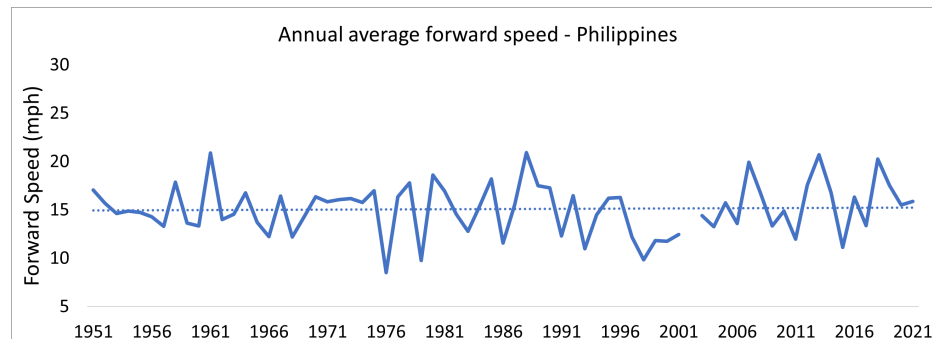


**Figure 190. Forward speed of typhoons at landfall – Philippines**

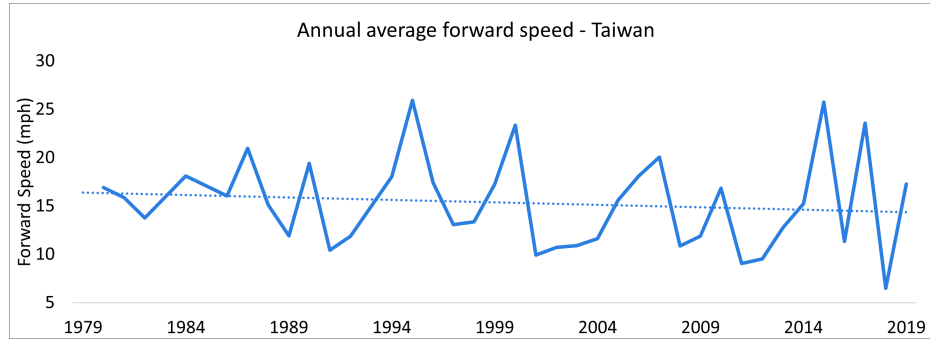


**Figure 191. Forward speed of typhoons at landfall –Taiwan forward**

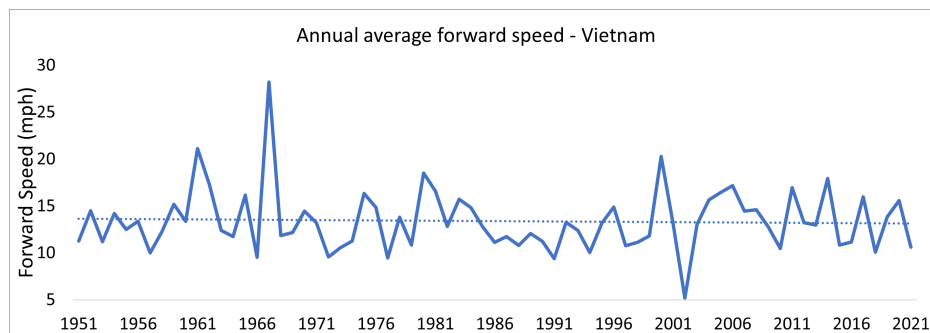


**Figure 192. Forward speed of typhoons at landfall –Vietnam**

## Published studies on trends in typhoon precipitation

Warmer oceans evaporate more, and a warmer atmosphere can hold more water vapor before reaching saturation. Therefore, all else being equal, increased ocean and atmosphere temperatures are expected to result in increased precipitation. Across much of the model domain, there has been an increase in typhoon-related precipitation, although some regions – notably around Hong Kong – have experienced a decreased trend.

- Nguyen-Thi et al. (2012) found increasing trends of tropical cyclone rainfall and tropical cyclone heavy rain days at most stations along the Vietnam’s central coastline from 1961 to 2008.
- Chang et al. (2013) found that major contributing factors to precipitation include slow-moving tropical cyclones and the location of their tracks relative to the mesoscale terrain.
- Tu and Chou, (2013) and Lee et al. (2020) found an increase in typhoon-related rainfall in the beginning of the twenty-first century in Taiwan – and a decrease in non-typhoon, lighter, rainfall.
- Li et al. (2015) found an intensification of autumn precipitation over central Vietnam since late 1990s.
- Bagtasa (2017) found that precipitation from typhoons has been increasing across the Philippines from 1951 to 2014 and the increase is considerably higher in northern Philippines than in southern Philippines (54% vs. 7%).

- Chu et al. (2018) found an increase in 100-year return-period typhoon rainfall across Taiwan, but little or no trend in shorter return period precipitation.
- Lee et al. (2020) found that, within a 500 km radius of Hong Kong, the annual rainfall per tropical cyclone and annual maximum hourly tropical cyclone rainfall from 1961 to 2018 has exhibited a slight decrease but it is not statistically significant. In nearby Macao, the trend is less.

## Verisk analysis on trends in typhoon precipitation

In the Verisk analysis of precipitation associated with typhoons in the model domain, precipitation was considered "typhoon precipitation" if a typhoon was within a 7.5 degree radius of stations within the country, regardless of whether the typhoon made landfall (there is "typhoon-day" precipitation even for those years that had no landfalling typhoons). The stations were then aggregated to a country-wide "typhoon-day precipitation" total.

Precipitation was obtained from the National Center for Environmental Information (NCEI) from the Global Summary of the Day archives for the Philippines, Taiwan, and Vietnam. Precipitation data for Hong Kong was obtained from the Hong Kong Observatory. In order to determine if observed trends were significant, Mann Kendall significance tests were done for typhoon-day precipitation trends over the time period 1989- 2020, and none were found to be significant.

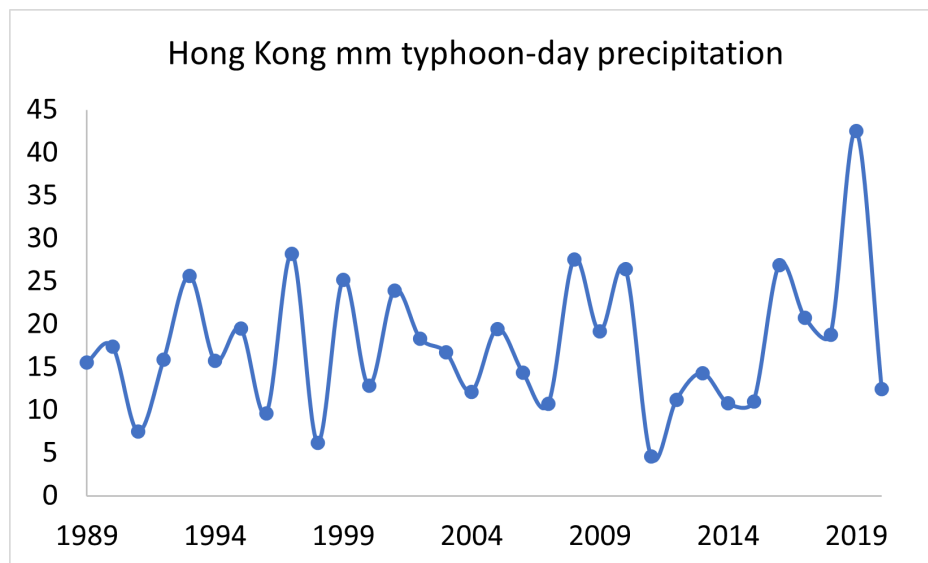


Figure 193. Hong Kong typhoon-day precipitation

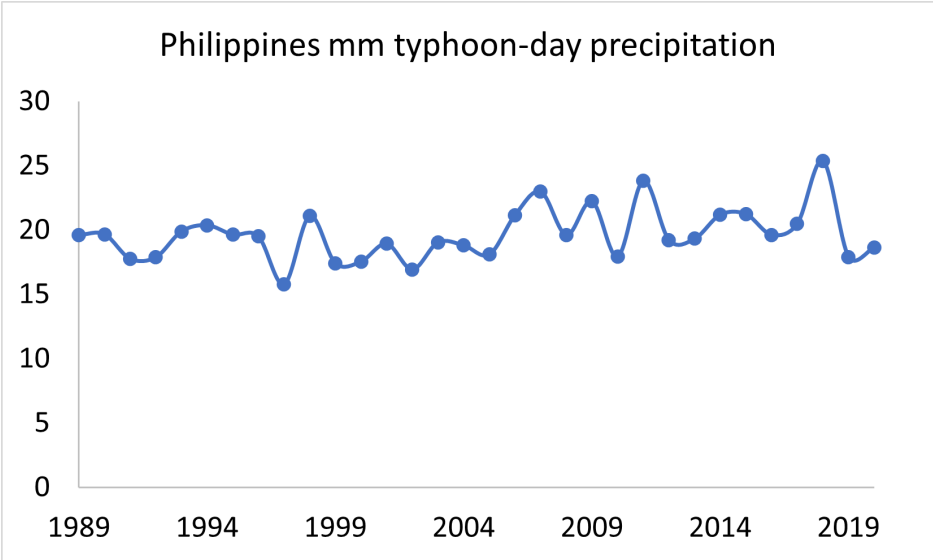


Figure 194. Philippines typhoon-day precipitation

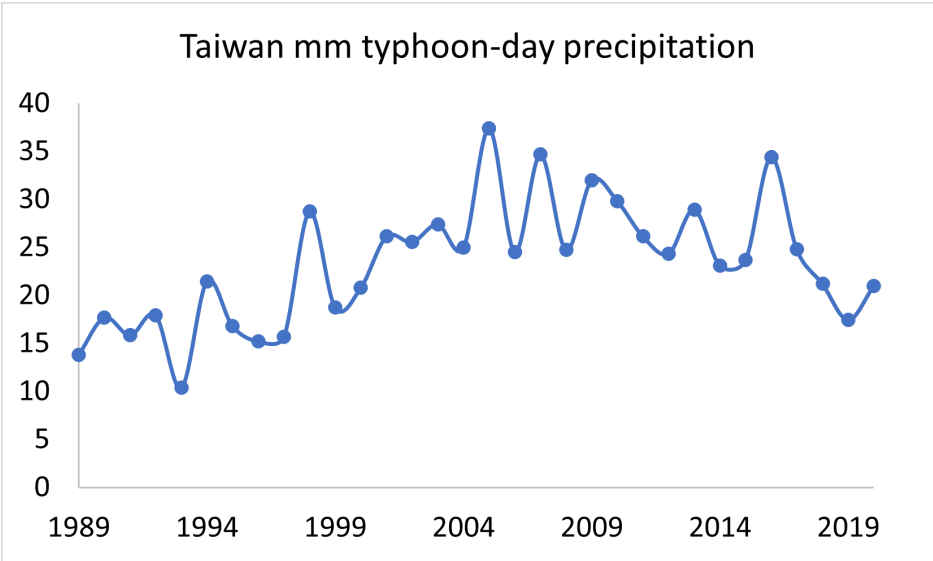
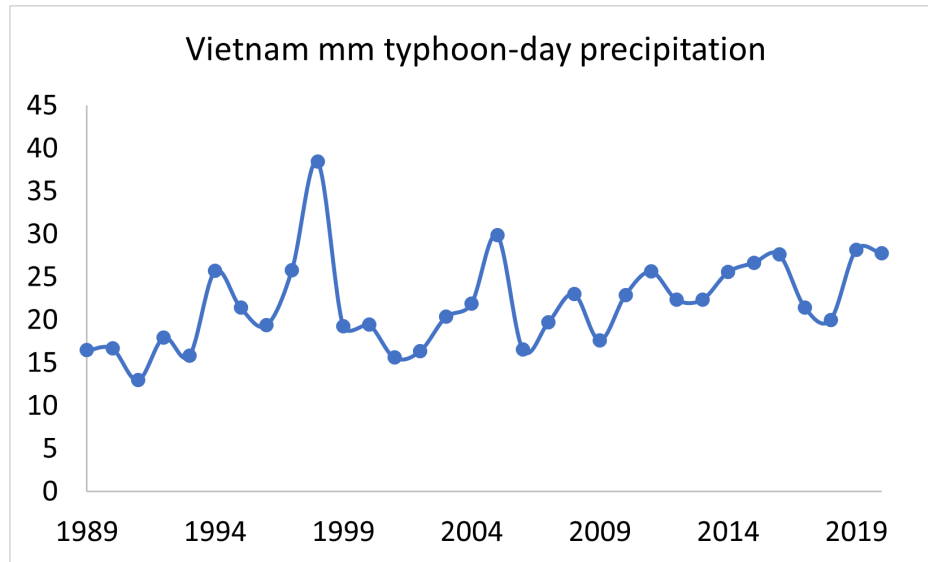


Figure 195. Taiwan typhoon-day precipitation



**Figure 196. Vietnam typhoon-day precipitation**

## 7.2 Model and catalog development

The primary data sources used to develop the model's stochastic catalog include typhoon track information from the Japan Meteorological Agency (JMA) and the Shanghai Typhoon Institute (STI) from 1949 to 2006. As the previous section showed, there are no significant trends that would motivate weighing more recent data more heavily or adjusting characteristics of early storms when developing a stochastic catalog that reflects the current climate. Therefore, in the catalog development for this model, all historical data were treated with equal weight throughout the entire historical interval.

Descriptions are provided below of how any precipitation and storm surge associated with the events in the stochastic catalog were simulated.

The precipitation model is parametric and accounts for precipitation within a circular shield but also accounts for asymmetries and interactions with other (non-tropical) precipitating weather systems. The primary data used for calibration was from the National Center for Environmental Information (NCEI) Global Summary of the Day Station Data (GSOD) for the period 1979-2013. Similarly to the Japan Meteorological Agency (JMA) and the Shanghai Typhoon Institute (STI) data, at the time of model development the more recent data did not show significant differences from older data; therefore equal weight was given to the entire historical interval in the calibration of the model.

To model the storm surge component for Hong Kong, Taiwan, and the Philippines, modern topographic and bathymetric datasets (referenced to modern sea levels) were used. Therefore, the storm surge model accounts for the current state of the sea level for the purposes of modern-day risk analysis.

Sampling variability was fully considered in the construction of the stochastic catalog. For example, because ocean heat content is critical to the genesis, development, and evolution of typhoons, a definition of climate that considers variability in basin-wide sea surface temperature is more appropriate than simple 30-year condition averages. For example, El Niño-Southern Oscillation (ENSO) is a climate phenomenon related to sea surface temperature and therefore affects typhoon climatology in the Northwest Pacific Basin. Annual changes in typhoon activity associated with ENSO are implicitly reflected in the historical data used for the catalog development.

**See Also**

[Local Intensity Calculation](#)

## 7.3 Model validation

The Verisk Typhoon Model for Southeast Asia has been validated using recent historical data to demonstrate that it reflects the near present climate and risk.

### Validating the model's typhoon frequency

The modeled landfall frequencies by Saffir-Simpson category were compared to the two periods 1951-1989 and 1990 to 2021 for locations across the model domain. The figures below show the modeled and historical values by individual category as well as by minor (Cat 0-2) and major (Cat 3-5) strength. Except for the figure showing all-basin landfall frequency, each storm is counted only once at its most intense landfall in the individual country.

There are no systematic differences in storm frequencies from one time period to another that would indicate a shift in typhoon frequencies between those time periods.

For both historical periods, the frequencies of the minor and major landfalls are within the 10% to 90% range of the modeled annual mean frequencies using 300 33-year samples from the 10k-year catalog (not shown).

Perhaps the most notable difference is that the number of modeled major-category landfalls across Taiwan is less than observed, primarily because there are fewer Cat 3 storms. However, the modeled frequencies in Taiwan agree better for the more recent historical time period.

As expected, the comparison for all landfalls (meaning there may be more than one landfall per event) across the domain shows better agreement than at the individual country level. In summary, the model captures the frequency of landfalling typhoons across the model domain for all storm categories remarkably well.

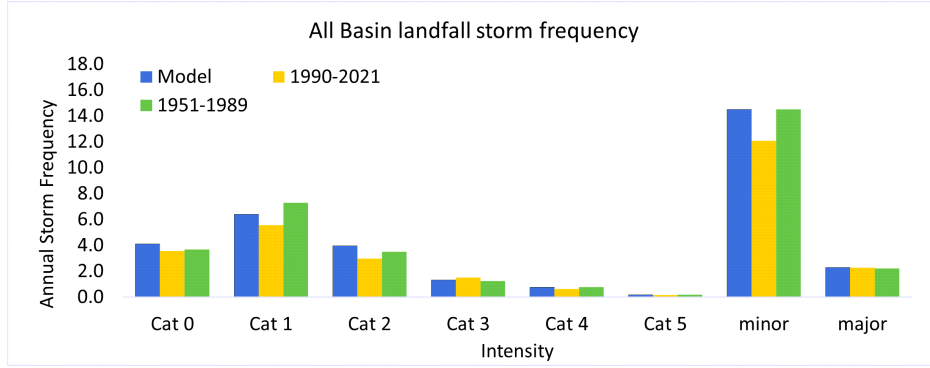


**Figure 197. Comparison of modeled and historic frequencies of typhoons making landfall across domain**

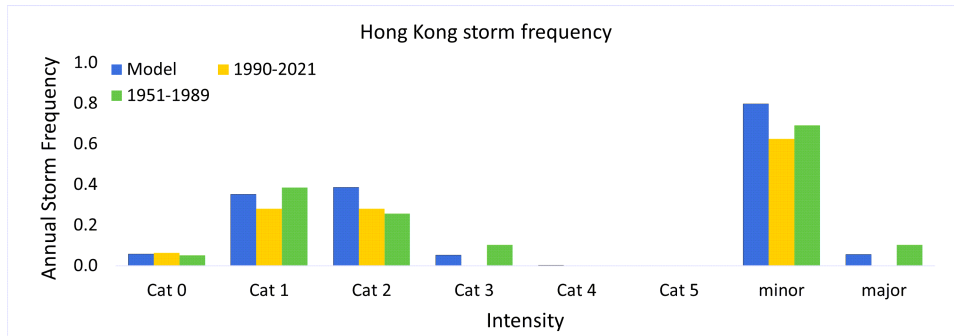


**Figure 198. Comparison of modeled and historic frequencies of typhoons making landfall—Hong Kong**

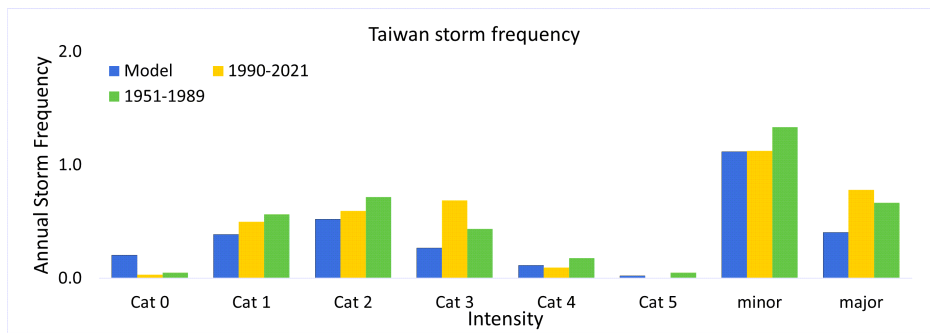


**Figure 199. Comparison of modeled and historic frequencies of typhoons making landfall—Taiwan**

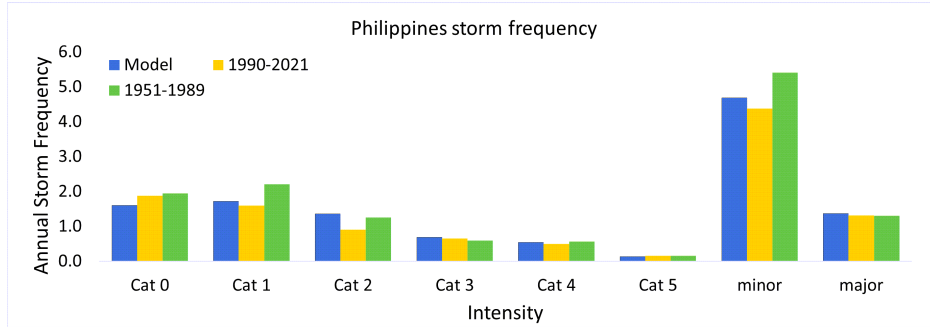


**Figure 200. Comparison of modeled and historic frequencies of typhoons making landfall—Philippines**

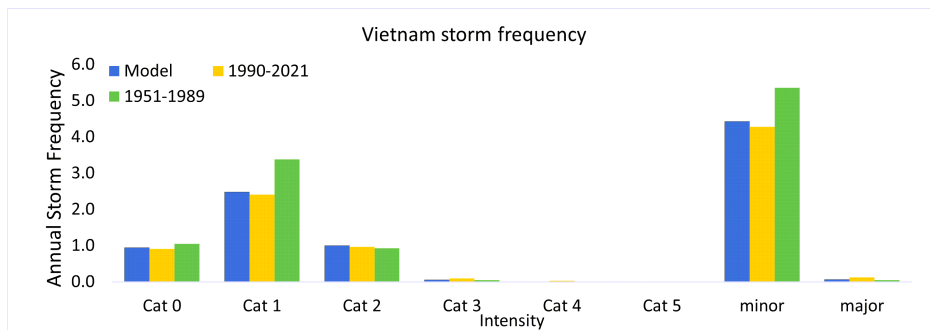


**Figure 201. Comparison of modeled and historic frequencies of typhoons making landfall—Vietnam**

**Validating the model's typhoon forward speed**

The figures below show comparisons of the modeled forward speed at landfall with the two time periods 1990 to 2021 and 1951-1989 for locations across the modeled domain. For this analysis all landfalls for all events are included. The two smallest regions shown, Hong Kong and Taiwan, both exhibit more modeled slow storms and fewer modeled fast storms than observed. The other countries show good agreement between modeled and observed speed categories, and as expected, good overall agreement is exhibited across the model domain.

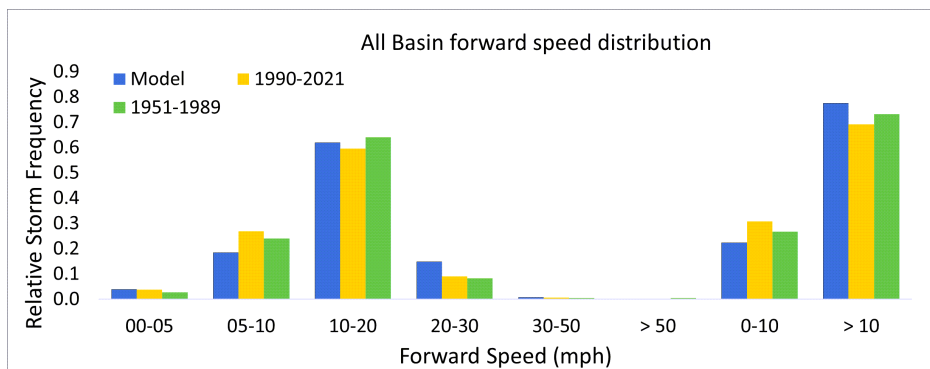


**Figure 202. Comparison of modeled and historic forward speed – model domain**

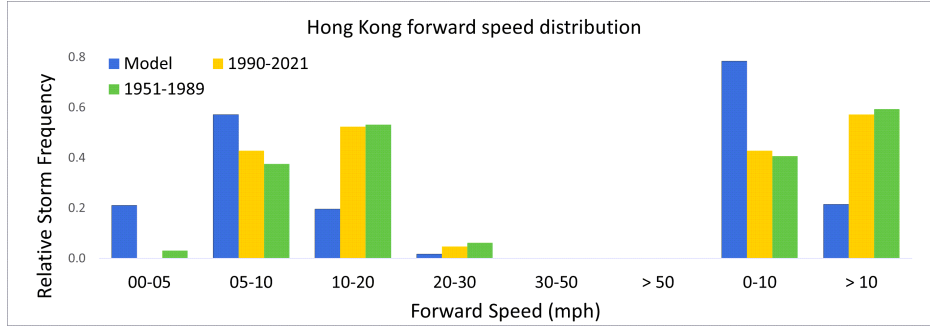


**Figure 203. Comparison of modeled and historic forward speed – Hong Kong**

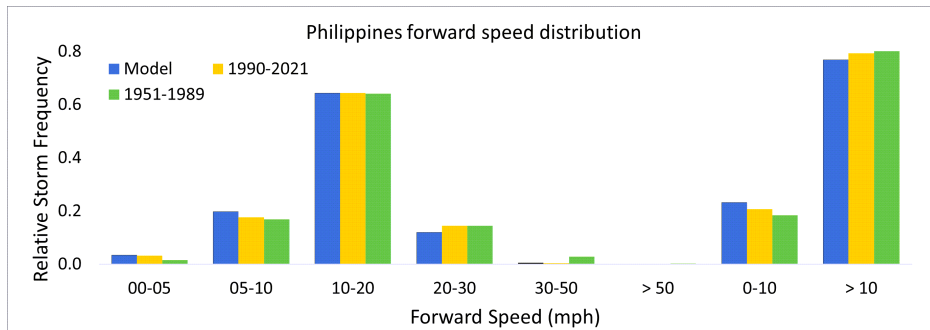


**Figure 204. Comparison of modeled and historic forward speed – Philippines**

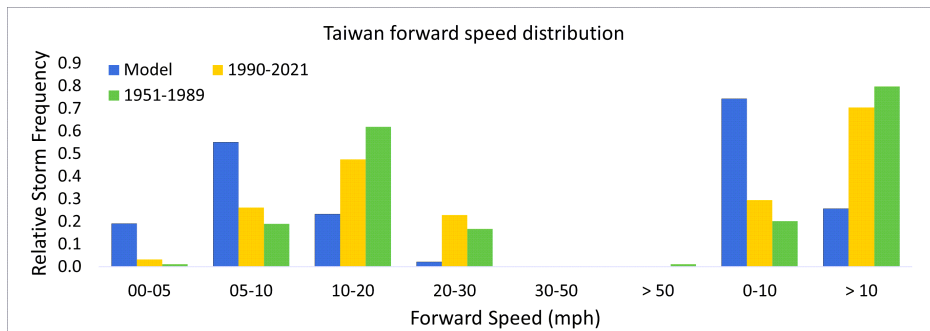


**Figure 205. Comparison of modeled and historic forward speed – Taiwan**

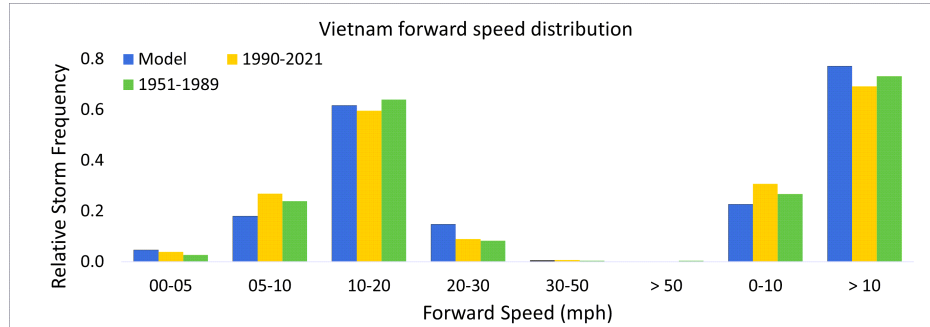


**Figure 206. Comparison of modeled and historic forward speed – Vietnam**

### Validating the model's precipitation

As was discussed in the Local Intensity Calculation chapter, evaluation of modeled precipitation relative to a historical period of any length is challenging. The figure from that discussion showing the 5-year return period precipitation values for several selected locations in the Southeast Typhoon domain for 1979-2013 is reproduced below. To examine climate variability, a comparison of the modeled 5-year return period precipitation for the more recent time period 1991-2020 is also shown (Figure 207).<sup>52</sup> Although the time periods are short, a comparison between observations and modelled results for 5-yr return periods strikes a balance between showing extreme event performance and having sufficient data to complete a valid comparison.

A comparison of the two figures shows that, except for Vietnam, the 5-year return period values have increased, although 5 of the 11 stations show an increase of only 5% or less.

The temperature dependence of saturation water vapor pressure would suggest that an increase of just a few degrees Celsius would lead to an increase in precipitation of a few percent.<sup>53</sup> Therefore, the differences between the two time periods shown in Figure 207 are greater than would be expected from global warming, and are likely due to interdecadal climate variability.

The figures below demonstrate that the Verisk model clearly captures recent climatology in typhoon-related precipitation across the model domain.

<sup>52</sup> Because there are only 40 years 1979-2020, the two time periods examined and shown in the figures overlap 2013-1991 to allow for longer time periods and more robust analyses.

<sup>53</sup> The temperature dependence of saturation water vapor pressure – described by the Clausius-Clapeyron equation – means that about 7% more water vapor can exist in the atmosphere for each degree Celsius increase, although globally, climate model projections give about a 2% to 6% water cycle amplification for each degree Celsius increase (Skirris, N., Zika, J., Nurser, G. *et al.* Global water cycle amplifying at less than the Clausius-Clapeyron rate. *Sci Rep* 6, 38752 (2016). <https://www.nature.com/articles/srep38752>

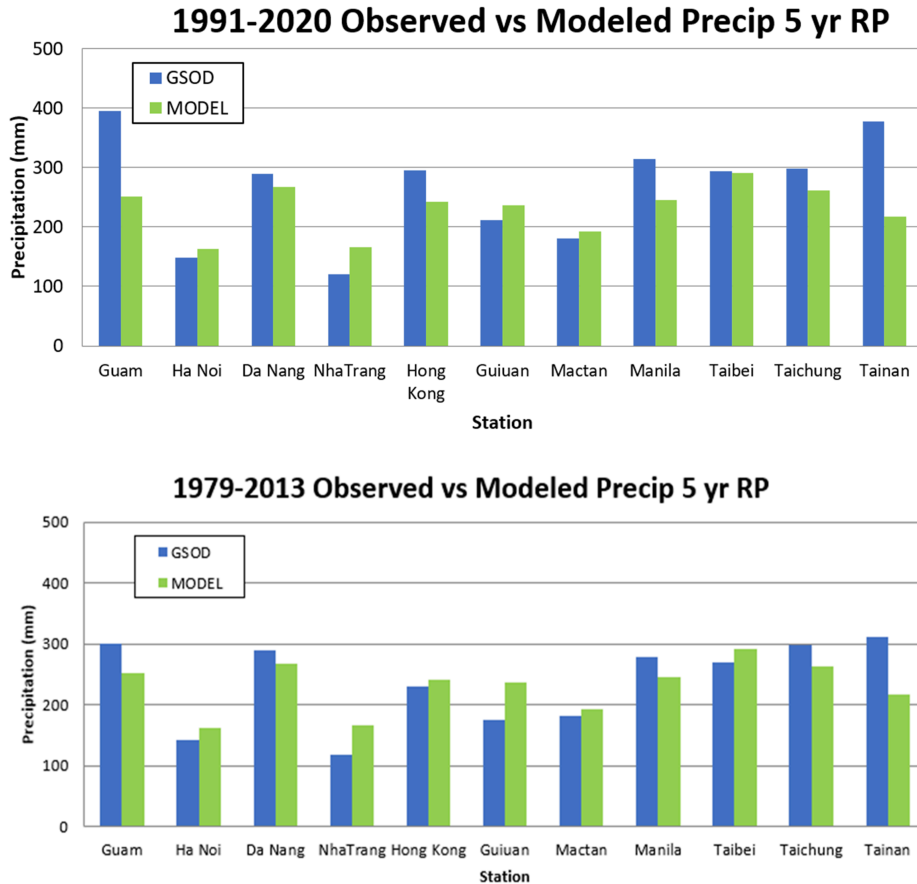


**Figure 207. Verisk modeled and observed 5-year (occurrence) return period typhoon related precipitation amounts. Observed values are computed from the National Climatic Data Center’s Global Summary of the Day data using the period of record shown.**

**See Also**  
[Validating local intensity](#)

## 7.4 Conclusion

The Verisk Typhoon Model for Southeast Asia captures the climate variability of the last few decades, and there are no strong trends in the historical record or predicted in the scientific literature that would warrant adjustments to the current model that would otherwise be necessary to account for changes in typhoon variability in the next few years.

# 8 Verisk Typhoon Model for Southeast Asia in CATRADER

## 8.1 Available catalogs

CATRADER supports a 10,000-year stochastic catalog. Also available in CATRADER is the World Scenarios event set, which includes EDS events.

Additionally, a historical event set is supported by CATRADER. The name and year of occurrence for each typhoon in the historical event set is presented in [Table 29](#).

**Table 29. The historical event set available in CATRADER for the Verisk Typhoon Model for Southeast Asia**

Year	Event Name	Year	Event Name	Year	Event Name
1958	Ida	1997	Winnie	2007	Sepat
1959	Sarah	1997	Paka	2008	Fengshen
1962	Karen	1998	Vicki	2008	Nuri
1970	Joan	1999	Sam	2008	Hagupit
1971	Rose	2001	Toraji	2009	Morakot
1975	Nina	2001	Nari	2009	Ketsana
1976	Pamela	2002	Pongsona	2010	Megi
1979	Hope	2004	Chaba	2011	Nesat
1983	Ellen	2005	Haitang	2011	Washi
1987	Thelma	2005	Nabi	2012	Vicente
1990	Mike	2006	Bilis	2012	Bopha
1991	Mireille	2006	Saomai	2013	Haiyan
1995	Angela	2006	Xangsane		
1996	Herb	2006	Durian		

### See Also

[Modeled losses for Extreme Disaster Scenarios](#)

[Extreme Disaster Scenarios \(EDS\)](#)

[Modeled industry losses](#)

[Significant historical Southeast Asia typhoons](#)

## 8.2 Resolution of analysis results

Modeled loss estimates are provided at country level for Guam, Macau, and Saipan; at CRESTA level for Taiwan and Vietnam; and at sub-CRESTA level for the Philippines and Hong Kong.

## 8.3 Verisk Industry Exposure Database

The Industry Exposure Database is an integral and highly valuable component of CATRADER. This database contains estimates of insured and insurable property exposure data at a high degree of resolution, including the number of risks, their replacement values (broken down by line of business, coverage, occupancy, and construction type), building attributes, and information regarding standard policy terms and conditions. Verisk uses a variety of public and private sources to estimate industry exposures, including government data, commercially-available demographic information, and other industry data. Verisk's Industry Exposure Database is extensively validated via comparison against values obtained from various insurance industry and governmental sources.

For more details about the Industry Exposure Database for this model, see the document *Verisk Industry Exposure Databases for Southeast Asia*, available with login from the [Client Portal](#). This publication provides further details about the Industry Exposure Database for this region and peril, including:

- How the Industry Exposure Database was developed
- The data sources used to develop the Industry Exposure Database
- Maps detailing the total exposure for the modeled region
- Share of Industry Exposure by LOB
- Construction splits by LOB
- Coverage splits by LOB
- Height band splits by LOB
- Assumed take-up rates
- Policy condition assumptions

## 8.4 Supported lines of business for reporting model losses

CATRADER supports the following Lines of Business (LOBs) for reporting losses (the components of each LOB are also indicated below):

- Residential Building: Building and Time Element
- Residential Contents: Contents
- Residential Building and Contents: Building, Contents, and Time Element

- Commercial/Industrial Building: Building and Time Element
- Commercial/Industrial Contents: Contents
- Commercial/Industrial Building and Contents: Building, Contents, and Time Element
- Agriculture:<sup>54</sup> Building and Contents
- Automobile

## 8.5 Policy conditions

This section provides summary statistics on policy conditions for insured property values the typhoon sub-perils, including wind policy conditions for all supported LOBs in CATRADER. To estimate policy terms and conditions in the Industry Exposure Database, Verisk draws on its global network of client companies for guidance. By working with local insurers, reinsurers, and brokers, Verisk has access to current data and market trends. To have as broad a view of the total market as possible, Verisk also takes into account third party research, such as the latest AXCO Insurance Market Reports.

**Table 30. Deductibles by line of business by country/territory**

Country/Territory	Residential	Commercial	Agriculture	Auto
Guam	USD 500	2% of building and content	NA	USD 500
Hong Kong	10% of loss (min HKD 1,500)	10% of loss (min HKD 5,000); 3 days for BI	N/A	HKD 5,000
Macau	10% of loss (min MOP 5,000)	10% of loss (min MOP 10,000); 3 days for BI	N/A	MOP 5,000
Philippines	2% SI	2% for building and content; 7 days for BI	2% SI	PHP 2,000
Saipan	USD 500	2% for building and content	N/A	USD 500
Taiwan	5% of loss	10% of loss	5% of loss	TWD 3,000
Vietnam	USD 100 for single-family; USD 500 for apartment	5% of loss (min USD 1,000)	USD 100	USD 25

<sup>54</sup> For Taiwan, the Philippines, and Vietnam only. Agriculture LOB is not reported for Hong Kong, Guam, Saipan, and Macau

**Table 31. Limits by line of business by country/territory**

Country/ Territory	Residential	Commercial	Agriculture	Auto
Guam	100% of building and content; time element limited to 10% SI	100%	N/A	100%
Hong Kong	100% of building and content; HKD 50,000 for time element	100%	N/A	100%
Macau	100% of building and content; MOP 50,000 for time element	100%	N/A	100%
Philippines	100%	100%	100%	100%
Saipan	100%	100%	N/A	100%
Taiwan	100%	75%	100%	100%
Vietnam	100%	100%	100%	100%

**Table 32. Assumed typhoon take-up rates by country/territory**

Country/ Territory	Residential Building	Residential Content	Commercial Building	Commercial Content	Agriculture	Auto
Guam	100%	100%	100%	100%	N/A	100%
Hong Kong	100%	35%	100%	75%	N/A	40%
Macau	100%	35%	100%	75%	N/A	40%
Philippines	Varies: see tables below	Varies: see tables below	Varies: see tables below	Varies: see tables below	2%	Varies: see tables below
Saipan	100%	100%	100%	100%	N/A	100%
Taiwan	1%	2%	Varies: see tables below	Varies: see tables below	1%	Varies: see tables below
Vietnam	Varies: see tables below	Varies: see tables below	Varies: see tables below	Varies: see tables below	0.5%	Varies: see tables below

**Table 33. Assumed typhoon take-up rates by CRESTA zone – the Philippines**

CRESTA	Residential Building	Residential Content	Commercial Building	Commercial Content	Agriculture	Auto
Z1. 1:Abra	3%	2%	15%	10%	2%	30%
Z1. 2:Aurora	3%	2%	15%	10%	2%	30%
Z1. 3:Batanes	3%	2%	15%	10%	2%	30%
Z1. 4:Benguet	3%	2%	15%	10%	2%	30%
Z1. 5:Cagayan	3%	2%	15%	10%	2%	30%

CRESTA	Residential Building	Residential Content	Commercial Building	Commercial Content	Agriculture	Auto
Z1. 6:Ifugao	3%	2%	15%	10%	2%	30%
Z1. 7:Ilocos Norte	3%	2%	15%	10%	2%	30%
Z1. 8:Ilocos Sur	3%	2%	15%	10%	2%	30%
Z1. 9:Isabela	3%	2%	15%	10%	2%	30%
Z1.10:Kalinga	3%	2%	15%	10%	2%	30%
Z1.11:La Union	3%	2%	15%	10%	2%	30%
Z1.12:Mountain	3%	2%	15%	10%	2%	30%
Z1.13:Quirino	3%	2%	15%	10%	2%	30%
Z1.14:Pangasinan	3%	2%	15%	10%	2%	30%
Z2:Makati	12%	8%	20%	15%	2%	45%
Z3:Manila Bay Reclamation Area	12%	8%	20%	15%	2%	45%
Z4:Santa Cruz Binondo Area	12%	8%	20%	15%	2%	45%
Z5:Rest of Metropolitan Manila	12%	8%	20%	15%	2%	45%
Z6. 1:Albay	3%	2%	15%	10%	2%	20%
Z6. 2:Bataan	3%	2%	15%	10%	2%	20%
Z6. 3:Batangas	3%	2%	15%	10%	2%	20%
Z6. 4:Bulacan	3%	2%	15%	10%	2%	20%
Z6. 5:Camarines Norte	3%	2%	15%	10%	2%	20%
Z6. 6:Camarines Sur	3%	2%	15%	10%	2%	20%
Z6. 7:Catanduanes	3%	2%	15%	10%	2%	20%
Z6. 8:Cavite	3%	2%	15%	10%	2%	20%
Z6. 9:Laguna	3%	2%	15%	10%	2%	20%
Z6.10:Marinduque	3%	2%	15%	10%	2%	20%
Z6.11:Masbate	3%	2%	15%	10%	2%	20%
Z6.12:Nueva Ecija	3%	2%	15%	10%	2%	20%
Z6.13:Occidental Mindoro	3%	2%	15%	10%	2%	20%
Z6.14:Oriental Mindoro	3%	2%	15%	10%	2%	20%
Z6.15:Pampanga	3%	2%	15%	10%	2%	20%
Z6.16:Quezon	3%	2%	15%	10%	2%	20%
Z6.17:Rizal	3%	2%	15%	10%	2%	20%
Z6.18:Romblon	3%	2%	15%	10%	2%	20%

CRESTA	Residential Building	Residential Content	Commercial Building	Commercial Content	Agriculture	Auto
Z6.19:Sorsogon	3%	2%	15%	10%	2%	20%
Z6.20:Tarlac	3%	2%	15%	10%	2%	20%
Z6.21:Zambales	3%	2%	15%	10%	2%	20%
Z7. 1:Aklan	3%	2%	20%	10%	2%	25%
Z7. 2:Antique	3%	2%	20%	10%	2%	25%
Z7. 3:Biliran	3%	2%	20%	10%	2%	25%
Z7. 4:Bohol	3%	2%	20%	10%	2%	25%
Z7. 5:Camotes	3%	2%	20%	10%	2%	25%
Z7. 6:Capiz	3%	2%	20%	10%	2%	25%
Z7. 7:Cebu	3%	2%	20%	10%	2%	25%
Z7. 8:Eastern Samar	3%	2%	20%	10%	2%	25%
Z7. 9:Guiamaras	3%	2%	20%	10%	2%	25%
Z7.10:Iloilo	3%	2%	20%	10%	2%	25%
Z7.11:Leyte	3%	2%	20%	10%	2%	25%
Z7.12:Negros Occidental	3%	2%	20%	10%	2%	25%
Z7.13:Negros Oriental	3%	2%	20%	10%	2%	25%
Z7.14:Northern Samar	3%	2%	20%	10%	2%	25%
Z7.15:Palawan	3%	2%	20%	10%	2%	25%
Z7.16:Siquijor	3%	2%	20%	10%	2%	25%
Z7.17:Southern Leyte	3%	2%	20%	10%	2%	25%
Z7.18:Western Samar	3%	2%	20%	10%	2%	25%
Z8. 1:Agusan Del Norte	3%	2%	15%	10%	2%	30%
Z8. 2:Agusan Del Sur	3%	2%	15%	10%	2%	30%
Z8. 3:Basilan	3%	2%	15%	10%	2%	30%
Z8. 4:Bukidnon	3%	2%	15%	10%	2%	30%
Z8. 5:Camiguin	3%	2%	15%	10%	2%	30%
Z8. 6:Lanao Del Norte	3%	2%	15%	10%	2%	30%
Z8. 7:Lanao Del Sur	3%	2%	15%	10%	2%	30%
Z8. 8:Misamis Occidental	3%	2%	15%	10%	2%	30%

CRESTA	Residential Building	Residential Content	Commercial Building	Commercial Content	Agriculture	Auto
Z8.9: Misamis Oriental	3%	2%	15%	10%	2%	30%
Z8.10: Surigao Del Norte	3%	2%	15%	10%	2%	30%
Z8.11: Surigao Del Sur	3%	2%	15%	10%	2%	30%
Z8.12: Zamboanga Del Norte	3%	2%	15%	10%	2%	30%
Z8.13: Zamboanga del Sur	3%	2%	15%	10%	2%	30%
Z9.1: Davao del Norte	3%	2%	15%	10%	2%	30%
Z9.2: Davao Oriental	3%	2%	15%	10%	2%	30%
Z9.3: Davao Del Sur	3%	2%	15%	10%	2%	30%
Z9.4: Maguindanao	3%	2%	15%	10%	2%	30%
Z9.5: North Cotabato	3%	2%	15%	10%	2%	30%
Z9.6: South Cotabato	3%	2%	15%	10%	2%	30%
Z9.7: Sultan Kudarat	3%	2%	15%	10%	2%	30%
Z9.8: Sulu	3%	2%	15%	10%	2%	30%
Z9.9: Tawi-Tawi	3%	2%	15%	10%	2%	30%

Table 34. Assumed typhoon take-up rates by CRESTA zone – Taiwan

CRESTA	Residential Building	Residential Content	Commercial Building	Commercial Content	Agriculture	Auto
Z 1.0: City of Taipei	1%	2%	14%	14%	1%	30%
Z 1.1: Rest of Taipei Keelung	1%	2%	5%	5%	1%	30%
Z 2.0: Taoyuan	1%	2%	18%	18%	1%	20%
Z 3.0: Hsinchu	1%	2%	27%	27%	1%	20%
Z 4.0: Maioli	1%	2%	23%	23%	1%	20%
Z 5.0: Taichung	1%	2%	8%	8%	1%	20%
Z 6.0: Nantou	1%	2%	10%	10%	1%	20%
Z 7.0: Changhua	1%	2%	8%	8%	1%	20%
Z 8.0: Yuanlin	1%	2%	17%	17%	1%	20%
Z 9.0: Chiai Tainan Penghu Islands	1%	2%	15%	15%	1%	20%
Z10.0: Kaohsiung Pingtung	1%	2%	14%	14%	1%	20%

CRESTA	Residential Building	Residential Content	Commercial Building	Commercial Content	Agriculture	Auto
Z11.0:Hualien Taitung	1%	2%	10%	10%	1%	20%
Z12.0:Ilan	1%	2%	8%	8%	1%	20%

**Table 35. Assumed typhoon take-up rates by CRESTA zone – Vietnam**

CRESTA	Residential	Commercial	Agriculture	Auto
Z 01: Lai Chau	1%	15%	0.5%	15%
Z 02: Lao Cai	1%	10%	0.5%	15%
Z 03: Ha Giang	1%	10%	0.5%	15%
Z 04: Cao Bang	1%	5%	0.5%	15%
Z 05: Son La	1%	15%	0.5%	15%
Z 06: Yen Bai	0.5%	10%	0.5%	15%
Z 07: Tuyen Quang	0.5%	10%	0.5%	15%
Z 09: Lang Son	0.5%	5%	0.5%	15%
Z 13: Quang Ninh	5%	10%	0.5%	15%
Z 14: Hoa Binh	0.5%	5%	0.5%	15%
Z 15: Ha Tay	0.5%	20%	0.5%	15%
Z 18: Ninh Binh	0.5%	10%	0.5%	15%
Z 20: Thai Binh	0.5%	10%	0.5%	15%
Z 21: Thanh Hoa	0.5%	15%	0.5%	15%
Z 22: Nghe An	1%	15%	0.5%	15%
Z 23: Ha Tinh	1%	5%	0.5%	15%
Z 24: Quang Binh	0.5%	30%	0.5%	15%
Z 25: Quang Tri	0.5%	5%	0.5%	15%
Z 26: Thua Thien - Hue	0.5%	10%	0.5%	15%
Z 27: Quang Nam	1%	25%	0.5%	15%
Z 28: Kon Tum	0.5%	5%	0.5%	15%
Z 29: Quang Ngai	2%	20%	0.5%	15%
Z 30: Gia Lai	2%	20%	0.5%	15%
Z 31: Binh Dinh	2%	15%	0.5%	15%
Z 32: Phu Yen	1%	20%	0.5%	15%
Z 33: Dak Lak	2%	15%	0.5%	15%
Z 34: Khanh Hoa	2%	15%	0.5%	15%
Z 35: Lam Dong	1%	5%	0.5%	15%
Z 36: Ninh Thuan	1%	5%	0.5%	15%

Verisk Typhoon Model for Southeast Asia in CATRADER

<b>CRESTA</b>	<b>Residential</b>	<b>Commercial</b>	<b>Agriculture</b>	<b>Auto</b>
Z 37: Tay Ninh	2%	15%	0.5%	15%
Z 39: Dong Nai	2%	30%	0.5%	15%
Z 40: Binh Thuan	2%	10%	0.5%	15%
Z 41: Long An	1%	30%	0.5%	15%
Z 43: Ba Ria - Vung Tau	10%	30%	0.5%	15%
Z 44: An Giang	2%	10%	0.5%	15%
Z 45: Dong Thap	1%	25%	0.5%	15%
Z 46: Tien Giang	0.5%	15%	0.5%	15%
Z 47: Kien Giang	3%	30%	0.5%	15%
Z 49: Vinh Long	0.5%	15%	0.5%	15%
Z 50: Ben Tre	1%	15%	0.5%	15%
Z 51: Tra Vinh	0.5%	15%	0.5%	15%
Z 52: Soc Trang	1%	15%	0.5%	15%
Z 53: Bac Kan	0.5%	2%	0.5%	15%
Z 54: Bac Giang	0.5%	10%	0.5%	15%
Z 55: Bac Lieu	0.5%	10%	0.5%	15%
Z 56: Bac Ninh	1%	20%	0.5%	15%
Z 57: Binh Duong	2%	30%	0.5%	15%
Z 58: Binh Phuoc	2%	30%	0.5%	15%
Z 59: Ca Mau	1%	15%	0.5%	15%
Z 61: Hai Duong	0.5%	15%	0.5%	15%
Z 63: Ha Nam	0.5%	20%	0.5%	15%
Z 66: Hung Yen	1%	30%	0.5%	15%
Z 67: Nam Dinh	0.5%	10%	0.5%	15%
Z 68: Phu Tho	0.5%	10%	0.5%	15%
Z 69: Thai Nguyen	0.5%	10%	0.5%	15%
Z 70: Vinh Phuc	2%	20%	0.5%	15%
Z 71: Dien Bien	0.5%	10%	0.5%	15%
Z 72: Dak Nong	0.5%	5%	0.5%	15%
Z 73: Hau Giang	1%	15%	0.5%	15%
Z CT: Can Tho	3%	25%	0.5%	15%
Z DN: Da Nang	2%	15%	0.5%	15%
Z HN: Ha Noi	10%	30%	0.5%	20%
Z HP: Hai Phong	2%	20%	0.5%	15%
Z SG: Ho Chi Minh City	10%	30%	0.5%	20%

# 9 Verisk Typhoon Model for Southeast Asia in Touchstone

## 9.1 Available catalogs

Touchstone supports a 10,000-year stochastic catalog. Also available in Touchstone is the World Scenarios event set, which includes EDS events.

Additionally, a historical event set is supported by Touchstone. The name and year of occurrence for each typhoon in the historical event set is presented in [Table 36](#).

**Table 36. The historical event set available in Touchstone for the Verisk Typhoon Model for Southeast Asia**

Year	Event Name	Year	Event Name	Year	Event Name
1958	Ida	1997	Winnie	2007	Sepat
1959	Sarah	1997	Paka	2008	Fengshen
1962	Karen	1998	Vicki	2008	Nuri
1970	Joan	1999	Sam	2008	Hagupit
1971	Rose	2001	Toraji	2009	Morakot
1975	Nina	2001	Nari	2009	Ketsana
1976	Pamela	2002	Pongsona	2010	Megi
1979	Hope	2004	Chaba	2011	Nesat
1983	Ellen	2005	Haitang	2011	Washi
1987	Thelma	2005	Nabi	2012	Vicente
1990	Mike	2006	Bilis	2012	Bopha
1991	Mireille	2006	Saomai	2013	Haiyan
1995	Angela	2006	Xangsane		
1996	Herb	2006	Durian		

### See Also

[Modeled losses for Extreme Disaster Scenarios](#)

[Extreme Disaster Scenarios \(EDS\)](#)

[Modeled industry losses](#)

[Significant historical Southeast Asia typhoons](#)

## 9.2 Supported geographic resolutions

The Touchstone-supported geographic resolutions for each of the modeled countries/territories in the Verisk Typhoon Model for Southeast Asia are listed in Table 42.

**Table 37. Supported geographic resolutions in Touchstone**

Country	Touchstone GeoLevel Code	Resolution
Guam	CRES	CRESTA
	SUBA	Province
	USER	User Lat/Long
Hong Kong	CRES	CRESTA
	AREA	Province
	SUBA	County
	CITY	City
	USER	User Lat/Long
Macau	CRES	CRESTA
	SUBA	District
	POST	Postal
	USER	User Lat/Long
Philippines	CRES	CRESTA
	AREA	Province
	POST	Postal
	CITY	City
	USER	User Lat/Long
Saipan	CRES	CRESTA
	USER	User Lat/Long
Taiwan	CRES	CRESTA
	AREA	County
	SUBA	District
	POST	Postal
	CITY	City
	USER	User Lat/Long
Vietnam	CRES	CRESTA
	SUBA	District
	POST	Postal
	CITY	City
	USER	User Lat/Long

## 9.3 Modeling aggregate data

During analysis, Touchstone can disaggregate risk at the CRESTA level resolution down to the 1-km grid cell level for all countries. In addition to that, for Philippines aggregate Province exposures are also automatically disaggregated to a 1-km grid. The exposure distribution is in accordance with the Verisk Industry Exposure Database, allowing the aggregated exposure to be placed where insurable properties are actually likely to be located within each administrative boundary.

When disaggregation is not selected, losses are analyzed at the exposure centroid of the administrative boundary. Further disaggregation allows users to take advantage of location-specific hazard characteristics. Note that selecting disaggregation may cause the analysis to take a significantly longer time due to the higher geographic resolution.

To the extent that the geographic distribution of risks in the portfolio reflects the industry-wide distribution, selecting disaggregation provides more accurate results.

## 9.4 Modeled coverages

The modeled coverages in the Verisk Typhoon Model for Southeast Asia in Touchstone are as follows: Coverage A: Buildings, Coverage B: Other Structures, Coverage C: Contents, and Coverage D: Business Interruption (Time Element).

## 9.5 Construction and occupancy classes, year built and height bands, and relative vulnerabilities

A structure's vulnerability depends on its construction and occupancy class combination as well as its age and height. With the goal of enabling clients to code their exposure data as specifically as possible, the Verisk Typhoon Model for Southeast Asia supports 116 construction classes and 116 occupancy classes, of which 62 are occupancy classes for large industrial facilities.<sup>55</sup>

Verisk has compiled all the supported construction and occupancy class information, along with relative vulnerabilities, into the *Verisk Typhoon Model for Southeast Asia Supplement*. This supplement is available with login on the [Client Portal](#).

Specifically, this workbook contains the following information for all the territories in the model:

---

<sup>55</sup> The industrial facilities set of occupancy classes refers to the 400-series, which include structures that are very different from the 300-series as they represent large, complex facilities comprised of many components. Small facilities (300-series) consist of mostly buildings and some machinery.

- Construction categories, codes and classes
- Occupancy categories, codes and classes
- Construction and occupancy class combinations (Coverage A)
- Height bands for wind damage
- Height bands for flood and storm surge damage
- Year-built bands for wind
- Year-built factors for wind by country
- Engineered and non-engineered building definitions
- Relative vulnerabilities to wind by year-built band, for combinations of selected construction classes and occupancy classes 301, 311, and 321, relative to unknown year-built (Coverage A)
- Relative vulnerabilities to wind for each construction and occupancy class combination, relative to the construction class 101 and occupancy class 302 combination (Coverage A)
- Relative vulnerabilities to flood for each construction and occupancy class combination, relative to the construction class 101 and occupancy class 302 combination (Coverage A)
- Relative vulnerabilities to surge for each construction and occupancy class combination, relative to the construction class 101 and occupancy class 302 combination (Coverage A) (available for Hong Kong, the Philippines, and Taiwan)
- Relative vulnerabilities to wind by height band, for combinations of selected construction classes and occupancy classes 301, 311, and 321, relative to unknown height (Coverage A)
- Relative vulnerabilities to flood by height band, for combinations of selected construction classes and occupancy classes 301, 311, and 321, relative to unknown height (Coverage A)
- Relative vulnerabilities to surge by height band, for combinations of selected construction classes and occupancy classes 301, 311, and 321, relative to unknown height (Coverage A) (available for Hong Kong, the Philippines, and Taiwan)

Note that detailed descriptions of the supported construction and occupancy classes are available in the *Touchstone Exposure Data Validation Reference*, which can be accessed from [www.unicede.com](http://www.unicede.com). The *Touchstone Exposure Data Validation Reference* serves as a comprehensive reference. In addition to including all relevant information from the original *UPX and UFX Preparer's Guides*, the *Touchstone Exposure Data Validation Reference* provides a robust series of exposure- and import-related information in a more import format-agnostic style. From lists of supported import fields and validation rules for these fields to robust reference information, including tables of supported construction, occupancy, CRESTA, and area codes per modeled country, the *Touchstone Exposure Data Validation Reference* gives you the information you need to import your exposure data successfully into Touchstone.

## 9.6 Supported secondary risk characteristics

The current release of the Verisk Typhoon Model for Southeast Asia in Touchstone does not support secondary risk characteristics.

## 9.7 Supported policy terms

Touchstone allows users to run wind-only, flood-only, and storm-surge-only (for applicable regions) or wind, flood, and storm surge combined sub-perils – thus, users can obtain loss estimates for these sub-perils separately or combined.

Touchstone supports a wide array of policy terms and conditions, including location limits and deductibles by site or by coverage, policy limits and deductibles, and facultative (assumed and ceded) and treaty reinsurances.

Touchstone includes a location deductible type which applies as the maximum of a specified amount or a percentage of loss (ML). When users specify the ML deductible type, Touchstone applies the maximum of the user-specified deductible or the percentage of loss at each point in the ground-up loss distribution. This deductible applies to building and content losses, while a separate deductible applies to business interruption losses.

Touchstone includes an additional location deductible type which applies as a percentage of combined loss from building, content, and business interruption losses (PL). When users specify the PL deductible type, Touchstone applies the percentage of combined loss from building, content, and business interruption losses at each point in the ground-up loss distribution.

For more information and a full list of supported policy terms, please see the *Touchstone Exposure Data Validation Reference*, which can be accessed from [www.unicede.com](http://www.unicede.com).

# A CRESTA Zones

The following sections show maps of CRESTA zones for each modeled country/territory. Tables that contain the CRESTA zone numbers and names corresponding to each map are also presented.

## A.1 Guam

[Figure 208](#) presents the CRESTA zone for Guam. [Table 38](#) provides the zone name.

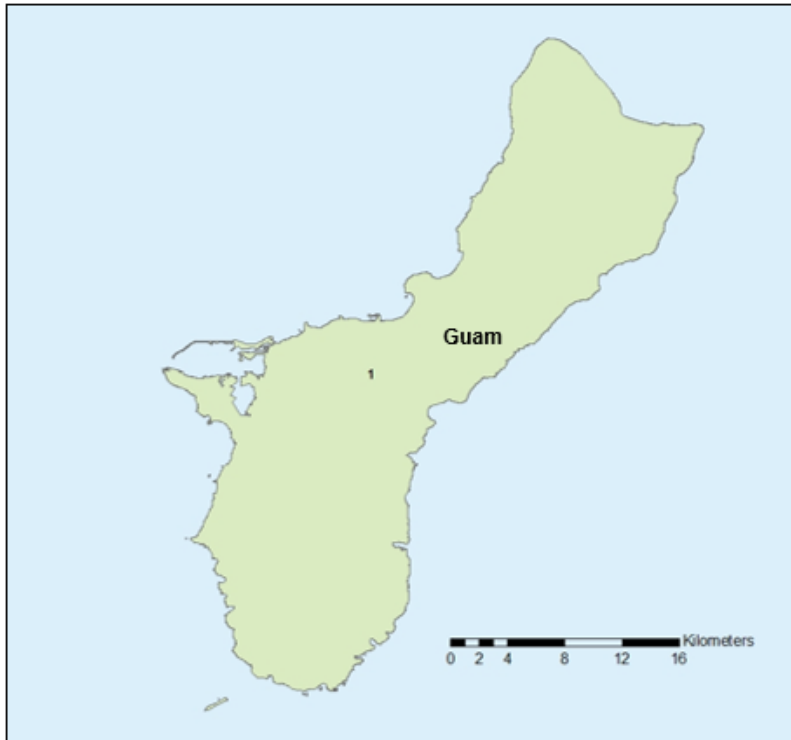


**Figure 208.** CRESTA zone in Guam

**Table 38.** CRESTA zone name in Guam

CRESTA Zone	Name
1	Guam

## A.2 Hong Kong

[Figure 209](#) presents CRESTA zones in Hong Kong. [Table 39](#) provides zone names.

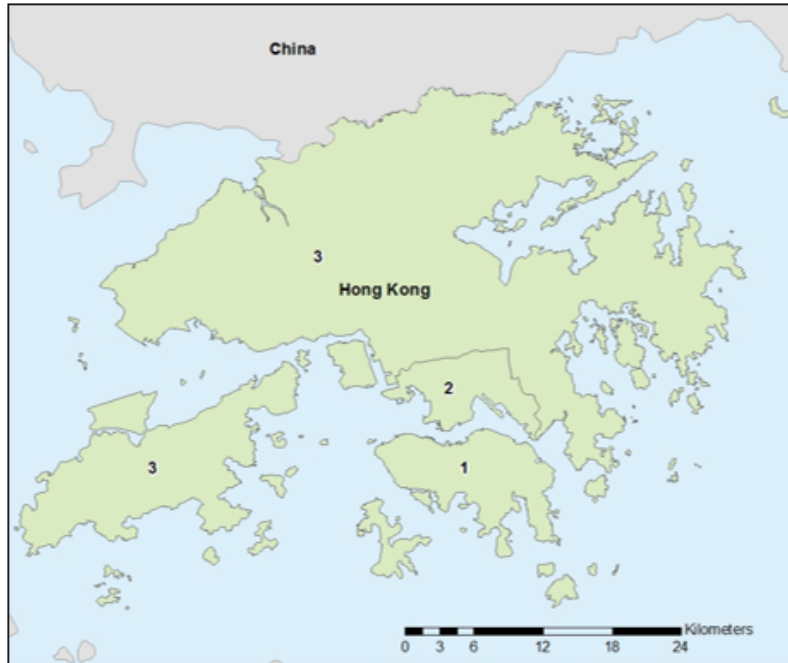


**Figure 209. CRESTA zones in Hong Kong**

**Table 39. CRESTA zone names in Hong Kong**

CRESTA Zone	Name
1	Hong Kong Island
2	Kowloon
3	New Territories

## A.3 Macau

[Figure 210](#) presents the CRESTA zone for Macau. [Table 40](#) provides the zone name.

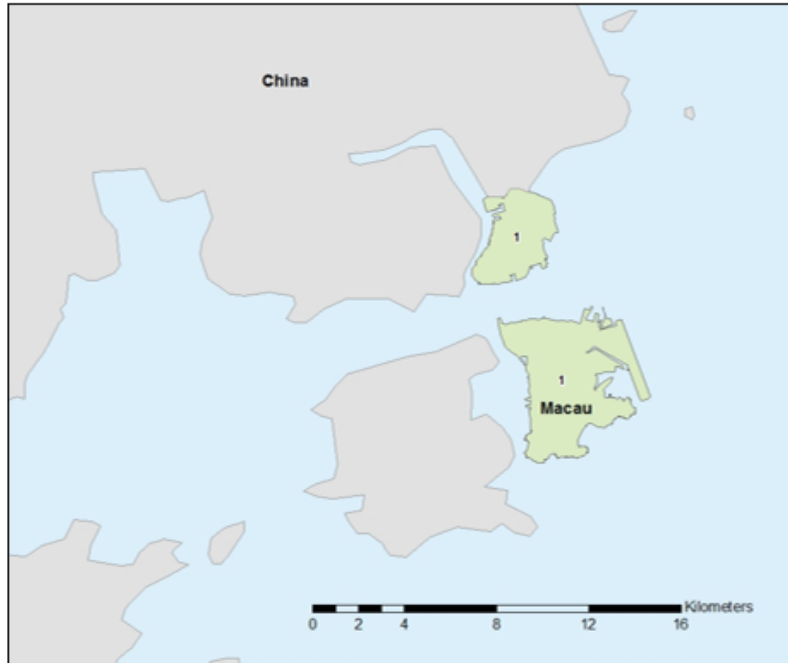


Figure 210. CRESTA zone in Macau

Table 40. CRESTA zone name in Macau

CRESTA Zone	Name
1	Macau

## A.4 Philippines

[Figure 211](#) presents CRESTA zones in the Philippines. [Table 41](#) provides zone names.

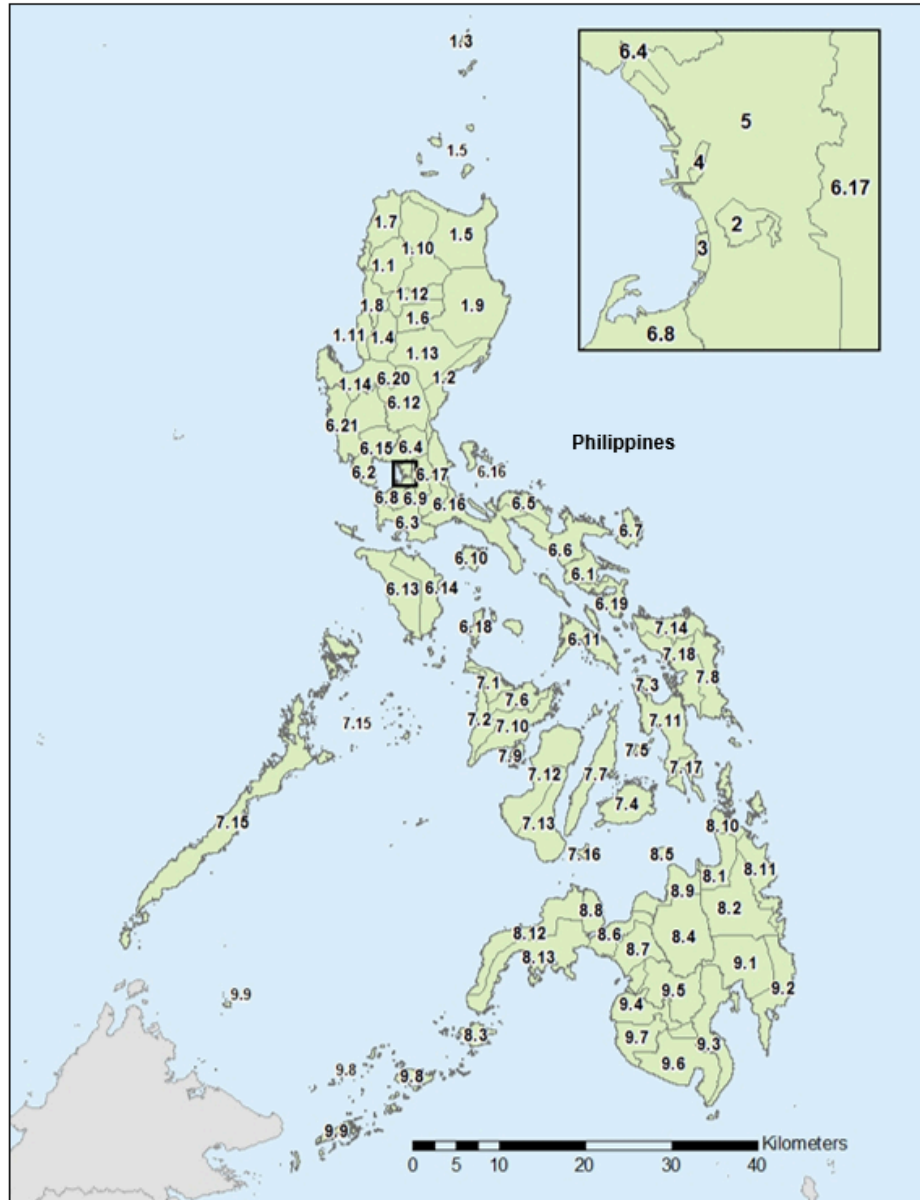


Figure 211. CRESTA zones in the Philippines

Table 41. CRESTA zone names in the Philippines

CRESTA Zone	Name
1.1	Abra
1.2	Aurora
1.3	Batanes
1.4	Benguet
1.5	Cagayan

CRESTA Zone	Name
1.6	Ifuagao
1.7	Ilocos Norte
1.8	Ilocos Sur (Quirino)
1.9	Isabela
1.10	Kalinga-Apayao
1.11	La Union
1.12	Mountain Province
1.13	Nueva Vizcaya
1.14	Pangasinan
2	Makati (Manila)
3	Manila Bay Reclamation Area (Manila Bay City)
4	Santa Cruz/Binondo Area (Manila)
5	Rest of Metropolitan Manila
6.1	Albay
6.2	Bataan
6.3	Batangas
6.4	Bulacan
6.5	Camarines Norte
6.6	Camarines Sur
6.7	Catanduanes
6.8	Cavite
6.9	Laguna
6.10	Marinduque
6.11	Masbate
6.12	Nueva Ecija
6.13	Occidental Mindoro
6.14	Oriental Mindoro
6.15	Pampanga
6.16	Quezon
6.17	Rizal
6.18	Ramblon
6.19	Sorsogon
6.20	Tarlac
6.21	Zambales

CRESTA Zone	Name
7.1	Aklan
7.2	Antique
7.3	Biliran
7.4	Bohol
7.5	Camotes
7.6	Capiz
7.7	Cebu
7.8	Eastern Samar
7.9	Guimaras
7.10	Iloilo
7.11	Leyte
7.12	Negros Occidental
7.13	Negros Oriental
7.14	Northern Samar
7.15	Palawan
7.16	Siquijor
7.17	Southern Leyte
7.18	Western Samar
8.1	Agusan Del Norte
8.2	Agusan Del Sur
8.3	Basilan
8.4	Bukidnon
8.5	Camiguin
8.6	Lanao Del Norte
8.7	Lanao Del Sur
8.8	Misamis Occidental
8.9	Misamis Oriental
8.10	Surigao Del Norte
8.11	Surigao Del Sur
8.12	Zamboanga Del Norte
8.13	Zamboanga Del Sur
9.1	Davao Del Norte
9.2	Davao Oriental
9.3	Davao Del Sur
9.4	Maguindanao

CRESTA Zone	Name
9.5	North Cotabato
9.6	South Cotabato
9.7	Sultan Kudarat
9.8	Sulu
9.9	Tawi-Tawi

## A.5 Saipan

Figure 212 presents the CRESTA zone for Saipan. Table 42 provides the zone name.



Figure 212. CRESTA zone in Saipan

Table 42. CRESTA zone name in Saipan

CRESTA Zone	Name
1	Saipan

## A.6 Taiwan

Figure 213 presents CRESTA zones in Taiwan. Table 43 provides zone names.

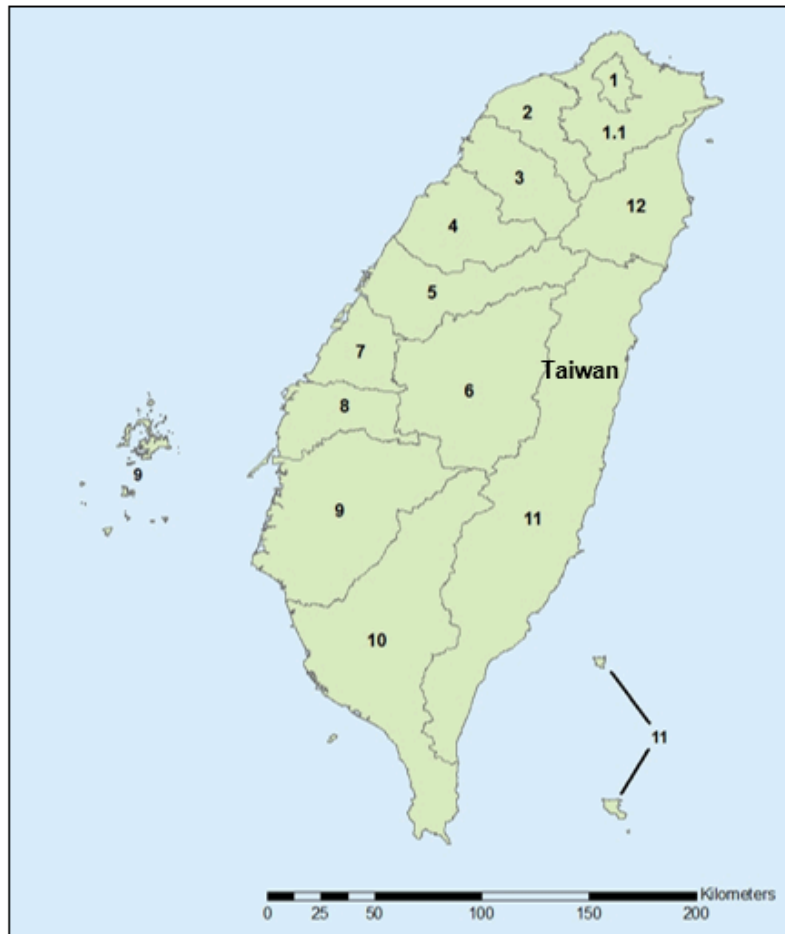


Figure 213. CRESTA zones in Taiwan

Table 43. CRESTA zone names in Taiwan

CRESTA Zone	Name
1	City of Taipei
1.1	Rest of Taipei, Keelung
2	Taoyuan
3	Hsinchu
4	Miaoli
5	Taichung
6	Nantou
7	Changhua

CRESTA Zone	Name
8	Yuanlin
9	Chiai, Tainan, Penghu Islands
10	Kaosiung, Pingtung
11	Hualien, Taitung
12	Ilan

## A.7 Vietnam

Figure 214 presents CRESTA zones in Vietnam. Table 44 provides zone names.

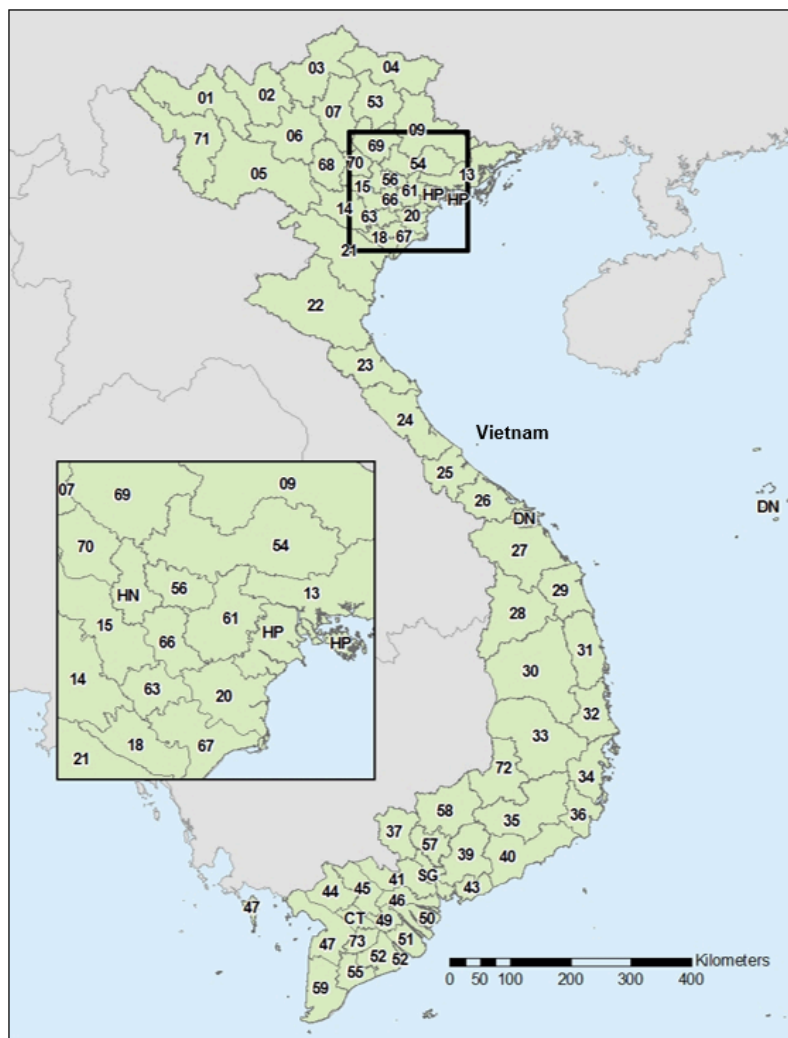


Figure 214. CRESTA zones in Vietnam

**Table 44. CRESTA zone names in Vietnam**

CRESTA Zone	Name
1	Tinh Lai Chau
2	Tinh Lao Cai
3	Tinh Ha Giang
4	Tinh Cao Bang
5	Tinh Son La
6	Tinh Yen Bai
7	Tinh Tuyen Quang
9	Tinh Lang Son
13	Tinh Quang Ninh
14	Tinh Hoa Binh
15	Ha Tay
18	Tinh Ninh Binh
20	Tinh Thai Binh
21	Tinh Thanh Hoa
22	Tinh Nghe An
23	Tinh Ha Tinh
24	Tinh Quang Binh
25	Tinh Quang Tri
26	Tinh Thua Thien Hue
27	Tinh Quang Nam
28	Tinh Kon Tum
29	Tinh Quang Ngai
30	Tinh Gia Lai
31	Tinh Binh Dinh
32	Tinh Phu Yen
33	Tinh Dak Lak
34	Tinh Khanh Hoa
35	Tinh Lam Dong
36	Tinh Ninh Thuan
37	Tinh Tay Ninh
39	Tinh Dong Nai
40	Tinh Binh Thuan
41	Tinh Long An
43	Tinh Ba Ria - Vung Tau

CRESTA Zone	Name
44	Tinh An Giang
45	Tinh Dong Thap
46	Tinh Tien Giang
47	Tinh Kien Giang
49	Tinh Vinh Long
50	Tinh Ben Tre
51	Tinh Tra Vinh
52	Tinh Soc Trang
53	Tinh Bac Kan
54	Tinh Bac Giang
55	Tinh Bac Lieu
56	Tinh Bac Ninh
57	Tinh Binh Duong
58	Tinh Binh Phuoc
59	Tinh Ca Mau
61	Tinh Hai Duong
63	Tinh Ha Nam
66	Tinh Hung Yen
67	Tinh Nam Dinh
68	Tinh Phu Tho
69	Tinh Thai Nguyen
70	Tinh Vinh Phuc
71	Tinh Dien Bien
72	Tinh Dak Nong
73	Tinh Hau Giang
CT	Thanh pho Can Tho
DN	Thanh pho Da Nang
HN	Ha Noi
HP	Thanh pho Hai Phong
SG	Thanh pho Ho Chi Minh

# Selected References

The following reference materials have been used in the development and refinement of the Verisk Typhoon Model for Southeast Asia.

AON Benfield, "Annual Global Climate and Catastrophe Report," report from AON Benfield, 2008.

AON Benfield, "Annual Global Climate and Catastrophe Report," report from AON Benfield, 2009.

AON Benfield, "Annual Global Climate and Catastrophe Report," report from AON Benfield, 2010.

AON Benfield, "Annual Global Climate and Catastrophe Report," report from AON Benfield, 2011.

AON Benfield, "Annual Global Climate and Catastrophe Report," report from AON Benfield, 2012.

AON Benfield, "Annual Global Climate and Catastrophe Report," report from AON Benfield, 2013.

Aquino, R. E. R., 2005, "Philippine Wind Information for Engineering, Research, and Mitigation," *APEC 21st century COE short term fellowship report*, Tokyo Polytechnic University, Kanagawa, Japan, June, 2005.

Atkinson, G. D., and C. R. Holliday 1977, "Tropical Cyclone Minimum Sea Level Pressure/ Maximum Sustained Wind Relationship for the Western North Pacific," *Monthly Weather Review*, 105, 421–427.

AXCO Insurance Information Services 2009, "Insurance Market Report: Japan Non-Life (P&C)," report from AXCO, November 2009.

AXCO Insurance Information Services 2010, "Insurance Market Report: Hong Kong Non-Life (P&C)," report from AXCO, September 2010.

AXCO Insurance Information Services 2010, "Insurance Market Report: Philippines Non-Life (P&C)," report from AXCO, July 2010.

AXCO Insurance Information Services 2010, "Insurance Market Report: Taiwan Non-Life (P&C)," report from AXCO, August 2010.

AXCO Insurance Information Services 2014, "Insurance Market Report: Guam: Non-Life (P&C)," report from AXCO, 2014.

AXCO Insurance Information Services 2014, "Insurance Market Report: Hong Kong: Non-Life (P&C)," report from AXCO, 2014.

- AXCO Insurance Information Services 2014, "Insurance Market Report: Macao: Non-Life (P&C)," report from AXCO, 2014.
- AXCO Insurance Information Services 2014, "Insurance Market Report: Philippines: Non-Life (P&C)," report from AXCO, 2014.
- AXCO Insurance Information Services 2014, "Insurance Market Report: Taiwan: Non-Life (P&C)," report from AXCO, 2014.
- AXCO Insurance Information Services 2014, "Insurance Market Report: Vietnam: Non-Life (P&C)," report from AXCO, 2014.
- Bagtasa, Gerry. 2017. Contribution of Tropical Cyclones to Rainfall in the Philippines. *Journal of Climate*, **30**: 3621-3633.
- Beckers, J.V.L., Diermanse, F.L.M., Tse, M.L. and Kan, F.Y.F. 2012, "Design of Flood Protection in Hong Kong," *Comprehensive Flood Risk Management, Research for Policy and Practice*, Nov. 2012. <http://www.crcnetbase.com/doi/abs/10.1201/b13715-20>.
- Brand, S., and J. Blesloch 1972 "Changes in the Characteristics of Typhoons Crossing the Philippines," *Journal of Applied Meteorology*, 12, 104–109.
- Brand, S., and J. Blesloch 1974 "Changes in the Characteristics of Typhoons Crossing the Island of Taiwan," *Monthly Weather Review*, 102, 708–713.
- Building Authority of Hong Kong, "Code of Practice on Wind Effects in Hong Kong – 1983," Hong Kong Building Department, 1983.
- Building Authority of Hong Kong, "Code of Practice on Wind Effects in Hong Kong – 2004," Hong Kong Building Department, 2004.
- Building Research Institute of Japan 1997, *Proceedings of the International Workshop on Harmonization of Performance-Based Buildings Structural Design in Countries Surrounding The Pacific Ocean*, Tsukuba, Japan, December 1–3, 1997.
- Campbell, S., 2005, "Typhoons affecting Hong Kong: Case studies," *APEC 21st century COE short-term fellowship report*, Tokyo Polytechnic University, Kanagawa, Japan, April, 2005.
- Campbell, S. 2005, "The history of wind damage in Hong Kong," *APEC 21st century COE short term fellowship report*, Tokyo Polytechnic University, Kanagawa, Japan, April, 2005.
- Chan, Johnny C. L. and Liu, Kin Sik; 2019. Inter-decadal variability of the location of maximum intensity of category 4–5 typhoons and its implication on landfall intensity in East Asia. *Int J Climatol.*, **39**, 1839– 1852. <https://doi.org/10.1002/joc.5919>
- Chan, K.T.F. 2019. Are global tropical cyclones moving slower in a warming climate? *Environ. Res. Lett.* **14**, 105015

- Chang, C.C., Hsu, W. and Su, M.D. 2008, "Modeling flood perils and flood insurance program in Taiwan," *In Proceedings of 2008 American Agricultural Economics Association Annual Meeting*, Orlando, Florida, July 27 – 29, 2008.
- Chang, C.-P., Y.-T. Yang, and H.-C. Kuo. 2013: Large Increasing Trend of Tropical Cyclone Rainfall in Taiwan and the Roles of Terrain. *Journal of Climate*, **26**, 4138-4147
- Change, C. H., and Cheng, C. M. 2010, "APEC-WW-2010 Country Report: Chinese Taipei," *Wind Engineering Research Center, Tokyo Polytechnic University*, 2010.
- Change, W. 2009, "The Updates of TREIF and Event Reports on Typhoon 'Morakot'," report to Taiwan Residential Earthquake Insurance Fund, Sept. 29, 2009.
- Cheng, C. M. and Chang, C. H. 2004, "Specifications on Building Wind Resistance Design and Wind Environmental Issues in Taiwan," *In Proceeding of Workshop on Regional Harmonization of Wind Loading and Wind Environmental Specifications in Asia-Pacific Economies*.
- Chen Jilong, Tam Chi-Yung, Cheung Kevin, Wang Ziqian, Murakami Hiroyuki, Lau Ngar-Cheung, Garner Stephen T., Xiao Ziniu, Choy Chun-Wing, Wang Peng. 2021. Changing Impacts of Tropical Cyclones on East and Southeast Asian Inland Regions in the Past and a Globally Warmed Future Climate. *Frontiers in Earth Science*, **9**, 234-235. <https://www.frontiersin.org/articles/10.3389/feart.2021.769005>
- Chu, Pao-Shin, Hanpei Zhang, Hui-Ling Chang, Tsui-Ling Chen and Kristine Tofte. 2018. Trends in return levels of 24-hr precipitation extremes during the typhoon season in Taiwan. *International Journal of Climatology* **38** 5107 - 5124.
- Cohen, J., Zhang, X., Francis, J. et al. 2020. Divergent consensus on Arctic amplification influence on midlatitude severe winter weather. *Nat. Clim. Chang.* **10**, 20–29. <https://doi.org/10.1038/s41558-019-0662-y>
- Cook, N. J. 1985, *The Designer's Guide to Wind Loading of Building Structures: Building Research Establishment Report*. London, England: Butterworth Heinemann Ltd.
- Cooperative Institute for Meteorological Satellite Studies (CIMSS), University of Wisconsin, Madison, Wisconsin. <http://cimss.ssec.wisc.edu/tropic2/>.
- Dartmouth Flood Observatory, Global Active Archive of Large Flood Events, <http://floodobservatory.colorado.edu/index.html>.
- De Graaf, Rutger, and F. Hooimeijer, 2008, "Urban Water in Japan," Taylor & Francis, xiii, 227.
- Dutta, D., S. Herath, and K. Musiak 2003, "A Mathematical Model for Flood Loss Estimation," *Journal of Hydrology*, **277**, 24–49.
- Duy, T.C., Xuan, C.N., Dai, M.N., Huu, H.N. and Tat, C.B. 2007, "Typhoons and technical solutions recommended for existing and new houses in the cyclonic regions

in Vietnam," *1st International Conference on Modern Design, Construction and Maintenance of Structures*, Hanoi, Vietnam, December, 2007.

- Ferritto, J. M. 1998, "Effective Stress Drydock Analysis," Technical Report TR-2093-SHR, Naval Facilities Engineering Service Center, September 1998. <http://www.dtic.mil/cgi-bin/GetTRDoc?Location=U2&doc=GetTRDoc.pdf&AD=ADA364716>.
- Gong, D., Tang, X., Chan, J. C. L., and Wang, Q., 2022. Trends of Tropical Cyclone Translation Speed over the Western North Pacific during 1980–2018, *Atmosphere*, **13** 896. <https://doi.org/10.3390/atmos13060896>.
- Government of Hong Kong, Drainage Services Department 2009, "Flood Prevention in Urban Areas." [http://www.dsd.gov.hk/TC/Files/publications\\_publicity/publicity\\_materials/leaflets\\_booklets\\_factsheets/Urban.pdf](http://www.dsd.gov.hk/TC/Files/publications_publicity/publicity_materials/leaflets_booklets_factsheets/Urban.pdf)
- Grimmond, C. S. B., and T. R. Oke 1999, "Aerodynamic Properties of Urban Areas Derived from Analysis of Surface Form," *Journal of Applied Meteorology*, **38**, 1262–1292.
- Guard, C., Hamnett, M.P., Neumann, C.J., Lander, M.A. and Siegrist Jr, H.G. 1999, "Typhoon vulnerability study for Guam." *University of Guam: Water and Environmental Research Institute of the Western Pacific*.
- Guy Carpenter, "Tropical Cyclone Review," annual report from Guy Carpenter, 2002.
- Guy Carpenter, "Tropical Cyclone Review," annual report from Guy Carpenter, 2006.
- Guy Carpenter, "Tropical Cyclone Review," annual report from Guy Carpenter, 2007.
- Guy Carpenter, "Tropical Cyclone Review," annual report from Guy Carpenter, 2008.
- Harr, P. A., and R. L. Elsberry 2000, "Extratropical Transition of Tropical Cyclones over the Western North Pacific, Part I: Evolution of Structural Characteristics during the Transition Process, *Monthly Weather Review*, **128**, 2613–2633.
- Harr, P. A., R. L. Elsberry, and T. F. Hogan 2000, "Extratropical Transition of Tropical Cyclones over the Western North Pacific, Part II: The Impact of Midlatitude Circulation Characteristics," *Monthly Weather Review*, **128**, 2634–2653.
- Hart, R. E., and J. L. Evans 2001, "A Climatology of the Extratropical Transition of Atlantic Tropical Cyclones," *Journal of Climate*, **14**, 546–564.
- Hart, R. E. 2003, "A Cyclone Phase Space Derived From Thermal Wind and Thermal Asymmetry," *Monthly Weather Review*, **131**, 585–616.
- Hernandez Jr., J. Y., and Veron, M. C. 2013, "Development of a Vulnerability Curve for RC Low-Rise residential Buildings to Severe Wind Hazard," *The 12th Americas Conference on Wind Engineering*, Seattle, Washington, USA, June 16 – 20, 2013.
- Higaki, M., H. Hayashibara, and F. Nozaki 2009, "Outline of the Storm Surge Prediction Model at the Japan Meteorological Agency," report by the Japan Meteorological Agency,

March 2009. <http://www.jma.go.jp/jma/jma-eng/jma-center/rsmc-hp-pub-eg/techrev/text11.pdf>.

- Ho, K.K.S., and K.S. Li 2003 (editors), *Geotechnical Engineering, Meeting Society's Needs, Volume 3*, Lisse, The Netherlands, Swets & Zeitlinger B. V.
- Ho, P.Y. 2003, *Weathering the storm: Hong Kong Observatory and social development*, Hong Kong University Press.
- Holmes, J. D., Tamura, Y., and Krishna, P. 2009, "Comparison of Wind Loads Calculated by Fifteen Different Codes and Standards, for Low, Medium and High-Rise Building," *11th Americas Conference on Wind Engineering*, San Juan, Puerto Rico, June 22 – 26, 2009.
- Holmes, J.D., Tamura, Y. and Krishna, P. 2008, "Wind loads on low, medium and high-rise buildings by Asia-Pacific codes," *In Proceedings of the 4th International Conference on Advances in Wind and Structures*, Jeju, Korea, May 29 – 31, 2008.
- Holmes, J. D. 2009, "Development in Codification of Wind Loads in the Asia Pacific," *The Seventh Asia-Pacific Conference on Wind Engineering*, Taipei, Taiwan, November 8 – 12, 2009.
- Hong Kong Observatory, Annual Tropical Cyclones Report, 1968 – 2012.
- Hong Kong Observatory (HKO), <http://www.hko.gov.hk/>.
- Hoskins, B. J., M. E. McIntyre, and A. W. Robertson 1985, "On the Use and Significance of Isentropic Potential Vorticity Maps," *Quarterly Journal of the Royal Meteorological Society*, 111, 877–946.
- Hsu, M.H., Chen, C.H., Chang, C.H., Liu, W.C., Chang, T.J., Lin, Y.C., Chen, A.S., Hammond, M.J., Djordjević, S. and Butler, D. 2013, "Flood Impact Assessment under Climate Change Scenarios in Central Taipei Area, Taiwan," *In International Conference on Flood Resilience*, UK.
- Insurance Market Report on Guam – Non-Life. Axco Insurance Information Services Ltd., Axco Reports: Guam (US).
- Jain, M.K., S.K. Mishra, P.S. Babu, K. Venugopal, and V.P. Singh, 2006, "Enhanced Runoff Curve Number Model Incorporating Storm Duration and a Nonlinear Ia–S Relation," *Journal of Hydrologic Engineering*, 11, 631–635.
- Jang, J.J., and J.R. Lee (1997), "Analysis of design wind speed distribution of Taiwan Area", *Journal of Marine Science and Technology*, 5(1), 55-63.
- Jeary, A.P. 1997, "The wind climate of Hong Kong," *Journal of wind engineering and industrial aerodynamics*, 72, 433-444.
- Jha, A.K., Bloch, R. and Lamond, J. 2012, "*Cities and flooding: a guide to integrated urban flood risk management for the 21st century*," World Bank Publications.

- Joint Typhoon Warning Center (JTWC)., Annual Tropical Cyclone Reports. <http://www.usno.navy.mil/JTWC/>.
- Jones, S., P. A. Harr, J. Abraham, L. F. Bosart, P. J. Bowyer, J. L. Evans, D. E. Hanley, B. N. Hanstram, R. E. Hart, F. Lalaurette, M. R. Sinclair, R. K. Smith and C. Thorncroft 2003, "The Extratropical Transition of Tropical Cyclones: Forecast Challenges, Current Understanding, and Future Directions," *Weather and Forecasting*, 18, 1052–1092.
- Kamoto, Minoru 2009, "Flood and Sediment Management in the Philippines, in view of Cooperation," Department of Public Works and Highways, Philippines
- Kaplan, J., and M. DeMaria 1995, "A Simple Empirical Model for Predicting the Decay of Tropical Cyclone Winds After Landfall," *Journal of Applied Meteorology*, 34, 2499–2512.
- Kato, F., Inagaki, S., Noguchi, K. and Fukuhama, M. (2005), "Coastal Disasters in 2004," technical note of National Institute for Land and Infrastructure Management, Ministry of Land, Infrastructure and Transport, Japan.
- Kato, F. and Torii, K. (2002), "Damages to General Properties due to a Storm Surge in Japan," *Solutions to Coastal Disasters*, 159-171.
- Kikitsu, H., and H. Okada 2000, "Characteristics of Across– Wind Response of Tall Building with Open Passage," *Proceedings of the 16th National Symposium on Wind Engineering*, 16, 435–440.
- Kim, S. Y., T. Yasuda, and H. Mase 2008, "Numerical analysis of effects of tidal variations on storm surges and waves," *Applied Ocean Research*, 311-322.
- Kitabatake, N. 2008, "Extratropical Transition of Tropical Cyclones in the Western North Pacific: Their Frontal Evolution," *Monthly Weather Review*, 136, 2066-2090.
- Klein, P. M., P. A. Harr, and R. L. Elsberry 2000, "Extratropical Transition of Western North Pacific Tropical Cyclones: An Overview and Conceptual Model of the Transformation Stage," *Weather and Forecasting*, 15, 373–396.
- Klein, P. M., P. A. Harr, and R. L. Elsberry 2000, "Extratropical Transition of Western North Pacific Tropical Cyclones: An Overview and Conceptual Model of the Transformation Stage," *Weather and Forecasting*, 15, 373–396.
- Knaff, J.A. and R.M Zehr 2007. "Reexamination of Tropical Cyclone Wind–Pressure Relationships," *Weather and Forecasting*, 22, 71–88.
- Knutson, Thomas; Camargo, Suzana J.; Chan, Johnny C. L.; Emanuel, Kerry; Ho, Chang-Hoi; Kossin, James; Mohapatra, Mrutyunjay; Satoh, Masaki; Sugi, Masato; Walsh, Kevin; Wu, Liguang. 2020. Tropical Cyclones and Climate Change Assessment: Part II. Projected Response to Anthropogenic Warming *Bulletin of the American Meteorological Society*, 101(3), E303-E322. <https://doi.org/10.1175/BAMS-D-18-0194.1>

- Kossin, J. P., Knapp, Kenneth; Olander, Timothy, Velden, Christopher. 2020. Global increase in major Tropical Cyclone Exceedence Probability over the past Four Decades. *PNAS* 117 (22) 11975-11980, <https://doi.org/10.1073/pnas.1920849117>
- Kossin, J.P. 2018. A global slowdown of tropical-cyclone translational speed. *Nature*, **558**, 104-107.
- Krayer, W. R., and R.D. Marshall 1992, "Gust Factors Applied to Hurricane Winds," *Bulletin of the American Meteorological Society*, 73, 613–617.
- Kubota, H., Matsumoto, J., Zaiki, M. et al. 2021. Tropical cyclones over the western north Pacific since the mid-nineteenth century. *Climatic Change* **164**, 29. <https://link.springer.com/article/10.1007/s10584-021-02984-7>
- Lagmay, Alfredo Mahar Francisco, Rojeelee P. Agaton, Mark Allen C. Bahala, Jo Brianne Louise T. Briones, Krichi May C. Cabacaba, Carl Vincent C. Caro, Lea L. Dasallas, Lia Anne L. Gonzalo, Christine N. Ladiero, John Phillip Lapidez, Maria Theresa Francia Mungcal, Jose Victor R. Puno, Michael Marie Angelo C. Ramos, Joy Santiago, John Kenneth Suarez, Judd P. Tablazon. Devastating storm surges of Typhoon Haiyan. 2015. *International Journal of Disaster Risk Reduction*, Volume 11, ages 1-12, <https://doi.org/10.1016/j.ijdr.2014.10.006>
- Lam, K.M. and To, A.P. 2009, "Statistical analysis of extreme wind speeds in Hong Kong and Macau," *HKIE Transactions*.
- Lee, C.S., Huang, L.R., Shen, H.S. and Wang, S.T. 2006, "A climatology model for forecasting typhoon rainfall in Taiwan," *Natural Hazards*, 37(1-2), 87-105.
- Lee, Tsz-Cheung, Thomas R. Knutson, Toshiyuki Nakaegawa, Ming Ying, Eun Jeong Cha. 2020. Third assessment on impacts of climate change on tropical cyclones in the Typhoon Committee Region – Part I: Observed changes, detection and attribution. *Tropical Cyclone Research and Review*, **Volume 9, Issue 1**, 1-22, <https://doi.org/10.1016/j.tcr.2020.03.001>
- Li, R.; Wang, Shih-Yu (Simon); Gillies, R. R.; Buckley, B.; Troung, L. H.; and Cho, C. 2015. "Decadal Oscillation of Autumn Precipitation in Central Vietnam Modulated by the East Pacific-North Pacific (EP-NP)". Plants, Soils, and Climate Faculty Publications. Paper 743. [https://digitalcommons.usu.edu/psc\\_facpub/743](https://digitalcommons.usu.edu/psc_facpub/743)
- Lin, Yong-Jun, Y-H. Chang, Y-C. Tan, J-S. Lai, H-Y. Lee, Y-J Chiu, and X-Y. He, "An Improved Watershed Management and Flood Mitigation Policy in Taiwan," *Interpraevent 2010*, International Symposium in the Pacific Rim, 810–819.
- Liu, K. S., and J. C. L. Chan, 199, "Size of Tropical Cyclones as Inferred from ERS–1 and ERS–2 Data," *Monthly Weather Review*, 127, 2992–3001.
- Liu, K. S., and J. C. L. Chan, 1999: Size of tropical cyclones as inferred from ERS-1 and ERS-2 data. *Mon. Wea. Rev.*, 127, 2992–3001.

- Matsuoka, M., K. Wakamatsu, K. Fujimoto, and S. Midorikawa 2006, "Average Shear-Wave Velocity Mapping Using Japan Engineering Geomorphologic Classification Map," *Japan Society of Civil Engineers*, 23, 57s-68s.
- Mei W., M., S.-P. Xie, F. Primeau, J. C. McWilliams, C. Pasquero. 2015. Northwestern Pacific typhoon intensity controlled by changes in ocean temperatures. *Science Advances*, **1:4**, 1-8.
- Mitsuta, Y., T. Fujii, and I. Nagashima 1996, "A Predicting Method for Typhoon Wind Damages," in *Proceedings of the 7th American Society of Civil Engineers Specialty Conference on Probabilistic Mechanics and Structural Reliability*, the American Society of Civil Engineers, Frangopol, D. M., and M. D. Grigoriu (eds.), Worcester, Massachusetts, USA, August 7-9, 1996, 970-973.
- Moon, I.-J., S.-H. Kim, and J. C. L. Chan. 2019. Climate change and tropical cyclone trend. *Nature*, 570, E3–E5
- Mori, Nobuhito, et al. "Local Amplification of Storm Surge by Super Typhoon Haiyan in Leyte Gulf." *Geophysical Research Letters* 41.14 (2014): 5106–5113. *PMC*. Web. 30 June 2016.
- Munich Re Group, "Topics Annual Review: Natural Catastrophes," Annual Report from Munich Re, 2001 – 2013.
- Murakami, Hiroyuki, Thomas L. Delworth, William F. Cooke, Ming Zhao, Baoqiang Xiang, Pang-Chi Hsu. 2020. Detected climatic change in global distribution of tropical cyclones. *Proceedings of the National Academy of Sciences*, **117 (20)**, 10706-10714.
- Muramatsu, T. 1985, "A Study on the Changes of the Three-Dimensional Structure and the Movement Speed of the Typhoon through Its Lifetime," technical report from the Meteorological Research Institute, 14, 117. <http://www.mri-jma.go.jp/>.
- National Aeronautics and Space Administration (NASA), Tropical Rainfall Measuring Mission (TRMM). <http://trmm.gsfc.nasa.gov/>.
- National Center for Atmospheric Research (NCAR) and Pennsylvania State University (PSU), NCEP-NCAR Global Reanalysis Data (1951-2008). <http://www.mmm.ucar.edu/mm5/>
- National Institute of Standards and Quality Vietnam, "Loads and Effects – Design Standard, TCVN 2737: 1995," *National Building Code of Vietnam*, 1995 (Vietnamese).
- National Oceanic and Atmospheric Administration (NOAA), National Climatic Data Center, Global Summary of the Day Data (NCDC).
- National Oceanic and Atmospheric Administration (NOAA), QuikSCAT. [http://manati.orbit.nesdis.noaa.gov/cgi-bin/qscat\\_storm.pl](http://manati.orbit.nesdis.noaa.gov/cgi-bin/qscat_storm.pl)
- National Oceanic and Atmospheric Administration (NOAA), Regional and Mesoscale Meteorology Branch (RAMMB). <http://rammb.cira.colostate.edu/>

- National Oceanic and Atmospheric Administration (NOAA) Technical Report NWS-23, 1981.
- National Reinsurance Corporation of the Philippines 2012, "Updates on the Philippines Reinsurance Market," *Philippines Non-Life Insurance Summit*, April 25, 2012.
- Nguyen-Thi, Hoang Anh, Jun Matsumoto, Thanh Ngo-Duc and Nobuhiko Endo 2012. A Climatological Study of Tropical Cyclone Rainfall in Vietnam. *SOLA (Scientific Online Letters on the Atmosphere)*. **8**, 41-44. <https://doi.org/10.2151/sola.2012-011>
- NOAA's National Hurricane Center, <http://www.nhc.noaa.gov/aboutsshws.php>.
- Oey, L-Y., and Chou, S. 2016. Evidence of rising and poleward shift of storm surge in western North Pacific in recent decades, *J. Geophys. Res. Oceans*, 121, 5181– 5192,
- Pacheco, B.M., Aquino, R.E., Tanchuling, M. A. N. and Tanzo, W.T. 2010, "APEC-WW-2010 Country Report: Philippines," *Wind Engineering Research Center, Tokyo Polytechnic University*, 2010.
- Pacheco, B.M., Aquino, R.E., Tanzo, W.T. and Rosaria, N.E. 2006, "Wind Loads and the Wind Environment in the Philippines: Recent Developments in 2006," *In Proceedings of the 3rd Workshop on Regional Harmonization of Wind Loading and Wind Environmental Specifications in Asia-Pacific Economies (APEC-WW-2006)*, New Delhi, India.
- Pacheco, B.M., Aquino, R.E. and Tanzo, W.T. 2005, "Wind Loading Code Provisions in the Philippines and Identified Future Improvements," *In Proc. Workshop on Regional Harmonization of Wind Loading and Wind Environmental Specifications in Asia-Pacific Economies (APEC-WW-2005)*.
- Pacheco, B.M., Tanzo, W.T. and Aquino, R.E. 2009, "Recent Wind Engineering Developments in the Philippines: 2007-2009," *In Proceedings of the 5th Workshop on Regional Harmonization of Wind Loading and Wind Environmental Specifications in Asia-Pacific Economies*. Taiwan, 2009.
- Rahmstorf, Stefan, Kerry Emanuel, Mike Mann and Jim Kossin. 2018. *Does global warming make tropical cyclones stronger?* Real Climate <https://www.realclimate.org/index.php/archives/2018/05/does-global-warming-make-tropical-cyclones-stronger/>
- Ritchie, E. A., and R. L. Elsberry 2001, "Simulations of the Transformation Stage of the Extratropical Transition of Tropical Cyclones," *Monthly Weather Review*, 129, 1462–1480.
- Rojas, R., P. Julien, and B. Johnson 2003, *CASC2D–SED v. 1.0 Reference Manual, A 2-Dimensional Rainfall–Runoff and Sediment Model*, Colorado State University, July 2003, 45.
- Sagala, S.A.H. 2006, "Analysis of flood physical vulnerability in residential areas. Case study: Naga City, The Philippines," *ITC*.

- Sakakibara, H., M. Ishihara, and Z. Yanagisawa 1985, "Structure of a Typhoon Rainstorm in the Middle Latitudes Observed by Doppler Radar," *Journal of the Meteorological Society of Japan*, 63, 901–922.
- Sato, T., Nakasu, T. (2011): 2009 Typhoon Ondoy Flood Disasters in Metro Manila. Natural Disaster Research Report, 45, 63-74.
- Saxton, K.E., W.J. Rawls, J.S. Romberger, and R.I. Papendick 1986. Estimating generalized soil-water characteristics from texture. *Soil Sci. Soc. Am. J.* 20:1031-1036.
- Saxton, K. E. and W.J. Rawls. 2006. Soil water characteristic estimates by texture and organic matter for hydrologic solutions. *Soil Science Society of America Journal* 70(5): 1569-1578.
- Schwerdt, R. W., F. P. Ho, and R. Watkins 1979, "Meteorological Criteria for Standard Project Hurricane and Probable Maximum Hurricane Wind fields, Gulf and East Coasts of the United States," U.S. Department of Commerce, National Oceanic and Atmospheric Administration, NOAA Technical Report NWS 23, September 1979.
- Simiu, E., and R. H. Scanlan 1996, *Wind Effects on Structures: Fundamentals and Applications to Design*. Malden, Massachusetts: Wiley InterScience.
- Sousounis, P. J. and J. Butke 2010, "The Climatological Significance of Extratropical Transitioning on Typhoon Precipitation over Japan," *Proceedings of the 29th American Meteorological Society Conference on Hurricanes and Tropical Meteorology*, Tucson, Arizona, May 10-14, 2010. <http://ams.confex.com/ams/pdfpapers/169244.pdf>.
- Sousounis, P. J. and M. Desflots 2010, "Evaluating the Impacts of Extratropical Transitioning on Typhoon Losses via Synoptic Case Studies," *Proceedings of the 29th American Meteorological Society Conference on Hurricanes and Tropical Meteorology*, Tucson, Arizona, May 10-14, 2010. <http://ams.confex.com/ams/pdfpapers/169228.pdf>.
- Su, E. C. M. 2002, *Building Structural Types in Taiwan*, National Center for Research on Earthquake Engineering (NCREE). [http://www.ncree.org.tw/itp2002/03\\_BuildingStructuralTypesInTaiwan.pdf](http://www.ncree.org.tw/itp2002/03_BuildingStructuralTypesInTaiwan.pdf)
- Subbaramayya, I., and S. Fujiwhara, 1979, "A Note on the Relationship Between Maximum Surface Wind and Central Pressure in Tropical Cyclones in Western North Pacific," *Journal of the Meteorological Society of Japan*, 57, 368–360.
- Sui, C. H., et al., 2002, Meteorology-hydrology study targets Typhoon Nari and Taipei flood, *Eos Trans. AGU*, 83(24), 265–270, doi:[10.1029/2002EO000186](https://doi.org/10.1029/2002EO000186).
- Sung-Hun Kim et al. 2020. *Environ. Res. Lett.* 15 094084. An increase in global trends of tropical cyclone translation speed since 1982 and its physical causes <https://iopscience.iop.org/article/10.1088/1748-9326/ab9e1f>
- Suzuki, K. 2000, "Characteristics of Extratropical Transition of Tropical Cyclones in Satellite Imagery," *Meteorological Satellite Center Technical Note*, 38, 21–42.

- Swiss Re, "Sigma: Natural Catastrophes and Man-made Disaster," Annual Report from Swiss Re, 2001– 014.
- Tagami, H., and T. Kanno, 2006, "Heavy Rainfalls during the Baiu Period and Remarkable Typhoons in 2004," a technical report from the Japan Meteorological Agency, 129, 281 (in Japanese).
- Taiwan Central Weather Bureau (CWB). <http://www.cwb.gov.tw/V6e/index.htm>
- Tajima, Y. et al. 2014, "Initial report of JSCE-PICE Joint Survey on the Storm Surge Disaster caused by Typhoon Haiyan." *Coastal Engineering Journal*, 56(1), DOI: [10.1142/S0578563414500065](https://doi.org/10.1142/S0578563414500065).
- Takagi, H., M. Esteban, T. Shibayama, T. Mikami, R. Matsumaru, M. De Leon,, N.D. Thao, T. Oyama, and R. Nakamura 2015, Track analysis, simulation, and field survey of the 2013 Typhoon Haiyan storm surge. *Journal of Flood Risk Management*. doi: 10.1111/jfr3.12136.
- Takagi, Hiroshi. 2019. Statistics on typhoon landfalls in Vietnam: Can recent increases in economic damage be attributed to storm trends?, *Urban Climate* **30**, <https://doi.org/10.1016/j.uclim.2019.100506>.
- Teng, Wei-Hsien, M.H. Hsu, C-H. Wu, and A.S. Chen, 2006, "Impact of Flood Disasters on Taiwan in the Last Quarter Century," *Natural Hazards*, 37, 191-207.
- The Board of the Civil Engineering of the Professional Regulation Commission, 1992. "National Structural Code of the Philippines," *Association of Structural Engineers of the Philippines*, 1, Fourth Edition.
- The Board of the Civil Engineering of the Professional Regulation Commission, 2001. "National Structural Code of the Philippines," *Association of Structural Engineers of the Philippines*, 1, Fifth Edition.
- The Board of the Civil Engineering of the Professional Regulation Commission, 2001. "National Structural Code of the Philippines," *Association of Structural Engineers of the Philippines*, 1, Sixth Edition.
- The Digital Typhoon Network, the National Institute of Informatics. <http://agora.ex.nii.ac.jp/digital-typhoon/index.html.en>.
- The Joint Typhoon Warning Center (JTWC) 1959, "1959 Annual Typhoon Report," report by the JTWC and the U.S. Navy.
- The Typhoon Research Department of the Meteorological Research Institute 2006, "Summary of Typhoons Landfalling on Japan in 2004," Technical Report, the Meteorological Research Institute. <http://www.mri-jma.go.jp/>.
- Tsubokawa, Hiroaki 2009, "The Report of the East Asian Seas Congress in Manila, Philippines – Partnerships at Work: Local Implementation and Good Practices," IGU-

Commission on Hazard and Risk. [http://www.homeofgeography.org/uk/news\\_2010/C08.18\\_Manila-nov09.pdf](http://www.homeofgeography.org/uk/news_2010/C08.18_Manila-nov09.pdf).

Tu, Jien-Yi and Chia Chou. 2013. Changes in precipitation frequency and intensity in the vicinity of Taiwan: typhoon versus non-typhoon events. *Environ. Res. Lett.* **8** 014023 DOI. <https://iopscience.iop.org/article/10.1088/1748-9326/8/1/014023>

Typhoon 2000 (Philippines). <http://www.typhoon2000.ph/>.

United States Department of Agriculture 1986, *Technical Release 55 (TR-55): Urban Hydrology for Small Watersheds*. Washington, D.C.: United States Department of Agriculture, Natural Resources Conservation Service, Conservation Engineering Division.

United States Department of Commerce 2003, *Super Typhoon Pongsona, December 8, 2002*, Silver Spring, Maryland: United States Department of Commerce, National Oceanic and Atmospheric Administration, National Weather Service.

Velden, C., B. Harper, F. Wells, J. L. Beven, R. Zehr, T. Olander, M. Mayfield, C. Guard, M. Lander, R. Edson, L. Avila, A. Burton, M. Turk, A. Kikuchi, A. Christian, P. Caroff, and P. McCrone 2006, "The Dvorak Tropical Cyclone Intensity Estimation Technique: A Satellite-Based Method That Has Endured For Over 30 Years," *Bulletin of the American Meteorological Society*, **87**, 1195–1210.

Wang, R. and L. Wu. 2019. Influence of Track Changes on the Poleward Shift of LMI Location of Western North Pacific Tropical Cyclones. *J Climate*, **32**, 8437-8445. (2019)

Water Resources Agency, Ministry of Economic Affairs, Taiwan, "Flood Characteristics in Taiwan." <http://eng.wra.gov.tw/lp.asp?ctNode=2299&CtUnit=619&BaseDSD=7>.

Willoughby, H. E., and M. E. Rahn 2004, "Parametric Representation of the Primary Hurricane Vortex. Part I: Observations and Evaluation of the Holland (1980) Model," *Monthly Weather Review*, **132**, 3033–3048.

Willoughby, H. E., R. W. R. Darling, and M. E. Rahn 2006, "Parametric Representation of the Primary Hurricane Vortex. Part II: A New Family of Sectionally Continuous Profiles," *Monthly Weather Review*, **134**, 1102–1120.

Wu, L., Wang, R., & Feng, X. 2018. Dominant role of the ocean mixed layer depth in the increased proportion of intense typhoons during 1980–2015. *Earth's Future*, **6**, 1518–1527. <https://doi.org/10.1029/2018EF000973>

Wu, L., Zhao, H., Wang, C. et al. 2022. Understanding of the Effect of Climate Change on Tropical Cyclone Intensity: A Review. *Adv. Atmos. Sci.* **39**, 205–221.

Yoshie, R., M. Watakabe, Y. Okuda, H. Okada 2001, "Comparison of Peak Pressure Coefficients for Wind Load on Cladding in National and International Standards," *Journal of Wind Engineering*, **89**, 597–600.

- Zhan, R., and Y. Wang. 2017. Weak tropical cyclones dominate the poleward migration of the annual mean location of lifetime maximum intensity of northwest Pacific tropical cyclones since 1980. *J. Climate*, **30**, 6873–6882, (2017)
- Zhang, Dongna, Han Zhang, Jiayu Zheng, Xuhua Cheng, Di Tian, and Dake Chen. 2020. "Changes in Tropical-Cyclone Translation Speed over the Western North Pacific" *Atmosphere* 11, no. 1: 93. <https://doi.org/10.3390/atmos11010093>

# Selected References for Accounting for Climate Change

The following reference materials have been used in the development and refinement of the Accounting for Climate Change chapter in the Verisk Typhoon Model for Southeast Asia.

Bagtasa, Gerry. "Contribution of Tropical Cyclones to Rainfall in the Philippines." *Journal of Climate*, 30 (2017): 3621-3633.

Chan, K.T.F. Are global tropical cyclones moving slower in a warming climate? *Environ. Res. Lett.* 2019, 14, 105015.

Chen Jilong, Tam Chi-Yung, Cheung Kevin, Wang Ziqian, Murakami Hiroyuki, Lau Ngar-Cheung, Garner Stephen T., Xiao Ziniu, Choy Chun-Wing, Wang Peng; 2021: Changing Impacts of Tropical Cyclones on East and Southeast Asian Inland Regions in the Past and a Globally Warmed Future Climate. *Frontiers in Earth Science*, 9, 234-235. <https://www.frontiersin.org/articles/10.3389/feart.2021.769005>

Chu, Pao-Shin, Hanpei Zhang, Hui-Ling Chang, Tsui-Ling Chen and Kristine Tofte. "Trends in return levels of 24-hr precipitation extremes during the typhoon season in Taiwan." *International Journal of Climatology* 38 (2018): 5107 - 5124.

Gong, D., Tang, X., Chan, J. C. L., and Wang, Q., "Trends of Tropical Cyclone Translation Speed over the Western North Pacific during 1980–2018", *Atmosphere*, vol. 13, no. 6, p. 896, 2022. doi:10.3390/atmos13060896.

Knutson, T., and co-authors (2020) Tropical cyclones and climate change assessment. Part II: Projected response to anthropogenic warming. *Bull. Amer. Meteor. Soc.*, **101**, E303-E322.

Kossin, J.P., 2018: A global slowdown of tropical-cyclone translational speed. *Nature*, **558**, 104-107.

Kossin, James P.; Knapp, Kenneth R.; Olander, Timothy L.; Velden, Christopher S (2020): Global increase in major tropical cyclone exceedance probability over the past four decades. *Proceedings of the National Academy of Sciences of the United States of America*. vol 117, 11975-11980

Kubota, H., Matsumoto, J., Zaiki, M. et al. Tropical cyclones over the western north Pacific since the mid-nineteenth century. *Climatic Change* 164, 29 (2021). <https://doi.org/10.1007/s10584-021-02984-7>

Lee, Tsz-Cheung, Thomas R. Knutson, Toshiyuki Nakaegawa, Ming Ying, Eun Jeong Cha, 2020: Third assessment on impacts of climate change on tropical cyclones in the Typhoon Committee Region – Part I: Observed changes, detection and attribution. *Tropical Cyclone Research and Review*, **Volume 9, Issue 1**, Pages 1-22, ISSN 2225-6032, <https://doi.org/10.1016/j.tccr.2020.03.001>.

Liu, KS, Chan, JCL. 2019: Inter-decadal variability of the location of maximum intensity of category 4–5 typhoons and its implication on landfall intensity in East Asia. *Int J Climatol.*, **39**, 1839– 1852. <https://doi.org/10.1002/joc.5919>

Mei W., M., S.-P. Xie, F. Primeau, J. C. McWilliams, C. Pasquero, 2015: Northwestern Pacific typhoon intensity controlled by changes in ocean temperatures. *Science Advances*, **1:4**, 1-8.

Murakami, Hiroyuki, Thomas L. Delworth, William F. Cooke, Ming Zhao, Baoqiang Xiang, Pang-Chi Hsu, 2020: Detected climatic change in global distribution of tropical cyclones. *Proceedings of the National Academy of Sciences*, **117 (20)**, 10706-10714. DOI: 10.1073/pnas.1922500117

Hiroshi Takagi, Statistics on typhoon landfalls in Vietnam: Can recent increases in economic damage be attributed to storm trends? *Urban Climate*, Volume 30, 2019, 100506, ISSN 2212-0955, <https://doi.org/10.1016/j.uclim.2019.100506>.

Wang, R. and L. Wu, 2019: Influence of Track Changes on the Poleward Shift of LMI Location of Western North Pacific Tropical Cyclones. *J Climate*, **32**, 8437-8445.

Wu, L., Wang, R., & Feng, X. (2018). Dominant role of the ocean mixed layer depth in the increased proportion of intense typhoons during 1980–2015. *Earth's Future*, **6**, 1518–1527. <https://doi.org/10.1029/2018EF000973>

Wu, L., Zhao, H., Wang, C. et al. Understanding of the Effect of Climate Change on Tropical Cyclone Intensity: A Review. *Adv. Atmos. Sci.* 39, 205–221 (2022).

Zhan, R., and Y. Wang, 2017: Weak tropical cyclones dominate the poleward migration of the annual mean location of lifetime maximum intensity of northwest Pacific tropical cyclones since 1980. *J. Climate*, **30**, 6873–6882, <https://doi.org/10.1175/JCLID-17-0019.1>.

Zhang, Dongna, Han Zhang, Jiayu Zheng, Xuhua Cheng, Di Tian, and Dake Chen. 2020. "Changes in Tropical-Cyclone Translation Speed over the Western North Pacific" *Atmosphere* 11, no. 1: 93. <https://doi.org/10.3390/atmos11010093>

## About Verisk

Verisk Analytics (Verisk) provides risk modeling solutions that make individuals, businesses, and society more resilient to extreme events. In 1987, a Verisk subsidiary founded the catastrophe modeling industry and today models the risk from natural catastrophes, terrorism, pandemics, casualty catastrophes, and cyber incidents. Insurance, reinsurance, financial, corporate, and government clients rely on Verisk's advanced science, software, and consulting services for catastrophe risk management, insurance-linked securities, longevity modeling, site-specific engineering analyses, and agricultural risk management. Verisk (Nasdaq:VRSK) is headquartered in Jersey City, New Jersey with many offices throughout the United States and around the world. For information on our office locations, visit <https://www.verisk.com/about/locations/>.

### Contact Information

Verisk Analytics  
Lafayette City Center, 2nd Floor  
Two Avenue de Lafayette  
Boston, MA 02111  
USA

Tel: (617) 267-6645  
Fax: (617) 267-8284

Verisk welcomes feedback on its documentation. If you need assistance in using the software or understanding the information in this document, please email us at [Documentation-Air@verisk.com](mailto:Documentation-Air@verisk.com).

